

GEOLOGICA ULTRAIECTINA

Mededelingen van de  
Faculteit Geowetenschappen  
Universiteit Utrecht

No. 256

**Neoproterozoic Tectonics of the Arabian-Nubian Shield**

**Bernard Blasband**

2006

Cover illustration: NE-SW trending dykes in the Wadi Kid Complex, Sinai, Egypt.

The research in this thesis was carried out at the structural geology and tectonics group of the Faculty of Geosciences at Utrecht University, the Netherlands. The author acknowledges financial support from the Dr. Schürmann Fund for the laboratory and field research in the Egypt and Saudi Arabia with grant numbers 1994/06, 1997/07, 1999/04 and 2000/04a.

Faculty of Geosciences  
Utrecht University  
Budapestlaan 4  
3584 CD Utrecht  
The Netherlands

<http://www.geo.uu.nl/>

ISBN-10: 90-5744-119-5

ISBN-13: 978-90-5744-119-6

# **Neoproterozoic Tectonics of the Arabian-Nubian Shield**

## **Neoproterozoische Tektoniek van het Arabische-Nubische Schild**

(met een samenvatting in het Nederlands)

### **PROEFSCHRIFT**

ter verkrijging van de graad van doctor aan de Universiteit Utrecht  
op gezag van de Rector Magnificus, Prof. Dr. W.H. Gispen,  
ingevolge het besluit van het College voor Promoties  
in het openbaar te verdedigen op maandag 3 april 2006 des ochtends te 10.30 uur

door

**Bernard Benjamin Blasband**  
geboren op 22 mei 1966, te Den Haag

Promotor: Prof. Dr. S.H. White  
Faculteit Geowetenschappen  
Universiteit Utrecht

Co-promotor: Prof. Dr. C.J. Spiers  
Faculteit Geowetenschappen  
Universiteit Utrecht



Members of the dissertation committee:

Dr. P.R. Johnson  
Saudi Geological Survey  
Jeddah, Saudi Arabia

Prof. Dr. H.J. Kisch  
Ben Gurion University of the Negev  
Be'er Sheva, Israel

Prof. Dr. C.W. Passchier  
Johannes Gutenberg Universität  
Mainz, Germany/  
Vrije Universiteit  
Amsterdam, The Netherlands

Prof. Dr. H.N.A. Priem  
Universiteit Utrecht  
Utrecht, The Netherlands

Prof. Dr. R.L.M. Vissers  
Universiteit Utrecht  
Utrecht, The Netherlands

# Contents

<b>Abstract</b>	<b>11</b>
<b>1. Introduction</b>	<b>13</b>
1.1 Preamble	13
1.2 Aims	15
1.3 Outline of thesis	15
<b>2. Geology of the Arabian Nubian Shield – An overview</b>	<b>17</b>
2.1 Introduction	17
2.2 Relicts of oceanic crust	17
2.3 Island-arc remnants	17
2.4 Features related to arc-accretion	19
2.5 Gneissic domes	26
2.6 Other late orogenic features	26
2.7 Proposed models for the Neoproterozoic in the ANS	30
<b>3. The Bi'r Umq Complex and Shear Zone: an ophiolitic suture in the Arabian-Nubian Shield</b>	<b>37</b>
Abstract	37
3.1 Introduction	37
3.2 Geological Background	39
3.2.1 Lithology	40
3.2.2 Metamorphism	42
3.2.3 Origin of igneous rocks	43
3.2.4 Geochronology	43
3.3 Structural Geology	44
3.3.1 Introduction	44
3.3.2 Previous studies	44
3.3.3 Shear Zone related structures	44
3.3.4 Structures outside the shear zones	56
3.4 Discussion and conclusions	57
3.4.1 Review of new data for the Bi'r Umq Complex	57
3.4.2 A tectonic model for the Bi'r Umq Complex	60
<b>4. Structural, geochemical and geochronological constraints on the tectonic evolution of the Tabalah and Wadi Tarj areas, central Asir, western Saudi Arabia</b>	<b>67</b>
Abstract	67

4.1 Introduction	67
4.2 Geological Background	70
4.2.1 Lithology	70
4.2.2 Metamorphism	73
4.3 Structural Geology	73
4.3.1 Introduction	73
4.3.2 Foliations	74
4.3.3 Lineations	74
4.3.4 Evidence for non-coaxial deformation	76
4.3.5 Conclusions on structural geology	77
4.4 Geochemistry	78
4.4.1 Introduction	78
4.4.2 Samples	79
4.4.3 Techniques	80
4.4.4 Major elements	80
4.4.4 Trace elements	81
4.5 Geochronology	86
4.5.1 Introduction	86
4.5.2 Previous geochronology studies	87
4.5.3 Description of samples	87
4.5.4 Results	88
4.5.5 Summary of geochronological studies	88
4.6 Discussion and conclusions	97
4.6.1 Summary of geological evidence	97
4.6.2 Tectonic model for the Tabalah and Wadi Tarj Complex	98
4.6.3 Conclusions	100
<b>5. A Pan-African core complex in the Sinai, Egypt</b>	<b>103</b>
Abstract	103
5.1 Introduction	103
5.2 Geological background	104
5.2.1 Introduction	104
5.2.2 Lithology	104
5.2.3 Metamorphism	107
5.2.4 Geochronology	108
5.3 The structural geology	108
5.3.1 Introduction	108
5.3.2 D1 structures	108
5.3.3 D2 structures	109
5.3.4 Evidence of non-coaxial strains during D2	111
5.4. Discussion	120
5.4.1 Interpretation of regional structural data	120



5.4.2 A core-complex model for the Wadi Kid area	121
5.4.3 Reversal in the sense of shear and coaxial overprint in core complexes	123
5.4.4 A model for the tectonic history of the Wadi Kid area	126
5.5 Conclusions	126
<b>6. A new geodynamic model for the Neoproterozoic of the Arabian-Nubian Shield</b>	<b>129</b>
6.1 Introduction	129
6.2 Summary of newly obtained data for the three main tectonic phases in the Arabian-Nubian Shield	129
6.2.1 Introduction	129
6.2.2 The Bi'r Umq Complex: Relicts of the oceanic stage and the arc-accretion stage	129
6.2.3 The Tabalah and Wadi Tarj Complex: Relicts of the oceanic stage and the arc-accretion stage	130
6.2.4 The Wadi Kid Complex: A core complex	131
6.3 A synthesis of the newly obtained data from the Bi'r Umq area, the Tabalah and Wadi Tarj area and the Wadi Kid area	136
6.4 A model for the tectonic evolution of the Arabian-Nubian Shield based on the Bi'r Umq Complex, the Tabalah and Tarj Complex and the Wadi Kid area	138
6.4.1 The oceanic/island-arc phase in the ANS	138
6.4.2 Arc-accretion phase in the ANS	139
6.4.3 Extensional features in the ANS	142
6.4.4 The transition from compression to extension in the ANS	143
6.5 Summary of a new tectonic scenario for the Arabian-Nubian Shield	148
6.6 Conclusions	150
6.7 Recommendations for future research	150
<b>References</b>	<b>153</b>
<b>Samenvatting (Summary in Dutch)</b>	<b>163</b>
<b>Acknowledgements</b>	<b>167</b>
<b>Curriculum Vitae</b>	<b>169</b>
<b>Appendices</b>	<b>171</b>
A1 Additional geological data for the Wadi Kid area, Sinai, Egypt	173
Abstract	173
A1.1 Introduction	173
A1.2 Geological background	173
A1.3 Geochemistry of undeformed igneous rocks in the Wadi Kid Complex	177

A1.4 Geochronology: Ar-Ar dating for the main lower-crustal amphibolite	179
A1.5 Conclusions	184
A.2 Geothermobarometric evidence for a metamorphic core-complex in Sinai, Egypt	187
Abstract	187
A.2.1 Introduction	187
A.2.2 Lithology	188
A.2.3 Structures	192
A.2.4 Petrology	193
A.2.5 Mineral composition	194
A.2.6 Evidence from PT-data for a core complex in the Wadi Kid Area	210
A.2.7 Conclusions	213

## Abstract

The Neoproterozoic tectonic development of the Arabian-Nubian Shield (ANS) can be divided in three parts: 1) the oceanic stage, which includes mainly remnants of intra-oceanic subduction; 2) the arc-accretion stage; 3) the extensional stage. Three key-areas in the Arabian-Nubian Shield, namely the Bi'r Umq Complex, The Tabalah and Tarj Complex and the Wadi Kid Complex, were studied in the framework of this research with the aim to investigate each of these three stages in detail and to integrate these stages into one geodynamic model for the Neoproterozoic of the ANS.

The Bi'r Umq Complex is part of the Bi'r Umq-Nakasib Suture that trends SW-NE in the central part of the ANS. It represents the border between the Jiddah and the Hijaz Terranes in the Arabian part of the ANS. The ophiolite of the Bi'r Umq complex was formed at ca. 830 Ma. The ophiolite was formed at a fore-arc or at a back-arc of an island-arc in the Mozambique Ocean. It was folded and extensively sheared during three phases of deformation. D1 resulted in regional folding and axial planar foliation, and regional deformation localized into shear zones with good shear sense indicators, and localized in shear zones, the development of foliations, and of steeply plunging stretching lineations, and the development of good shear indicators. These structures resulted from SE-vergent thrusting on the Bi'r Umq Shear Zone (BUSZ), the main shear structure, and on minor shear zones within the Bi'r Umq Complex. The D1-deformation phase was a result of NW-SE compression and was responsible for the emplacement of the ophiolites in the overriding plate. The second phase, D2, was marked by dextral strike-slip in the central zone of the WSW-ENE-trending BUSZ and resulted in the formation of sub-horizontally WSW-plunging elongated clast-lineations. This phase resulted from WNW-ESE compression. The third phase, D3, involved sinistral strike-slip shear reversal on the BUSZ and resulted from NNE-SSW compression. Deformation in the Bi'r Umq Complex (BUC) occurred during obduction of the Bi'r Umq ophiolite and ended at ca. 760 Ma. The changes of the sense of movement on the shear zones of the Bi'r Umq Complex were related to a change in the direction of plate motion of the subducting plate. The structures and structural history in the region are associated with the closure of an oceanic basin by subduction and are relicts of the "off-shore amalgamation" of a number of island-arcs in the Arabian shield. The "off-shore amalgamation" led to the formation of the Amennakhte Superterrane.

The Tabalah and Wadi Tarj Complex in the central part of the Neoproterozoic Asir Terrane in Saudi Arabia, display typical intra-terrane features. The Tabalah and Wadi Tarj areas contain gabbros and quartz-diorites, which were intruded in an island arc, together with tonalites and granodiorites, which display characteristics of intrusion during subduction at an active continental margin. These rocks were deformed during two deformation-phases: D1 and D2. The D1-phase was characterized by thrusting as illustrated by steep lineations and hanging wall over footwall shear sense indicators. This phase was dated at ca. 779 Ma and resulted from E-W to WNW-ESE compression. The D2-phase was characterized by dextral strike slip that resulted from NNE-SSW compression. This event was dated at ca. 765 Ma. The observed deformation phases and late intrusions in the Tabalah and Wadi Tarj area are also related to the

“off-shore amalgamation” along NE-SW trending sutures which formed the Amennakhte Superterrane.

In the Wadi Kid Complex in the Sinai, Egypt, a sequence of thick sub-horizontal amphibolite HT/LP grade schists, was interpreted as low-angle normal shear zones which displayed top-to-the-NW movement and was associated with upper-crustal extension. Undeformed granites, similar to the A-type granites found in other parts of the ANS and interpreted to be related to extension, intruded the area. The intrusion of NE-SW trending dykes, perpendicular and synchronous to the movement on the shear zone, indicated that the shear zones were formed in a NW-SE extensional regime. The activity on the low-angle shear zone was dated at ~595 Ma. These geological features indicate that the Wadi Kid Complex represent a core complex that was formed during NW-SE extension. Other “gneissic domes” in the ANS can also be interpreted as core complexes.

Published data show that the extension as observed in the Wadi Kid Complex, was predated by a phase of arc-accretion at the N-S trending active continental margins of East- and West Gondwanaland at 700-650 Ma. During this phase, independent island-arcs and superterranees that were formed off-shore, accreted upon these continental margins. In summary, the arc-accretion at the continental margins led to lithospheric thickening. When convergence slowed down, thermal re-equilibration led a decrease of strength in the lithosphere. This led, in turn, to the gravitational collapse of the thickened lithosphere and the extension that caused the formation of the core complexes. The Neoproterozoic development of the ANS is thus similar to the Mesozoic development of the Cordillera in western North America.

# Introduction

## 1.1 Preamble

The Arabian-Nubian Shield contains the remnants of the Neoproterozoic basement in the Middle East and NE Africa (Figure 1-1). This shield was formed between ca. 900 Ma and ca. 560 Ma. The hydrocarbon industry has performed much research in the Phanerozoic sedimentary cover of the Middle East due to its high contents of oil and gas. Occasionally, the research into the petroleum geology of the Middle East also involved research in its Neoproterozoic basement. A study of the Neoproterozoic sediments of the Arabian-Nubian Shield in Egypt was one of the first assignments of dr. H.M.E. Schürmann at Royal Dutch/Shell in the 1920s. This study was performed to allow differentiation between the oil-bearing Phanerozoic sediments and the “dry” Neoproterozoic sediments. In recent times, the understanding of the Neoproterozoic structures in the Middle East was regarded as a crucial part of petroleum geological research (e.g. Hussein, 2000). However, geological research in the Arabian-Nubian Shield started much earlier than any of the oil-industry related research.

The Nubian part of the Arabian-Nubian Shield (current day Egypt, Sudan, Eritrea and Ethiopia) is actually the location of the earliest known geological research to have been recorded. The pharaonic Egyptians explored their country for gold and found this in the Neoproterozoic basement of their country, the Nubian part of the Arabian-Nubian Shield. A map that describes the geology of the Wadi Hammamat area in the Eastern Desert was made by the Theban scribe Amennakhte at ~1150 B.C. during the reign of Ramesses IV (Harrel and Brown, 1992). The map (Figure 1-2) contains different colors which can be correlated with different rock-formations in the field as the granites, siliclastic sediments, volcanics and serpentinites of the area (Harrel and Brown, 1992). The map highlights gold-workings and a quarry for decorative stones (Harrel and Brown, 1992).

Another landmark of Arabian-Nubian geology, was the recognition of Neoproterozoic ophiolitic sequences in the 1970s. A number of authors (e.g. Garson and Shalaby, 1976; Shackleton, 1977 and Bakor et al., 1976; Shanti and Roobol, 1979) interpreted sequences of ultramafics, gabbros and marine sediments in Egypt and Saudi Arabia as ophiolites. Until the late 1980s, the ophiolites of the Arabian-Nubian Shield (dated at ca. 800-900Ma) were thought to be the oldest in the world and consequently this shield was believed to contain the oldest remnants of plate tectonics as we see it today. However since then, ophiolites have been found in the Late Archean and Early Proterozoic (Stern, 2005).

The presence of the ophiolites led most authors to view the Neoproterozoic tectonics of the Arabian-Nubian Shield as being associated with continuing compression that was associated with the obduction of the ophiolites. It was in recent years, that the importance of tectonic regimes other than compression has been proposed (e.g., Greiling et al., 1994; Stern, 1994). Another reason that makes the Arabian-Nubian Shield a very interesting area for geological

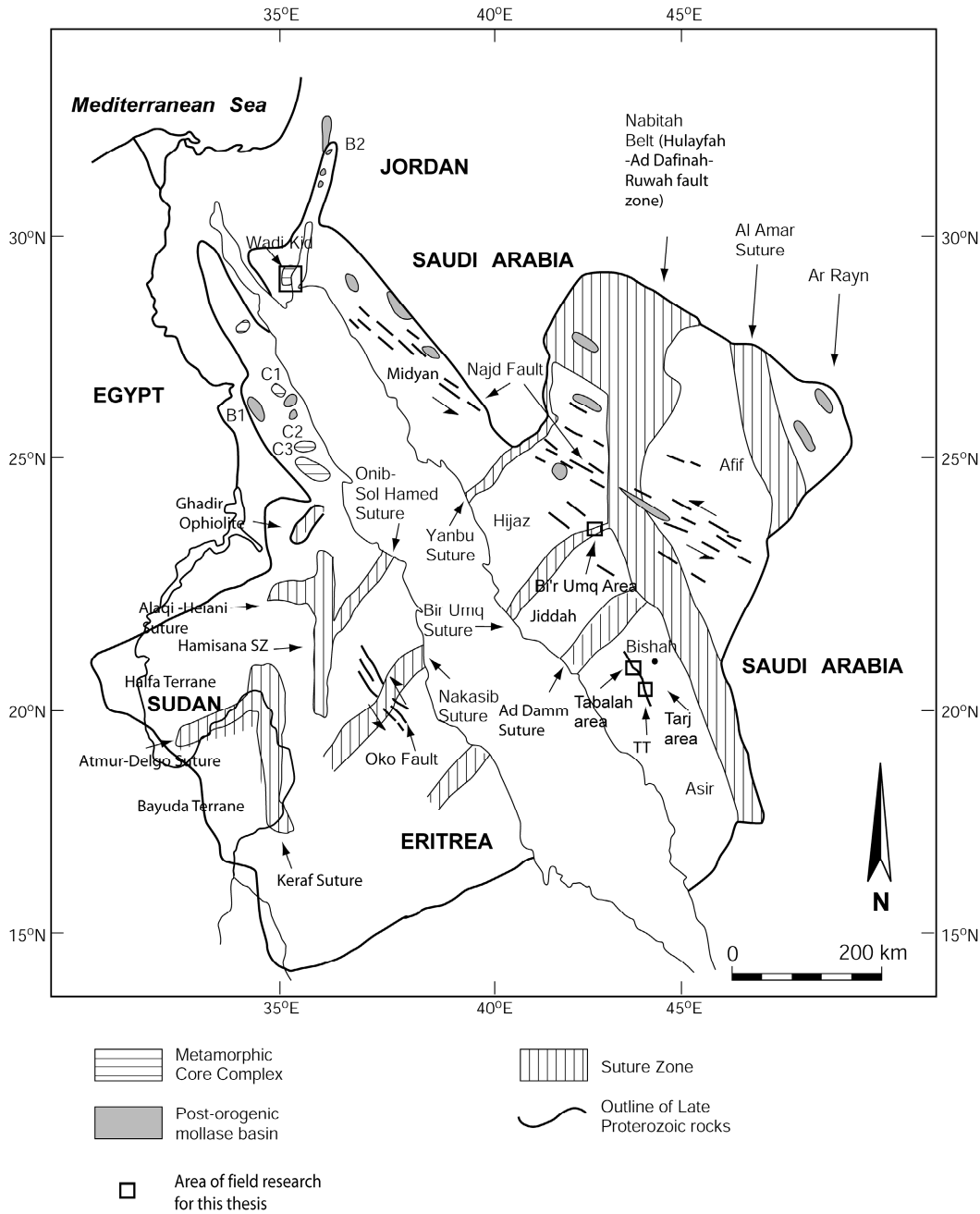


Figure 1-1 A map showing the main Neoproterozoic features in the Arabian Nubian Shield.

WK = Wadi Kid Complex, C1 = Meatiq Dome, C2 = El Sibai Dome, C3 = Wadi Ghadir Complex, C4 = Hafafit Dome, C5 = Taif area, C6 = Abha Complex, B1 = Basin with Hammamat sedimentary sequence, B2 = Basin with Saramuj Conglomerate. Compiled from maps by Vail (1985); Stoesser and Camp (1985); Brown et al., (1989), Greiling et al., (1994) and Abdelsalam and Stern (1996).

research is the fact that it contains a very high percentage of outcrop. This makes the area also suitable for the study of fundamental geological problems such as the interplay between compression and extension during the tectonic development of an orogen. This problem will be discussed in this thesis.

## **1.2 Aims**

The aim of this study is to improve the understanding of the Neoproterozoic geodynamic development of the Arabian-Nubian Shield. To achieve this, the different tectonic phases in the evolution of the Arabian-Nubian Shield and their relationships will be evaluated in order to define a tectonic model for the Neoproterozoic of the Arabian-Nubian Shield. Blasband et al. (2000) identified three main tectonic phase: 1) the oceanic phase; 2) the arc-accretion phase; 3) the late orogenic phase. The main structural trends in the Arabian-Nubian Shield are NE-SW, N-S to NNE-SSW, NW-SE and sub-horizontal structures that are associated with the late orogenic phase (Blasband et al. 2000). Most of previous the studies in the Arabian-Nubian Shield focused on petrology and geochemistry data however detailed kinematic studies are rare. These studies are crucial for a full understanding of the tectonic development of the shield. Detailed field-based structural research, with limited geochemical and geochronological research, was undertaken in three key areas of the Arabian-Nubian Shield (Figure 1-1):

1. The Bi'r Umq Complex – a complex that contains an accreted ophiolitic sequence and is thought to represent an ophiolitic suture, a relict of the oceanic phase (Pallister et al., 1988). This area contains a large NE to ENE trending shear zone.
2. The Tabalah and Tarj area – an area that contains remnants of an island-arc and major NNW ductile shear zones (Greenwood et al., 1986).
3. The Wadi Kid Complex – a complex that contains one of the “gneissic domes” of the Arabian Nubian Shield (Habib et al., 1985).

Geochemical and geochronological research was performed to allow correlation with other studies in the Arabian-Nubian Shield. The integration of data from the studied areas forms the basis for the construction of a tectonic model for the Arabian-Nubian Shield.

## **1.3 Outline of thesis**

Chapter 2 contains a review of published data of the Arabian-Nubian Shield and the ideas on its tectonic development. In chapter 3, a detailed structural study of the Bi'r Umq Complex in Saudi Arabia is presented. Chapter 4 describes a structural study of the Tabalah and Tarj areas Saudi Arabia. Geochemical and geochronological data, in addition to the structural data, are used to define a tectonic model for this area. Chapter 5 presents the structural data for the Wadi Kid Complex, Egypt. This chapter was published as Blasband et al. (1997). In chapter 6, the data presented in the chapters 3-5 are integrated together with published data from key-areas in the Arabian-Nubian Shield, to form the basis for a new geodynamic model for the Neoproterozoic of the Arabian-Nubian Shield. Chapter 6 also includes the conclusions of this thesis and recommendations for further research. Appendix 1 contains structural, geochemical and geochronological data from research that was performed after the publication chapter 5 as Blasband et al. (1997). Appendix 2 presents a detailed metamorphic study of the Wadi Kid Complex by Brooijmans et al. (2003) of which I was co-author. The results of this metamorphic study add information regarding the evolution of the Wadi Kid Complex.

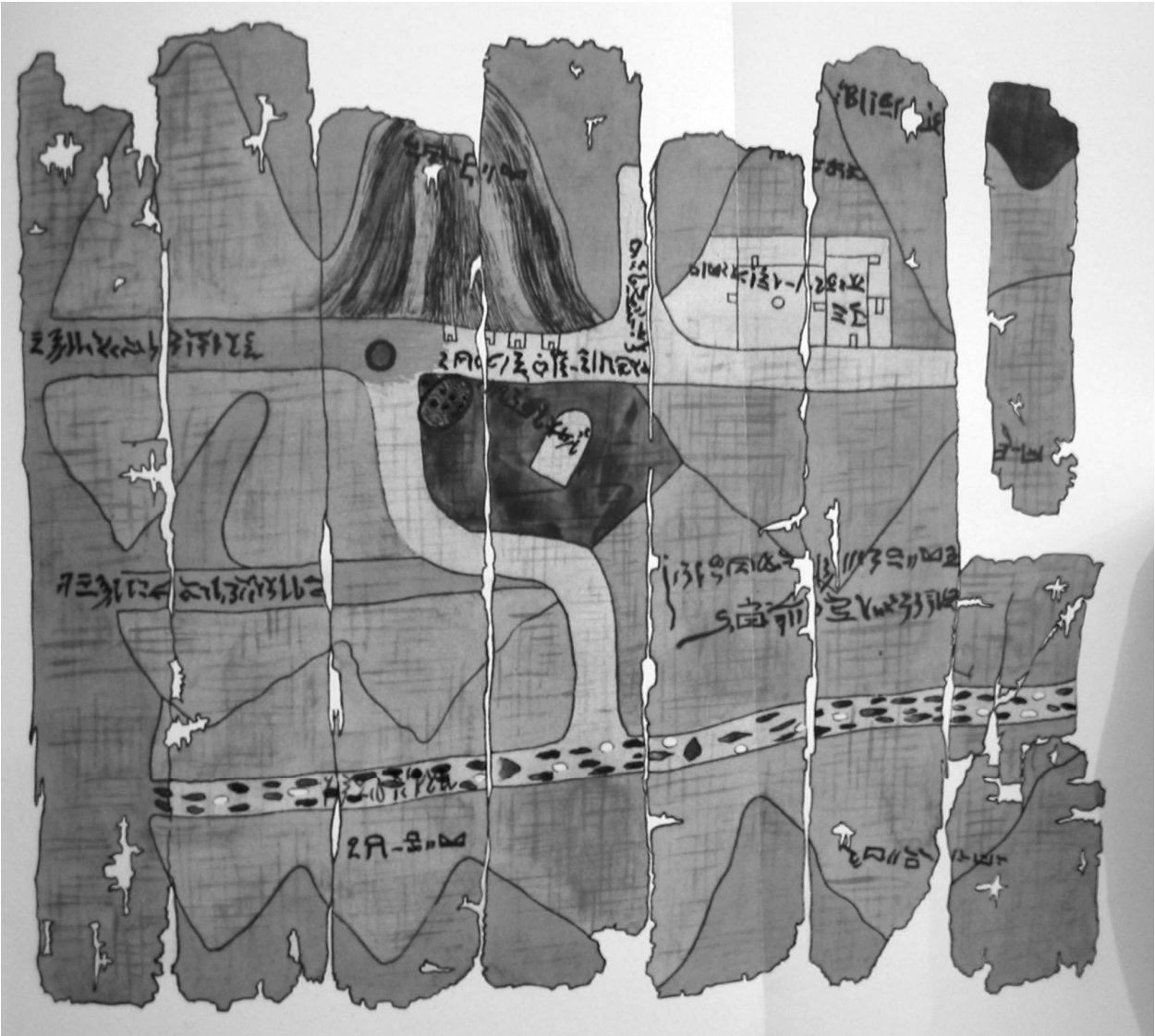


Figure 1-2 A photo of the oldest geological map in the world: the Wadi Hammamat map that was prepared at ~1150 B.C.



## **Geology of the Arabian Nubian Shield – An overview**

### **2.1 Introduction**

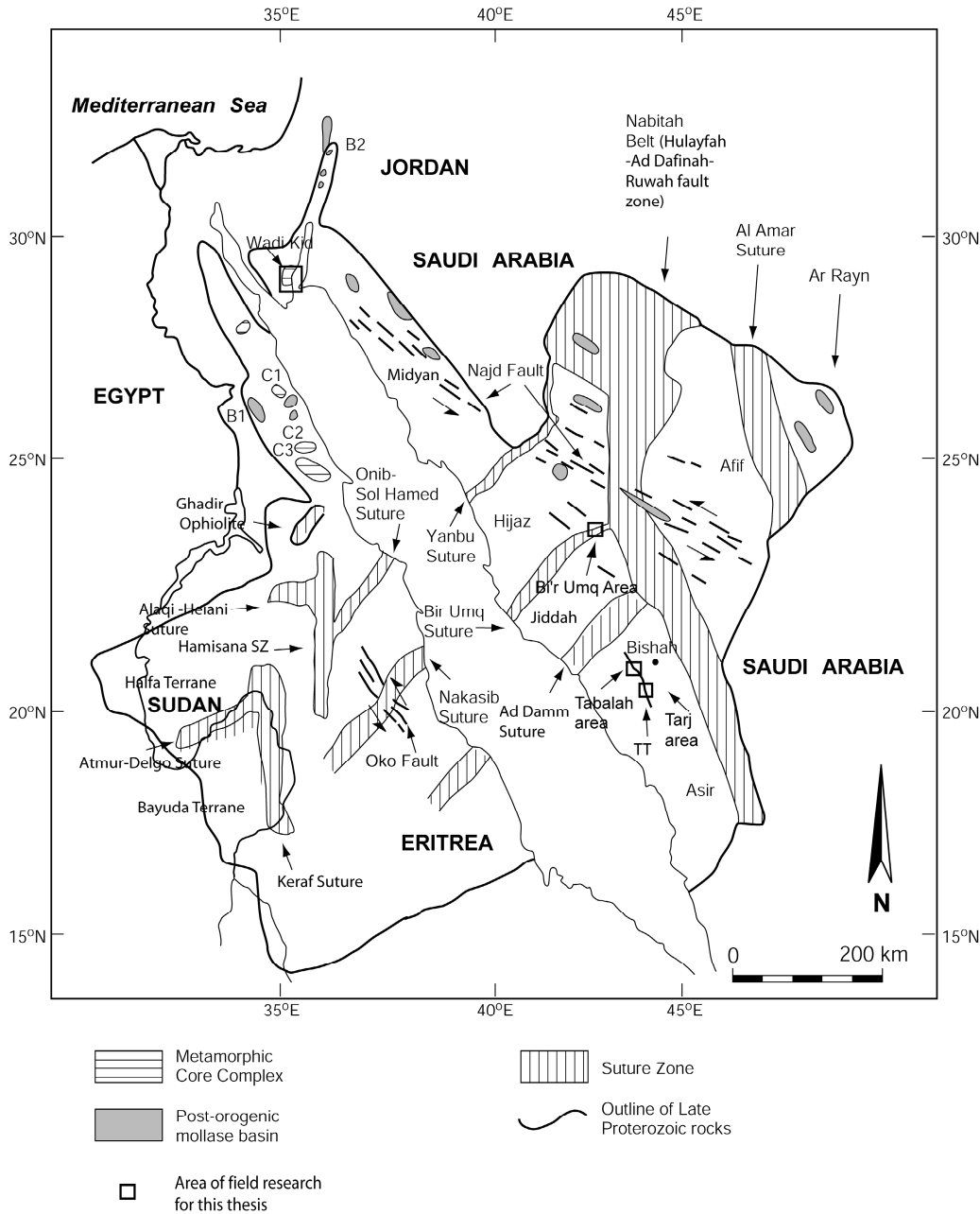
This chapter aims to provide an overview of the regional geology of the Arabian Nubian Shield (ANS) as published in the literature. The ANS extends from Jordan and southern Israel in the north to Eritrea and Ethiopia in the south and from Egypt in the west to Saudi Arabia and Oman in the east (Figure 2-1). The ANS consists of gneisses, granitoids, various (meta)volcanic and (meta)sedimentary rocks. Many authors interpret the early evolution of the ANS as the accretion of island arcs and of oceanic terranes (e.g. Vail 1985; Stoeser and Camp 1985; Harris et al., 1990; Samson and Patchet 1991; Abdelsalam and Stern 1996; Johnson and Kattan, 2001). The Afif and Ar Rayn Terranes in Saudi Arabia, both with a continental signature have also been included in the Arabian-Nubian Shield (Stoeser and Camp, 1985; Abdelsalam and Stern, 1996). Occasionally attention has been given to features that are generally associated with extension, such as dykes and sedimentary basins (e.g. Schürmann, 1966; Grothaus et al., 1979; Stern et al., 1984; Hussein 1989; Rice et al., 1991; Greiling et al., 1994; Blasband et al., 2000).

### **2.2 Relicts of oceanic crust**

The ANS contains many remnants of oceanic crust, in the form of ophiolites. Typical ophiolite sequences are found in the Eastern Desert, Egypt, in Sudan and in western Saudi Arabia (Table 2-1). Locally, complete ophiolitic sequences can be observed including peridotites, gabbros, sheeted dykes, pillow lavas and sedimentary rocks that reflect a deep-sea environment (Table 2-1). In many cases, the ophiolites have been dismembered and are now found in tectonic mélanges. The ophiolites were dated at approximately 870-740 Ma (Table 2-1; Stern et al., 2004 and Johnson et al., 2004). Geochemistry of a number of mafic schistose units throughout the ANS indicates a MORB provenance (Bentor 1985; El Gaby et al., 1984; El Din et al., 1991; Rashwan 1991). Some interpret the ophiolites to have been formed in back-arc basins and others believe that they were formed at mid oceanic spreading ridges (Bentor 1985; El Gaby et al., 1984; El Din et al., 1991; Rashwan 1991; Pallister et al., 1988). The ophiolites are thought to have been formed in the Mozambique Ocean that was formed upon rifting of Rodinia (Abdelsalam and Stern, 1996; Stern, 1994).

### **2.3 Island-arc remnants**

Typical island-arc related rocks are found throughout the ANS (Table 2-2). Tonalites, gabbros, basalts, andesites and metavolcanics with a calc-alkaline island-arc geochemistry are common in the Eastern Desert and the Sinai, Egypt (Bentor 1985; El Gaby et al., 1984; El Din et al., 1991; Rashwan, 1991). Gabbro-diorite suites are typically observed in plutonic complexes in



**Figure 2-1** A map showing the main Neoproterozoic features in the Arabian Nubian Shield. WK = Wadi Kid Complex, C1 = Meatiq Dome, C2 = El Sibai Dome, C3 = Wadi Ghadir Complex, C4 = Hafafit Dome, C5 = Taif area, C6 = Abha Complex, B1 = Basin with Hammamat sedimentary sequence, B2 = Basin with Saramuj Conglomerate. Compiled from maps by Vail (1985); Stoesser and Camp (1985); Brown et al., (1989) , Greiling et al., (1994) and Abdelsalam and Stern (1996).

ancient island-arcs as the Umm Naggat Complex in the Eastern Desert of Egypt (Mohamed and Hassanen, 1996). Many amphibolites throughout the Eastern Desert, Egypt have island-arc protoliths (Bentor 1985; El Din 1993). The formation of the island-arc rocks has been dated at ca. 900-700 Ma (Table 2-2).

The oldest island-arc remnants in Saudi Arabia (900-850 Ma) consist of tholeiitic andesites (Jackson 1986; Brown et al., 1989) and are thought to represent young immature island arcs (Jackson 1986). Thickening and melting of the immature tholeiitic crust caused the

formation of more mature island arcs with rocks of calc-alkaline character. Low- to high K tonalites, trondhjemites and andesites were formed during this phase and have been dated at 825-730 Ma (Schmidt et al., 1980; Jackson 1986; Brown et al., 1989).

Many of the island-arc related rocks are also thought to have been formed in the Mozambique Ocean, as the ophiolites (Abdelsalam and Stern 1996).

#### **2.4 Features related to arc-accretion**

A number of deformed linear belts of ophiolitic rocks have been observed throughout the ANS (Table 2-3) and these were interpreted as sutures (e.g. Ries et al., 1983; Vail 1985; Abdelsalam and Stern 1996). The NE-SW trending Yanbu and Bi'r Umq Sutures represent examples of the ophiolitic linear belts in the Neoproterozoic shield of Saudi Arabia (Figure 2-1). These belts separate little deformed domains that are distinguished from each other on the basis of different petrology, geochemistry and ages. This led several authors to interpret the Asir, Midyan, Afif, Ar Rayn and Hijaz Domains (Figure 2-1) as accreted terranes and helped to identify the linear belts as ophiolitic sutures (Vail 1985; Stoeser 1986; Johnson et al., 1987). A number of sutures display significant strike-slip overprint after the initial compressional phase (Quick 1991; Abdelsalam and Stern 1996; Johnson and Kattan 2001). Little reliable geochronological constrains are available for these NE-SW sutures, however interpretations of intrusives relations led Johnson et al. (2002) to date the suturing on the Bi'r Umq Suture at ca. 780-760 Ma. The deformation along the Yanbu Suture was estimated at 740-700 Ma (Johnson, 1999; Stoeser and Camp, 1985).

The two most easterly outcropping terranes in the ANS, the Ar Rayn and the Afif Terranes, have a continental signature as shown by their geochemical characteristics (Al-Salah and Boyle, 2001). The ophiolites of the Al-Amar suture, that separate these two terranes, is thought to have originated in a back-arc basin that was formed as a result of back-arc extension above the subduction zone (Al-Salah and Boyle, 2001). The formation of the back-arc took place at ca. 700 Ma and the closure of the back-arc, which is represented by the Al Amar Suture, took place at ca. 680 Ma (Al-Salah and Boyle, 2001).

The Nabitah Belt (referred to as Hulayfah-Ad Dafinah-Ruwah fault zone by Johnson and Kattan, 2001) in Saudi Arabia is the largest and most complicated feature that was formed during the arc-accretion phase in the ANS (Johnson and Kattan, 2001; Quick, 1991; Stoeser and Camp, 1985). It is some 1000 km long, up to 100 km wide and trends N-S. It forms the contact between the continental Afif Terrane and the juvenile Hijaz, Jiddah and Asir Terranes. Therefore, the Nabitah Belt also may represent the continental margin between the continental and the oceanic parts of the eastern ANS. The Nabitah Belt consists of ophiolites and sheared ophiolites in the form of N-S trending and steeply dipping mylonites and phyllonites (Quick 1991; Johnson and Kattan, 2001). These main structures were formed during a phase of left-lateral transpression from ca. 680 Ma (Quick 1991; Johnson and Kattan 2001). The closure of the oceanic basin between juvenile terranes and the Afif Terrane was completed by 630 Ma (Johnson and Kattan, 2001). The Siham Group in the Afif Terrane contains low-grade mixed sedimentary and volcanic sequences that were deposited on the high grade rocks which formed

Table 2-1 A review of lithologies and ages of rocks that are regarded as remnants of oceanic crust.

Oceanic crust (ophiolitic sequences)		
Area	Lithology	Age (Ma) Reference
Wadi Ghadir, Egypt	Serpentinities, layered gabbros, sheeted dykes, pillow lavas, black shales.	746±19 (Pb-Pb) 1985; El Akhal, 1993; Kroner
Qift-Quseir, Egypt	The Eastern Desert Ophiolitic Melange Group/Abu Ziran Supergroup: Dunites, peridotites, layered gabbros, sheeted dykes, pillow lavas and deep sea sediments (red pelites).	ca. 800 1985; El Gaby et al., 1984
Onib and Gerf, Sudan	Ultramafic cumulates, interlayered gabbros, sheeted dykes and pillow basalt.	ca. 840-740, e.g. 808±14 (Pb-Pb) 741±21 (Pb-Pb) Stern et al., 1990; Kroner et al., 1987; Zimmer et al., 1995
Halaban Ophiolite, Al Amar Suture,	Ultramafics, gabbros, cherts. Gabbros indicate that ophiolites were formed in back-arc basin	Ca. 700 Al-Saleh et al., 1998
Ophiolites throughout Saudi Arabia	Peridotites, gabbros, sheeted dykes, pillow lavas, cherts, pelagic metasediments and marble.	882±12 (U-Pb) to 743±24 (Sm-Nd) Brown et al., 1989; Kemp et al., 1980; Claesson et al., 1984; Pallister et al., 1988

the continental basement (Agar, 1985). Agar (1985) found these sedimentary sequences to be similar to those that were formed along the continental margins of western North and South America. This is confirmed by geochemical analyses of volcanic rocks of the Siham Group (Agar, 1985). Consequently Agar (1985) interpreted the Siham Group to have formed at the continental margin west of the Afif Terrane. The Nabitah Belt formed the relict of this continental margin (Agar, 1985).

Ophiolitic sutures have been observed in Sudan and Egypt (Table 2-3; Figure 2-1). The NE-SW trending Nakasib and Onib-Sol Hamed Sutures in Sudan are continuations of the Yanbu and Bi'r Umq sutures in Saudi Arabia (see Figure 2-1). These structures are interpreted to separate island-arcs terranes (Abdelsalam and Stern 1996). The Nakasib Suture displays relicts of an E-W compressional regime which represents the suturing phase. Strike-slip movement overprints the earlier structures and represents the later stages of arc-accretion (Abdelsalam and Stern 1996). The N-S trending Hamisana shear zone also contains ophiolitic remnants (Abdelsalam and Stern 1996). It recorded dextral strike-slip movement at 640-600 Ma and displaced Onib-Sol Hamid Suture (Abdelsalam et al., 2003). The N-S trending Keraf Suture in Sudan separates the continental Bayuda Terrane and the juvenile Gebeit Terrane and may thus be a relict of an active continental margin (Abdelsalam and Stern, 1996; Kuster and Liegeois, 2003). Structures in this terrane and the Keraf and Atmur-Delgo Sutures display evidence for closure of the ocean that is represented by the ophiolitic rocks of these sutures at ca. 700 Ma (Abdelsalam, 2003). N-S trending supra-subduction shear zones in Eritrea, which were related to arc-accretion, display HP metamorphism (Beyth et al., 2003; De Souza Filho and Drury, 1998). The collisional event that caused the HP-metamorphism ended before 650 Ma (De Souza Filho and Drury, 1998). Throughout the ANS, the N-S trending sutures postdate the NE-SW trending ophiolitic sutures.

Large NW-SE trending strike slip zones, such as the Najd Shear Zone in Saudi Arabia and the Oko Shear Zone in Sudan, represent another important structural feature in the ANS (e.g. Fleck et al., 1980; Stern 1985; Dixon et al., 1987). They cross-cut the NE-SW and N-S trending structures in the ANS (Stern 1985; Dixon et al., 1987). The Najd shear zone, the largest of the NW-SE strike-slip zones, started its activity around 680 Ma when it was formed during arc-accretion and collision (Stern, 1985; Johnson and Kattan, 1999). Its activity continued until 600 Ma or even later (Abdelsalam and Stern, 1996; Johnson and Kattan, 1999; Shalaby et al., 2005); however, no conclusive data are available for the age of its latest activity. NW-SE trending strike-slip faults are also observed next to the “gneissic domes” (Bregar et al., 2002; Fritz et al., 1996), which will be discussed late in this chapter.

I-type calc-alkaline magmas, which form, among others, granodiorites, tonalites and andesites, are igneous relicts of subduction at continental margins and of arc-accretion (Wilson, 1989). Also in the ANS, these rock-types were often associated with arc-accretion (Brown et al., 1989). For example, the tonalites and granodiorites from the El-Bula area in Central Eastern Desert in Egypt display geochemical characteristics of I-type intrusives that were formed at a continental margin (El-Shazly and El-Sayad, 2000). In the ANS, the I-type granitoids were generally interpreted to result from melting of an amphibolitic crust (e.g. Hassanen et al., 1996; Jarrar et al., 2003; Kuster and Liegeois, 2001). The I-type granitoids the ANS were dated at

Table 2-2 A review of lithologies and ages of rocks that are regarded as island-arc remnants.

Island-arc remnants			
Area	Lithology	Age (Ma)	Reference
Wadi Hafafit, Egypt	Meta-andesites with an island-arc chemistry.	N/A	Rashwan, 1991
E. Desert, Egypt	Tonalites, trondhjemites, basalts, andesites. Volcanics with island-arc chemistry.	ca 900-700	Bentor, 1984; El Gaby et al., 1984; El Din, 1991; Rashwan, 1991
Umm Naggat, Egypt	Gabbro-diorite suite with island-arc geochemistry	N/A	Mohamed and Hassanen, 1996
Asif, Saudi Arabia	Basaltic to andesitic lavas and tuffs with calc alkaline to low K-chemistry.	ca. 900-800	Jackson and Ramsay, 1980
Throughout Saudi Arabia	Tholeiitic andesites and basalts, andesites, pillow basalts, tonalites and trondhjemites. Chert, marble, graywackes (no sedimentary structures), turbidites, claystone, siltstone (sediments were in part deposited in back-arcs), back-arc basins trend NE (perpendicular to principal direction of compression).	ca. 900-780, e.g. 912±76 (Rb-Sr) 785±96 (Rb-Sr)	Hadley and Schmidt, 1980; Brown et al., 1989; Schmidt et al., 1980; Johnson et al., 1987
El-Arardiya area, Eastern Desert, Bayuda Desert, Sudan	Gabbros and dolerites dykes display an island-arc geochemistry	NA	Abu El-Ela, 1999
Nakfa Volcanics, Northern Erutra	Amphibolite schists with tholeiitic island-arc geochemistry Basalts and Rhyolites, deformed at greenschist grade with island-arc geochemistry	806 (Sm-Nd, WR) 854±3 (U-Pb, SHRIMP)	Kuster and Liegeois, 2001 Teklay et al, 2002

Table 2-3 A review of lithologies, metamorphism, structural data and ages of rocks that contain remnants of the arc-accretion phase.

Arc-accretion remnants					
Area	Lithology	Metamorphis m	Structural data	Age (Ma)	Reference
Idsas, Yanbu and Bir Umq sutures, Saudi Arabia	NW-SE trending linear ophiolitic belts.	Greenschist to lower amphibolite- grade	Folds, foliations, lineations, thrusts.	Ca. 780 -700	Johnson, 1999; Johnson et al., 2002
Alaqi-Heiani suture, Egypt	Ophiolites	Greenschist- to amphibolite grade	Early N- and S-dipping nappes and thrusts formed during N-dipping subduction followed by NW-striking folding phase due to NE-SW compression and N-striking folding phase due to E-W compression (Hamisana trend)	N-S compression: 770-730 NE-SW to E-W compression:	Abdelsalam et al., 2003a
Nakasib, Sudan	Ophiolitic suture, folded ophiolitic nappes, diorite	N/A	E-NE trending suture zone: Early (ca. 750Ma) SE-verging tight folds, overprinted by NE-trending upright folds (ca 700Ma),	ca. 840-760 arc- arc ca. 760-700 arc- continent	Abdelalam, 1994; Abdelsalam and Stern, 1996; Schandemeier et
Onib-Sol Hamed, Sudan	Ophiolitic suture. Granodiorite with I-type geochemistry	Greenschist to amphibolite-grade	Suture zone: Early S-to SE verging ophiolitic nappes, late E-NE-trending	ca. 750-720	Stern et al., 1990; Abdelsalam and

Continuation Table 2-3 A review of lithologies, metamorphism, structural data and ages of rocks that contain remnants of the arc-accretion phase.

Location	Lithology	Metamorphism	Structural Data	Age	Reference
Throughout Saudi Arabia	Synorogenic diorites and granodiorites.	N/A	Syn-kinematic	ca. 763-660	Stoeser, 1986; Brown et al., 1989
Nabitah Belt/ Hufayfah-Ad	N-S trending ophiolites and sheared ophiolites, phyllonites and mylonites	Non-metamorphosed to amphibolite	Open folds with NE-SW trending fold axes and subvertical axial planes, overprinted by N-S trending steeply dipping mylonites (Nabitah trend). Steeply NE-dipping foliation, lineation and folds. Sinistral shear indicators.	Quartz diorite: 710	Quick, 1991 Johnson and Kattian, 2001
Dafinah-Ruwah fault zone, Saudi Arabia	juxtaposes terranes with different petrological characteristics. Intruded by quartz diorites.			Sinistral strike – slip: 680-630	
Halaban ophiolite, Al Amar suture, Saudi Arabia	N-S trending linear ophiolitic belt.	Amphibolite-grade	Ophiolitic sutures	679±6 (Ar-Ar)	Al-Saleh et al., 1998; Al-Salah and Boyle, 2001
El-Bula area	Tonalites and granodiorites with an I-type geochemistry	N/A	N/A	NA	El-Shazy and El-Sayed, 2000
Dineibit/El-Quleib, South Eastern Desert, Egypt	Calc-alkaline granite with I-type geochemistry	Non-metamorphosed	Undeformed	NA	El-Sayed and El-Nisr, 1999
Gabal Igla Ahmar, Eastern Desert, Egypt	Deformed tonalites and granodiorites with an I-type geochemistry. Diorites and granodiorites with I-type geochemistry. Interpreted to have been formed through melting of amphibolitic crust	Amphibolite	North-west directed thrusting	680	Bregar et al., 2002; El Din, 1991; Hassanen et al., 1996



Continuation Table 2-3 A review of lithologies, metamorphism, structural data and ages of rocks that contain remnants of the arc-accretion phase.

Guseir-Marsa Alam, Egypt	Ophiolitic melanges.	Greenschist	Suture zone: mylonites interpreted as thrusts dipping NE, and folds.	N/A	Ries et al., 1983
Hamisana shear zone	Ophiolites	NA	Different folding phases. E-W shortening followed by dextral strike-slip movement	640-600	Abdelsalam and Stern, 1996; Abdelsalam et al., 2003a Jarrar et al., 2003
Aqaba, Jordan	Tonalites and granodiorites. Geochemistry indicates that they resulted from melting of an amphibolitic crust above a subduction zone	NA	NA	640	
Roded Area, Israel	Diorites with I-type geochemistry. Formed through melting of amphibolite crust	Non-metamorphosed	Undeformed	NA	Bogoch et al, 2002
Kerf Suture, Sudan	Ophiolitic suture, diorites, granodiorites and gneiss. Diorites and granodiorites intruded at active continental margin as indicated by geochemistry	Upper amphibolite	N-S striking thrusts. Main deformation-phase resulted from E-W shortening	730 for diorites and granodiorites	Abdelsalam and Stern, 1996 Kuster and Liegeois, 2001 Abdelsalam et al., 2003b
Bayuda Terrane	Gneiss and volcano-sedimentary sequences (interpreted as continental terrane). A-type granites	NA	Phase 1: S-verging thrusts; Phase 2: N-trending folds; Phase 3: N-S trending sinistral strike slip; Phase 4: W-dipping normal faults	Phase 1: 700 Phase 2: 659-650 Phase 3: 590-550 Phase 4: <550	
Nacfu and Ghedem Terranes, Eritrea	Meta-volcanics and meta-sediments.	Amphibolite (HP-HT)	Steep S1-foliation and F1-folds (D1)	650 Ma	Ghebreab, 1999; Beyth et al., 2003

approximately 760-650 Ma (e.g. Bregar et al., 2002; Jarrar et al., 2003; Kuster and Liegeois, 2003).

From the scarcely available geochronological data, it appears that deformation on the NE-SW trending ophiolitic belts took place at ca. 780-700 Ma (e.g. Abdelsalam and Stern, 1996; Johnson et al., 2002; Pallister et al., 1989). The deformation on the N-S trending faults took place at ca. 700-620 Ma (e.g. Abdelsalam and Stern, 1996; Quick, 1991; De Souza Filho and Drury, 1998).

## 2.5 Gneissic domes

A number of gneissic domes have been described in the Eastern Desert, Egypt (Table 2-4). The Meatiq, Hafifit, Gebel El Sibai and Wadi Kid areas (Figure 2-1) contain the most studied of these gneissic domes which show a broad similarity in structure. The gneissic domes have lower- and upper-crustal units. The lower-crustal units comprise deformed tonalites, diorites and granodiorites, and metasedimentary, metavolcanic and meta-ophiolitic schists. The schists have been generally metamorphosed at amphibolite-grade HT/LP conditions. The upper crustal unit consists of folded and thrustured island-arc volcanics, island-arc related sedimentary sequences and ophiolites. This unit displays low-grade metamorphism. Many of the gneissic domes are bordered at their NE- and SW-margins by NW-SE trending strike-slip faults (Bregar et al., 2002; Fritz et al., 1996).

The Meatiq Dome is one of the most studied gneissic domes in the ANS. It consists of a lower-crustal unit of gneiss and amphibolite-schists and an upper-crustal unit of ophiolitic mélanges, low-grade island-arc related rocks and other volcano-sedimentary rocks (Loizenbauer et al., 2001; Sturchio et al., 1983). The lower- and upper-crustal units are separated by a cataclasite (Habib et al., 1985). The foliation in the lower crustal rocks is mainly subhorizontal to moderately dipping (Loizenbauer et al., 2001; Sturchio et al., 1983). A NW-SE trending mineral lineation is developed on the foliation (Loizenbauer et al., 2001; Sturchio et al., 1983). Evidence for non-coaxial strain was observed in the schists in the form of S-C fabrics, asymmetric porphyroclasts and asymmetric boudins (Loizenbauer et al., 2001; Sturchio et al., 1983; El Din 1993). Consequently, the schists were interpreted as low-angle mylonitic shear zones that formed under lower-crustal conditions (Greiling et al., 1994; Fritz et al., 1996). HT/LP metamorphism took place during the final stages of formation when the Meatiq Dome received its domal structure (Loizenbauer et al., 2001). The low-angle shear zone of the Meatiq Dome was dated at 590 Ma (Fritz et al., 2002). Late anorogenic granites are associated with the doming of the complexes (Greiling et al., 1994). The lower-crustal mylonitic shear zones of the gneissic domes in the ANS were formed at approximately 620-580 Ma (Table 2-4).

## 2.6 Other late orogenic features

A number of geological features, namely dykes, sedimentary basins and alkaline granites, have been formed at the latest stages of the Neoproterozoic development of the ANS (Table 2-5 and

Table 2-6). These features were formed simultaneously to, or slightly after the low-angle shear zones in the “gneissic domes” (Tables 2-4, 2-5 and Table 2-6).

The Hammamat Group in the Eastern Desert, Egypt contains one of the best preserved clastic sedimentary sequences found in this part of the ANS. Grothaus et al., (1979) have described this sequence in detail. The sedimentary rocks of the Hammamat Gp. unconformably overlie metamorphic rocks and consist of thick sequences of unsorted to well-sorted conglomerates, sandstones and siltstones (Grothaus et al., 1979). The sequence contains several types of sedimentary structures such as debris flows, alluvial fans and channel fills (Grothaus et al., 1979). Grothaus et al., 1979 believed syn-sedimentary normal faulting to be necessary to explain the sedimentary sequence of the Hammamat Gp. Other Neoproterozoic sedimentary basins in the Eastern Desert were interpreted as molasse-type basins (Fritz et al., 1996). They are bordered by major NE-SW striking normal faults and display internal syn-sedimentary normal faulting (Fritz et al., 1996).

The Saramuj Conglomerate Gp., Wadi Araba, SW Jordan, dated at 600-550 Ma, is similar to the Hammamat Group (Jarrar et al., 1991). It consists of a post-orogenic molasse-type basin with poorly-sorted conglomerates and sandstones. Sedimentary structures include alluvial fans, channel fills and debris flows. The Saramuj Conglomerate Gp. was deposited in a fan-type depositional system in grabens that were formed during NW-SE extension (Jarrar et al., 1991). NE-SW striking dykes cross-cut this sequence.

Throughout Saudi Arabia, Neoproterozoic post-orogenic molasse sequences, deposited in environments similar to the Hammamat and Saramuj Conglomerate Groups, overlie basement rocks (e.g. Jackson and Ramsay 1980; Hadley and Schmidt 1980; Brown et al., 1989). Evaporitic and clastic basins in Oman, formed at 620-580 Ma, were bordered by NE-SW trending faults Husseini (1989).

Widespread intrusions of mostly undeformed alkaline granites into the lower-crustal sequences in the ANS were dated at ~620-530 Ma (e.g. Schmidt et al., 1980; Habib et al., 1985; El Din et al., 1991; Greiling et al., 1994; Harms and Kuster, 1998). On the basis of geochemical studies, these granitoids have been interpreted as A-type granites that were derived from mantle magmas (Beyth et al., 1994; Kessel et al., 1998; Kuster and Harms, 1998; Moghazi, 2003).

Reconnaissance maps by Schürmann (1966) and Eyal and Eyal (1987) show the presence of NE-SW striking Precambrian dykes in large parts of the Eastern Desert, Egypt. The bimodal mafic and felsic dykes in the Eastern Desert were dated at ca. 620-550 Ma (Stern et al., 1984). In the Midyan region of northwestern Saudi Arabia and the Uyaijah area of central Saudi Arabia, mafic to intermediate and felsic dykes striking NE-SW were described (Dodge 1979; Clark 1985). Jarrar et al., (2003) and Kessel et al., (1998) showed that these late mafic and felsic dykes were formed from mantle-derived magmas, similar to the A-type granites.

Throughout the ANS, undeformed basalts and rhyolites overlie the lower- and upper crustal metamorphic sequences. The Dohkan Volcanics, in the central part of the Eastern Desert of Egypt, consist of basalts and rhyolites (Moghazi, 2003). Detailed geochemical studies show that the volcanics originate from mantle derived magmas that were extruded from a thinned and extending crust (Moghazi, 2003).

Table 2-4 A review of lithologies, metamorphism, structural data and ages of rocks associated with the “gneissic domes”.

“Gneissic domes”					
Area	Lithology	Metamorphism	Structural data	Age (Ma)	Reference
Meatiq,	Supracrustal: folded ophiolites, cataclasites;	greenschist to upper-	Subhorizontal to moderately dipping	596±0.5 and	Sturchio et al., 1983; El
Egypt	Infracrustal: amphibolite schists, tonalitic and dioritic gneisses, late A-type granites.	amphibolite-grade (LP) and relicts of HP.	foliation interpreted as thick mylonite, NW-SE stretching lineation, cataclasites.	588±0.3 (Ar-Ar)	Gaby et al., 1984; Greiling et al., 1994; Fritz et al., 1996; Loizenbauer et al., 2001; Fritz et al., 2002
Wadi Hafafit,	Supracrustal: ophiolites, cataclasites;	High grade (HP)	NE-SW folds at upper crustal levels,	585	Greiling et al., 1984;
Egypt	Infracrustal: metavolcanic and metasedimentary schists, gneisses, late A-type granites.	overprinted by amphibolite-grade (LP).	large mylonitic shear zones with NW-SE stretching lineation, cataclasites.		Greiling et al., 1994; Fritz et al., 2002
Gebel El Sibai,	Gneisses, migmatites overlain by amphibolite schists, overlain by low grade metavolcanics and metasediments.	Upper amphibolite-grade	Sub-horizontal foliation with NW-SE trending lineation and shear indicators. This structure was interpreted as a low-angle shear zone by Greiling et al., (1994).	615	El Din, 1991; Bregar et al., 2002; ; Fritz et al., 2002
Egypt			Cataclasites.		

Continuation Table 2-4 A review of lithologies, metamorphism, structural data and ages of rocks associated with the “gneissic domes”.

Um Had area, Egypt	Core: Gneiss and schists; “Overthrusting units”: ophiolitic mélange, volcanics and clastic sediments	Core: M1 – upper amphibolite; M2 – greenschist; M3 – amphibolite;	Core: Sub-horizontal foliation and NW-SE sub-horizontal stretching lineation. “Overthrusting units”: Folding, SW- and NE-dipping thrusts. NW-SE striking sinistral strike-slip.	NA	Fowler and Osman, 2001
Nacfu and Ghedem Terranes, Eritrea	Meta-volcanics and meta-sediments	Upper-amphibolite	Sub-horizontal shear zones with flat-lying S2-foliation	640	Ghebreab, 1999
East Eritrea and northern Ethiopia	Deformed granodiorites and diorites, undeformed granites, (meta)volcanics, (meta)sediments, (cap-)carbonates In Eritrea; Gneiss and schist in Ethiopia	Greenschist-amphibolite	W-dipping low-angle ductile shear zones with top-to-W shear indicators, overprinted by low-angle cataclases	590-545	Beyth et al., 2003

## 2.7 Proposed models for the Neoproterozoic in the ANS

It is generally thought that the ophiolitic rocks and island-arc related rocks of the ANS, described in Table 2-1 and Table 2-2, were formed in the Mozambique Ocean which was formed upon the rifting of Rodinia (e.g. Abdelsalam and Stern, 1996; Rogers et al, 1995; Shackleton, 1996; Unrug, 1996). The rifting of Rodinia and the formation of the Mozambique Ocean started at ~900 Ma (e.g. Abdelsalam and Stern, 1996; Rogers et al, 1995; Shackleton, 1996; Unrug, 1996). The formation of oceanic crust continued until ca. 740 Ma. Meanwhile, intra-oceanic subduction in the Mozambique Ocean formed the island-arcs (e.g. Abdelsalam and Stern, 1996; Bentor, 1985; Brown et al., 1989; Greiling et al., 1994). The relicts of these island-arcs are found in the form of the juvenile terranes of the ANS, as the Asir, Jiddah and Hijaz Terranes in Saudi Arabia (e.g. Brown et al., 1989; Harris et al., 1990; Johnson et al., 1987; Stoesser and Camp, 1985). The island-arcs were formed at ~900-780 Ma (see Table 2-2).

The ophiolites, described above, are found in strongly deformed linear belts which trend NE-SW or N-S (see Figure 2-1 and Table 2-3). They mark the borders between the terranes (e.g. Abdelsalam and Stern, 1996; Johnson et al., 1987; Stoesser and Camp, 1985). They are thought to represent the zones of closure of the oceanic basins between the juvenile terranes and between the juvenile terranes and the continental terranes (e.g. Abdelsalam and Stern, 1996; Stoesser and Camp, 1985). The closure took place along subduction zones and so these ophiolitic sutures are thought to represent relicts of ancient subduction zones (Abdelsalam and Stern, 1996; Shackleton, 1996; Stoesser and Camp, 1985). Consequently arc-accretion is regarded as the process responsible for the assemblage of the different terranes in the ANS (Pallister et al., 1988; Harris et al., 1990; Samson and Patchet 1991). The accretion-phase was accompanied by the intrusion of I-type plutons (Brown et al., 1989; Kuster and Liegeois, 2001; Stoesser 1986). It took place at 780-630 Ma (see Figure 2-2 and Table 2-3). The earliest evidence for arc-accretion was found in the NE-SW trending Bi'r Umq Suture where suturing was dated at 780-760Ma (Johnson et al., 2002). The Nabitah Belt, the contact between the juvenile terranes in Saudi Arabia and the continental Afif Terrane, is believed to represent the active continental margin of East Gondwanaland (Abdelsalam and Stern, 1996; Al-Salah and Boyle, 2001). The activity along the Nabitah Belt is thought to have started at 700 Ma however this date is not regarded as robust (Johnson and Kattan, 2001). The Keraf Suture is part of the continental margin at the southwestern side of the ANS and should thus be the continental margin of Western Gondwanaland (Abdelsalam et al., 2003b; Abdelsalam and Stern, 1996; Unrug, 1996). Calc-alkaline magmatism in the Saharan craton, which contains the relicts of western Gondwanaland, indicated that subduction started at 730 Ma (Bailo et al., 2003). From the limited available geochronological data on arc-accretion, it appears that the NE-SW trending sutures pre-date the N-S trending sutures.

Some authors regard the NW-SE trending Najd sinistral strike-slip shear zone as the major structure in the later development of the ANS (e.g. Stern, 1985; Sultan et al., 1988) however recent research indicates that the faults that represent the Najd shear zone may not form the major system as initially thought (Johnson and Kattan, 1999; Shalaby et al., 2005). Abdelsalam and Stern (1996) and Stern (1994) believe that the Najd shear zone formed due to

Table 2-5 A review of geological lithologies, structural data and ages of rocks associated with “late orogenic” sedimentary basins.

“late orogenic” sedimentary basins			
Area	Feature/Lithology	Structural data	Age (Ma) Reference
Hammamat	Hammamat Gr.; Basin and Range-type	Syn-sedimentary normal faults	585±15 (Rb-Sr) Grothaus et al., 1979; Willis et al., 1988
Egypt	molasse: sandstones, conglomerates with debris flows, channel fills	forming NE-SW trending basins.	
Wadi Igla,	Post-orogenic molasse: basal	NE-SW striking normal faults.	ca. 595-575 Greiling et al., 1994
Wadi Hafafit,	conglomerates overlain by volcanics and pyroclastics		
Wadi Araba	Saramuj Conglomerate; post-orogenic	NE-SW striking normal faults	ca. 600-550 Jarrar et al., 1991; Jarrar et al., 1992
Jordan	molasse: sandstones, conglomerates with debris flows, channel fills	NE-SW trending dykes	Dyke at 545±13 (K-Ar)
	Bimodal dykes		
Saudi Arabia	Sedimentary basins; Fatima, Murdama, Jibalah and Shammar Groups: conglomerates, sandstones, deposited in shallow water, high-energy environments.	N/A	ca. 620-540 Jackson and Ramsay, 1980; Hadley and Schmidt, 1980; Brown et al., 1989; Kemp, 1996; Johnson, 2003
Oman	Salt basins	Basins bounded by NE-SW striking normal faults.	ca. 620-540 Husseini, 1989

Table 2-6 A review of lithologies, structural data and ages of "late orogenic" igneous rocks. .

<b>"late orogenic" igneous rocks</b>				
<b>Area</b>	<b>Feature/Lithology</b>	<b>Structural data</b>	<b>Age (Ma)</b>	<b>Reference</b>
E. Desert Egypt	Dykes: bimodal, mafic and felsic	Dykes trend NE-SW	ca. 620-550	Schürmann, 1986; Stern and Gottfried, 1986 Greiling et al., 1994
Midyan Saudi Arabia	Dykes: bimodal, mafic and felsic; silicic volcanics and pyroclasts.	Dykes trend NE-SW, volcanics and pyroclasts in fault basins.	ca. 625-575	Clark, 1985; Agar, 1986
Wadi Araba	Dykes: bimodal, mafic and felsic	Dykes trend NE-SW	550±13 (K-Ar)	Jarrar et al., 1991
Dokhan Volcanics Sudan, Eritrea	Basalts and rhyolites Potassic and metaluminous granites that are interpreted as A-type granites	Undeformed	N/A	Moghazi, 2003
Araba, Southeastern	A-type granites, mafic and felsic volcanics. Geochemistry indicates that derived from	Undeformed	580-470 600-540	Küster and Harms, 1998 Jarrar et al., 2003



Continuation Table 2-6 A review of lithologies, structural data and ages of “late orogenic” igneous rocks.

Shalatin- Halaib, south Eastern Desert, Egypt Eilat, Southern Israel Entire Shield	Granites with A-type geochemistry	Undeformed	NA	El-Nisr et al, 2001
	Granites with A-type geochemistry. Mafic and felsic dykes. All were derived from a mantle derived magma	Undeformed	NA	Beyth et al., 1994; Kessel et al., 1998
	Alkaline granites: A-type granite geochemistry, intruded in thinned and extending crust.	None to slightly lineated.	ca. 600-540 Granite at 594±4 (Rb-Sr) and granite at 544 (Rb-Sr)	Stern and Hedge 1985; Hussein, 1989; Beyth et al., 1994; Greiling et al., 1994; Brown et al., 1989; Hassanen, 1997

continuing collision of East- and West-Gondwanaland after the closure of the oceanic basins and after the end of the actual arc-accretion.

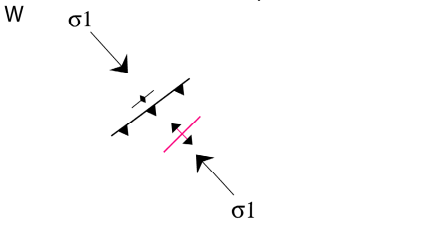
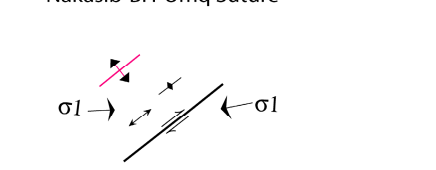
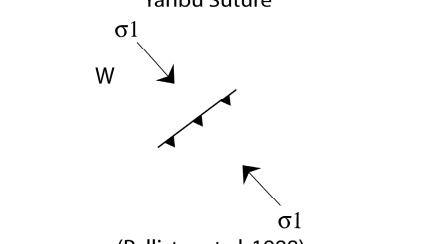
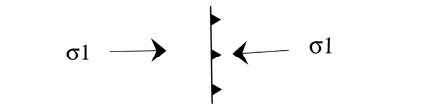
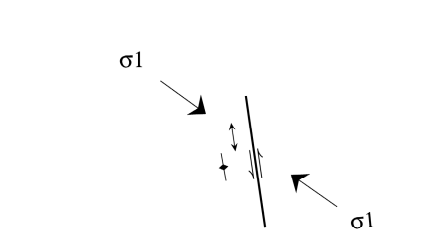
The formation of the gneissic domes postdates the arc-accretion and is the latest Neoproterozoic features that was formed in the ANS (Blasband et al., 2000; Greiling et al., 1994). Most authors interpret the “gneissic domes” as core complexes (e.g. Blasband et al., 2000; Bregar et al., 2002; Greiling et al., 1994; Loizenbauer et al., 2001). Disagreement exists, however, about their mode of formation. Some believe that the low-angle shear zones of the core complexes are thrusts (Fowler and Osman, 2001; Habib et al., 1985). Others interpret the core complexes in the ANS as expressions of local extension in the NW-SE strike-slip shear zones as the Najd shear zone (e.g. Bregar et al., 2002; Fritz et al., 2002; Loizenbauer et al., 2001). For this model, the NW-SE strike-slip shear zones were thought to have been formed during the later stages of collision in the ANS (e.g. Bregar et al., 2002; Fritz et al., 2002; Loizenbauer et al., 2001). Recently, a number of authors have interpreted the core complexes as structures that were formed during regional extension throughout the ANS at the latest stages of its development (Blasband et al., 2000; Greiling et al., 1994). The core complexes were formed when the collision had ceased completely (Beyth et al., 2003; Blasband et al., 2000). Consequently, these core complexes were thought to have been formed in similar way as the Cordilleran core complexes in western North America (Blasband et al., 2000). Thick low-angle high-grade shear zones in Eritrea and Ethiopia, similar to those in core complexes, were also related to regional extension during the latest stages of the development of the ANS (Beyth et al., 2003; Ghebreab, 1999). The “gneissic domes” or core complexes were formed at ca. 620-580 Ma (see Table 2-4).

Granitoid intrusions, dykes, and sedimentary basins represent other notable geological features that were formed simultaneously with the gneissic domes. Alkaline granites are found throughout the ANS. On the basis of their geochemistry, they are generally thought have been derived from mantle and to have intruded in an extending and thinned crust (e.g. Beyth et al., 1994; Jarrar et al., 2003; Kessel et al., 1998; Kuster and Harms, 1998).

Undeformed felsic and mafic dykes, and undeformed rhyolites and basalts, dated at ~620-550 Ma (see also Table 2-6), were also interpreted to have been formed in a thinned and extending crust (Jarrar et al., 2003; Kessel et al., 1998). These dykes trend generally NE-SW and this led Blasband et al., (2000) and Jarrar et al., (1992) to postulate that they were intruded during NW-SE extension.

Little to undeformed sedimentary basins were interpreted to have been formed at ca. 620-540 Ma (see Table 2-5). These basins contain many different types of clastic sequences. Salt and carbonates fill the Neoproterozoic basins in Oman (Husseini, 1989). Some sedimentary basins were formed during extension in a NW-SE extension (Jarrar et al., 1991; Grothaus et al., 1979; Husseini, 1989). Other “late orogenic” basins were interpreted as pull-apart basins that were related to the NW-SE strike-slip shear zones (Fritz et al., 1996; Johnson, 2003).

A number of authors state that compression and collision continued until the end of the Neoproterozoic in the ANS (e.g. Abdelsalam and Stern, 1996, Bregar et al., 2002; Shackleton, 1996; Stern, 1999). Alternatively, those who relate the “gneissic domes” and the other “late orogenic” geological features to extension, state that the transition from arc-accretion and

NE-SW trending structures	N-S trending structures	Age
<p>Nakasib-Bi'r Umq Suture</p>  <p>D1/D2 in Bi'r Umq-Nakasib Suture (Wipfler, 1996; Abdelsalam and Stern, 1993) D1 in Bi'r Umq Nakasib Suture (Johnson, 1998)</p>		<p>E</p> <p>&gt;780 Ma</p>
<p>Nakasib-Bi'r Umq Suture</p>  <p>D3 in Bi'r Umq Nakasib Suture (Wipfler, 1996; Abdelsalam and Stern, 1993) D2 Bi'r Umq Nakasib Suture (Johnson, 1998)</p>		<p>780-760Ma</p>
<p>Yanbu Suture</p>  <p>(Pallister et al, 1988)</p>		<p>740-700Ma</p>
	 <p>Quick, 1991</p>	<p>700 Ma</p>
	 <p>Quick, 1991 Johnson, 2001</p>	<p>680-630 Ma</p>

**Figure 2-2** Sketch table of major structures that are related to arc-accretion in the Arabian-Nubian Shield as described in literature.

Note: the ages in the right column are not according to a scale.

collision towards extension was caused by gravitational collapse (e.g. Abdelsalam et al., 2003b; Beyth et al., 2003; Blasband et al., 2000; Kessel et al., 1998; Moghazi, 2003).

## The Bi'r Umq Complex and Shear Zone: an ophiolitic suture in the Arabian-Nubian Shield

### Abstract

The Bi'r Umq Complex (BUC) is a Neoproterozoic ophiolite complex (ca. 830 Ma) at the northern margin of the Mahd Group in the central part of the Arabian part of the ANS. Locally, it defines the contact between the Jiddah and Hijaz Terranes. It has been folded and extensively sheared during three phases of deformation. The D1-deformation phase resulted in folding, development of foliation, the formation of steeply plunging mineral lineations, and shear indicators. D1 took place under ductile conditions during a phase of greenschist-facies metamorphism. D1 involved SE-vergent thrusting on the Bi'r Umq Shear Zone (BUSZ) at the southern margin of the BUC, and on the minor shear zones within the BUC. The D1-deformation phase was a result of NW-SE compression and was responsible for the emplacement of the Bi'r Umq ophiolite in the overriding plate. The second deformation phase, D2, was marked by dextral strike-slip with a minor transpressive component in the central zone of the WSW-ENE-trending BUSZ and resulted in the formation of sub-horizontally WSW-plunging stretching lineations that are marked by elongated clasts. D2 took place during WNW-ESE compression. The third phase, D3, involved shear reversal and resulted in sinistral strike-slip with a minor transtensional component on the BUSZ. This phase took place during NNE-SSW directed compression. The D1-D3 deformation phases in the Bi'r Umq Complex (BUC) occurred during obduction of the Bi'r Umq ophiolite and ended at ca. 760 Ma. The structures and structural history in the region are of the type expected to be associated with the closure of an oceanic basin by subduction and are consistent with the history of arc-accretion in the Arabian shield established elsewhere. The changes of the sense of movement on the main structures in the BUC can be attributed to a change in plate motion of the subduction plate, as observed during Mesozoic arc-accretion in western North America.

### 3.1 Introduction

The formation of the Neoproterozoic rocks of the Arabian part of the ANS is thought to be a result of arc-accretion of juvenile crust that was formed in island-arcs and oceanic basins (see Chapter 2). The oldest juvenile rocks of the Shield were formed at about 900 Ma and accretion- and subduction-processes continued to approximately 650 Ma (Blasband et al, 2000). The concept of terrane-accretion for the Arabian Shield was based on lithological and geochemical observations (Johnson et al, 1987). However, few structural/kinematic studies, which have been so important for the understanding of the geotectonic evolution of other areas where arc-accretion was established, were performed in the Arabian Shield. It is only in recent years, that

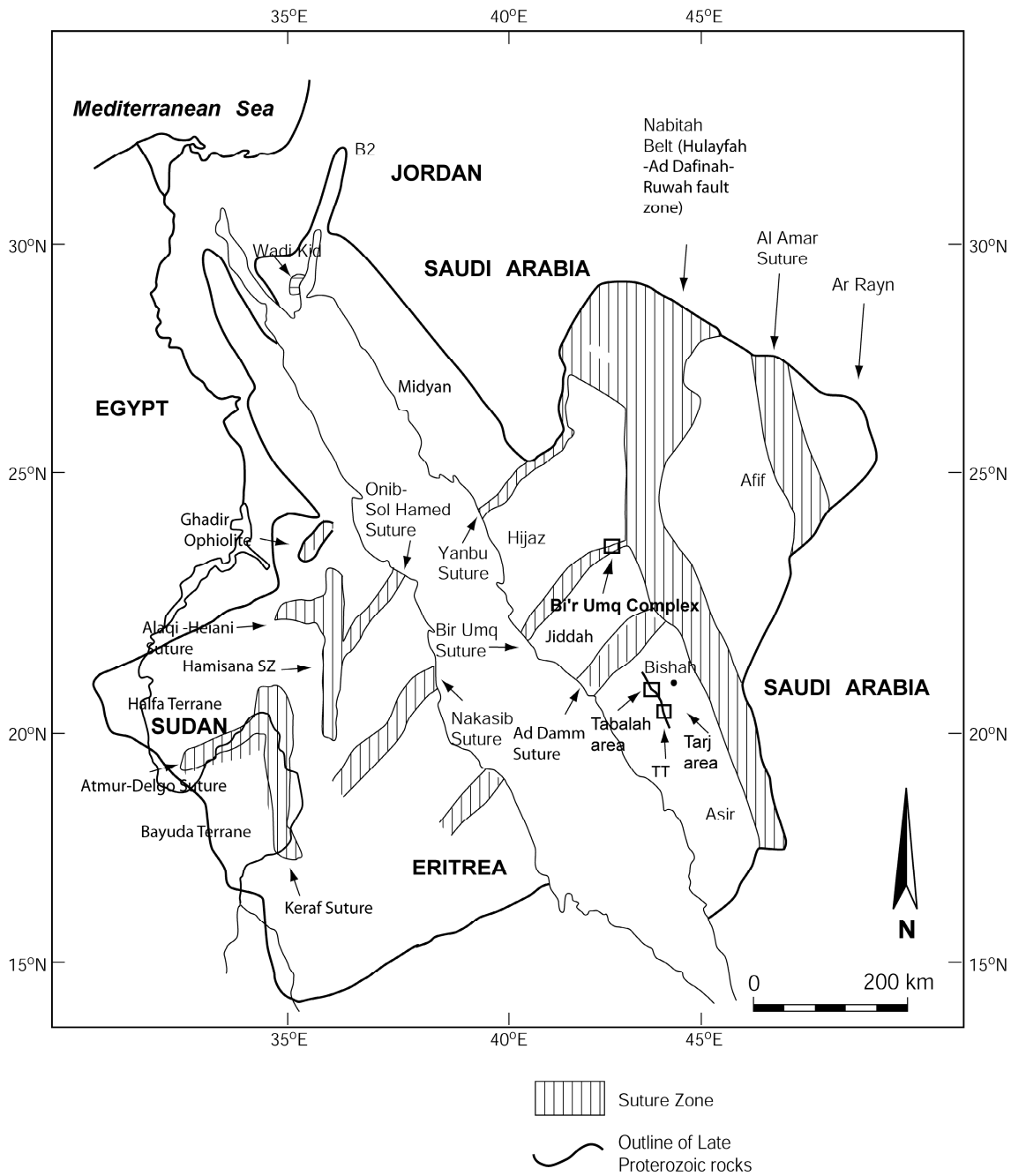


Figure 3-1 Overview map of the Arabian-Nubian Shield with main features and the site of the Bi'r Umq Complex.

Johnson (1998, 1999a, 1999b) has demonstrated the importance of these studies in the Arabian Shield. Shear zones, related to the arc-accretion, are represented by NE-SW trending linear belts such as the Bi'r Umq-Nakasib Suture and the Yanbu Suture, the NNW-SSE trending Hulayfah-Ad Dafinah-Ruwah shear zone and the N-S trending Nabitah Belt (see also Chapter 2 and references within for more details on these structures). These shear zones are interpreted as ophiolite-bearing sutures (Stoeser and Camp, 1985; Johnson et al., 2001). The results of a detailed structural study of the Bi'r Umq Complex (BUC) and its surrounding areas are presented in this chapter. The BUC itself is thought to be a typical example of a part of an ophiolitic suture (e.g. Pallister et al. 1988; Johnson et al., 2002).

Detailed structural and kinematic studies are crucial for the understanding of the complicated accretion processes, which are assumed to be responsible for the formation of the Arabian-Nubian Shield (Stoeser and Camp, 1985; Johnson et al., 1987; Blasband et al., 2000). The aim of this chapter is to more fully understand these tectonic processes through integrated structural and kinematic studies. These studies will in turn provide a basis for a more comprehensive interpretation of the tectonic evolution of the ANS. Through this structural and kinematic study, it will be shown that the observed structural features are indeed typical of an area that has experienced arc-accretion.

The Bi'r Umq Complex (BUC), the subject of this study, forms the NE portion of the Saudi part of the generally NE-SW trending Bi'r Umq/Nakasib suture (Figure 3-1). The total length of the suture is some 600 km (Johnson et al., 2002). The Saudi part of the suture, referred to as the Bi'r Umq suture, defines the border between the Jiddah and Hijaz terranes (Johnson et al., 2002). The BUC trends WSW-ENE and is some 25 km long and 10-15 km wide. It consists of a sequence of rocks that are thought to form a dismembered/disrupted ophiolite (Stoeser and Camp 1985; Pallister and others 1988). This assumption is based on the presence of ultramafic rocks, basalts, and chert in the BUC. The rocks in the BUC are locally deformed. The Bi'r Umq Complex derives its name from the village of Bi'r Umq, which lies in the middle of the area. The main tectonic feature in the complex is the Bi'r Umq Shear Zone (BUSZ) in the southern part of the complex. This shear zone defines the contact between the Jiddah Terrane and the less deformed part of the BUC. Minor shear zones are found within the BUC, and south of the BUSZ, within the Jiddah Terrane. The border between the Bi'r Umq Complex and the Hijaz Terrane in the north is not visible due to the lack of outcrop.

This chapter concentrates on the structural features of the Bi'r Umq Complex and its surrounding areas, and consequently special attention was given to the structurally complicated areas as the BUSZ. The results from study of the Bi'r Umq Complex will be integrated in Chapter 6 with results from the studies of other areas that were performed in the framework of this thesis, and will be integrated with data from other key areas of the Arabian-Nubian Shield.

### **3.2 Geological Background**

### 3.2.1 Lithology

The lithological sequence of the Bi'r Umq area will be described from south to north starting with the *Mahd Group*. Figure 3-2 shows a simplified geological map of the Bi'r Umq Complex. The *Mahd Group* forms the northernmost part of the Jiddah terrane and southernmost of the studied area. The BUC itself is regarded as one lithological entity. The northern border of the BUC is not visible because it is covered by Quaternary sediments.

The rocks that are found to the south of the BUC belong to the *Mahd Group*. The rocks of this unit were studied in order to define the southern contact of the Bi'r Umq Complex. The *Mahd Group* consists of (meta)basalts, (meta)andesites, and different varieties of (meta) sedimentary rocks. The metasediments are slates, very fine-grained (meta)sandstones and chlorite-schists. The chlorite-schists contain quartz, plagioclase, chlorite and minor white mica. Locally the schists are carbonated. Rhyolites, andesites and basalts are found close to the contact with the Bi'r Umq Complex. The basalts are found in massive and vesicular varieties. Locally the volcanics are foliated and form bands of schist with a thickness of up to approximately 5 meters. Towards the contact with BUC the rocks become increasingly deformed as indicated by increasing foliation intensity. Outside of the studied area, the *Mahd Group* is intruded by many (grano)dioritic plutons (Johnson et al., 2002).

The BUC, which forms the main subject of this chapter, starts north of the *Mahd group*. The rocks at the contact with the *Mahd Group* consist of an orange-pale red carbonate-rich rock. Most workers in the area interpreted these rocks as peridotites that were carbonated (Hopwood 1979, Bowden and others 1981, Al-Rahaili 1982). The *carbonated ultramafics* are between 100 and 500 m thick. Occasionally the carbonated ultramafic rocks disappear laterally and instead serpentinite is found at the contact of the BUC with the *Mahd Group*. The carbonated rocks are generally undeformed but locally foliated carbonated ultramafics were found and close to the contact with the *Mahd Group*, the carbonated ultramafics are always foliated. The *carbonated ultramafics* consist of carbonates and minor chlorite and serpentine. Towards the contact between BUC and the *Mahd Group*, an increasing number of elongated basaltic clasts from the latter formation are found.

A dark gray to dark brownish gray *serpentinite* layer is found north of the carbonated ultramafic rocks and continues along the contact with the *Mahd Group* where carbonated ultramafics are lacking. This layer is also 100 to 500 meters in thickness and strikes ENE-WSW. The *serpentinite* contains up to 90% serpentine with olivine pseudomorphs and minor Fe-oxide, carbonates and chlorite. Occasionally pyroxene pseudomorphs are observed in the *serpentinite*. The *serpentinite* is found in a foliated and in a massive variety. The massive serpentinite grades into layers of serpentinite schist that are 10 to 100 of meters thick. Serpentinite schists contain clasts of undeformed massive serpentinite, ranging in size from a few millimeters to 10s of centimeters. The schistose parts form mostly low ground in the wadis and good outcrop of the *serpentinite* schist only occurs where schist is adjacent to massive outstanding ridges of dyke rock or basalt.

The *serpentinite* is thought to be meta-harzburgite (Hopwood, 1979). The serpentinite schist contains biotite in places, but only when close to a contact with the *Mahd Group* and the Basalts north of the *serpentinite*. All visible contacts with other lithologies are foliated.



Figure 3-2 A simplified geological map of the Bi'r Umq Complex and its surrounding areas. A-A'-B-B' represents cross-section of Figure 3-12.

However, poor outcrop masks most contacts and in many cases the nature of the serpentinites at the contacts could not be studied. Close to the contact with the *Mahd Group*, the *serpentinite* schist contains many clasts of undeformed basalts, ranging in size from a few centimeters to 10s of meters. These clasts are locally foliated and oriented (sub)parallel to the main foliation of the serpentinite schist.

A large ENE-WSW trending basalt and chert layer is found north of the main serpentinite. The basalt, which locally grades to andesite, is mostly massive and stands out in ridges. It is locally foliated, mainly near its contacts with the ultramafic rocks where it forms chlorite-or biotite-schist. The undeformed basalts are often silicified and contain fine-grained chlorite. Locally pillow structures are found in the basalts. Occasionally bands of serpentinite-schist were found within the basalts. These layers are as much as several 10s of meters thick. In the northern part of the BUC, a carbonated peridotite layer is associated with such serpentinite schist. Chert, which also forms prominent ridges, is mainly found in the northern part of the complex as interbeds in the basalt. Some of the chert-basalt contacts are strongly schistose.

A large ENE-WSW layer of *carbonated ultramafics* cross-cuts the basalt- and chert sequence in the central part of the BUC. In the northern part of the BUC a carbonated ultramafic lens of some 100 m thick and 1 km wide is observed within the basalt- and chert sequence.

The northern most outcrop of the BUC consists of (meta)andesites, (meta)dacites and chlorite-schists. The chlorite-schists contain up to 20% quartz and large amounts of chlorite and appear to have a volcanic or sedimentary origin. The northern edge of the BUC is not exposed and the location of the northern contact of the BUC is therefore uncertain.

Basaltic to andesitic dikes occur in the area and are generally undeformed. Late dykes cross-cut all other lithologies. The undeformed ENE-trending basaltic dykes contain mainly plagioclase and hornblende and are in part chloritized. N-S trending dykes have an andesitic composition, containing plagioclase and minor amounts of hornblende and quartz. They are not chloritized and this indicates that the ENE-trending dykes have undergone some form of metamorphism. The N-S trending dykes postdate the phase of greenschist metamorphism and should thus be youngest.

An undeformed microdiorite body is found in the southeastern part of the BUC. It is intrusive to the surrounding serpentinites and basalts. An undeformed plagiogranite intrudes the serpentinite schist in the southwestern part of the BUC.

Although no complete ophiolitic sequence was observed in BUC, the presence of a variety of ultramafics next to basalts and cherts justifies the interpretation of the BUC as a dismembered ophiolite. This interpretation is in accordance with those of others who worked in the area (e.g. El-Rahaili 1982; Pallister et al., 1988; Johnson et al., 2002).

### 3.2.2 Metamorphism

The inferred metamorphic conditions are based on microscopic observations together with earlier reports (e.g. Hopwood, 1979; El-Rehaili, 1980; Bowden and others, 1981). The rocks of the *Mahd Group* are typically non- to slightly metamorphosed. The meta-sediments of the *Mahd Group* contain chlorite and occasionally actinolite. This indicates lower-middle

greenschist facies. Within the BUC, serpentine, minor amounts of talc, chlorite and biotite are found. These rocks, like the rocks in *Mahd Group*, display low- to medium-greenschist grade metamorphism.

### *3.2.3 Origin of igneous rocks*

Most of the rocks in the BUC and the Mahd group are of magmatic origin. Geochemical studies of these rocks may present useful information on their tectonic environment. The igneous rocks in the Mahd Group consist of rhyolites, andesites and basalts. Johnson and others (2002) concluded, on the basis of geochemistry and on the basis of the geology of adjacent areas, that they were formed in a supra-subduction setting. The rocks of the BUC consist of ultramafic rocks as harzburgite and dunite and combined with (pillow) basalts and cherts, they resemble ophiolites (e.g. Al-Rahaili, 1980; Stoesser and Camp, 1985). Le Metour and others (1982) suggested that the serpentinites were formed from peridotites which have Cr-spinel compositions that are comparable to Tethyan ophiolites. Johnson and others (2001) compared the geochemical data of Le Metour and others (1982) with the standardized chromian spinel diagrams of Dick and Bullen (1984). On the basis of these diagrams, Johnson et al. (2002) concluded that the Bi'r Umq serpentinized peridotite was formed at a juvenile mid-oceanic ridge close to an island-arc or at a fore-arc. The (grano)diorites that are found south of the BUC are thought to be intruded in to a volcanic arc (Pallister et al., 1988; Johnson et al., 2002)

### *3.2.4 Geochronology*

Pallister et al. (1988) performed a geochronologic study (U-Pb zircons) in several ophiolitic sequences of Saudi Arabia. They dated a number of rocks from the Bi'r Umq area. A diorite in the northeastern part of the BUC was dated at  $838 \pm 10$  Ma. This date was related to the formation of the ophiolite in the BUC. An undeformed plagiogranite in the southwestern part of the complex (named "keratophyre" by Pallister et al., 1988) that intrudes the serpentinite schist was dated at  $764 \pm 3$  Ma. This date should give an upper limit of the age of the deformation phase that was responsible for formation of the serpentinite schist. Dunlop et al. (1986) dated a nearby trondhjemite and a pyroxene separate from a gabbro, thought to be related to the formation of the ophiolite, at  $828 \pm 47$  Ma. Diorites in the Jiddah Terrane, intruded in to a volcanic arc south of the BUC, were dated at approximately 810 Ma (Calvez and Kemp, 1982; Stoesser and Stacey, 1988; Pallister et al, 1988). A rhyolite of the Mahd group was dated at  $772 \pm 28$  Ma (Calvez and Kemp, 1982). Other intrusives related to arc magmatism south of the BUC, intruded at 780-760 Ma (Johnson et al., 2002).

From these geochronologic data, it can be concluded that the ophiolite was formed before 820 Ma. The tectonic phase that caused the deformation in the serpentine schists, ended by 760 Ma. The beginning of the deformation phase is temporally unconstrained, however it should post-date the age of the youngest ophiolite-related rocks that were dated at ca. 820 Ma (Dunlop et al., 1986; Pallister et al., 1989).

### 3.3 Structural Geology

#### 3.3.1 Introduction

The structural features in the Bi'r Umq area, will be described according to their inferred mode of formation, namely those which have been classified as part of a shear process (shear zone related structures) or those which have been classified to have formed independently from the shear process (structures outside the shear zones). As implied by the terminology, shear-zone related structures occur in foliated and sheared rocks that displays indications of non-coaxial shear; non-shear-zone related structures are outside such shear zone. The main structural trend of the Bi'r Umq Complex is WSW-ENE.

For the structural study, reference will be made to the 3 principal structural domains: a) the Mahd group area in the south, b) the main Bi'r Umq Shear Zone (BUSZ), and c) the BUC, excluding the BUSZ. The BUSZ itself marks the contact between *Mahd Group* (Jiddah Terrane) and the BUC (Al-Rehaili, 1980; Johnson et al., 2002). Strictly speaking, on the basis of lithology, the BUSZ is part of the BUC but since it is much larger in comparison with other structures in the BUC and records a significantly more complicated structural history than any other structure in the area, it is described as a separate structural entity.

#### 3.3.2 Previous studies

Most authors, who worked in the area, have concentrated on the BUSZ, and many have interpreted it as a thrust-complex related to a southward dipping subduction zone (Al-Rahaili, 1982; Stoeser and Camp, 1985; Pallister et al., 1988; Johnson et al., 2002). A post-thrust dextral strike-slip phase has been postulated for the entire Bi'r Umq/Nakasib Suture (Johnson et al, 2002).

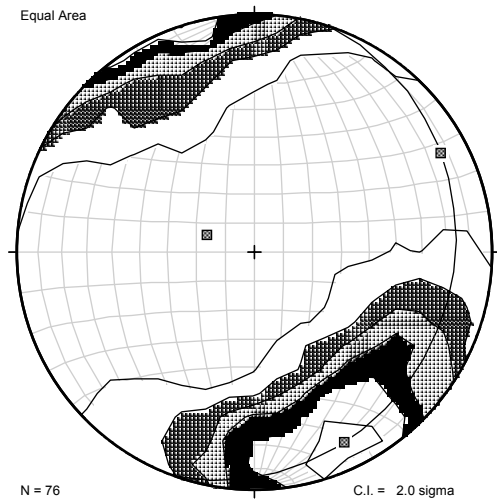
#### 3.3.3 Shear Zone related structures

##### 3.3.3.1 Introduction

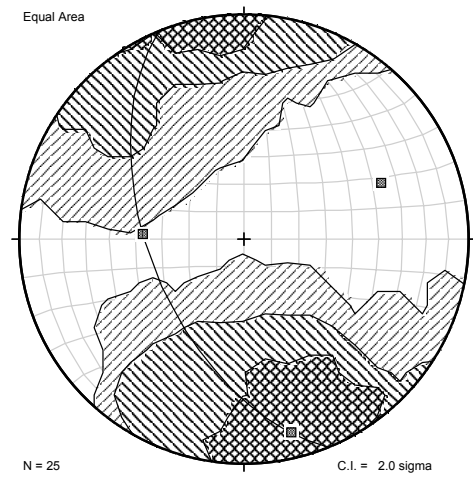
This section describes lineations, foliations, and structures associated with non-coaxial deformation, which are observed in the shear zones that are present in the study area. These include minor shear zones in the Mahd group with widths up to 50 m; the Bi'r Umq Shear Zone (BUSZ) which is 200-1000 m wide and is the main shear structure in the area; and minor shear zones in the BUC, north of the BUSZ, with widths up to 50 m. The southern margin of the BUSZ is drawn at the southernmost outcrop of ultramafic rocks, either the orange colored carbonated ultramafics or, where these are absent, serpentinite schist. The northern margin is drawn at the southernmost outcrop of massive basalt of the BUC.

##### 3.3.3.2 Foliation

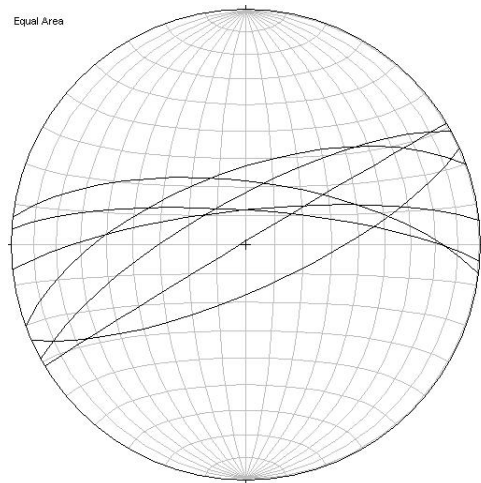
Foliations are pervasive structures in the shear zones, and are particularly well developed in serpentinite schists and carbonated ultramafic rocks along the contact between the Mahd Group and the Bi'r Umq Complex. This contact-zone is referred to in the literature as the Bi'r Umq



a



b



c

Figure 3-3 Stereoplots of planar structures in the shear zones; (a) contour-plot of the poles to the foliation in the BUSZ; (b) contour-plot of the poles to the foliation in the minor shear zones of the BUC; (c) Stereoplot of the foliations in the minor shear zones in the Mahd Group.

Shear Zone (e.g. El Rahaili, 1980; Johnson et al., 2002) and this term will also be used in this chapter. The foliated rocks in the BUSZ are formed by serpentine schist, foliated carbonated ultramafics, biotite schists and chlorite schists. The foliation in the BUSZ is mainly defined by serpentine, whereas foliations in the minor shear zones in the BUC and the Mahd group are defined by serpentine, biotite and chlorite. The foliation in all shear zones is sub-vertical and strikes WSW-ENE to SW-NE (Figure 3-3a and Figure 3-3b). Outcrops of the Mahd Group next to the BUSZ are also well foliated.

### 3.3.3.3. Lineations

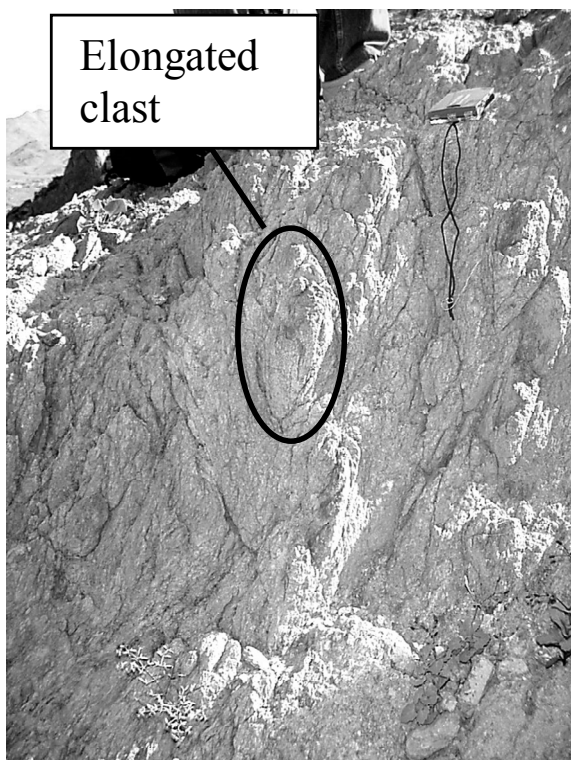
Lineations, defined by elongate minerals or mineral aggregates, and elongated clasts, are well developed in the BUSZ and in the minor shear zones of the BUC and Mahd group. Mineral lineations mostly consist of fibrous serpentine (Figure 3-4) but in places they also consist of elongate quartz pods, actinolite needles and elongate pods of biotite. Fibrous serpentine is formed on the foliation planes and individual fibers reach lengths of 2 cm. Other mineral lineations are not longer than 2-3 mm and are also formed on the foliation planes. The mineral lineations throughout the BUSZ plunge generally steep-moderate to the NW (Figure 3-6a) and are found on NNW dipping planes. Sub-horizontal mineral lineations were rarely observed in the BUSZ (see Figure 3-6a). Mineral lineations in minor shear zones in the *Mahd Group* and BUC were observed on SSE-dipping foliations and mostly plunge moderately to the SE (Figure 3-7a) but some lineations in minor shear zones in the *Mahd Group* and BUC plunge steeply to the NW in shear zones with NW-dipping foliations (Figure 3-7a).

Throughout the BUSZ, the clast lineations are the most commonly observed type of lineation (Figure 3-5). These clast-lineations consist of elongated clasts of basalt, carbonated ultramafics and massive undeformed serpentinite-clasts within the serpentinite schist and carbonated ultramafic rocks. These clasts are several centimeters to several decimeters long; several centimeters to a decimeter wide; and several centimeters to a decimeter thick. Their shortest axes are perpendicular to the foliation and their longest axes trend in generally uniform directions as indicated by clearly defined maxima in Figure 3-6b. In the BUSZ, the clast-lineations plunge mostly sub-horizontally to the WSW but also have a secondary maximum plunging steeply to the NW (Figure 3-6b). It is only close to the contacts of the BUSZ with the Mahd Group and the contacts of the BUSZ with the non-sheared parts of the BUC that the clast lineations are plunging steeply instead of sub-horizontally (Figure 3-5). Close to the contact with the Mahd Group, the clasts are basaltic and away from this contact more massive serpentinite clasts were found. In the minor shear zones of the BUC itself and the *Mahd Group*, clast-lineations plunge mainly toward the NW (Figure 3-7 b).

On the outcrop scale, no overprinting relations were observed between the steeply NW-plunging lineations, the moderately SE plunging lineations and the sub-horizontally WSW-plunging lineations. However, the conditions at which the different lineations trends were formed, may give an indication of their relative age relations. The presence of fibrous serpentine lineations and actinolite lineations indicates that their formation took place under greenschist-facies conditions. These mineral lineations were only observed as the steeply NW-



*Figure 3-4 Fibrous serpentine lineation in the BUSZ.*



*Figure 3-5 Steep clast lineation (dark elongate structures in carbonated ultramafic).*

plunging lineations in the BUSZ and moderately SE-plunging lineations in the minor shear zones of the BUC. Clast-lineations can form at the very lowest metamorphic grades when rocks were deformed by very low-grade deformation processes as pressure solution. No indications of thermal overprinting were observed with respect to the mineral lineations in the BUSZ, and therefore it is inferred that the steeply NW-plunging mineral lineations reflect the earliest phase of formation of lineations in the BUSZ because they developed at a higher temperature than the

Chapter 3

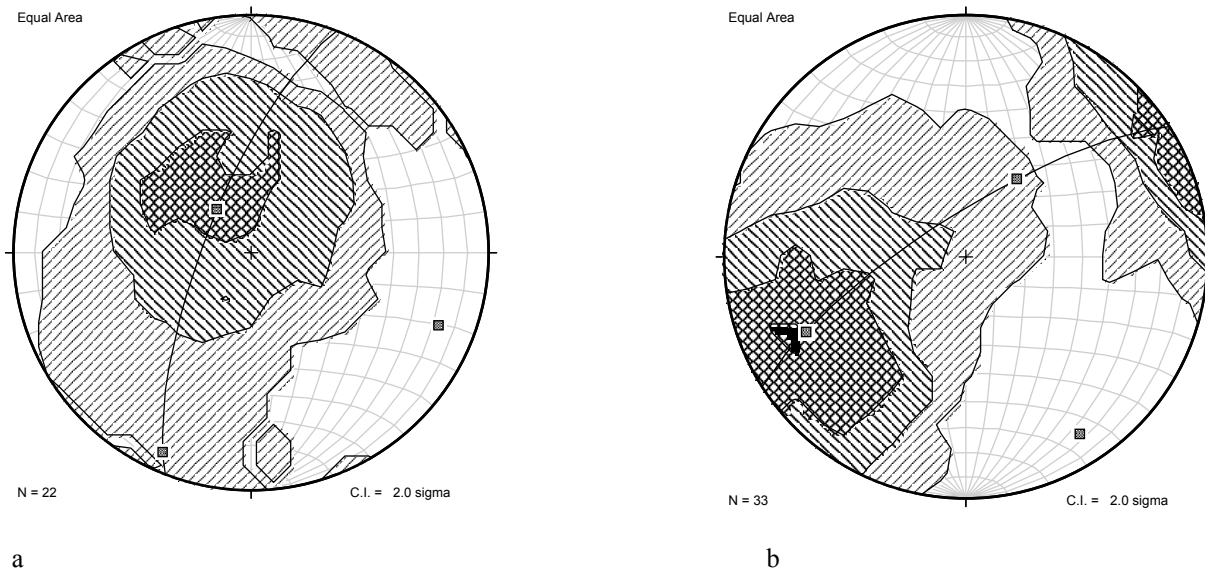


Figure 3-6 Contour-plots of linear features in the BUSZ; (a) mineral lineations in the BUSZ; (b) clast lineations in the BUSZ.

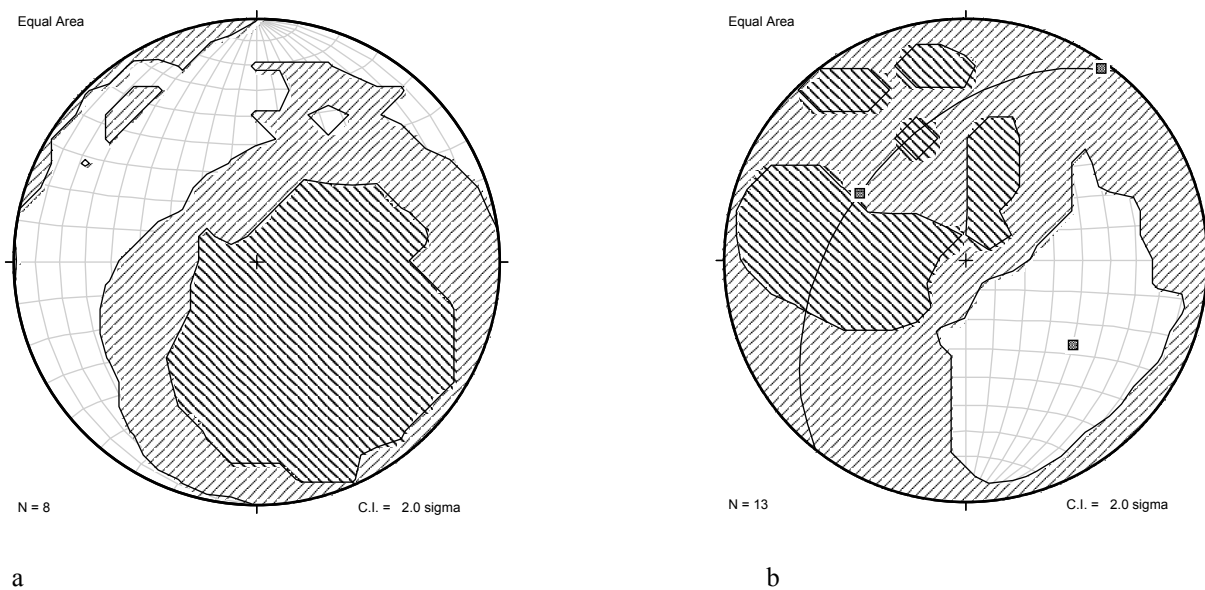


Figure 3-7 Contour-plots of linear features in the minor shear zones outside of the BUSZ; (a) mineral lineations in the shear zones outside of the BUSZ; (b) clast lineations in the shear zones outside of the BUSZ.

sub-horizontally plunging WSW clast-lineations. By association it is interpreted that all steeply plunging linear structures, other than the mineral lineations in the BUSZ (see also Figure 3-2 and Figure 3-6), are a part of the early, relative high temperature phase of deformation.

The mineral lineations in the BUC and in the *Mahd Group* have a different trend but were formed at the same metamorphic grade as the mineral lineations in the BUSZ; namely under greenschist conditions. Also in the *Mahd Group*, no thermal overprinting was observed on outcrop scale with respect to the mineral lineations. Therefore, like in the BUSZ, the mineral lineations in the BUC and the *Mahd Group* are interpreted to be the oldest linear features observed.



In summary, it can be concluded that the lineation in the BUSZ trends can be divided into two groups: a) steep-moderate plunge to NW-N; b) shallow plunge to WSW; and into two groups in the BUC and *Mahd Group*: moderate plunge to SE; b) steep-moderate plunge to NW. Steeper plunging clast- and mineral-lineations pre-date the sub-horizontal clast-lineations. Furthermore the mineral lineations were formed at a higher grade than the clast lineations. Any clast lineations that formed parallel to mineral lineations should have formed in the same deformation phase. For the complete interpretation of the tectonic significance of lineations and foliations, other structural information is required such as shear sense indicators and fold geometries. These features will be described in the section below.

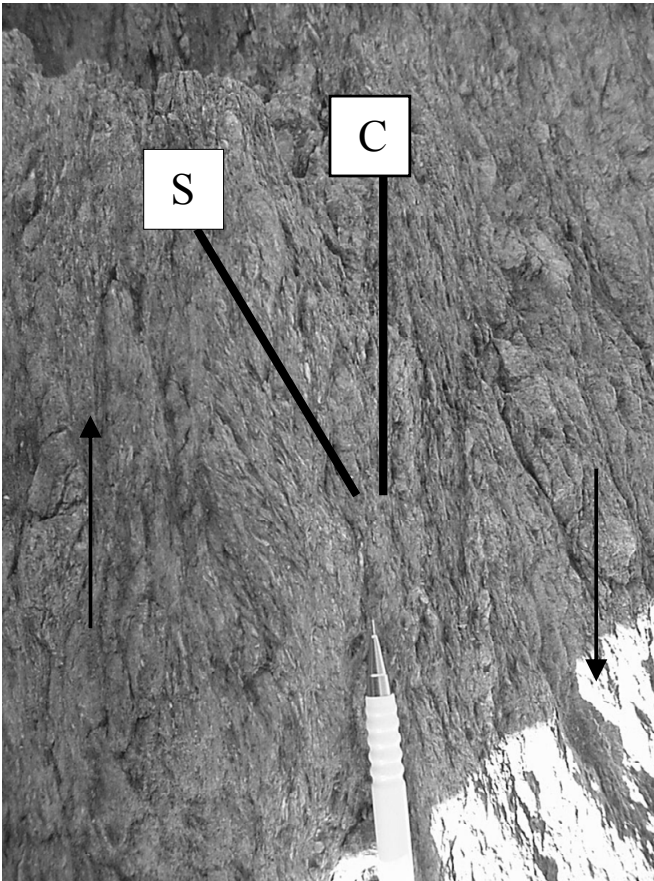
#### 3.3.3.4 Evidence for non-coaxial deformation

In order to understand the tectonic significance of the foliations and lineations, other structural features such as shear-sense indicators and fold geometries were studied. Lineations formed during non-coaxial deformation will be associated with asymmetric shear indicators when viewed parallel to the lineation and perpendicular to the foliation. Lineations that are related to regional folding will often form parallel to the fold-hinges (Price and Cosgrove, 1990; Twiss and Moores, 1992). In the BUSZ and in the distinct schistose zones in the Mahd Group and BUC, referred to as shear zones, no structures were observed that are indicative for regional folding as axial planar cleavages, intersection lineation and “fold-hinge lineations”, however indicators of non-coaxial deformation were widespread.

Prior to the use of shear sense indicators to ascertain non-coaxial deformation, it is important that the lineation-trends are analyzed carefully. From Figure 3-6 and Figure 3-7 it was concluded that the lineation trends in the BUSZ can be divided into two groups: a) steep-moderate to NW; b) shallow to WSW; and into two groups in minor shear zones of the BUC and *Mahd Group*: a) moderate to SE; b) steep-moderate to NW. Each of these sets is associated with indicators of non-coaxial movement.

The shear sense indicators associated with the lineations that plunge steeply to the NW in the steeply dipping ENE-WSW striking BUSZ, include asymmetric clasts, SC-fabrics (Figure 3-8a), and asymmetric folds (Figure 3-8b). These indicators all display top-to-SE movement along NNW dipping shear zones. The shear sense indicators in the schists of the Mahd Group near the contact with the BUSZ also display top-to-SE movement through their steep lineation and asymmetric basalt clasts.

The clast-lineations that plunge shallowly to the WSW are the most commonly observed linear structures in the ENE-trending BUSZ. Rotated clasts, asymmetric pressure shadows, C-C'-fabrics, S-C fabrics, microscopic tension gashes and asymmetric folds are the typical indicators of movement that are related to the shallowly dipping clast lineation in the BUSZ. Both, a dextral sense of shear (Figure 3-9) and a sinistral sense of shear were observed perpendicular to the shallowly WSW plunging lineations. The shear indicators with the dextral sense of shear are the most abundantly observed ones in the BUSZ and are ductile in nature. Brittle to brittle-ductile C-C'-fabrics display a sinistral sense (Figure 3-10) and overprint the



a



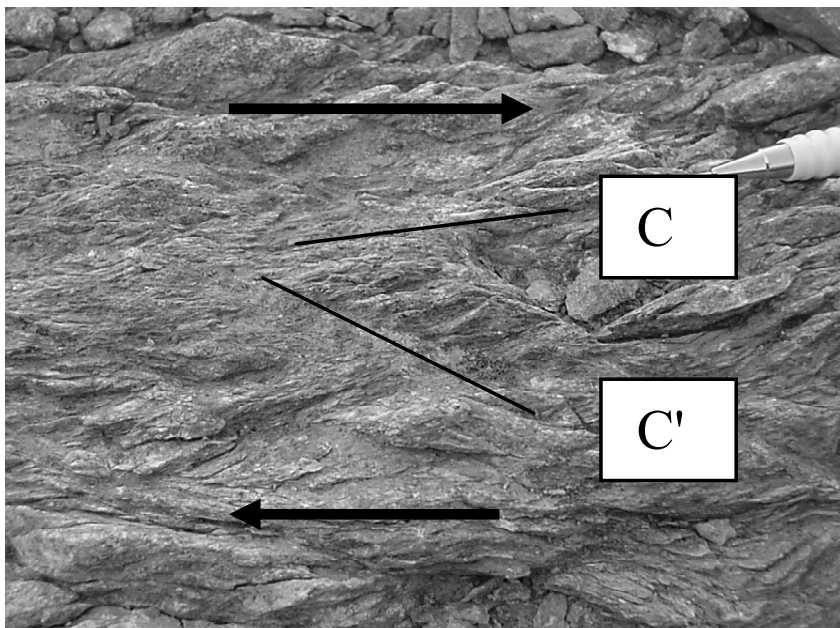
b

Figure 3-8 (a) SC fabric indicating top to the SE on NNW- dipping plane in the BUSZ (b) Asymmetric fold indicating top to SE-movement on NNW-dipping plane (fold axis is perpendicular to lineation) in the BUSZ.

ductile dextral structures. On the microscopical scale, sinistral brittle C-C'-fabrics overprint dextral asymmetric folds.



a



b

Figure 3-9 (a) Rotated clast of a non-deformed ultramafic clast with pressure shadows of serpentine schist (b) Ductile extensional crenulation cleavage in the BUSZ indicating dextral movement.

Since no other linear features were observed in these outcrops than the shallowly WSW plunging clast lineation, it is interpreted that the brittle sinistral C-C'-fabrics also to be associated to the elongated clasts with a shallowly plunging WSW trend. Since the sinistral brittle C-C'-fabrics overprint the ductile structures on outcrop scale, it is interpreted that they to postdate the formation of the ductile structures that are related to the steeply plunging lineations and the ductile dextral structures related to the WSW plunging lineation. The brittle shear indicators that display a sinistral overprint on the sub-horizontal lineations represent thus a

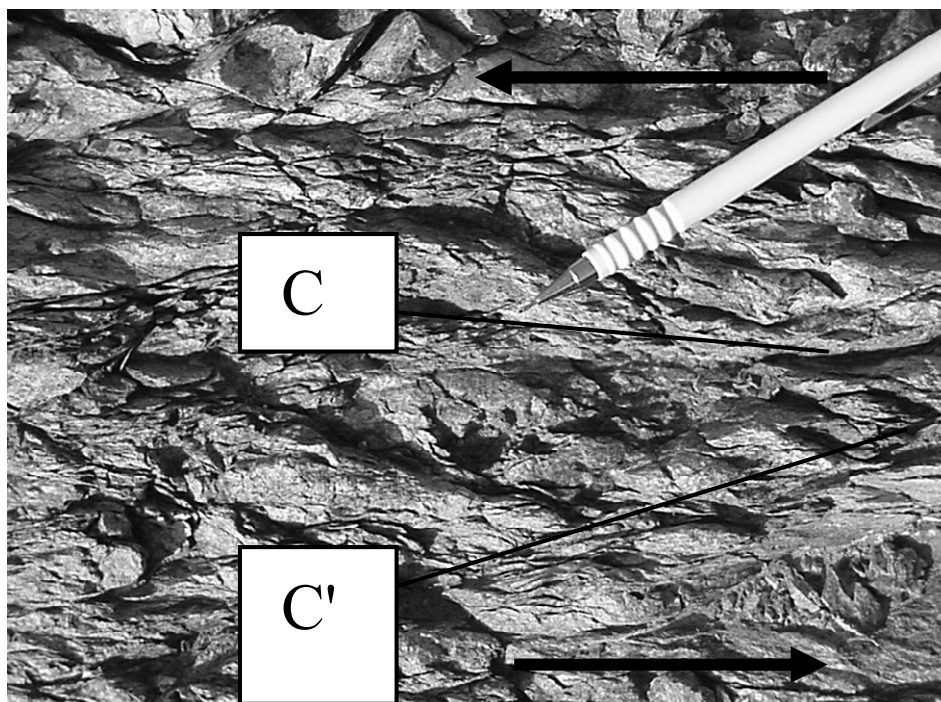


Figure 3-10 Late brittle-ductile extensional crenulation cleavage in the BUSZ indicating sinistral sense of shear.

phase of shear-sense reversal. The relationships between the plunge of lineations and their associated shear sense in the BUSZ is shown in Figure 3-11.

Shear sense indicators were associated with moderately SE plunging lineations in the ENE-WSW striking minor greenschist grade shear zones in the northern part of the BUC (Figure 3-2 and Figure 3-7). The shear indicators include asymmetric folds, asymmetric pressure shadows and C-C'-fabrics. They all record top-to-the NW movement, and so these shear zones record NW-vergent thrusting. In the ENE-WSW striking minor shear zones of the central BUC, the lineations plunge moderately to the NW (Figure 3-2 and Figure 3-7). The shear sense indicators associated with lineations in the minor shear zones of the central BUC all indicate top-to-the-SE movement and thus display thrusting. Rarely, SSW shallowly dipping elongated clasts were observed in the northern part of the BUC (Figure 3-2). Shear indicators associated with this lineation, namely rotated clasts and extensional crenulation cleavages, display sinistral movement.

### 3.3.3.5 Formation of shear-related structures

The co-occurrence of foliations and lineations together with indicators of non-coaxial shear in the ENE-trending BUSZ and in parts of the ENE-trending schistose units of the BUC and the *Mahd Group* (see Figure 3-11 and Figure 3-12) indicate that all these structures developed during non-coaxial deformation.

The lineation trends were divided into two groups in the BUSZ: a) steep-moderate to NW; b) sub-horizontal to WSW; and into two groups in the minor shear zones of BUC and Mahd Group: moderate to SE; b) steep-moderate to NW (see Figure 3-11). Indicators of non-coaxial deformation trends were associated with all of the lineation-trends. The steeply NW-

plunging lineations in the BUSZ and the moderately SE plunging lineations in the northern BUC were developed at the highest grade of metamorphism in the region and no thermal overprint was observed (see section 3.3.2). For this reason, they were interpreted to have been formed at the same time. Shear indicators that were associated with the steeply NW-plunging lineations in the BUSZ, indicate top-to-SE movement which would imply thrusting with a minor dextral component in its current geographic position. This would indicate a NW-SE compressional regime, however thrusts rarely form as steep as observed at the BUSZ. In the minor SE -dipping shear zones of the BUC, SE-plunging lineations are associated with top-to-the-NW shear indicators, suggesting NW-vergent thrusting in a NW-SE compressional regime (Figure 3-2, Figure 3-11 and Figure 3- 12). The minor NW-dipping shear zones with NW-plunging lineations in the BUC and in the Mahd Group also display thrusting to the SE and, consequently, were also formed in a NW-SW compressional stress regime.

Since the NW- and SE-plunging mineral lineations were formed in the same stress regime and at the same metamorphic condition, they were interpreted to have been formed simultaneously during the same phase of deformation. The NW-plunging clast-lineations throughout the entire Bi'r Umq area were also associated with the shear indicators that indicate thrusting to the SE and were thus also formed in the same NW-SW compressional stress regime, as the mineral lineations. Therefore, these NW-plunging clast-lineations and their associated top-to-SE shear indicators also belong to the earliest deformation event in the Bi'r Umq area.

Since the steep lineations in the BUSZ, and the other NW- and the SE-plunging lineations, represent the oldest observed phase of deformation in the Bi'r Umq area, they were named L1-lineations which were formed during a D1-deformation phase. Only one foliation was formed in the shear zones and this must have formed simultaneously with the L1-lineation because these lineations were formed on the foliations. This foliation, formed during D1, is thus named S1.

To conclude, the D1-deformation was responsible for the formation of shear zones in the Bi'r Umq area with a sub-vertical WSW-ENE striking foliation (S1), the steeply plunging NW- and SE-plunging mineral lineations and the steeply NW-plunging clast-lineations (L1), and the shear indicators that indicate thrusting with a minor dextral component along all L1-lineations. These D1-features were formed in a NW-SE compressional regime. Thrusting on steep shear zones as the BUSZ is rare, however this issue can only be discussed when all the structural features of the area have been assessed and therefore this will be discussed at a later stage in this chapter.

Sub-horizontally WSW-plunging lineations on the ENE-trending BUSZ exclusively consist of elongated clasts that formed at a lower grade than the mineral lineations and other steep linear features. These sub-horizontally plunging clast-lineations were interpreted to be the younger set of lineations observed in the Bi'r Umq area because no thermal overprint was observed with respect to the steeply plunging mineral lineations. Consequently, the sub-horizontally WSW plunging lineations are referred to as L2-lineations. The L2-lineations in the core of the WSW-ENE trending BUSZ are associated with ductile shear indicators displaying dextral movement and brittle shear indicators displaying sinistral movement. The brittle

Bi'r Umq Shear Zone

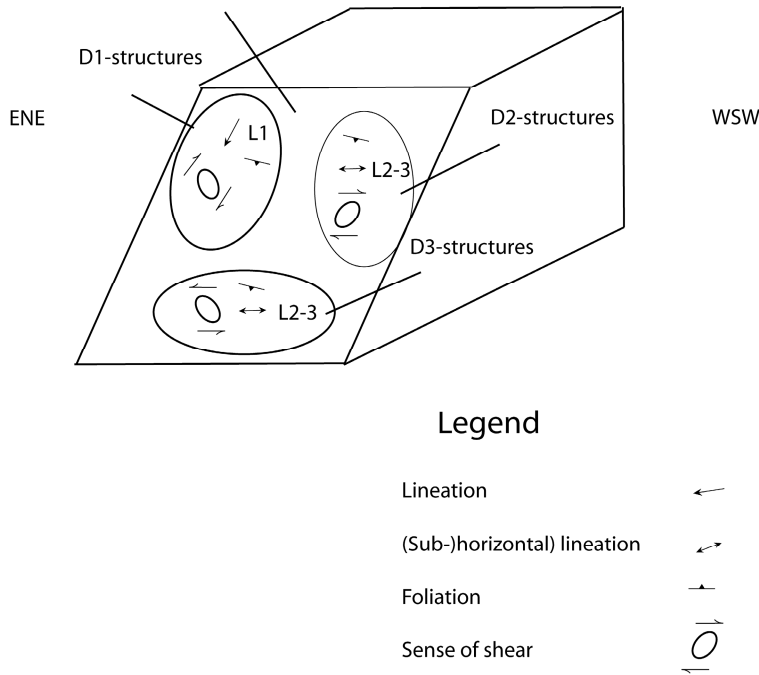


Figure 3-11 Block diagram of main structural features (foliations, lineations, and shear sense indicators) in the BUSZ.

sinistral shear indicators overprinted the ductile dextral shear indicators. Therefore the dextral ductile shear indicators are interpreted to be older than the sinistral brittle shear indicators and thus belong to the deformation phase that is referred to as D2. The brittle shear indicators that display a sinistral overprint on the sub-horizontal lineations represent thus a phase of subsequent shear-reversal which is referred to as the D3-deformation phase. The D2- movement along the sub-horizontally WSW-plunging lineations of the BUSZ displayed dextral strike-slip with a minor transpressive component and resulted thus from WNW-ESE directed  $\sigma_1$ . The D3-sinistral movement along these same lineations displayed sinistral strike-slip with a minor transtensional component and resulted consequently from NNE-SSW directed  $\sigma_1$ .

Since no other foliation was found then S1, it is assumed that both, the D2- and D3-deformation events used the S1-foliations to accommodate their planar deformation. The L2-lineation accommodated the linear deformation during D3. It should be noted that the strike-slip deformation did not affect the contacts of the BUSZ since L2 and horizontal shear indicators are absent over here.

It is assumed that no strike-slip movement took place on the minor shear zones because they only contain steeply plunging lineations and infer, consequently, that the minor shear zones were only active during D1, with the exception of the northernmost shear zone where sub-horizontal lineations are locally observed together with brittle sinistral shear sense indicators (Figure 3-2). Therefore it is assumed that the later deformation mainly concentrated on the BUSZ.

In summary, the history of shearing in the Bi'r Umq area is:

SE

Cross-section of the Bir Umq Complex

NW

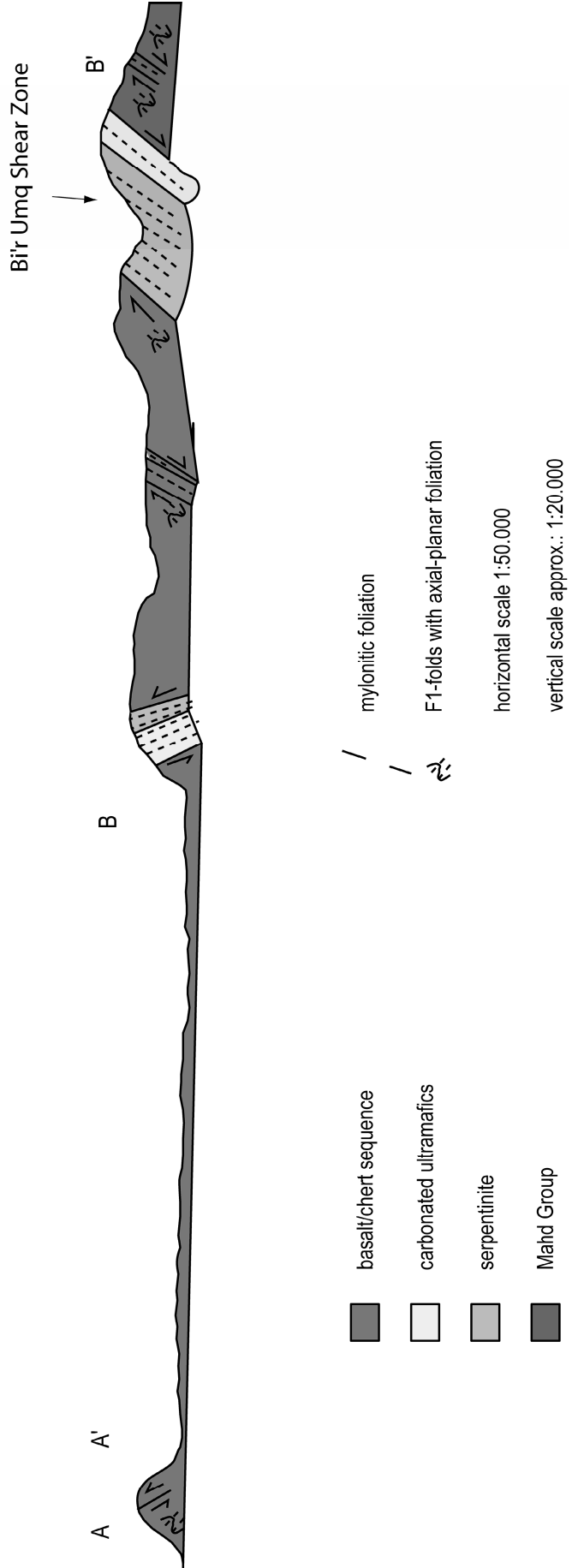


Figure 3- 12 NW-SE cross-section of the Bi'r Umq Area.

1. Thrusting with a minor dextral component along NW-plunging lineations on the WSW-ENE trending BUSZ and the minor shear zones in the BUC at greenschist grade (D1, NW-SE shortening)
2. Dextral strike-slip with a minor transpressive component at very low greenschist grade on the WSW-ENE trending BUSZ (D2, WNW-ESE directed  $\sigma_1$ ).
3. Sinistral strike-slip with a minor transtensional component – a phase of shear reversal - on the BUSZ (at brittle conditions) and locally at the northern most shear zone in the BUC (D3, NNE-SSW directed  $\sigma_1$ ).

No reliable ages are available for the start of the deformation at the Bi'r Umq Complex, however the youngest available date of formation for any ophiolite related rocks in this area is ca. 825 Ma (Pallister et al., 1989). The end of deformation in the Bi'r Umq Complex is constrained by the undeformed microdiorite in the Bi'r Umq Complex that was dated at ca. 760 Ma (Dunlop et al., 1986; Pallister et al., 1989). Consequently it may be concluded that D1-deformation should have started after 820 Ma and that D3-deformation should have ceased by 760 Ma.

### 3.3.4 Structures outside the shear zones

#### 3.3.4.1 Introduction

Some of the foliated rocks in the BUC and the Mahd group contain no indicators of non-coaxial deformation. They are treated as not being directly related to the shear zones, and they are described below.

#### 3.3.4.2 Folding

Meso-scale folds were observed to fold S0 bedding (Figure 3-13) and they define F1-folds. Folding of the S0 bedding defines a NE to ENE trending fold-axis (Figure 3-14a). The meso-scale fold axes are sub-horizontal and trend NE to ENE (Figure 3-14d), indicating NW-SE to NNW-SSE compression. In places, a WSW-ENE striking axial planar foliation (Figure 3-14e) was observed in the meso-scale folds. The trend of these planes is parallel to the main foliation outside of the shear zones and therefore, this foliation is interpreted to be the result of the folding about WSW-ENE fold axes.

#### 3.3.4.3 Foliation

Slates and schists in the Mahd group constitute foliated sequences of a centimeter to a few meters wide within otherwise undeformed volcanic and sedimentary rocks that occur outside of the shear zones in the Bi'r Umq area (Figure 3-13). The schists belong mainly to greenschist-facies as indicated by the presence of quartz, albite chlorite and white mica. Bedding (S0) was occasionally observed and in places where bedding and foliation were observed together, the foliation appears bedding-parallel. This relationship is commonly observed as the initial bedding foliation relationship in regionally folded rocks (Ramsey and Huber, 1983). Foliated



sections in the BUC consist mainly of biotite schist (Figure 3-13b). Bedding (S0) in these rocks strikes WNW-ESE and dips steeply to vertical (Figure 3-14a). The main trend of foliation in the Mahd group and the BUC is WSW-ENE (Figure 3-14b and Figure 3-14c).

#### *3.3.4.4 Formation of structures outside the shear zones*

The structures observed outside the shear zones as outlined above, comprise folds and foliations. The main trend of the regional foliation strikes NE-SW to WSW-ENE (Figure 3-14b and Figure 3-14c) similar to fold axial planar foliation (Figure 3-14e). Associated fold axes trend WSW-ENE (Figure 3-14d), and all the structures are consistent with a NW-SE to NNW-SSE directed shortening. Folding of S0 indicates a similar trend (Figure 3-14a). This indicates that this phase of deformation was related to NW-SE to NNW-SSE shortening and that the regional foliation is related to F1-folding. Although no evidence of non-coaxial strain was observed in the areas where S0-bedding and F1-folding, the relative proximity to the BUSZ justifies a relationship between the structures observed in the BUSZ and those outside which provide evidence for non-coaxial deformation. NW-SE to NNW-SSE shortening can be related to NW-SE to NNW-SSW compression during coaxial strain, it can be related to dextral strike-slip movement on an E-W trending N-dipping shear zone, or it can be related to sinistral strike-slip movement on an N-S trending W-dipping strike-slip shear zone. The orientation of shortening indicated by the folds and foliation is (sub-)parallel to the D1-shortening that was deduced from the shear zone-related structures. Therefore it is assumed that the F1-folds and the foliation that developed outside the shear zones were formed during that same D1-deformation event.

### **3.4 Discussion and conclusions**

#### *3.4.1 Review of new data for the Bi'r Umq Complex*

Table 3-1 and Figure 3-15 summarize the Neoproterozoic history of the Bi'r Umq area. The Bi'r Umq Complex and its surrounding areas are interpreted as ophiolitic sequences, which were formed before 820 Ma. The presence of ultramafics, pillow basalts and cherts in the BUC support this. Layered gabbros and sheeted dykes are missing and therefore, together with the sequence of ultramafics, pillow basalts and cherts in the BUC, they form a dismembered ophiolite. The ophiolite is characterized by mixed MORB/island-arc geochemistry (Johnson et al., 2002).

The rocks of the Bi'r Umq area display a variety of structures that can be related to one of the three of deformational events described in this chapter. Structures within the shear zones, namely S1-foliations, L1-lineations and shear indicators, as well as structures outside the shear zones, namely F1-folds and an associated foliation, are remnants of the oldest (D1) ductile deformation phase. This phase involved thrusting with a minor dextral component on the BUSZ and on the minor shear zones in the BUC, and represents a regional NW-SE to NNW-SSE compression event at greenschist conditions.



Figure 3-13 Example of non-shear zone related structures away from the shear zones: Foliated basalt in Mahd group, close to contact with BUSZ. A mesoscale late kinkfold is shown in this photograph.

D1 was followed by D2, which is characterized by dextral strike-slip with a minor transpressive component along the WSW-ENE trending BUSZ. It occurred during lower greenschist grade. The deformation is recorded by sub-horizontally WSW plunging elongated clasts and an abundance of dextral shear indicators. These structures resulted from WNW-ESE directed  $\sigma_1$ .

D2 was followed by sinistral-strike slip with a minor transtensional component along the same WSW-ENE trending shear zone at brittle conditions. This phase is referred to as the D3-deformation phase and formed during NNE-SSW directed  $\sigma_1$ . The D1- to D3-deformation events postdated formation of the ophiolite at ~820 Ma and predated the emplacement of ca. 760 Ma undeformed intrusives that cross-cut the BUSZ (Pallister et al, 1988).

As mentioned previously, thrusts do not form initially as steeply as the BUSZ, and so other indications of thrusting are required, such as metamorphic breaks between rocks at both sides of a shear zone. The Mahd Group, S of the BUSZ, consists of upper-crustal volcanics, and the rocks in the BUC (including those in the BUSZ), just N of the contact with the Mahd Group, consists of lower parts of an oceanic crust. Consequently it can be assumed that SE-vergent thrusting along the steep NW plunging lineation at the BUSZ juxtaposed the Mahd Group and BUC. This justifies the conclusion that the top-to-the SE movement along the steeply NW plunging lineations took place during SE-vergent thrusting. The BUSZ is a steeply dipping shear zone and this is very rare for thrusts. However, strike-slip shearing took place along steep shear zones and since the strike-slip movement in the BUSZ took place along the same shear zone as the thrusting, the strike-slip events is assumed to have caused the steepening of the foliation during D2 and D3. The fact that the metamorphic conditions of deformation on the moderately dipping minor shear zones of the BUC, formed during NW-SE compression, were the same as the highest metamorphic conditions on the steeply plunging lineations of the

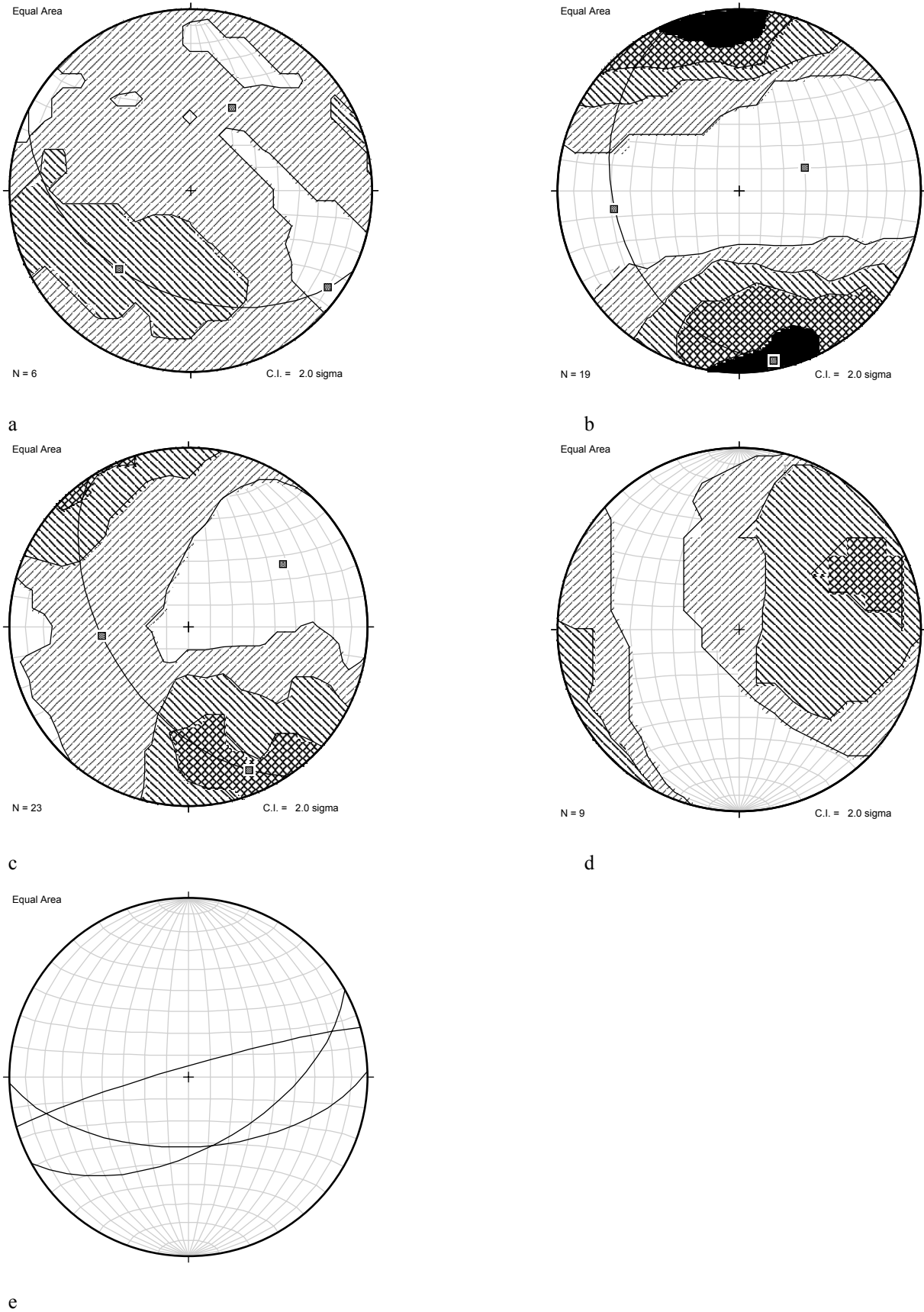


Figure 3-14 Stereo plots of structural features outside shear zones in the BUC and Mahd Group. (a) Contour plot of the poles to the  $S_0$  bedding in the Mahd Group (no data from shear zones included); (b) Stereo plot of poles

to the foliation in the Mahd group (no data from shear zones included). (c) Stereo plot of poles to the foliation in the BUC (no data from the shear zones included). (d) Stereo plot of fold axes in the Mahd group and the BUC (no data from the shear zones included). (e) Stereo plot of axial planes of folds in the Mahd group and the BUC (no data from the shear zones included).

BUSZ indicates that the steepening on the BUSZ didn't lead to a rotation of the lineations. Therefore the steeper L1-lineations of the BUSZ were also formed at a NW-SE compressional regime, however initially at a moderate plunge.

### 3.4.2 A tectonic model for the Bi'r Umq Complex

In the past, ophiolites were thought to be relicts of oceanic crusts that were formed at mid oceanic ridges (Dilek, 2003). However, over the past two decades, evidence was found for the formation of ophiolites in suprasubduction zones (e.g. Dilek, 2003; Hawkins, 2003; Pearce, 2003). In these cases, the formation of ophiolites is related to "local" extension above a subduction zone (e.g. Flower, 2003; Stern and Bloomer, 1992). The extension, that forms these suprasubduction ophiolites, takes place in the back-arcs and in fore-arcs of island arcs (e.g. Flower, 2003; Stern and Bloomer, 1992). Ophiolites from fore-arcs form at the initial stages of subduction when extension occurs and is related to early slab roll-back that forms the actual subduction zone (Flower, 2003; Stern and Bloomer, 1992). In such a scenario, asthenospheric material flows into area between the future overriding plate and the subsiding plate (Fowler, 2003; Stern and Bloomer, 1992). Back-arc ophiolites form due to extension that is related to continuing slab roll-back after the initial stages of the intra-oceanic subduction (Hawkins, 2003). The geochemical characteristics of back-arc ophiolites are close to those of ophiolites that are supposed to be derived from mid oceanic ridges but may also contain characteristics of nearby island-arcs. Fore-arc ophiolites have geochemical characteristics that are intermediate between mid oceanic ridges and island-arcs (Pearce, 2003). The geochemistry of the Bi'r Umq Complex is intermediate between typical mid oceanic ridges and island arcs (Johnson et al., 2002). Detailed geochemical data are required to differentiate between the two modes of ophiolite-formation presented here, however this is not available for the Bi'r Umq Complex. The fact that the ophiolites of the Bi'r Umq Complex have a mixed MORB/OIB geochemistry, together with the fact that the Bi'r Umq Complex is actually close to the island-arc relicts of the Jiddah Terrane and Hijaz Terrane, suggest that the Bi'r Umq Complex as a suprasubduction ophiolite that was formed in a fore-arc or a back-arc in accordance with the interpretation of Johnson et al. (2002) and Dilek and Ahmed (2003). In recent studies other ophiolites in the ANS, as the Halaban ophiolite, the Garf ophiolites and the Fawakhir ophiolite, have also been interpreted to have been formed in fore- or back-arcs (Al-Salah and Boyle, 2001; El-Sayed and El-Nisr, 1999; Zimmer et al., 1995).

Two important environments of emplacement of ophiolites are recognized (e.g. Ernst, 2003; Wakabayashi and Dilek, 2003): 1) emplacement at Alpine (or Thetyan) orogenic belts; 2) emplacement at Pacific (or Cordilleran) orogenic belts. Emplacement of ophiolites at Alpine orogenic belts is characterized by presence of a granitic gneiss basement, UHP metamorphism, a large age differences between the different units and little to no calc-alkaline magmatism

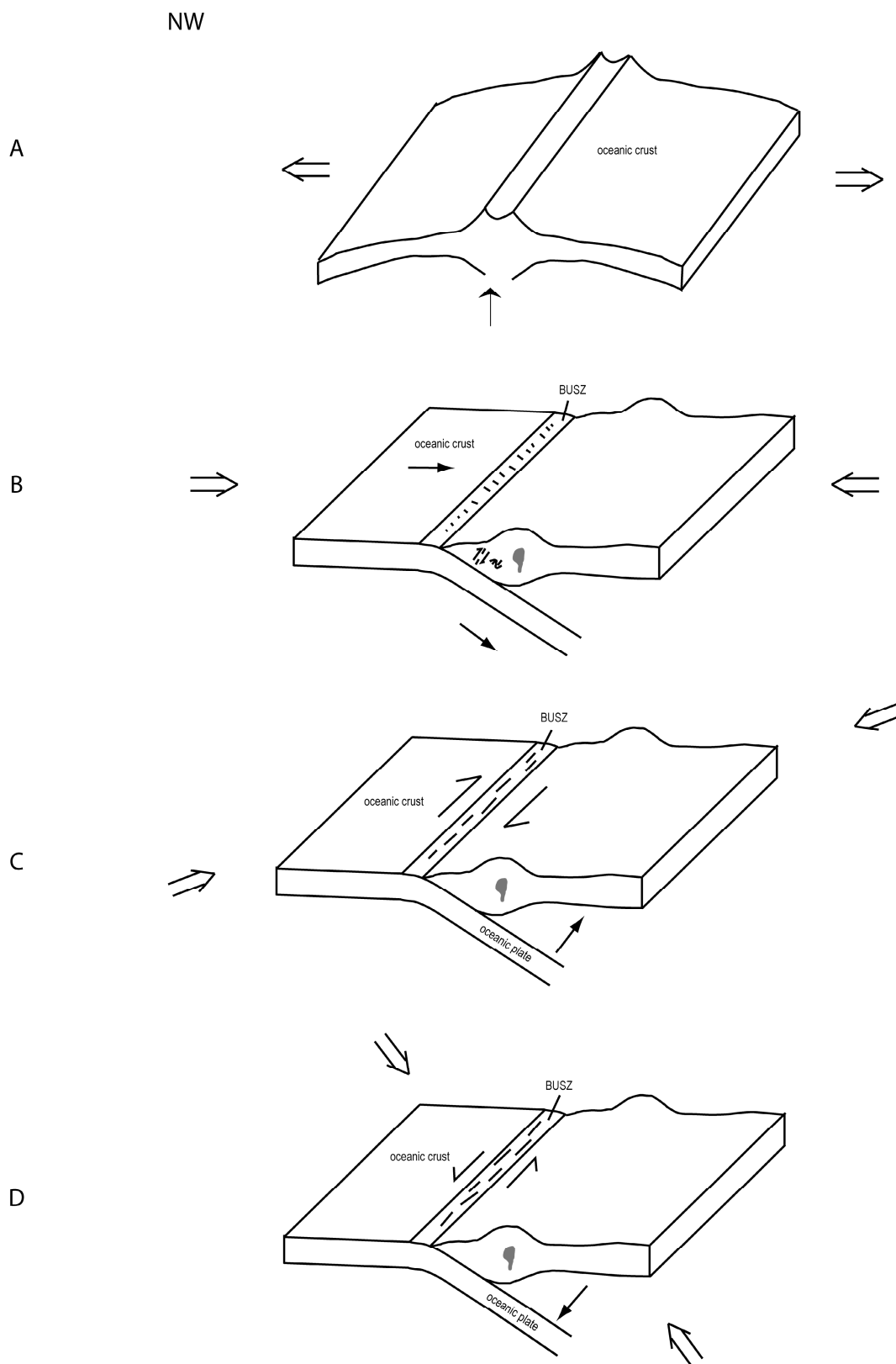


Figure 3-15 The tectonic evolution of the Bi'r Umq Complex: (a) Formation of an ophiolites recorded by the presence of ultramafics; (b) Subduction and arc-accretion led to thrusting during NW-SE compression in the BUC; (c) A change in plate-motion results in WNW-ESE compression as recorded by dextral transpressional strike-slip movement along the BUSZ during continuing arc-accretion; (d) Another change in plate-motion results in shear reversal along the BUSZ results in NNE-SSW compression.

(Ernst, 2003). The emplacement of ophiolites at a Pacific orogenic belt is characterized by presence of large amounts of island-arc remnants (in the form of island-arcs and suspect terranes), HP metamorphism, a small range of ages, calc-alkaline magma associated with emplacement and the presence of paired metamorphic belts (Ernst, 2003). The differences are related to the fact that at Alpine orogenic belts parts of continental crusts are subducted together with the oceanic lithosphere (Ernst, 2003). This typically happens in smaller oceanic basins that are close to continental margins (Ernst, 2003; Wakabayashi and Dilek, 2003). During Pacific-type orogenies, enormous amounts of oceanic crust with island-arcs are subducted and this leads to the extensive calc-alkaline magmatism (Ernst, 2003). This type of ophiolite emplacement is often associated with arc-accretion (Wakabayashi and Dilek, 2003). The Bi'r Umq Complex and its surrounding areas display mainly geological features that can be associated with emplacement during a Pacific-type orogen, as the island-arc remnants of the Hijaz Terrane and the Jiddah Terrane, a small range of ages, a lack of UHP metamorphism and abundant calc-alkaline intrusives. The ophiolites would be thrust into the accretionary prism during subduction of the oceanic crust below the overriding plate. The subduction that caused the emplacement the ophiolites took place at 820-760 Ma. In this period no subduction at was recorded an active continental margin in the ANS (see chapter 2). The emplacement of the ophiolite of the Bi'r Umq Complex should thus have taken place at an island-arc.

It is generally accepted that the ANS went through a period of subduction and arc-accretion from ca. 800-620 Ma (see Chapter 2 and references within). The structures of D1, D2 and D3 in the Bi'r Umq Complex were thus formed in a period when the Shield was mainly experiencing compression through subduction processes and arc-accretion. The D1-phase of NW-SE compression fits well into the arc-accretion along the NW-SE trending ophiolitic sutures that took place at ca. 800-700 Ma in the Arabian Nubian Shield (see Chapter 2). This phase should thus also have been responsible for the initial emplacement of the ophiolitic rocks of the Bi'r Umq Complex. The timing of the deformation of D2 and D3 indicates that these deformation phases also took place during the arc-accretion along the NE-SW trending sutures in the ANS. Consequently, the WNW-ESE directed  $\sigma_1$  of D2, that caused the dextral strike-slip with a minor transpressional component along the BUSZ, resulted from WNW-ESE compression. The NNE-SSW directed  $\sigma_1$  of D3, which caused sinistral movement with a minor transtensional component on the same ENE trending BUSZ, resulted from NNE-SSW compression.

The changes in the style of deformation, from thrusting to strike-slip deformation (with oblique components), during arc-accretion, is commonly observed in "traditional arc-accretion" systems such as those that were form during the Mesozoic and Cenozoic in western North America (e.g. Oldow et al., 1989; Cole et al., 1999; Wolf and Saleeby, 1992). As an example, the accretion of the Wrangelia Terrane to Southern Alaska, from 85 to 55 Ma, went through an era of pure shortening, and was followed by strike-slip movement at the later stages of arc-accretion (Cole et al., 1999). The shift in the compression-field during the Wrangelia accretion onto Alaska was related to a change in plate motion of the subducting plate (Cole et al., 1999).

Table 3-1 Table with the main Neoproterozoic geological events in the Bi'r Umq Complex.

<b>Main geological and deformation phases in the Bi'r Umq Complex</b>				
<b>Phase</b>	<b>Lithology</b>	<b>Metamorphism</b>	<b>Structures produced</b>	<b>Age constraints (in Ma)</b>
Ophiolitic phase	Chert, basalt, peridotites (now as carbonated ultramafic), harzburgite (now as serpentinite)	N/A	None.	> 820
D1	Serpentinite, greenschist, diorites in Jiddah Terrane	greenschist	F1 folds, S1, L1, reverse shear indicators (thrusting) -> NW-	820-760
D2	N/A	Very low greenschist	SE compression L2, dextral shear indicators -> WNW-ESE	820-760
D3	N/A	Brittle	compression Sinistral shear indicators -> NNE-SSW $\sigma_1$	820-760

Strike-slip movement with oblique components is commonly associated with oblique subduction during Pacific-style arc-accretion (Oldow et al., 1989). As an example, the Kings River Ophiolite in Western U.S.A. recorded a component of transpressional strike-slip movement during subduction and arc-accretion in the early Mesozoic during the Cordilleran Orogeny (Saleeby, 1982). Transtension along strike-slip faults was also observed during arc-accretion and during subduction at Pacific-style orogenies. Examples for this type of deformation have been described for the Cenozoic in the Pacific Northwest and Alaska in North America (Oldow et al., 1989), the Nevadan Orogeny (Saleeby, 1982; Shervais et al., 2005) and faulting that was related to the subduction of the Cocos Ridge beneath Costa Rica (Fisher et al., 1994). The shift from compression to transtension during the Nevadan Orogeny in the North American Sierra Nevada was also attributed to the changes in plate-motion, in this case by a change in plate motion of the subducting Proto-Pacific plate (Wolf and Saleeby, 1992).

As demonstrated above, the combination of an ophiolitic sequence with a deformation history of thrusting followed by strike-slip movement (with an oblique component) is typical for "ophiolitic sutures" related to obduction of oceanic crust followed by the closure of an oceanic basin along a subduction zone during arc accretion. The obduction of a fragment of oceanic crust and emplacement within the overriding plate took place through thrusting during D1 in the BUC in a NW-SE to NNW-SSE compression regime. The abundance of arc-related

igneous rocks to the south of the Bi'r Umq Complex, would imply a SE dipping subduction zone during D1. Continuing subduction with changes in the direction of plate motion led to dextral strike-slip movement with a transpressional component (D2). Sinistral strike-slip shear reversal occurred at brittle-ductile conditions (D3), reflecting another change in the trend of plate motion and consequently a change in the trend of collision of an oceanic plate upon the new continental plate, following incorporation of the Bi'r Umq ophiolitic complex.

It should be noted that the Bi'r Umq Suture in the Saudi Arabian part of the Arabian-Nubian Shield, of which the ENE-trending BUSZ is the main structural remnant in the BUC, and the Nakasib Suture, which is the Sudanese continuation of the Bi'r Umq Suture, trend NE-SW (see Figure 3-1). No description exists in generally available literature for shear related lineations in other parts of the Bi'r Umq Suture and the Nakasib Suture. It is however generally assumed that the initial movement on the Nakasib and Bi'r Umq Sutures (named D1 in most studies) was related to NW- or SE-vergent thrusting (e.g. Abdelsalam and Stern, 1993; Abdelsalam and Stern, 1996; Wipfler, 1996; Johnson et al., 2002). These NW- and SE-vergent thrusts were formed during NW-SE compression, parallel to the D1-phase in the Bi'r Umq area. Because the earliest phase of deformation in the Bi'r Umq area and in the other parts of the Bi'r Umq and Nakasib Sutures are parallel, it can be concluded that during D1, the BUSZ was already trending WSW-ENE, at a small angle with the general NE-SW trend of the Bi'r Umq and Nakasib Sutures. Most studies of the Nakasib and Bi'r Umq Sutures also indicate that early thrusting was followed by a major phase of dextral transpression (e.g. Abdelsalam and Stern, 1996; Wipfler, 1996; Johnson et al., 2002) as observed for the D2-phase in the Bi'r Umq area.

Summarizing, it can be concluded, from the geological observations that were presented in this chapter, that the main geological features observed in the Bi'r Umq Complex, an ophiolite that recorded thrusting and significant phases of (oblique) strike-slip movement, justify the interpretation as an ophiolitic suture that was obducted during arc-accretion in the Neoproterozoic. The time-spans and the shifts in compression-fields are similar to those observed in "traditional arc-accretion" systems. The Bi'r Umq Suture, of which the Bi'r Umq Complex is part, represents the contact between the Jiddah Terrane and the Hijaz Terrane. Both terranes consist of remnants of island-arc complexes (Johnson et al., 1987; Stoesser and Camp, 1985). The deformation that was recorded in the Bi'r Umq Complex should thus reflect the kinematics that was responsible for the emplacement of the ophiolites of the Bi'r Umq Complex and the juxtaposition of the Jiddah Terrane and the Hijaz Terrane. Since ophiolite-emplacement and the juxtaposition of terranes should have been taken place in a relatively short time-interval of less than 50 Ma, they should be related to each other.

The following tectonic model is suggested for the Bi'r Umq Complex:

- 1) An oceanic sequence was formed at a fore-arc or back-arc before 820 Ma. Ultramafics, basalts and cherts are remnants of this phase.



2) After ca. 820 Ma, obduction of a fragment of oceanic crust started in a NW-SE trending compressional field due to SW-directed subduction and caused emplacement of the ophiolite in the overriding plate. The D1-phase of deformation resulted in the formation of a shear zones at the border of *Mahd Group* and the Bi'r Umq Complex and within the Bi'r Umq Complex. The NW-SE to NNW-SSE compression resulted in the formation of folds with an axial planar cleavage outside the shear zones. The emplacement of the ophiolite took place at an island-arc. The NW-SE compression was also described in literature for other parts of the Bi'r Umq Suture, and its Sudanese continuation, the Nakasib Suture.

3) Dextral strike-slip deformation with a minor transpressive component (D2) overprinted the thrusting phase (D1). During this phase, the BUSZ was steepened. Strike-slip movement is a common feature at the later stages of arc-accretion. This is for example observed in the ophiolites of Western North America. D2 took place during WNW-ESE compression. A change in plate motion causes the observed structural changes in the shear zones of the Bi'r Umq Complex.

4) A second change in plate-motion resulted in shear reversal along the Bi'r Umq Shear Zone. Brittle structures that were formed during sinistral strike-slip with a minor transtensional component overprinted D2-structures. This phase of deformation was referred to as D3. This phase took place during NNE-SSW compression.



## **Structural, geochemical and geochronological constraints on the tectonic evolution of the Tabalah and Wadi Tarj areas, central Asir, western Saudi Arabia**

### **Abstract**

The Tabalah and Wadi Tarj areas in the central part of the Neoproterozoic Asir Terrane in Saudi Arabia, display typical intra-terrane features. The Tabalah and Wadi Tarj areas contain gabbros and quartz-diorites, which were intruded in an island arc, and tonalites and granodiorites, which were formed during subduction at an active continental margin. These rocks were deformed during two phases of deformation: D1 and D2 as recorded by the Tabalah/Ta'al Shear Zone. The D1-phase displayed thrusting as illustrated by steep lineations and hanging wall over footwall shear sense indicators. This phase was dated at 779Ma and resulted from E-W compression. The D2-phase displayed dextral strike slip and resulted from NNE-SSW compression. This event was dated at 765 Ma. A granodiorite that displayed characteristics of intrusion at an active continental margin, was dated at 761 Ma.

Early intrusives were intruded in an island-arc environment. The observed deformation phases and late intrusions in the Tabalah and Wadi Tarj area are best explained as intra-terrane deformation and magmatism that resulted from arc-accretion. The change in the directions of compression from D1 to D2 can be best explained by an anti-clockwise change in plate motion of the subducting plate during the arc-accretion.

### **4.1 Introduction**

The formation of the Neoproterozoic Arabian Shield is thought to be a result of arc-accretion of mainly juvenile crust, formed in island-arcs and in oceanic basins (see chapter 2). The terrane concept for the Arabian Shield was based on lithological and geochemical observations (Stoeser and Camp, 1985; Johnson et al., 1987). However few structural studies were performed, which have been important for other areas where arc-accretion was established as in the North American Cordillera. It is only recently that Johnson (1998) and Johnson and Kattan (1999a, 1999b) have demonstrated the importance of such studies in the Arabian Shield, by describing the structural features of thrusts and strike slip zones that were related to arc-accretion. The shear zones, related to the arc-accretion, are represented by NE-SW trending linear belts, and ophiolitic sutures, such as the Bi'r Umq Suture and the N-S trending Nabitah Fault Zone.

The aim of this chapter is to improve the understanding of what happened during island-arc formation and arc-accretion in the Arabian-Nubian Shield. In order to achieve this, a detailed study was undertaken of an area that includes the "traditional" intra-terrane features of a Neoproterozoic terrane.

The Asir Terrane (see Figure 4-1) is the largest and most deformed terrane of the Arabian Shield (Stoeser and Camp, 1985). The Tabalah/Wadi Ta'al "Tectonic Zone" is one of the main intra-terrane structures of the Asir Terrane and is found in the central part of this terrane. Two key-areas on the Tabalah/Wadi Ta'al "Tectonic Zone" were chosen for detailed research, namely the Tabalah and Wadi Tarj areas (see Figure 4-1). These areas display lithologies that are typical of the Neoproterozoic in the Arabian Shield, namely different types of igneous rocks like diorite/gabbro complexes, tonalites and granodiorites (Ernst Anderson, 1977; Greenwood et al., 1986). These rock-types are believed to reflect intrusives related to intra-oceanic and continental subduction (Ernst Anderson, 1977; Greenwood et al., 1986).

The main study area was the Tabalah area, located in the northern central part of the Asir Terrane, some 30-40 km southwest of Bishah (Figure 4-1). The Wadi Tarj area is located 20 km south of the Tabalah area (Figure 4-1). The Tabalah/Wadi Ta'al "Tectonic Zone" is the major structure that runs through the Tabalah and Wadi Tarj areas. In the Tabalah area, the Tabalah/Wadi Ta'al "Tectonic Zone" is represented by a NNW-SSE trending zone of intense ductile deformation. There is a minor bend in the Tabalah/Wadi Ta'al "Tectonic Zone" between the Tabalah and Tarj areas and therefore it trends NW-SE in the Wadi Tarj area. The Tabalah/Wadi Ta'al "Tectonic Zone" is a ca. 5 kilometres wide and over 100 kilometres long in total. Ernst Anderson (1977) and Greenwood et al. (1986) mapped the Tabalah/Wadi Ta'al "Tectonic Zone" in the Tabalah area as two separate "Tectonic Zones", the Tabalah "Tectonic Zone" and the Wadi Ta'al "Tectonic Zone". In the Tabalah area, Greenwood et al., (1986) mapped 5 km or less deformed sequence between the two main tectonic zones. Towards the south, in the Wadi Tarj area, the Tabalah/Wadi Ta'al "Tectonic Zone" grades into one intensely deformed belt and is named "Tabalah Tectonic Zone" (Greenwood et al., 1986).

Most authors believe that these linear belts of intense deformation are relicts of faulting, and therefore refer to them as shear zones (SZ). The Tabalah "Tectonic Zone" was thought to result from "wrench tectonics" (Greenwood et al., 1986). Deformation on the Wadi Ta'al "Tectonic Zone" was attributed to thrusting (Greenwood et al., 1986).

This chapter presents results of field-, microscopical, geochemical and geochronological studies. It will be shown that the Tabalah area contains one broad shear zone instead of the two separate "Tectonic" zones that were described by Greenwood et al. (1986). It is concluded that thrusting at ca. 779 Ma is the oldest deformation phase that occurred in the studied areas. The thrusting took place during subduction at an active continental margin and allowed the accretion of island-arcs onto a continental mass. Intra-terrane strike-slip movement on the Tabalah/Wadi Ta'al SZ followed the thrusting-phase. The strike-slip movement was dated at ca. 765 Ma and took place during continuing subduction at the margin of the terrane. Finally, at ca. 761 Ma a granodiorite has been intruded. This granodiorite shows characteristics of intrusion at an active continental margin.

The results from study of the Tabalah and Tarj areas will be integrated in Chapter 6 with results from the studies of other areas that were performed in the framework of this thesis, and will be integrated with data from other key areas of the Arabian-Nubian Shield.

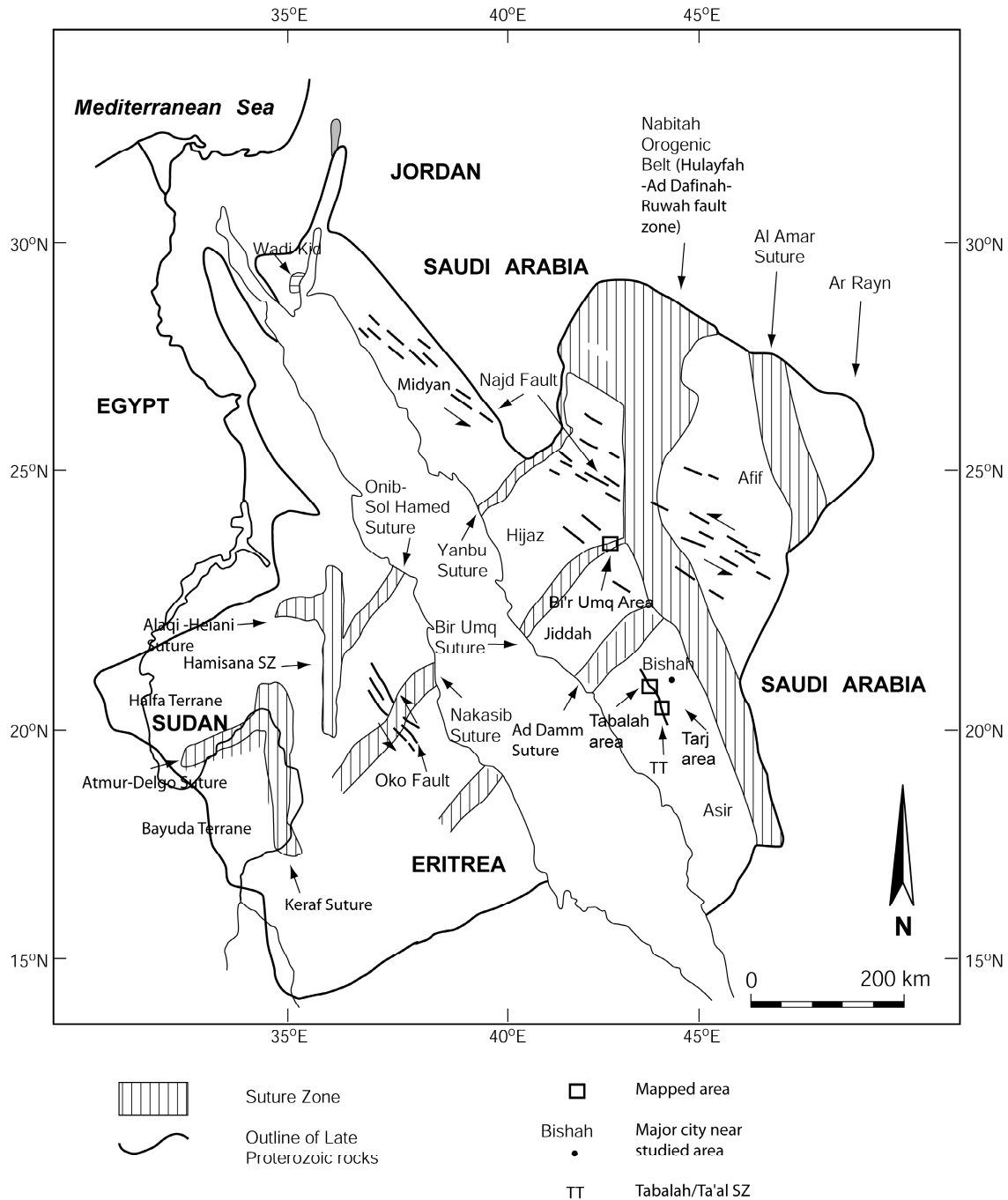


Figure 4-1 Map of the Arabian Nubian Shield that displays the location of the Tabalah and Wadi Tarj areas. TT = Tabalah/Wadi Ta'al Tectonic zone.

## 4.2 Geological Background

### 4.2.1 Lithology

The Tabalah and Wadi Tarj areas consist of undeformed and deformed intrusives and schists which are typical for the Asir Terrane as described by Brown et al. (1989). Figure 4-2 shows the main lithologies and structures of the Tabalah area and Figure 4-3 shows the main lithologies and structures of the Wadi Tarj area. The western and eastern parts of the Tabalah area and large parts of the Wadi Tarj area consist of a *mixed gabbro-diorite suite*. The *mixed gabbro-diorite* consists of gabbro rich in pyroxene, with plagioclase and hornblende, and diorite containing plagioclase, hornblende, biotite and quartz. In the Wadi Tarj area, the *mixed gabbro-diorite suite* has a mainly dioritic composition.

The rocks of the *mixed gabbro-diorite suite* are generally undeformed but locally a foliation and a lineation have developed. These ductily deformed NNW-SSE striking bands have thicknesses of 0.5 meter up to 25 meter and are dipping steeply to the ENE. The deformed layers within the *mixed gabbro-diorite suite* are phyllitic. The rocks of the *mixed gabbro-diorite suite* become increasingly foliated towards the schists of the main Tabalah/Wadi Ta'al Shear zones. Here, they grade into hornblende-biotite schists.

The *quartz diorite-tonalite* occupies the central part of the Tabalah area and is found between what was referred to as the Tabalah Shear Zone and Wadi Ta'al Shear zone by Greenwood et al. (1986). This rock is a rather uniformly massive, medium- to coarse-grained linear body that is parallel to the "shear zones". It contains plagioclase, quartz, hornblende and minor amounts of biotite. Occasionally this rock type contains mafic xenoliths. The *quartz diorite-tonalite* is well foliated and lineated. It is strongly deformed in many places and in these places, it grades into quartzo-feldspathic schist that is similar to the quartzo-feldspathic variety of the *amphibolite* described below.

An undeformed homogeneous *diorite* intrudes deformed gabbro and biotite-schist in the southwestern part of the Tabalah area. This *diorite* is very rich in plagioclase and relatively low in mafic constituents.

A large undeformed homogeneous *granodiorite* body was observed in the southern Wadi Tarj area. It consists of plagioclase, hornblende and minor amounts of quartz. Intrusive and structural relations indicate that the *granodiorite* is the youngest feature in this area.

The *amphibolites* are found in the Tabalah and Wadi Ta'al Shear Zones, in contact with the less- to non-deformed *mixed gabbro-diorite suite* and the strongly deformed *quartz diorite-tonalite*. There are two components to the *amphibolites*: a hornblende-biotite schist and a quartzo-feldspathic schist. The hornblende-biotite schist is rich in hornblende, biotite, plagioclase and minor quartz. These components are observed in all zones of *amphibolites* in the Tabalah and Wadi Tarj areas. Occasionally, clasts of diorite (up to 5 cm in diameter) are found within the biotite-hornblende schists. The quartzo-feldspathic schists are very rich in plagioclase and quartz and contain some minor hornblende and biotite. Locally, schists with an intermediate composition were observed. At the northwestern part of the Tabalah area, a garnet-biotite schist was found in the *amphibolites*. Most of the schists are fine-grained,  $\pm 0.1$  mm, but also a coarser variety is observed with grain sizes of approximately 0.5 mm. In places, the

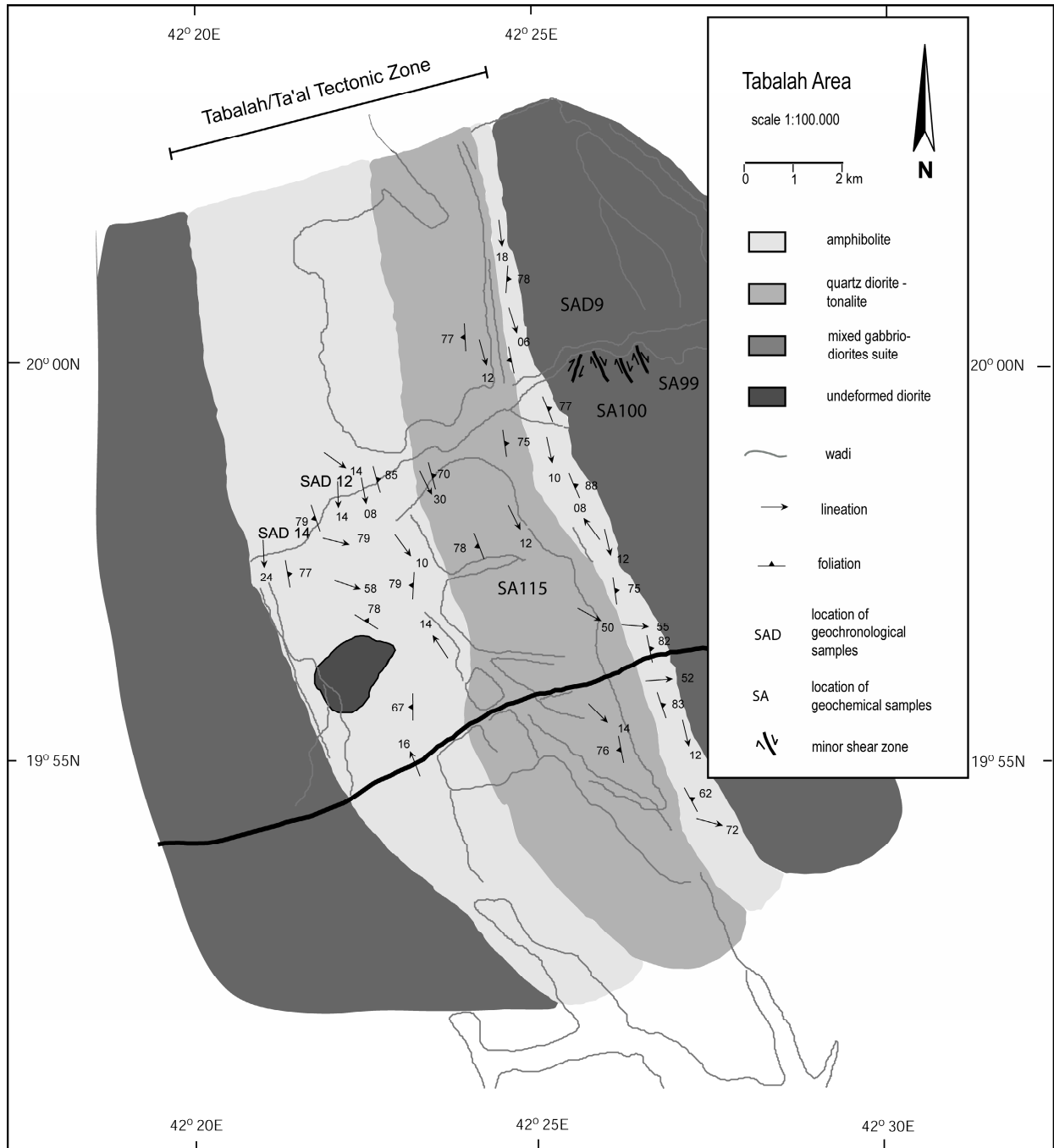


Figure 4-2 Geological map of the Tabalah area (1:100.000).

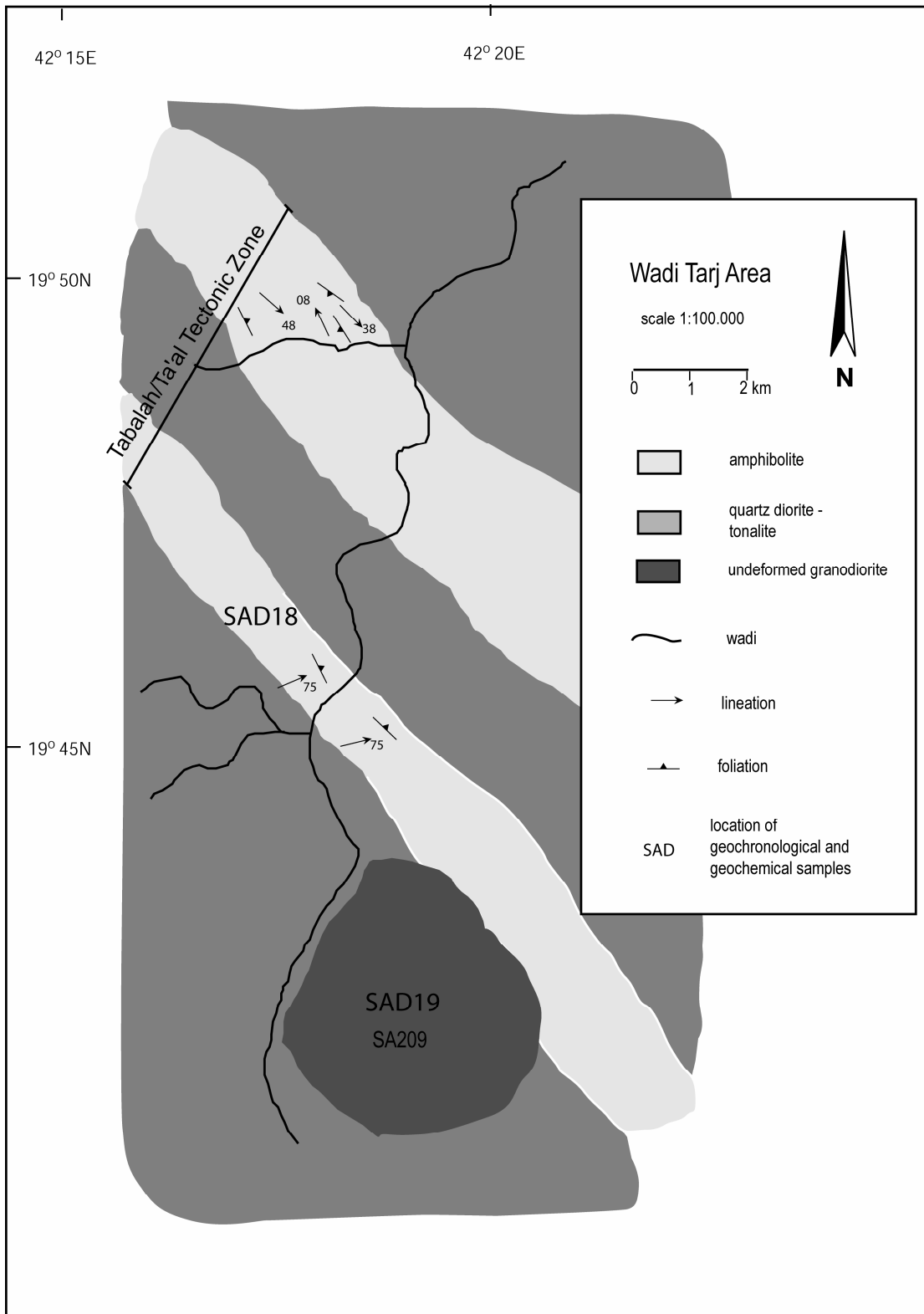


Figure 4-3 Geological map of the Wadi Tarj area (1:100.000).



*amphibolites* were found interlayered with *quartz diorite-tonalite*, often close to the contact with the main *quartz diorite-tonalite* body. Locally, the *amphibolite* has a gneissic appearance with alternating dark and light coloured bands of approximately 1 to 10 cm thickness. The dark bands consist of fine to coarse hornblende-rich schistose rock. The light coloured bands consist of plagioclase- and quartz rich schistose rocks with minor biotite and hornblende. Occasionally, less deformed parts of *gabbro-diorite suite* and *quartz diorite-tonalite* are found in the schists of *amphibolite*.

A small number of *dykes* was observed. They are slightly to non-foliated and have an andesitic to a basaltic composition with large amounts of plagioclase and minor amounts of hornblende and biotite. They intrude the *mixed gabbro-diorite suite*, *quartz diorite-tonalite* and the *amphibolite*. The dykes strike W-E in the western part of the Tabalah area but have more NW-SE trend in the eastern part (Greenwood et al., 1986).

#### 4.2.2 Metamorphism

The metamorphic conditions were deduced from microscopical studies. The schists of the *amphibolites* and the *quartz diorite-tonalite* display evidence of metamorphism and are thus the only ones for which the metamorphic conditions were assessed. The *mixed gabbro-diorite suite* preserved its primary igneous texture and mineralogy, however locally pyroxene has been replaced by green hornblende. Bluish-green hornblende, as observed in the *amphibolites* and the *quartz diorite-tonalite*, is typical for metamorphic conditions of lower amphibolite facies with relatively low to medium pressure and medium temperature conditions (Miyashiro, 1994). Brown hornblende, which indicates a higher temperature than the bluish-green variety, is only observed in the *amphibolites* at the Wadi Tarj area. Deformation in the *amphibolites* in the latter area occurred thus at intermediate amphibolite-facies conditions. The thin schistose bands in the otherwise undeformed *mixed gabbro-diorite suite* are generally rich in green hornblende and contain minor amounts of biotite. The presence of green hornblende indicates that these rocks were also formed at lower amphibolite grade.

It can be concluded that generally deformation took place at low to intermediate amphibolite grade. Typical temperatures for such grade are 450-530° C and pressures of 4-8 kbar (Miyashiro, 1994). In the Wadi Tarj area, the presence of brown hornblende indicates a slightly higher temperature, at about 550 C (Miyashiro, 1994).

### 4.3 Structural Geology

#### 4.3.1 Introduction

This section will focus on the ductile structures in the Tabalah area and the Wadi Tarj area. The main structures in the studied areas are the Tabalah and Wadi Ta'al SZ. As stated in the introduction, the Wadi Ta'al SZ was previously interpreted as a thrust (Greenwood et al., 1986). The Tabalah SZ was interpreted as a strike slip fault with sinistral sense of movement that post-dated movement on the Wadi Ta'al SZ (Greenwood et al., 1986).

The belt of *amphibolites* represents the most highly deformed zone in the Tabalah and Wadi Tarj area. The *quartz diorite-tonalite* in the Tabalah area, between the Wadi Ta'al and Tabalah shear zones, is also foliated and lineated and, as will be demonstrated in this chapter, is part of the shear zone-complex. The thickness of the Tabalah SZ is ca. 800-1200 m. The Wadi Ta'al SZ is slightly thicker: 1200 – 2000 m. The total thickness of the foliated sequence, including the *amphibolites* and the *diorite-tonalite*, is about 6-10 km in the Tabalah area (Figure 4-2). Here, the main shear zones trend NNW-SSE (Figure 4-2). The total thickness of the foliated sequence in the Wadi Tarj area is ca. 3-4 km (Figure 4-3). In the Wadi Tarj area, the main structure trends NW-SE (Figure 4-3).

Foliated bands occur within the mainly non-deformed *mixed gabbro-diorite suite*, adjacent to the Tabalah SZ. Their thickness ranges from 0.5 meter, in the eastern part of the area, up to 50 meters close to the main shear zone. The fact that the *mixed gabbro-diorite suite* and the *quartz diorite-tonalite* grade into the deformed units and that relicts of the *mixed gabbro-diorite suite* and the *quartz diorite-tonalite* are found in the deformed units indicates that the *amphibolites* are the deformed equivalent of the *mixed gabbro-diorite suite* and the *quartz diorite-tonalite*.

#### 4.3.2 Foliations

The *amphibolites* and the *quartz diorite-tonalite* form a well-foliated sequence. The foliation is mainly defined by biotites and by flattened recrystallised quartz grains. The foliation in the Tabalah area is steeply dipping to ENE to vertical and strikes NNW-SSE (Figure 4-4). The foliation trend in the *quartz diorite-tonalite* has the same trend as the foliation in the *amphibolites*. The foliations of the thin schistose layers within the *mixed gabbro-diorite suite* also have a similar trend as the main foliation. The contact between the foliated rocks and the undeformed rocks is gradational. In the Wadi Tarj area the foliation shows a NW-SE trend and dips NE (Figure 4-3 and Figure 4-5). The difference in the trend of foliation between the Tabalah area and the Wadi Tarj area is best explained by the fact that the overall trend of the main structure changes slightly from the Tabalah area to the Wadi Tarj area. Throughout the Tabalah and Wadi Tarj areas, no evidence of regional folding was found.

#### 4.3.3 Lineations

Lineations are observed on the foliation-planes of the *amphibolites* and the *quartz diorite-tonalite*. They are mainly defined by growth of minerals and occasionally by the stretching of minerals and stretched xenoliths. The growth of hornblende in a uniform direction represents the mineral lineation. The hornblendes are up to 0.5 cm long. However, in the southern part of the Wadi Tarj area, larger hornblendes were observed. Quartz, plagioclase, hornblende and biotite form the stretching lineation and are parallel to the mineral lineation that is defined by hornblende. Figure 4-6 shows that the lineation in the Tabalah area trends mainly sub-horizontally NNW-SSE. A secondary maximum shows lineations plunging steeply to E to ESE (Figure 4-2 and Figure 4-6). Rarely, randomly orientated hornblendes were also observed near the undeformed diorite of the SW Wadi Tabalah area. This may indicate some form of late thermal overprint due to the intrusion of this diorite. Mineral lineations in the Wadi Tarj area

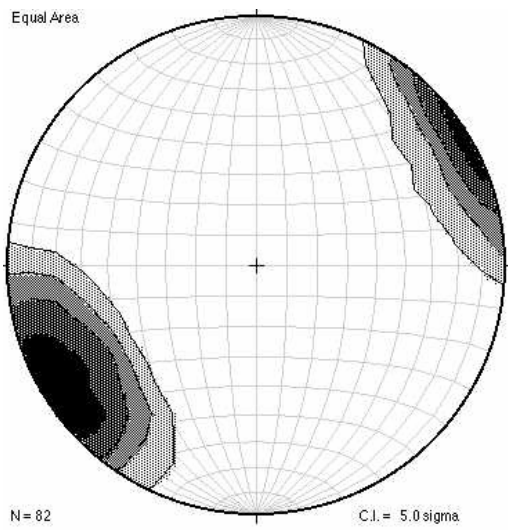


Figure 4-4 Poles to the foliation in Tabalah area.

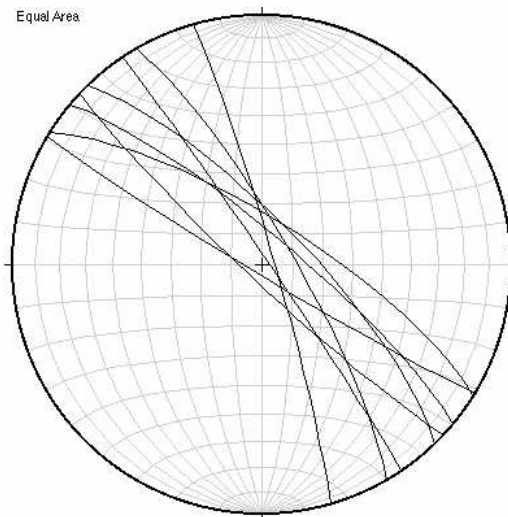


Figure 4-5 Foliation in the Tarj area.

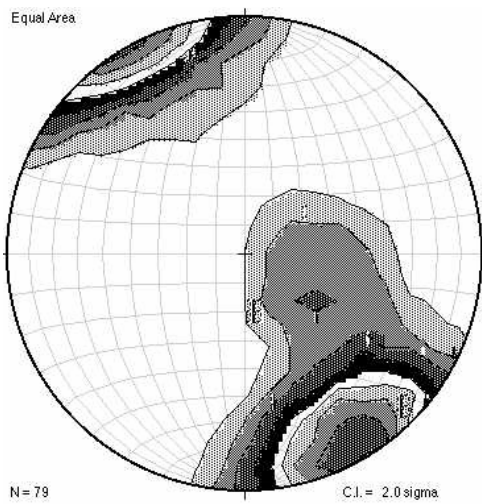


Figure 4-6 Contour of lineations in the Tabalah area.

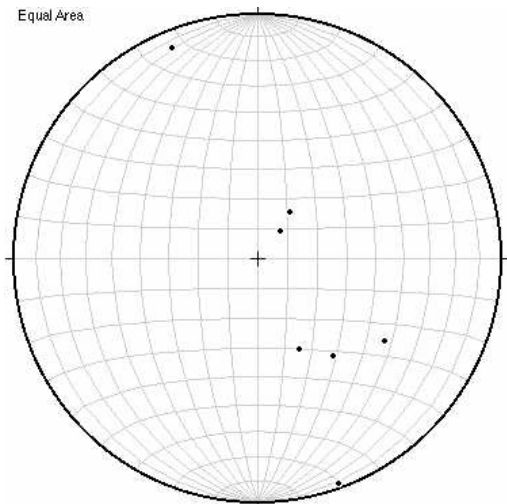


Figure 4-7 Lineations in the Wadi Tarj area.

plunge generally moderately SE and steeply ENE (Figure 4-3 and Figure 4-7). These differences in the trends of lineations is best explained by the fact that the overall trend of the main shear zone and the foliations has a slightly different trend of the main structure in the Wadi Tarj area than in the Tabalah area. The temporal relations between the steep and sub-horizontal lineations could not be assessed from the observed geological features in the field or through the microscopical studies. It will be further assessed in the geochronological section of the chapter.

#### 4.3.4 Evidence for non-coaxial deformation

A number of indicators of non-coaxial deformation were observed in the schistose units of the Tabalah and Wadi Tarj areas. The *amphibolites* and the *quartz diorite-tonalite* contain these indicators. C-C' fabrics, rotated clasts (Figure 4-8 and Figure 4-10) and mica fish are typical indicators of non-coaxial deformation that are observed in all the schistose units of the Tabalah and Wadi Tarj areas. The C-C' fabrics and "mica-fish" are generally defined by hornblendes. This indicates that the deformation took place at amphibolite-facies conditions. The rotated  $\sigma$ -clasts consist mainly of plagioclase and rarely of pyroxene relicts. The pressure shadows that are associated with the rotated clasts consist of quartz and hornblende. When formed by hornblendes, these strain shadows are of the displacement-controlled type with deformable fibres as described by Ramsey and Huber (1983). Also massive strain shadows were observed containing quartz. Both types of strain shadows indicate simple shear progressive deformation (Passchier and Trouw, 1996).

The shear sense indicators that are associated with the SSE to SE trending sub-horizontal lineation in the Tabalah and Wadi Tarj areas indicate dextral movement. E to ESE moderately to steeply plunging lineations in the Wadi Tarj and Tabalah areas were associated with shear indicators that displayed top-to-the-W movement, which would indicate thrusting in its current position. The temporal relations between the steep and sub-horizontal lineations and their associated non-coaxial shear indicators could not be assessed from the observed geological



Figure 4-8 A rotated diorite clast indicates a dextral sense of shear.



Figure 4-9 An extensional crenulation cleavage indicates dextral sense of shear in one of the minor shear zones east of the main Tabalah SZ.

features in the field or through the microscopical studies. The fact that indicators of non-coaxial deformation were observed in schistose sequences, shows that these have a mylonitic origin.

Evidence for non-coaxial deformation is also observed in the schists that contain NNW-SSE trending foliations and sub-horizontal lineations within the *mixed gabbro-diorite suite*. Macroscopic diorite clasts and C-C' fabrics (Figure 4-9) display dextral movement. Microscopical extensional crenulation cleavages in the minor mylonites of the *mixed gabbro-diorite suite* also display dextral movement.

#### 4.3.5 Conclusions on structural geology

The *amphibolites* and *quartz diorite-tonalite* contain structures that were formed at amphibolite

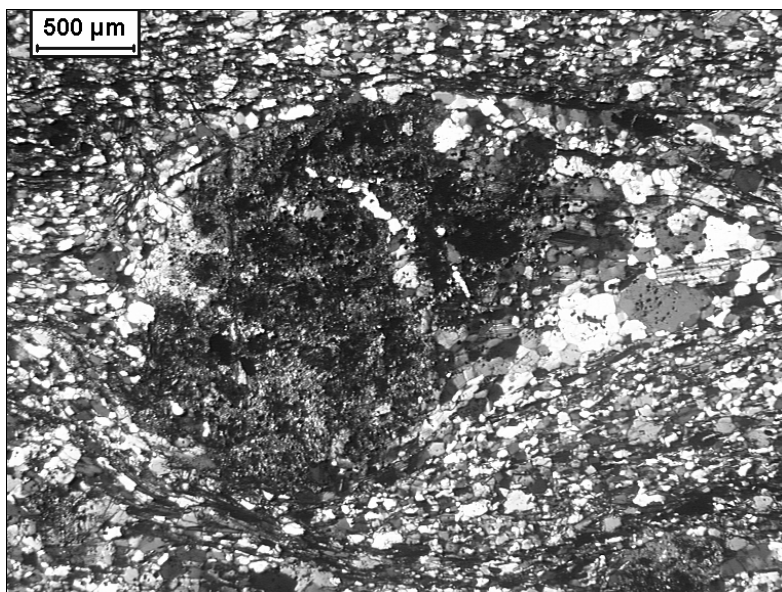


Figure 4-10 Rotated clast with strain shadows indicating dextral movement.

metamorphic grade. A steep NNW-SSE (in the Tabalah area) to NW-SE (in the Wadi Tarj area) striking foliation and a sub-horizontal lineation are the main structural features in these formations. Occasionally, steeply plunging lineations were observed. Top-to-the-W movement was observed along these steeply E-plunging lineations. Dextral strike-slip movement was associated with the sub-horizontal NNW-SSE lineations. Since no temporal relations were observed between the different lineation-trends, it was not possible to assess the temporal relationships between the different phases of shearing. Randomly oriented hornblendes near an undeformed diorite in the SW Tabalah area indicate post-deformational heating at lower amphibolite conditions.

## 4.4 Geochemistry

### 4.4.1 Introduction

Much geochemical research has been performed in the Arabian Nubian Shield and it was used as a basis for many of the existing theories regarding the tectonic development of the Arabian-Nubian Shield (e.g. Schmidt et al., 1980; Bendor, 1985; Jackson, 1986; Brown et al., 1989; Harms et al., 1994; Mohammed and Hassanen, 1996). In order to put the structural and geochronological results in a tectonic framework, a limited geochemical study was undertaken, that can then be used as a reference tool with respect to other studies in the Arabian-Nubian Shield. The results of the geochemical analyses were compared to published geochemical data from the Arabian-Nubian Shield and the interpretations of these published studies were integrated over here.

The magmatic rocks have been generally interpreted to belong to one of the three main phases in the Arabian-Nubian Shield: 1) oceanic phase (sub-divided into island-arc and ophiolitic phases) (Bendor, 1985; Brown et al., 1989; Blasband et al., 2000), 2) arc-accretion

(Brown et al., 1989; Blasband et al., 2000), and 3) late orogenic extension (Blasband et al., 2000). Brown et al. (1989) compared some 500 geochemical analyses and concluded that the plutonic rocks in the Arabian part of the Arabian Nubian Shield can be divided into 3 groups:

- I) The earliest phase of plutonic activity (900–700 Ma) consists of diorites and gabbros that were intruded in island-arcs and gabbros that were related to ophiolitic sequences;
- II) Tonalites and granodiorites intruded during a collisional event around 740-650 Ma;
- III) Granodiorites to granites intruded from 650-550 Ma and were related to the late stages of collision and post-tectonic cratonisation.

#### *4.4.2 Samples*

Five samples, that are representative for the Tabalah and Tarj areas, were analysed for geochemical studies using XRF and ICP-MS. These samples were selected because they represent the main non- to little deformed and non-metamorphosed lithologies from the Tabalah and Wadi Tarj areas (see also Figure 4-2 and Figure 4-3)

- *An undeformed gabbro* (sample SA99; N 20°01.565' E42°15.960') from the *mixed gabbro-diorite suite* in the eastern Tabalah area. It is rich in pyroxene and consists of minor plagioclase, biotite and hornblende. This sample was analyzed because it is one of the main lithologies in the area and pre-dates deformation. Its analysis will give information about the early overall setting of the area.
- *A slightly deformed diorite* (sample SA100; N 20°01.565' E42°15.960') from the *mixed gabbro-diorite suite* in the Tabalah area. The sample consists of plagioclase, pyroxene and minor quartz. Like sample SA99, this sample was analyzed because it is one of the main lithologies in the area and pre-dates deformation, and because its analysis may give information about the initial tectonic regime in the areas.
- *A slightly deformed tonalite* (sample SA115; N 19°59.257' E42°13.539') taken from the *quartz diorite-tonalite suite* in the central Tabalah area. This sample consists mainly of quartz and plagioclase and some minor biotite. This sample is a major rock-type in the area. It was only observed in a slightly deformed state.
- *An undeformed granodiorite* (sample SA209; N 19°43.244' E42°21.969') from the Wadi Tarj area. It consists of hornblende, plagioclase and some quartz and biotite. This granodiorite intrudes the main Wadi Ta'al Shear Zone and should thus give indications on the tectonic setting of the area after the activity on the shear zone ceased.
- *An andesitic basalt* from a dyke (sample SAD9; N 20°01.509' E42°15.392') in the central Tabalah area that trends 120° and intrudes the *mixed gabbro-diorite suite*. It consists mainly of plagioclase and hornblende. This undeformed sample was analyzed because it is one of the youngest rocks in the areas and this should give indications on the later tectonic regime in the area.

#### 4.4.3 Techniques

Only non- to slightly deformed rocks were used for geochemical analyses. The samples were ground in a Tungsten-carbide mill. XRF major element analyses were carried out with a Siemens SRS 3440 spectrometer at Utrecht University, the Netherlands. ICP-MS was used for the trace element analyses. 0.1 of sample powder was dissolved in 4 ml HNO<sub>3</sub>, 3 ml HClO<sub>4</sub>, and 5 ml HF acid, in Teflon bombs. They were heated to 180° C for 5 hours. The samples were analyzed on an Agilent 7500a ICP-MS instrument at Utrecht, the Netherlands. The analyses were undertaken by the staff of the integrated geochemical laboratory of the Faculty of Geosciences at the Utrecht University.

#### 4.4.4 Major elements

The geochemical analysed samples can be classified on the basis of major elements. This classification is used for the comparison with other geochemical studies on the Arabian Nubian Shield. Table 4-1 shows the results of the major-element analyses of the selected rock samples from the Tabalah and Wadi Tar areas. Diagramic representations of the data obtained are shown in Figure 4-1.

Brown et al. (1989) presented the most extensive geochemical overview study of the Arabian Shield to date. Brown et al. (1989) mainly used Na<sub>2</sub>O-CaO-K<sub>2</sub>O diagrams for the classification of their plutonic samples because this type of diagram is suitable for the differentiation between calc-alkaline rocks and others. The analyses of the samples from the Tabalah and Tarj areas were compared to the results of Brown et al. (1989) and followed their interpretations. The *undeformed gabbro* and the *slightly deformed diorite*, both from the *mixed gabbro-diorite* in the Tabalah area, display a similar position in the Na<sub>2</sub>O-CaO-K<sub>2</sub>O diagram (Figure 4-11) as the gabbros and quartz-diorites from the “Jiddah Group” and “Baish-Bahah Group” in Brown et al. (1989; figs 19-21). Brown et al. (1989) interpreted these rock-types to have been formed in an island-arc environment. The *slightly deformed tonalite* and *undeformed granodiorite* display a similar position in the Na<sub>2</sub>O-CaO-K<sub>2</sub>O (Figure 4-11) diagram as the “Halaban Group” and “Culminant-orogeny rocks” of Brown et al. (1989, figs 19-21). Both, the “Halaban Group” and “Culminant-orogeny rocks” consist mainly of granodiorites (Brown et al., 1986). These granodiorites intruded into a thickened crust (Brown et al., 1986), which typically could have formed during arc-accretion. Jackson (1986) and Stoesser (1986) interpreted tonalites and granodiorites diorites in the Arabian-Nubian Shield to have been formed during subduction at continental Andean-type margins and arc-accretion. The *andesitic basalt*, an undeformed dyke, displays a similar position in the Na<sub>2</sub>O-CaO-K<sub>2</sub>O diagram (Figure 4-11) as samples from the “Halaban Group” of Brown et al. (1989) which were related to the arc-accretion.



Table 4-1 Major elements of selected samples from the Tabalah Area measured through XRF (in weight %).

	SAD9	SA99	SA100	SA115	SA209
SiO <sub>2</sub>	48,1	40,7	45,9	64,6	57,1
Al <sub>2</sub> O <sub>3</sub>	13,2	16,0	24,2	15,8	16,1
TiO <sub>2</sub>	2,50	0,94	0,20	0,40	0,71
CaO	10,0	13,9	13,9	4,71	6,92
MgO	5,65	8,44	4,19	1,98	3,80
Na <sub>2</sub> O	2,04	0,67	1,59	3,78	3,25
K <sub>2</sub> O	0,32	0,12	0,20	1,14	1,21
Fe <sub>2</sub> O <sub>3</sub>	15,0	12,8	4,44	3,83	7,13
MnO	0,21	0,12	0,075	0,070	0,11
P <sub>2</sub> O <sub>5</sub>	0,37	0,093	0,11	0,21	0,24
LOI	0,85	2,37	1,80	1,37	0,59

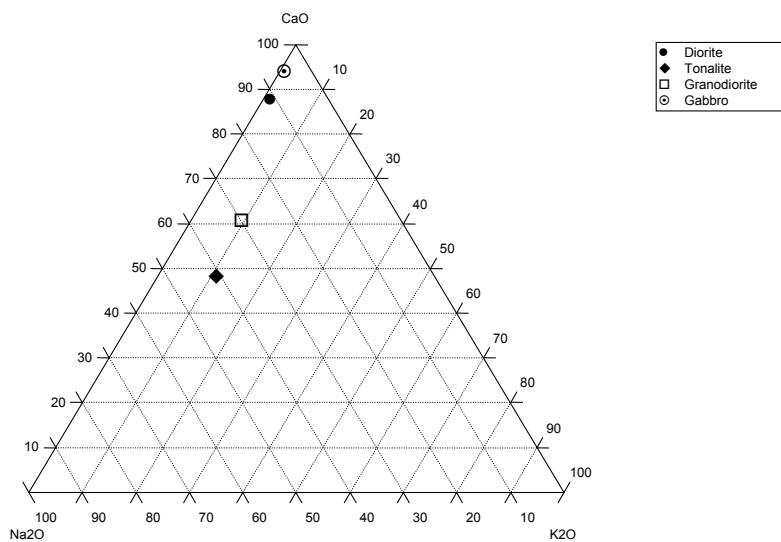


Figure 4-11 Na<sub>2</sub>O-CaO-K<sub>2</sub>O diagram for plutonic samples from the Tabalah and Tarj Complex.

#### 4.4.4 Trace elements

## 4.4.4.1 Introduction

Trace elements are useful in discriminating between magmatic processes and tectonic regimes and have been widely used to assist in tectonic interpretations in the Arabian-Nubian Shield (e.g. Hassanen et al., 1996; Marzouki and Divi, 1989; Mohamed and Hassanen, 1996; Teklay et al., 2002). In this paragraph, the results of the trace element analyses from the Tabalah and Wadi Tarj areas were compared with those of published trace element studies in the Arabian-Nubian Shield. The trace element concentrations for the samples from the Tabalah area are listed in Table 4-2.

The trace elements are presented through N-MORB normalized multi-element diagrams and REE chondrite-normalized diagrams. N-MORB normalized diagrams are especially useful for samples which have originated from of oceanic rocks or underwent an evolution as arc-related rocks from intra-oceanic subduction zones or active continental margins (Rollinson, 1993).

Table 4-2 Trace element analysis through ICP-MS (in PPM).

Sample	SA 99	SA 100	SA 115	SA 209	SAD 9
Rb	1,92	4,16	19,48	28,43	5,21
Sr	215,15	458,98	478,58	346,68	264,32
Y	4,72	4,70	11,42	14,73	63,36
Zr	5,58	6,95	14,08	14,58	144,02
Nb	0,30	0,88	2,92	1,68	8,59
Ba	24,08	68,18	278,88	243,52	97,79
La	0,36	0,79	9,63	9,16	14,78
Ce	1,02	1,90	24,75	22,30	40,95
Pr	0,22	0,32	2,81	3,00	6,39
Nd	1,40	1,60	11,52	13,19	31,96
Sm	0,61	0,56	2,54	3,16	9,33
Eu	0,33	0,50	0,80	0,87	3,07
Gd	0,85	0,74	2,40	3,06	11,07
Tb	0,16	0,14	0,38	0,51	2,00
Dy	1,01	0,93	2,12	2,96	12,18
Ho	0,21	0,20	0,44	0,61	2,67
Er	0,58	0,56	1,28	1,70	7,22
Tm	0,08	0,09	0,20	0,25	1,09
Yb	0,55	0,64	1,39	1,70	6,91
Lu	0,09	0,11	0,24	0,27	1,04
Hf	0,29	0,26	0,76	0,73	4,45
Ta	0,41	1,63	0,43	0,30	1,02
Th	0,03	0,11	2,92	1,72	1,03

The N-MORB normalized diagrams in Figure 4-12 and the REE chondrite-normalized diagrams in Figure 4-13 justify the division into 2 groups of the samples from the Tabalah and Tarj areas:

- I) The undeformed gabbro (sample SA99) and the slightly deformed diorite (sample SA100)
- II) The slightly deformed tonalite (sample (SA115), undeformed granodiorite (sample SA209) and the andesitic basalt from a dyke (sample SAD9)

The samples of *Group I*, namely the samples SA99 and SA100, have the lowest trace element concentrations and both rock-types have identical trace-element patterns (Figure 4-12 and Figure 4-13). The rock-types of *Group II*, namely the samples SA115, SA209 and SAD9 are more enriched in trace elements than the samples of *Group I*. Their trends are similar to each other but differ from the samples from *Group I* (Figure 4-12 and Figure 4-13).

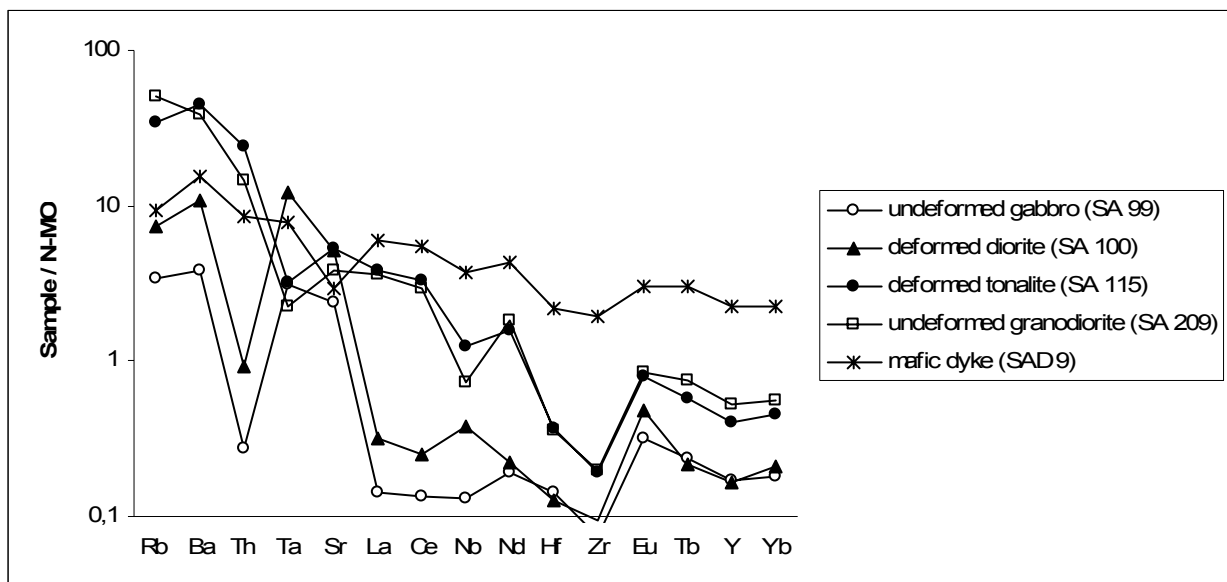


Figure 4-12 N-MORB normalized multi-element diagram for the samples from the Tabalah and Tarj Complex area. N-MORB values from McDonough and Sun (1995).

#### 4.4.4.2 Group I: The undeformed gabbro (SA99) and the slightly deformed diorite (SA100)

The N-MORB normalized pattern for the undeformed gabbro and the slightly deformed diorite show an overall enrichment of the LFS-elements relative to the HFS-elements with a pronounced Th-trough, a notable La-Ce trough for the gabbro and a minor Nb-peak. The REE-pattern for both rock-types of this group displays a slight depletion for LREE relative to the HREE. Both rock-types have a positive Eu-anomaly.

The LFS-enrichment, as observed in the N-MORB patterns of the *Group I* samples of the Tabalah and Tarj areas, is also observed in a number of other gabbro-diorite suites the Arabian Nubian Shield as the gabbro-diorite suite from the Umm Naggat district in the Eastern Desert of Egypt (Mohamed and Hassanen, 1996) and the gabbro-diorite suite from the Ariab complex in Sudan (Schandelmeier et al., 1994). Mohamed and Hassanen (1996) attribute enrichment of the LFS-element enrichment the fact that these elements are easily mobilized by

hydrous fluids that are derived from subducting oceanic crust by dehydration of this subducting slab. The hydrous fluids will then "contaminate" the magma source with LFS-elements. This explanation for LFS-enrichment in island-arc related rocks is similar to the explanation that was put forward by Wilson (1989). Mohamed and Hassanen (1996) further found their samples to plot close to the typical island-arc rock composition in the Nb-Zr-Y tectonic classification diagrams of igneous rocks by Pearce (1982). The gabbro-diorite suite in the Ariab complex was also interpreted to have been formed in an immature island arc (Schandelmeier et al., 1994).

For the samples from *Group I* in the Tabalah and Tarj areas, the diorite has an overall higher trace-element concentrations than the gabbro. This can be best explained by the fact that primitive island arcs will have relatively less enrichment of LFS-elements than the more evolved island arc rocks (Wilson, 1989). Consequently, the undeformed gabbro represents an older immature island arc. Jackson (1986) also indicated that generally island-arc related gabbros in the Arabian Nubian Shield were formed in immature island arcs and the diorites were formed in a more mature island arc

Based on N-MORB normalized diagrams, it can be concluded that the samples of *Group I* are similar to gabbros and diorites from other areas in the Arabian Nubian Shield. They were formed in an island-arc environment. The undeformed gabbro was formed in a younger immature island-arc. The slightly deformed diorite was formed when the island-arc was mature.

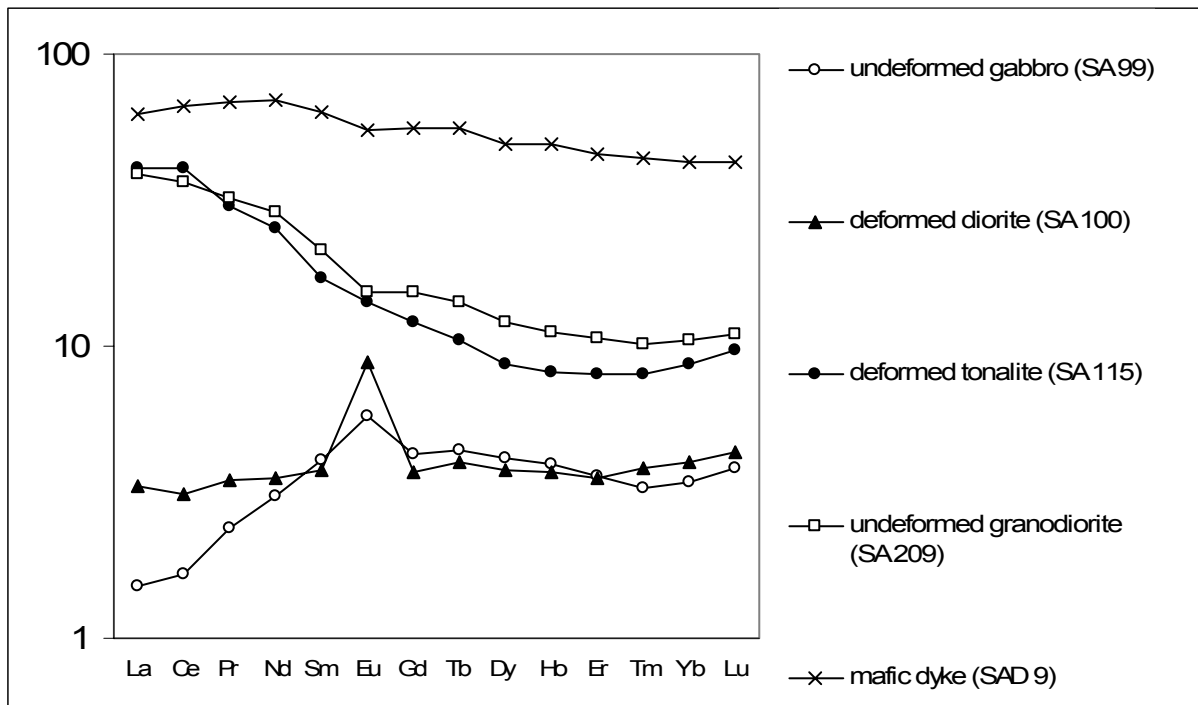


Figure 4-13 Chondrite normalized REE diagram for the samples from the Tabalah and Tarj Complex area. Chondrite values from McDonough and Sun (1995).

4.4.4.3 *Group II: the slightly deformed tonalite (SA115), the undeformed granodiorite and the andesitic basalt from a dyke (SAD9)*

The samples of *Group II* have higher concentrations of trace elements than the samples of *Group I*. The N-MORB patterns display a strong LFS enrichment relative to the HFS elements. The rocks of this group display a Ta trough, an Nb trough, and an Nd peak. The slightly deformed tonalite and the granodiorite are enriched in LREE over HREE. Furthermore, the undeformed granodiorite has a slight negative Eu-anomaly and a slight concavity in the DY-YB region (Figure 4-13).

The LFS-enrichment as observed in the samples of the tonalite and the granodiorite, is found in many geochemical studies of tonalites and granodiorites in the Arabian Nubian Shield. For example, geochemical patterns of the granodiorites and tonalites from the Homrit Waggat and El-Yatima areas, eastern Egypt (Moghazi et al., 1996) and the Roded Complex, southern Israel (Bogoch et al., 2002) resemble the geochemical patterns of those of the Tabalah and Tarj areas. The N-MORB patterns for the granodiorites and tonalites from both of these areas display an enrichment of LFS-elements relative to HFS-elements. The Nb-trough is also observed for both areas. These are typical features for plutonic rocks that are formed at an active continental margin where the LFS-enrichment results from dehydration of this subducting slab Wilson (1989). On the basis of the trace element studies, Bogoch et al. (2002) and Moghazi et al. (1999) interpret the granodiorites and tonalites in their respective areas to have been formed by melting of an amphibolitic crust in a subduction setting. This could typically take place during accretion of an island-arc at an active continental margin (Moghazi et al., 1996).

REE-patterns similar to the intrusives of *Group II* in other parts of the Arabian Nubian Shield, are observed for other granodiorites and tonalites in the Arabian Nubian Shield. The granodiorites and tonalites from the Al Amar-Idsas area, Saudi Arabia (Le Bel and Laval, 1986) and the Keraf area, northern Sudan (Bailo et al., 2003), display enrichment of LREE with respect to HREE, the lack of a significant Eu-anomaly and the concavity in the Dy-Yb region. On the basis of their REE-patterns, these rocks were interpreted to have been formed by melting of an amphibolitic or eclogitic crust (Le Bel and Laval, 1986). Le Bel and Laval (1986) found the REE-patterns of the granodiorites from Al Amar-Idsas area to be similar to subduction-related plutonic rocks in western North- and South America. Bailo et al., (2003) interpreted granodiorites in the Keraf area to be indicative of subduction.

The observed Th-, La- and Ce-enrichment for the intrusives of *Group II* in the N-MORB normalized plots is typical for plutonic rocks that are formed at an active continental margin compared to island-arc related rocks (Wilson, 1989; Tormey et al., 1991). This enrichment is explained by the fact that these elements are typically enriched in a sedimentary or amphibolitic continental crust (Wilson, 1989; Tormey et al., 1991).

The enrichment of LREE relative to HREE is generally attributed to garnet fractionation (Rollinson, 1993). Garnet fractionation can indicate melting of an amphibolitic crust (Rollinson, 1993).

Based on N-MORB normalized diagrams and the REE patterns found in this study and their similarity to those published in other studies in the ANS, it can be concluded that the

granodiorites and tonalites from the Tabalah and Tarj areas are very similar to tonalites and granodiorites in the ANS that were intruded during subduction at a continental margin.

The *andesitic basalt* is the only non-plutonic rock of the analysed samples. This rock-type has generally the highest concentration of trace elements. The MORB-normalized diagram displays an enrichment of LFS-elements relative to HFS elements with a pronounced Nb trough, and a significant Nd peak, similar to the tonalites and granodiorites. The REE normalized diagram shows LREE enrichment relative to the REE and a small negative Eu-anomaly.

Examples of andesitic basalts from other areas in the Arabian Nubian Shield with similar trace element patterns as for sample SAD9, are found in the Bir Safsaf area, south-west Egypt (Pudlo and Franz, 1994) and in Eritrea (Teklay et al., 2002). Trace element studies from both areas display similar trace element patterns as *andesitic basalt* in the Tabalah area. Their N-MORB normalized diagrams display a pronounced LFS enrichment which is explained by the fact that these rocks were formed in a subduction environment (Pudlo and Franz, 1994; Teklay et al., 2002). The negative Nb-anomaly in the Bir Safsaf samples was interpreted to indicate formation at an active continental margin (Pudlo and Franz, 1994).

Poll and Franz (1994) performed model-calculations on REE data from andesitic basalts in the Bir Safsaf area, Egypt, with a similar pattern to the REE-pattern as the andesitic basalt from the Tabalah area. Their calculations show that the andesitic basalts resulted from melting of garnet-bearing peridotite in the lower crust. According to Poll and Franz (1994), this fact together with the negative Nb-anomaly, indicates that these basalts were formed during subduction at a continental margin.

The *andesitic basalt* displays, like the samples of tonalite and the granodiorite, Th-, La- and Ce-enrichments that indicate proximity of a continental crust. The general enrichment of trace elements in the *andesitic basalt* indicates a higher level of fractionation than for the other studied samples from the Tabalah and Tarj areas.

Based on the trace elements, it can be concluded that the *andesitic basalt* is similar to andesitic basalts in other parts of the Arabian Nubian Shield and that were formed at an active continental margin similar to the one where the tonalites and the granodiorites.

## 4.5 Geochronology

### 4.5.1 Introduction

A number of key-samples was dated in order to temporally constrain the tectonic phases that were observed throughout the Tabalah and Wadi Tarj areas. These studies are needed because of the lack of evidence on the relative timing of the observed tectonic events through field relationships. The  $^{40}\text{Ar}/^{39}\text{Ar}$ -method was chosen for the dating because this allows dating of amphibolite-grade as well as plutonic rocks through dating of hornblendes. Furthermore, hornblende has good argon retentivity properties with a closure temperature of 525° C for well

crystallized hornblende (McDougall & Harrison, 1999). The hornblendes in the samples of the shear zones define the highest metamorphic grades found in these rock-types so their dates are expected to define the age for the peak tectono-metamorphic event.

The samples from the Tabalah and Wadi Tarj areas were crushed, sieved and washed before the actual mineral separation. Sieve fractions of 250-500 $\mu$ m and 125-250  $\mu$ m were used for hornblende separation with a roll-magnet. The fractions that remained after the separation, were cleaned ultrasonically in demineralised water. Approximately 15 grains of cleaned hornblende were hand-picked microscopically. The samples were irradiated at the ECN/EU high flux nuclear reactor in Petten, The Netherlands. I analysed the samples at the geochronological laboratory of the "Vrije Universiteit", Amsterdam, The Netherlands. The step-heating degassing experiments were carried out with an argon laserprobe as described by Wijbrans et al. (1995). The age- and error-calculations for  $^{40}\text{Ar}/^{39}\text{Ar}$  in hornblende were done as discussed in detail in McDougall and Harisson (1999). A short outline of previous geochronological studies will be given first.

#### 4.5.2 Previous geochronology studies

Previous geochronological data are only available for the intrusives. Diorites in the Wadi Tarj area were dated at 818 $\pm$ 95 Ma (Rb-Sr whole rock by Fleck et al., 1980). A quartz-diorite/granodiorite southeast of Bisha was dated at 723 $\pm$ 107 Ma (Rb-Sr whole rock by Fleck *et al.*, 1980). A granodiorite north of Bisha was dated at 623 $\pm$ 18 (Rb-Sr whole rock by Fleck *et al.*, 1980). More recently, Johnson et al. (2001) published an age for the undeformed Al Khalij tonalite that intrudes the Tabalah Shear Zone north of the studied area. The tonalite was dated through SHRIMP U-Pb zircon dating at 755  $\pm$  7 Ma. This means that the Tabalah Shear Zone should not have been active after 755 Ma.

#### 4.5.3 Description of samples

Four samples were selected for geochronological studies. These samples represent the rocks of which dating information could present crucial information for the tectonic history of the Tabalah and Wadi Tarj areas. The geographic positions of the samples are shown in Figure 4-2 and Figure 4-3.

- *Sample SAD 12* (N19°59,654' E042°12,318') is hornblende schist from the *amphibolite* in the central Tabalah area. The sample is well foliated and lineated and comes from the main portion of the Wadi Ta'al Shear Zone. It contains plagioclase, metamorphic hornblende, quartz and minor biotite and pyroxene. The hornblendes define a strong uniformly trending lineation, which was subhorizontal in the outcrop from where the sample was taken. Shear indicators at the sample location, displayed dextral shearing.
- *Sample SAD 14* (N20°01,245' E042°14,731') is a hornblende schist from the *amphibolite* in the central Tabalah area. The sample is well foliated and lineated and comes from the main portion of the Wadi Ta'al Shear Zone. It contains plagioclase, metamorphic greenish-brownish hornblende and minor quartz. The hornblendes define a strong uniformly trending lineation, which was subhorizontal

in the outcrop from where the sample was taken. Shear indicators at this location, displayed dextral shearing.

- *Sample SAD 18* (N19°43,261' E042°21,817') is a hornblende schist from the *amphibolite* in the Wadi Tarj area. The sample is foliated and lineated. This sample comes from an outcrop with a steep NE-plunging lineation. It contains plagioclase, metamorphic brown hornblende and minor quartz and pyroxene. The hornblendes define the lineation. The lineations plunge steeply to the ENE and top-to-the-WSW movement was observed along these lineations.
- *Sample SA 209* (N19°41' E042°19') is a sample from the non-deformed *granodiorite* from the Wadi Tarj area and it intrudes the Tabalah/Ta'al Shear Zone over here. It contains hornblende, plagioclase and some quartz and biotite. SAD 209 was also geochemically analysed.

#### 4.5.4 Results

The age spectra for the analyzed samples from the Tabalah and Wadi Tarj areas are shown in Figure 4-14 to Figure 4-17. The detailed data of the individual step-heating experiments can be found in Table 4-3 to Table 4-6. The identification of plateau ages was done according to the following criteria: a minimum of 3 contiguous steps of ages within a  $2\sigma$  error is required; these steps should yield a well-defined isochron; and a significant portion of the  $^{39}\text{Ar}$ -release should have taken place during these steps (McDougall and Harrison, 1999). All analyzed samples display clear plateaus with no evidence of a secondary event outside of event that formed the main plateau.

The results of  $^{40}\text{Ar}/^{39}\text{Ar}$  dating for sample SAD 18, with hornblendes forming a steeply plunging ENE plunging lineation are presented in Figure 4-16. This sample was dated at  $779 \pm 7$  Ma and represents the oldest age found in the Tabalah and Wadi Tarj areas during this study. Kinematics indicated that these hornblendes were associated with WSW directed thrusting. The samples which were taken from the sections of the Tabalah and Tarj Shear Zones where lineated hornblendes were associated with a sub-horizontal NNW-SSE trending lineation, SAD 12 (Figure 4-14) and SAD 14 (Figure 4-15), yield ages of respectively,  $765 \pm 5$  Ma and  $764 \pm 7$  Ma. Kinematics for both samples indicated dextral strike-slip and so it can be concluded that this event took place around 765 Ma. The results of  $^{40}\text{Ar}/^{39}\text{Ar}$  dating for the undeformed *granodiorite* in the Wadi Tarj area (sample SAD 19) are presented in Figure 4-17. This sample was dated at  $761 \pm 6$  Ma.

#### 4.5.5 Summary of geochronological studies

From the  $^{40}\text{Ar}/^{39}\text{Ar}$ -studies, it can be concluded that the thrusting was the oldest event dated during this study with a date of ca. 779 Ma. The dextral strike slip event, as recorded for the main Wadi Ta'al Shear Zone by samples SAD 12 and SAD 14, has an age of approximately 765 Ma. The undeformed granodiorite recorded an age of 761 Ma. The ages of the dextral strike slip event and the cooling of the undeformed granodiorite are very close to each other and fall within each others error. However, field observations show clearly that the granodiorite intruded the shear zone and the granodiorite must have formed later than the dextral strike slip



Table 4-3 Detailed data of the individual step-heating for sample SAD 12.

<b>Incremental Heating</b>										
	$^{36}\text{Ar(a)}$	$^{37}\text{Ar(ca)}$	$^{38}\text{Ar(c)}$	$^{39}\text{Ar(k)}$	$^{40}\text{Ar(r)}$	Age $\pm 2\sigma$ (Ma)	$^{40}\text{Ar(r)}$ (%)	$^{39}\text{Ar(k)}$ (%)	K/Ca	$\pm 2\sigma$
01M0243A	0,00057	0,18213	0,00268	0,03277	0,76634	613.41 $\pm$ 37.96	82,09	4,47	0,077	$\pm$ 0,019
01M0243B	0,00036	5,98142	0,08478	0,44038	13,43907	765.44 $\pm$ 3.48	99,21	60,04	0,032	$\pm$ 0,003
01M0243C	0,00001	0,66321	0,00675	0,04181	1,26662	760.94 $\pm$ 28.16	99,68	5,70	0,027	$\pm$ 0,004
01M0243D	0,00000	0,68144	0,00772	0,04347	1,31919	761.90 $\pm$ 4.01	99,99	5,93	0,027	$\pm$ 0,003
01M0243F	0,00010	1,07567	0,01348	0,07504	2,29595	767.07 $\pm$ 17.66	98,74	10,23	0,030	$\pm$ 0,003
01M0243G	0,00009	0,42878	0,00491	0,02919	0,88444	761.09 $\pm$ 33.56	96,97	3,98	0,029	$\pm$ 0,004
01M0243H	0,00000	0,27414	0,00267	0,01388	0,42701	770.27 $\pm$ 10.48	99,99	1,89	0,022	$\pm$ 0,005
01M0243I	0,00000	0,23043	0,00206	0,01221	0,37886	775.95 $\pm$ 13.29	99,99	1,66	0,023	$\pm$ 0,005
01M0243K	0,00002	0,40986	0,00463	0,02734	0,85345	779.66 $\pm$ 35.54	99,26	3,73	0,029	$\pm$ 0,004
01M0243L	0,00000	0,09249	0,00022	0,00245	0,07696	783.84 $\pm$ 50.32	99,99	0,33	0,011	$\pm$ 0,004
01M0243M	0,00022	0,29544	0,00266	0,01495	0,47807	795.04 $\pm$ 64.68	88,11	2,04	0,022	$\pm$ 0,004
$\Sigma$	0,00137	10,31500	0,13258	0,73349	22,18595					
<b>Information on Analysis</b>										
Sample Material	<b>Results</b>					Age $\pm 2\sigma$ (Ma)	MSW	$^{39}\text{Ar(k)}$ (% <sub>0,n</sub> )	K/Ca	$\pm 2\sigma$
VU38-A12 hornblende						764.70 $\pm$ 4.52 $\pm$ 0,59%	1,05	89,43 <sub>7</sub>	0,028	$\pm$ 0,002
Saudi Arabia Brigitte						External Error $\pm$ 15.95 Analytical Error $\pm$ 2.53				
Project Bernard2001						759.91 $\pm$ 5.67 $\pm$ 0,75%		11	0,031	$\pm$ 0,002
Irradiation VU38						External Error $\pm$ 16.22 Analytical Error $\pm$ 4.27				
J-value 0,017318										
Standard 98,3										

90 Table 4-4 Detailed data of the individual step-heating for sample SAD 14.

		<sup>36</sup> Ar(a)	<sup>37</sup> Ar(ca)	<sup>38</sup> Ar(cl)	<sup>39</sup> Ar(k)	<sup>40</sup> Ar(r)	Age ± 2σ (Ma)	<sup>40</sup> Ar (r) (%)	<sup>39</sup> Ar (k) (%)	K/Ca ± 2σ
<b>Incremental Heating</b>										
01M0244A	0,20 W	0,00054	0,08847	0,00183	0,00427	0,09443	585.52 ± 253.16	37,12	0,49	0,021 ± 0,011
01M0244C	0,25 W	0,00026	0,03209	0,00064	0,00240	0,02286	275.17 ± 550.54	22,74	0,28	± 0,031
01M0244D	0,30 W	0,00037	0,14238	0,00369	0,01074	0,23183	573.16 ± 141.74	67,89	1,24	0,032 ± 0,014
01M0244E	0,35 W	0,00003	0,25694	0,00796	0,01695	0,47790	717.35 ± 75.51	97,97	1,96	0,028 ± 0,006
01M0244F	0,40 W	0,00021	1,14448	0,02738	0,04434	1,28859	735.40 ± 30.55	95,37	5,13	0,017 ± 0,002
01M0244H	0,45 W	0,00043	5,34062	0,12598	0,17837	5,39849	760.30 ± 8.74	97,70	20,65	0,014 ± 0,001
01M0244I	0,50 W	0,00053	6,83250	0,17907	0,23707	7,23138	765.15 ± 7.43	97,88	27,44	0,015 ± 0,002
01M0244J	0,55 W	0,00038	5,24763	0,13762	0,18119	5,49905	762.03 ± 10.78	97,97	20,97	0,015 ± 0,001
01M0244K	0,60 W	0,00010	1,78620	0,04767	0,06747	1,98719	743.58 ± 19.08	98,56	7,81	0,016 ± 0,002
01M0244M	0,65 W	0,00000	0,48384	0,01021	0,01626	0,48592	752.58 ± 10.03	99,99	1,88	0,014 ± 0,002
01M0244N	0,70 W	0,00024	0,84984	0,01738	0,02659	0,74537	713.90 ± 72.69	91,41	3,08	0,013 ± 0,002
01M0244O	0,80 W	0,00000	0,60548	0,01321	0,02024	0,62988	777.78 ± 7.86	99,99	2,34	0,014 ± 0,002
01M0244P	0,90 W	0,00009	0,68167	0,01452	0,02268	0,68431	758.44 ± 76.95	96,18	2,62	0,014 ± 0,002
01M0244R	fusion	0,00004	1,18924	0,02464	0,03540	1,08230	766.66 ± 29.87	98,81	4,10	0,013 ± 0,001
	Σ	0,00323	24,68137	0,61181	0,86395	25,85949				
<b>Information</b>										
<b>on Analysis</b>										
Sample	VU38-A13									
Material	hornblende									
Location	Saudi Arabia									
Analyst	Brigitte									
Project	Bernard2001									
Irradiation	VU38									
J-value	0,017318									
Standard	98,3									
<b>Results</b>										
<b>Error Plateau</b>		30,4169	± 0,3168	± 1,04%	40(r)/39(k) ± 2σ	Age ± 2σ (Ma)	MSW	D	K/Ca ± 2σ	
					763.39	3,00	97,99	11	0,015	± 0,001
					External Error					
					Analytical Error					
					6.48					
<b>Total Fusion Age</b>		29,9317	± 0,2879	± 0,96%	753.44		14		0,015	± 0,001
					External Error					
					Analytical Error					
					± 16.61					
					± 5.92					

Table 4-5 Detailed data of the individual step-heating for sample SAD 18.

<b>Incremental Heating</b>											
	<sup>36</sup> Ar(a)	<sup>37</sup> Ar(ca)	<sup>38</sup> Ar(rl)	<sup>39</sup> Ar(k)	<sup>40</sup> Ar(r)	Age ± 2σ (Ma)	<sup>40</sup> Ar(r) (%)	<sup>39</sup> Ar(k) (%)	K/Ca	± 2σ	
01M0245A	0,20 W	0,00120	0,11678	0,08205	0,14058	647.41 ± 10.34	3,50437	0,14058	0,518	± 0,265	
01M0245B	0,25 W	0,00027	0,27318	0,03427	0,06984	632.91 ± 14.80	1,69482	0,06984	0,110	± 0,033	
01M0245C	0,30 W	0,00029	0,65023	0,10269	0,15263	694.93 ± 7.04	4,14163	0,15263	0,101	± 0,015	
01M0245E	0,35 W	0,00032	1,19622	0,20596	0,25615	729.27 ± 3.45	7,36804	0,25615	0,092	± 0,011	
01M0245F	0,40 W	0,00128	5,40952	0,95880	0,95120	778.83 ± 2.54	29,65339	0,95120	0,076	± 0,008	
01M0245G	0,45 W	0,00131	9,59005	1,59531	1,58630	783.13 ± 1.95	49,78869	1,58630	0,071	± 0,007	
01M0245I	0,50 W	0,00011	0,65871	0,12019	0,12220	775.77 ± 10.06	3,79108	0,12220	0,080	± 0,011	
01M0245J	0,55 W	0,00004	0,19493	0,04483	0,04926	749.90 ± 18.71	1,46599	0,04926	0,109	± 0,032	
01M0245K	0,60 W	0,00000	0,18714	0,01159	0,01461	757.79 ± 5.88	0,44041	0,01461	0,034	± 0,010	
01M0245L	0,65 W	0,00000	0,10639	0,00784	0,00974	767.97 ± 7.31	0,29834	0,00974	0,039	± 0,017	
01M0245N	0,70 W	0,00000	0,11352	0,00843	0,00971	762.04 ± 8.60	0,29465	0,00971	0,037	± 0,017	
01M0245O	0,75 W	0,00000	0,12933	0,01710	0,01746	780.41 ± 4.56	0,54557	0,01746	0,058	± 0,022	
01M0245P	0,80 W	0,00000	0,11041	0,00782	0,00821	798.62 ± 9.34	0,26415	0,00821	0,032	± 0,016	
01M0245Q	0,90 W	0,00000	0,21240	0,01560	0,01516	799.12 ± 8.16	0,48791	0,01516	0,031	± 0,009	
01M0245S	fusion	0,00015	0,55655	0,05103	0,05225	767.08 ± 14.03	1,59870	0,05225	0,040	± 0,006	
Σ		0,00498	19,50536	3,26350	3,45530		105,33772				

<b>Information on Analysis</b>		<b>Results</b>	
Sample	Material	40(r)/39(k) ± 2σ	MSW
VU38-A14	hornblende	31,1704 ± 0,2946 ± 0,95%	D
Location	Saudi Arabia	778.74 ± 7.08 ± 0,91%	17,58
Analyst	Bernard	External Error ± 17.11 Analytical Error ± 5.98	79,39 7
Project	Bernard2001		
Irradiation	VU38		
J-value	0,017318	30,4859 ± 0,0678 ± 0,22%	15
Standard	98,3	External Error ± 15.81 Analytical Error ± 1.39	0,076 ± 0,004

92 Table 4-6 Detailed data of the individual step-heating for sample SAD 19.

<b>Incremental Heating</b>										
	$^{36}\text{Ar}(a)$	$^{37}\text{Ar}(ca)$	$^{38}\text{Ar}(cl)$	$^{39}\text{Ar}(k)$	$^{40}\text{Ar}(r)$	Age $\pm 2\sigma$ (Ma)	$^{40}\text{Ar}(r)$ (%)	$^{39}\text{Ar}(k)$ (%)	K/Ca	$\pm 2\sigma$
01M0247A	0,20 W	0,00055	0,03719	0,00252	0,00745	1236,90	0,42381	0,00745	0,086	$\pm 0,118$
01M0247B	0,25 W	0,00028	0,03179	0,00068	0,00804	687,87	0,21562	0,00804	0,109	$\pm 0,172$
01M0247C	0,30 W	0,00055	0,00000	0,00041	0,01111	612,71	0,25948	0,01111	0,000	$\pm 0,000$
01M0247E	0,35 W	0,00076	0,00869	0,00180	0,03318	700,22	0,90848	0,03318	1,642	$\pm 10,195$
01M0247F	0,40 W	0,00022	0,02615	0,00183	0,02041	679,24	0,53871	0,02041	0,336	$\pm 0,405$
01M0247G	0,45 W	0,00046	0,01811	0,00277	0,01900	598,76	0,43179	0,01900	0,451	$\pm 0,761$
01M0247H	0,50 W	0,00037	0,20361	0,01053	0,04211	742,11	1,23744	0,04211	0,089	$\pm 0,019$
01M0247J	0,55 W	0,00010	0,89280	0,04456	0,14000	779,59	4,36972	0,14000	0,067	$\pm 0,008$
01M0247K	0,60 W	0,00025	1,01290	0,04602	0,14411	762,34	4,37608	0,14411	0,061	$\pm 0,007$
01M0247L	0,65 W	0,00035	1,30919	0,05033	0,16392	763,02	4,98305	0,16392	0,054	$\pm 0,006$
01M0247M	0,75 W	0,00017	0,85469	0,03348	0,11587	768,88	3,55542	0,11587	0,058	$\pm 0,007$
01M0247O	0,80 W	0,00012	0,25450	0,01476	0,05269	752,42	1,57454	0,05269	0,089	$\pm 0,020$
01M0247P	0,90 W	0,00030	0,60075	0,02967	0,09841	754,57	2,95105	0,09841	0,070	$\pm 0,009$
01M0247Q	fusion	0,00045	2,76779	0,08177	0,26401	771,47	8,13496	0,26401	0,041	$\pm 0,004$
$\Sigma$		0,00494	8,01816	0,32114	1,12032		33,96015			
<b>Results</b>										
Sample Material Location Analyst					$^{40}(r)/^{39}(k) \pm 2\sigma$	Age $\pm 2\sigma$ (Ma)	MSW D	$^{39}\text{Ar}(k)$ (%,n)	K/Ca	$\pm 2\sigma$
	VU38-A15 hornblende Saudi Arabia Brigitte				$\pm 0,2364$ $\pm 0,78\%$	760,84 External Error Analytical Error	2,18	51,33 5	0,060	$\pm 0,008$
Project Irradiation J-value Standard	Bernard2001 VU38 0,017318 98,3				$\pm 0,1627$ $\pm 0,54\%$	761,26 External Error Analytical Error		14	0,060	$\pm 0,003$

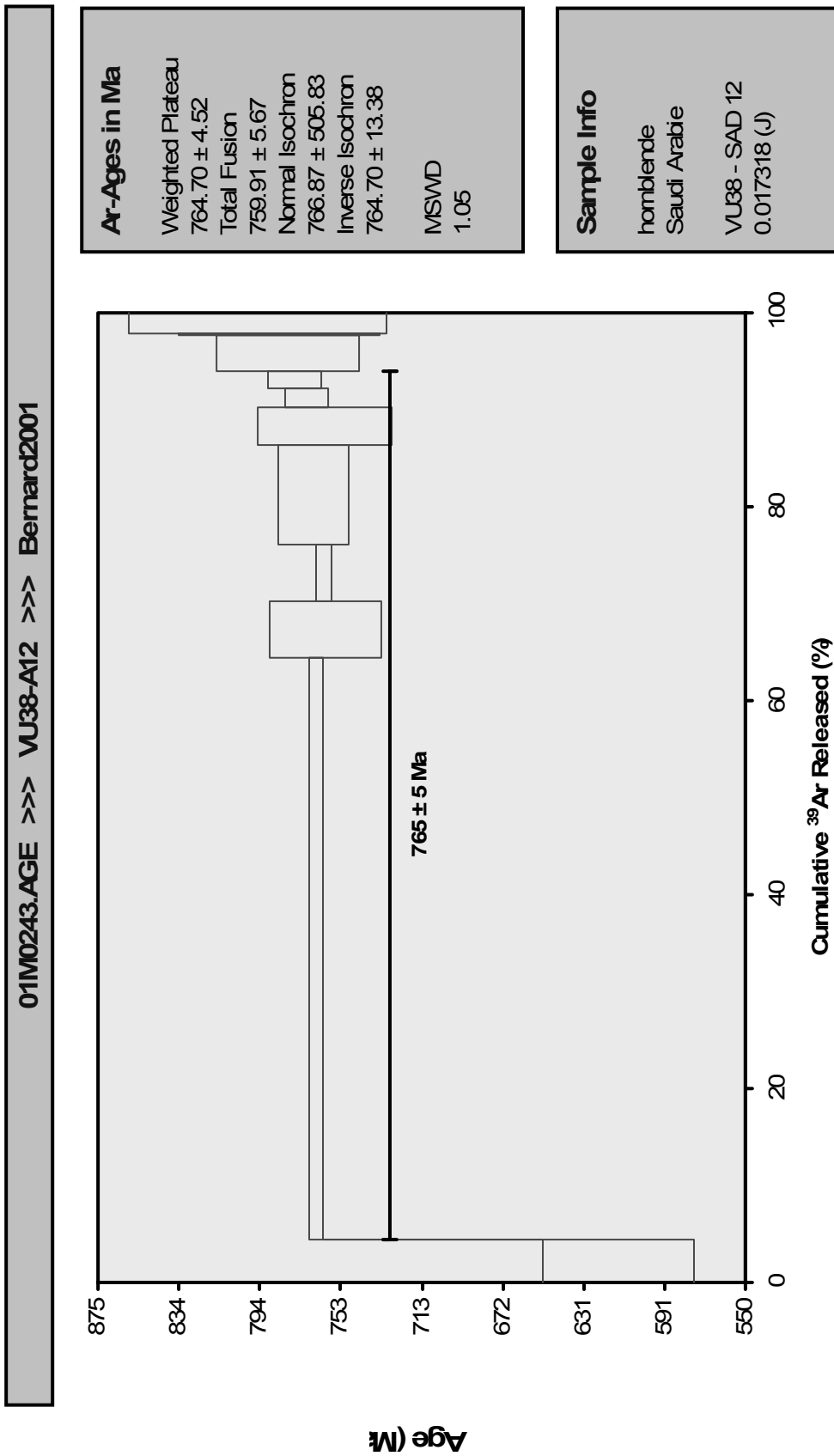


Figure 4-14 Results of <sup>40</sup>Ar/<sup>39</sup>Ar dating for sample SAD 12.

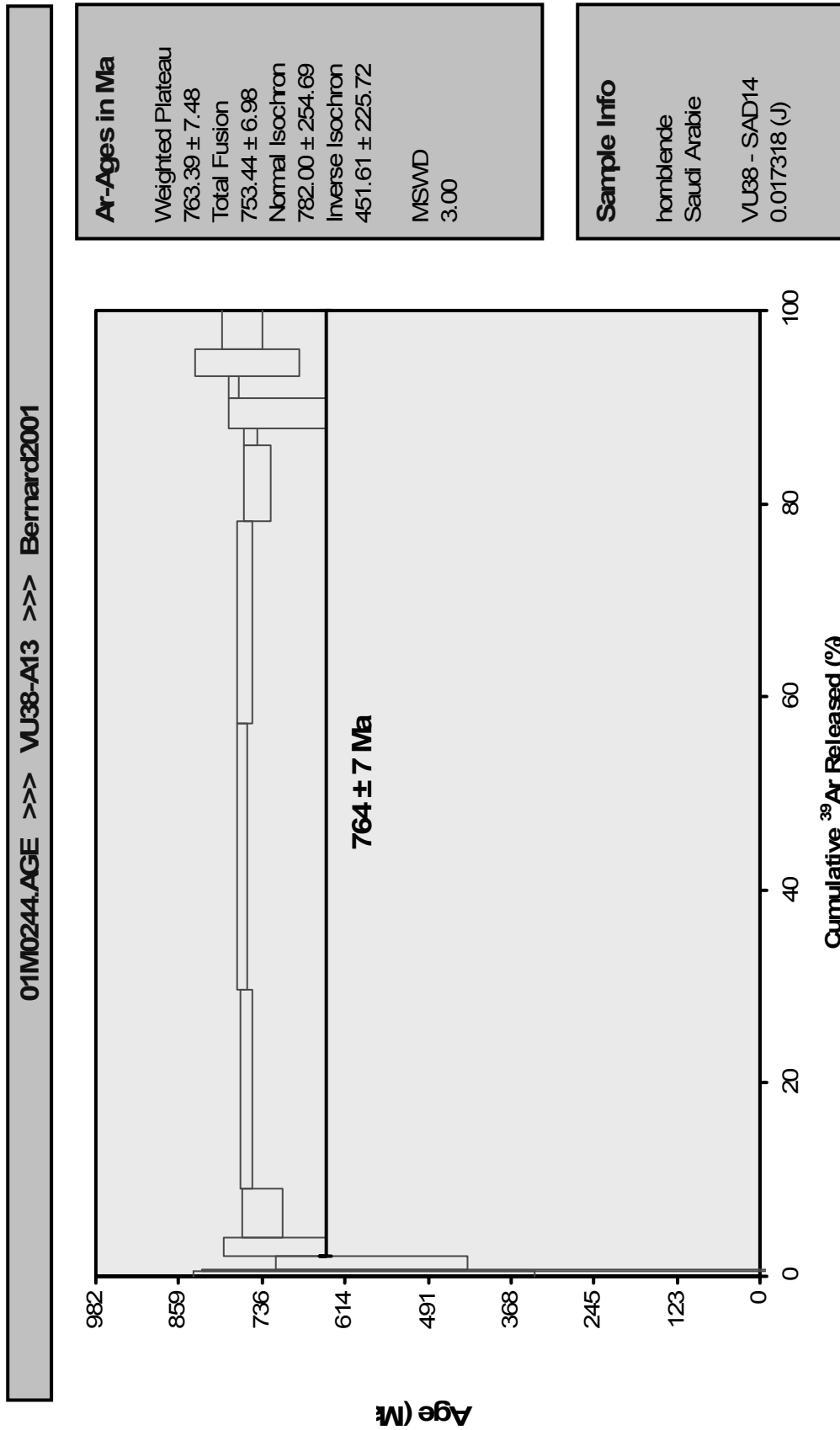


Figure 4-15 Results of  $^{40}\text{Ar}/^{39}\text{Ar}$  Ar dating for sample SAD 14.

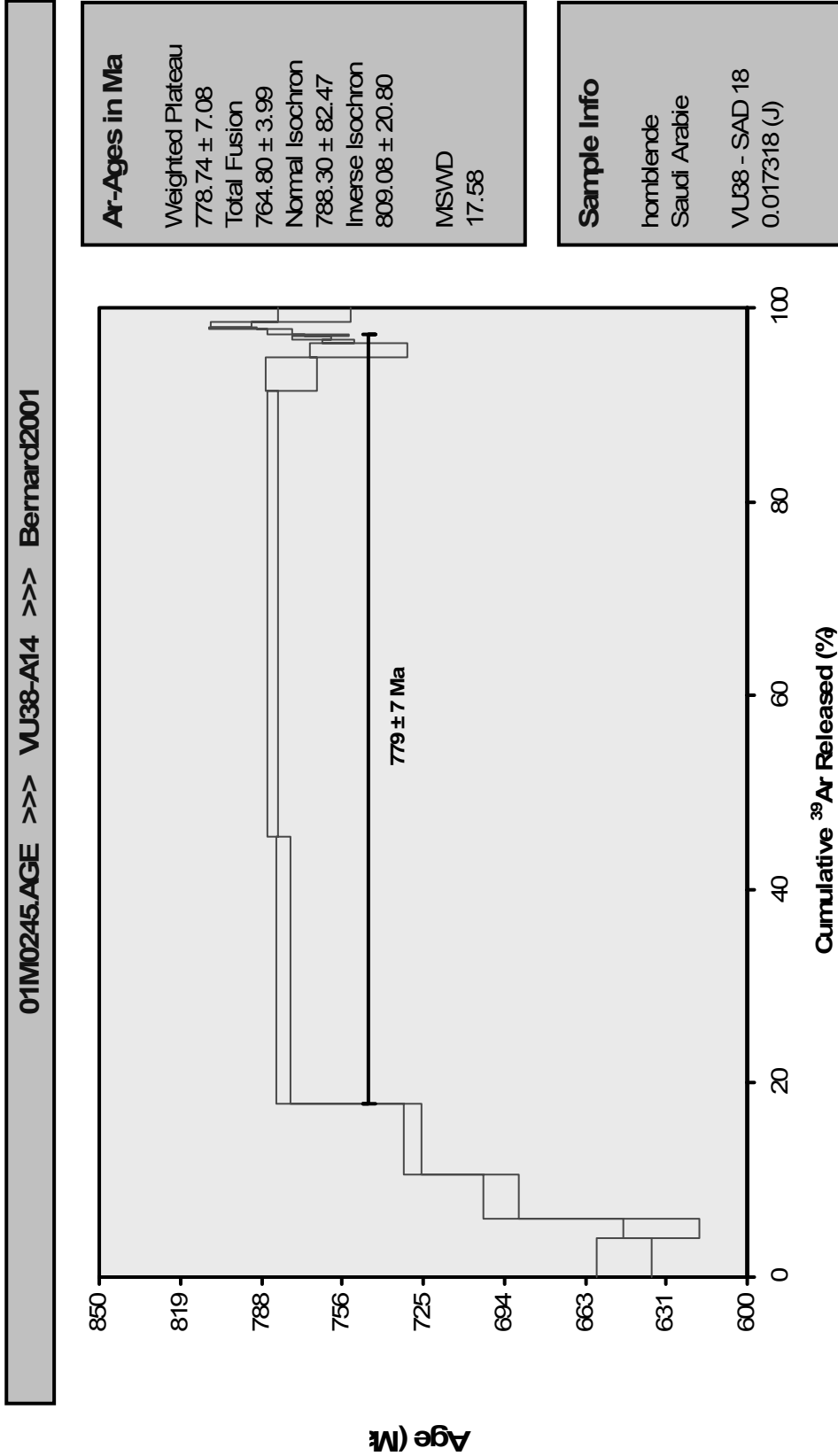


Figure 4-16 Results of <sup>40</sup>Ar/<sup>39</sup>Ar dating for sample SAD 18.

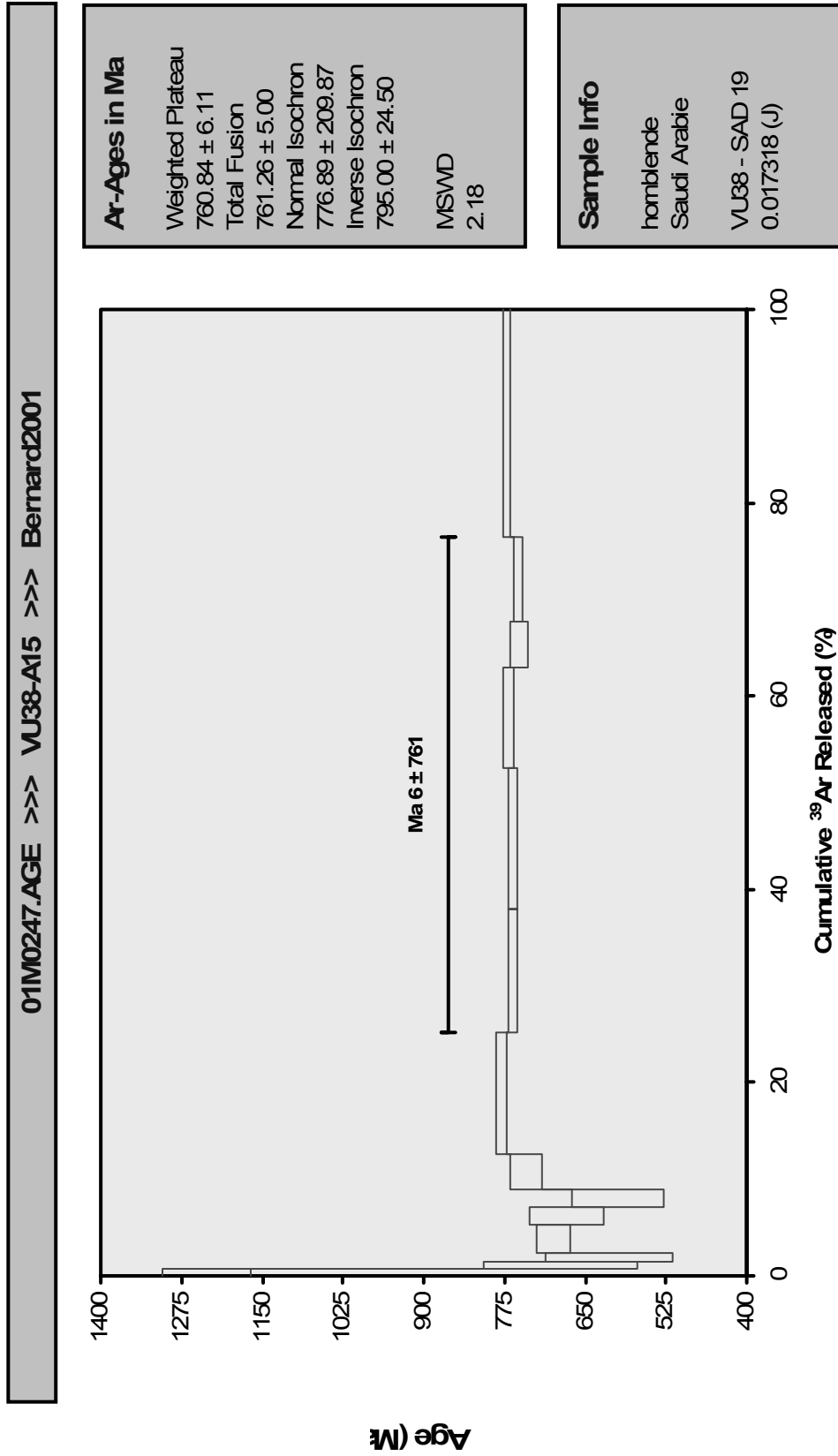


Figure 4-17 Results of  $^{40}\text{Ar}/^{39}\text{Ar}$  Ar dating for sample SAD 19.



event.

## 4.6 Discussion and conclusions

### 4.6.1 Summary of geological evidence

The Tabalah area and Wadi Tarj area contain features that are typical of the Neoproterozoic terranes in the Arabian Nubian Shield as plutons and schistose sequences. The foliated and lineated sequences in the Tabalah and Wadi Tarj areas represent shear zones.

The main lithological units are the *mixed gabbro-diorite suite*, which consists of gabbros and diorites and the *quartz diorite-tonalite*, which consists mainly of tonalite. These intrusives are crosscut by *amphibolites*. Some dikes were observed and they trend W-E. An undeformed *granodiorite* intruded the *amphibolites* in the Wadi Tarj area.

Geochemical studies were conducted on the most important non-metamorphosed and non-deformed rocks to analyse the tectonic environment from which they originate. The results of the analyses were compared to published geochemical studies of similar rocks in other parts of the ANS. The geochemistry of the rocks in the *mixed gabbro-diorite suite* is similar to gabbros/diorites suites in Egypt, Sudan and Saudi Arabia. These gabbros/diorite suites were interpreted to have been formed in island-arc environments. The gabbros were formed in immature island-arcs and the diorites were formed in more mature island-arcs. The geochemical studies indicate that tonalites from the *quartz diorite-tonalite*, the granodiorite in the Wadi Tarj area and the W-E dykes are very similar to tonalites, granodiorites and calc-alkaline volcanics from other parts of the ANS. These were generally interpreted to have been formed in an active continental margin setting. No dates are available for the rocks that were formed in an island-arc setting however the earliest activity on the shear zone that deforms these rocks is dated at approximately  $779 \pm 7$  Ma and so the island-arc phase must have predated  $779 \pm 7$  Ma. The cooling of the granodiorite in the Wadi Tarj area is dated at  $761 \pm 6$  Ma.

The structural studies indicate that the Wadi Ta'al and Tabalah shear zones and the deformed *quartz diorite-tonalite* in between, represent one zone of intense deformation since the main structural features, the foliations, the lineations and the shear indicators, are identical and continuous through these three neighbouring units. The *mixed gabbro-diorite suite* and *quartz diorite-tonalite* grade into the *amphibolites* and are their deformed equivalents. The *amphibolites* are the lithological entities that record the most intense deformation. The small shear zones in the *mixed gabbro-diorite* were also formed during the deformation event that was responsible for the formation of the main Tabalah/Wadi Ta'al SZ. Lineations and shear sense indicators show that there are three phases of deformation:

- 1) The top-to-WSW movement in the Wadi Ta'al/Tabalah shear zone along steeply NE plunging lineations was dated at ca. 779 Ma. This indicates thrusting in its current position.
- 2) Dextral strike-slip movement along sub-horizontal NNW-SSE lineations on the Tabalah/Wadi Ta'al shear zone. This event was dated at ca. 765 Ma. It appears to be the main phase of deformation that can be currently observed.

- 3) Dextral strike-slip movement with a top-to-the-SE component along moderately SE plunging lineations. No dates are available for this phase however the Tabalah/Tarj shear zone system is intruded by the *undeformed granodiorite* that was dated at  $761 \pm 6$  Ma. This should be the lower age limit for the structures that are associated with the SE plunging lineations.

From the available data, it can be concluded that the steep ENE plunging hornblende lineations are older than the NNW-SSE subhorizontal hornblende lineations and consequently the thrusting pre-dates the strike-slip event. However no assumptions can be made of the relative age of the SE plunging lineation relative to the other the ages of the other features.

#### 4.6.2 Tectonic model for the Tabalah and Wadi Tarj Complex

The island-arc related rocks, as found in the Tabalah and Tarj Complex, were formed during intra-oceanic subduction, as indicated by their geochemical characteristics. The subduction is thought to initiate at an existing weakness within an oceanic plate, as a strike-slip fault, when plates of a different density are juxtaposed (e.g. Flower, 2003; Stern and Bloomer, 1992; Wakabayashi and Dilek, 2003). The older and denser plate will subside and this will initiate the subduction (e.g. Flower, 2003; Stern and Bloomer, 1992). The colder subducted oceanic lithosphere will dehydrate at depth (Wilson, 1989). The fluids that are derived from the dehydration of the subducting slab will cause partial melting of the mantle wedge and the actual formation of the island-arc with its associated magmatism (Wilson, 1989). This scenario is also applicable for the island-arc related rocks in the Tabalah and Tarj areas which form part of the Asir Terrane which is composed of island-arc related rocks (e.g. Stoeser and Camp, 1985; Johnson et al., 1987; Brown et al., 1989).

Chapter 2 indicates that the earliest evolution of the ANS is explained by formation of ophiolites and island-arc remnants that represent relicts of the oceanic phase which took place at 900-750 Ma. Arc-accretion is the process that caused the amalgamation of island-arcs in the Arabian-Nubian Shield (Stoeser and Camp, 1985). Island-arcs that reach a subduction zone at a margin with characteristics of a continental crust will behave buoyant. They will resist subduction and will accrete upon the continental crust to become part of that same crust. The arc-accretion in the ANS is thought to have been taken place at 810-650 Ma. The sites of obduction are supposed to be represented by ophiolitic suture zones (e.g. Stoeser and Camp, 1985). The ophiolitic sutures in the Arabian Nubian Shield have two trends: 1) SW-NE ophiolitic sutures such as the Bi'r Umq suture and Yanbu suture, with the main period of activity at 800-700 Ma (Johnson, 2001; all of these are found to the N of the Tabalah and Tarj areas); and 2) NNW-SSE to N-S trending sutures such as the Nabitah Suture and Ruwah Suture with the main period of activity around 700-650 Ma (Quick, 1991; Johnson, 2001). From an age perspective, it can thus be assumed that the Tabalah and Tarj areas should contain remnants of the oceanic phase and intra-terrane remnants of the arc-accretion along the NE-SW trending sutures. The timeframes of deformation along the Tabalah/Ta'al SZ, as described in the paragraph on geochronology in this chapter, indicate that the structures in the Tabalah and Wadi Tarj area are likely to be related to tectonic processes that were recorded at the NE-SW trending margins of terranes in the Arabian Shield. They should thus be regarded as intra-

terrane responses to arc-accretion at the terrane margins, which are represented by the ophiolitic sutures. This also justifies relating the shear zones in the Tabalah and Wadi Tarj areas to a compressional regime. In such a regime, the E-dipping lineations with the top-to-W-movement indicate thrusting in an E-W compressional regime at ca. 779 Ma. Thrusts do not typically form as steep as the observed current dip of the Tabalah/Ta'al Shear Zone but the steepening of the shear zone after the initial thrusting will be discussed later in this chapter.

Dextral strike-slip movement along NNW-SSE trending lineations at the Tabalah/Ta'al Shear Zone took place at ca. 765 Ma. The lineations associated with the strike-slip event were dated at younger ages than the lineations that were associated with thrusting and consequently the strike-slip movement post-dates the thrusting. Dextral strike-slip movement along a NNW-SSE trending shear zone should result from NNE-SSW directed  $\sigma_1$ . As demonstrated above, the deformation in the Tabalah and Tarj areas took place in a period of arc-accretion and compression within the ANS and therefore it can be concluded that the dextral strike-slip along NNW-SSE trending lineation should have resulted from NNE-SSW compression. Since strike-slip faulting takes place along steep shear zones, it is this phase that is assumed to have caused the steepening of the initial moderately dipping thrusts.

Strike-slip overprint of thrusting is a commonly observed feature of intra-terrane deformation during arc-accretion in the North American Cordillera (Monger et al., 1982; Van der Heyden, 1992; Chardon et al., 1999; Cole et al., 1999). Over here, the thrusting represents an intra-terrane response to arc-accretion at the terrane boundary (Monger et al., 1982; Van der Heyden, 1992; Chardon et al., 1999; Cole et al., 1999). The intra-terrane shortening features in the North American Cordillera are mostly parallel to the movement of the subducting plate (Monger et al., 1982; Van der Heyden, 1992; Chardon et al., 1999; Cole et al., 1999). The strike-slip movement obscured much of the earlier thrusting and caused steepening of the shear zones (Chardon et al., 1999; Cole et al., 1999). The intra-terrane strike-slip shear zones in the North American Cordillera were related to oblique convergence that resulted from changes in the direction of plate motion of the subducting plate (Van der Heyden, 1992; Chardon et al., 1999; Cole et al., 1999). The changes in the direction of plate motions can occur within short time-frames of 5-20 Ma as shown for the Middle Cretaceous shear zones of the Coast Plutonic Complex, British Columbia and for the Late Cretaceous McKinley Fault in south Alaska (Cole et al., 1999).

On the basis of the observations in this chapter, a scenario, as described above for intra-terrane arc-accretion related shear zones in the Cordillera of North America, is also suggested for the Tabalah Complex. In such a model, the Tabalah/Ta'al shear zone is initially formed as an intra-terrane thrust in E-W compression due to accretionary processes at a terrane boundary. This happened at  $779 \pm 7$  Ma. The main structural phase that was recorded on the Tabalah/Ta'al Shear Zone was defined by the dextral strike slip along NNW-SSE trending lineations at ca. 765 Ma. This phase resulted from NNE-SSW compression. Such a change in the direction of compression during arc-accretion can thus be best explained by an anti-clockwise change in plate motion of the subduction plate. On the basis of the above discussion, the different deformation phases can be named as follows:

- D1-phase: A phase of thrusting at  $779 \pm 7$  Ma formed foliations (S1), ENE-plunging lineations (L1) and top-to-W shear sense indicators.
- D2-phase: A phase of dextral strike-slip movement steepened the foliations, and formed NNW-SSE trending lineations (L2) and dextral shear sense indicators. This phase took place at ca. 765 Ma as is indicated by  $^{40}\text{Ar}/^{39}\text{Ar}$  dating of sub-horizontal NNW-SSE trending hornblendes at  $765 \pm 5$  Ma and  $764 \pm 7$  Ma.

The geochemical data from this study indicate that the Tabalah/Ta'al Shear Zone deformed the *quartz diorite-tonalite* that was emplaced at a lithosphere with characteristics of an active continental margin but predates the *granodiorite*, which intruded at a lithosphere with characteristics of an active continental margin.

#### 4.6.3 Conclusions

The tectonic development of the Tabalah and Tarj areas is illustrated in Figure 4-18 and Table 4-7. The Tabalah and Tarj areas contain many of the features that are typical for an intra-terrane deformation in terranes that participate in arc-accretion events. Examples of these features are the gabbros and diorites that were formed in island-arcs and the granodiorites and the tonalites which contain characteristics of intrusion at continental margins.

Finally, it should be noted that no explanation was found, in the form of folding, for the minor bend in the Tabalah/Wadi Ta'al "Tectonic Zone" between the Tabalah and Tarj areas. It is therefore assumed that later faulting, possibly along the Najd trend, caused the bend in the Tabalah/Wadi Ta'al "Tectonic Zone".

The following tectonic model is suggested for the Tabalah and Wadi Tarj areas:

- 1) Island-arc related plutons formed probably at ca 820 Ma but surely prior to 779 Ma. The *mixed gabbro-diorite* and the *quartz diorite-tonalite* are the principal relicts of this phase.
- 2) The thrusting as observed along some parts of the shear zone are intra-terrane remnants of plate movements along a subduction zone at the margin of the terrane of which the Asir was part at the time of deformation. It is dated at about 779 Ma (D1).
- 3) A major dextral strike-slip event overprinted the thrusting phase. This took place at about 765 Ma (D2). This structure was also related to arc-accretion. Large strike-slips are common features in areas where arc-accretion takes place. In this respect, the Wadi Tabalah area resembles the Coast Plutonic Complex, British Columbia, where large strike slip shear zones were formed within magmatic arcs and overprint earlier thrusting (see Chardon et al., 1999). The change from thrusting towards strike-slip movement is typically due to a change in plate motion of the subducting plate. In the case of the Tabalah/Ta'al Shear Zone, an anti-clockwise change in motion of the subducting plate should have resulted in the change of the style of deformation on the Tabalah/Ta'al Shear Zone.

4) Finally, an arc-accretion related granodiorite was emplaced at about 761 Ma. This indicates that the subduction still continued after the main phase of strike-slip movement in the Tabalah and Wadi Tarj areas.

Table 4-7 Table with the main stages of the tectonic history in the Tabalah and Tarj areas.

<b>Main Geological phases in the Tabalah area</b>				
<b>Phase</b>	<b>Lithology</b>	<b>Metamorphism</b>	<b>Structures</b>	<b>Age (Ma)</b>
Island-arc	mixed gabbro-diorite and the quartz diorite-tonalite	N/A	None.	820-779
D1	Amphibolites and deformed the quartz diorite-tonalite	Lower amphibolite	Foliation, steep lineations, shear indicators -> thrusting;	779 Ma
D2	Amphibolites and deformed the quartz diorite-tonalite	Lower amphibolite	Foliation, subhorizontal lineations, shear indicators -> strike slip movement; NNE-SSW	765 Ma
Active continental margin	Granodiorite	N/A	None	761 Ma

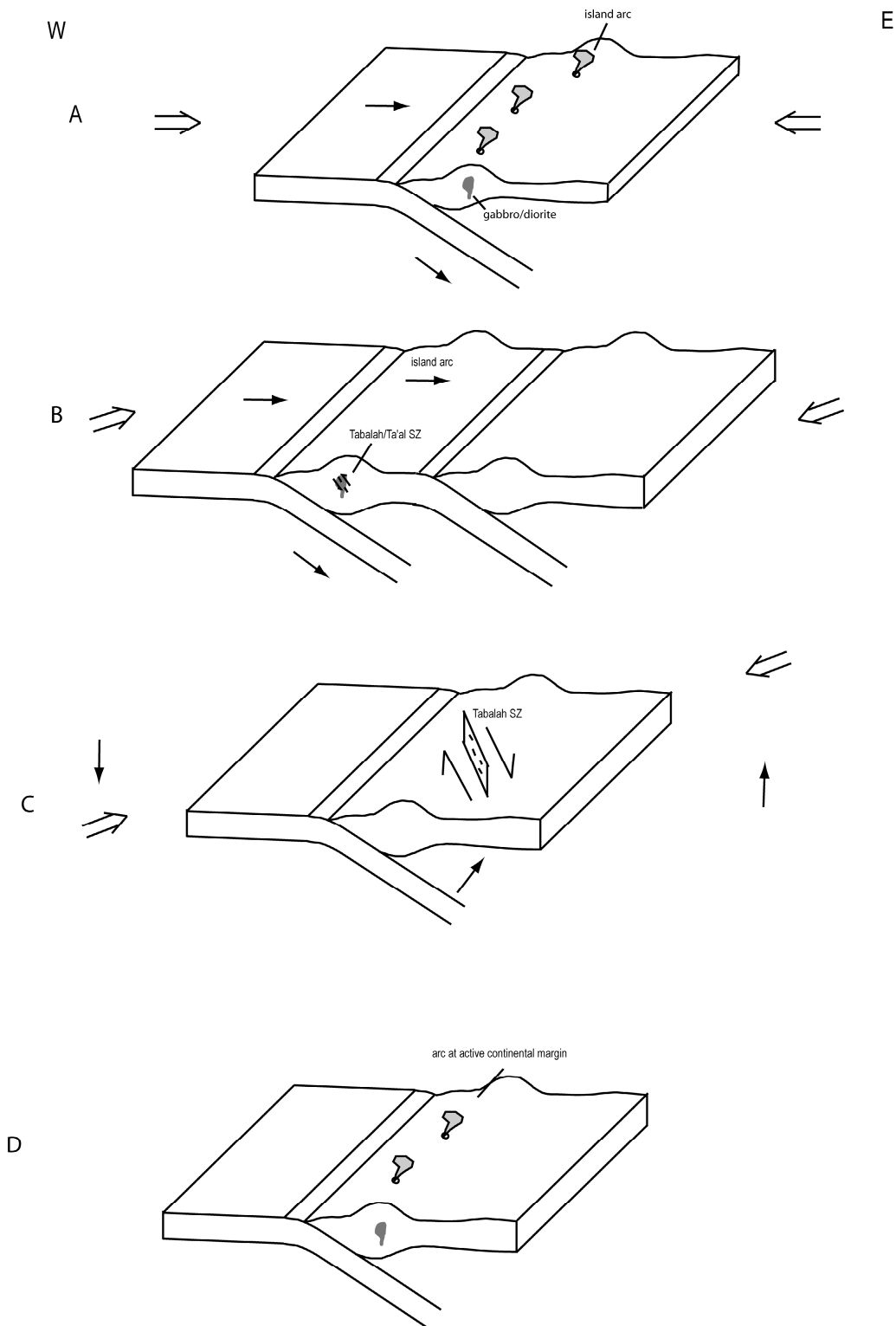


Figure 4-18 Diagrams illustrating the tectonic history of the Tabalah and Tarj areas

a) Formation of island arcs

b) The formation of an intra-terrane thrust (D1) at 779 Ma due to arc-accretion at the terrane margin

c) Continuing arc-accretion leads to dextral strike slip (D2) at 765 Ma. Anti-clockwise change in the direction of plate motion of the subducting plate is responsible for the change in deformation along the Tabalah/Ta'al Shear Zone.

d) Granodiorite intrusion at active margin at 761 Ma

## **A Pan-African core complex in the Sinai, Egypt**

Published in “Geologie en Mijnbouw: B. Blasband, P. Brooijmans, P. Dirks, W. Visser and White, S., 1997. A Pan-African core complex in the Sinai Egypt. *Geologie en Mijnbouw*, 73, 247-266

*After the publication of this paper, additional research was performed in the Wadi Kid Complex. This research, presented in Appendix 1, confirmed the core complex model for this area and showed that the low-angle shear zone was active at ~595 Ma*

### **Abstract**

In the late Precambrian history of the Wadi Kid area in the Sinai, Egypt, two deformation phases are clearly recognized. The first phase, D1 (pre-620 Ma), produced a steep regional foliation, axial planar to upright F1 folds, in rocks of a lower-greenschist grade. This compressional phase of deformation is interpreted in terms of subduction in an island-arc setting.

The second phase, D2 (post-620 Ma), is mainly expressed by the widespread development of sub-horizontal mylonitic zones with a total thickness of 1.5 km. Shear sense indicators give a consistent regional transport direction to the northwest, with local indications of reversal to the southeast. This event is associated with regional LP/HT metamorphism, indicative of high thermal gradients. Because of the LP/HT metamorphism, the change in geochemical nature of the granitoids, and the orientation of the dykes, we interpret the mylonitic zones as low-angle normal shear zones related to core-complex development during an extensional event with the transport reversal being induced by doming. We postulate that orogenic collapse was responsible for the transition from the D1 compressional phase to the D2 extensional phase.

### **5.1 Introduction**

The nature of the Pan-African orogeny in the Arabo-Nubian Shield has been subject of debate over the last years. Many geologists believe that a compressional regime in an island-arc setting was responsible for the main tectonic features (e.g. Shackleton et al. 1980; Bentor 1985; Vail

1985; Ragab 1993). However, in some recent studies large strike-slip zones are regarded as being the important tectonic feature; they are associated with extensional structures such as sedimentary basins and dykes (Stern 1985; Hussein 1988).

The Wadi Kid area in the Sinai, Egypt, was chosen as a key area to study the structural geology and tectonics of the Precambrian rocks of the Arabo-Nubian Shield. Just as two models exist for the overall evolution of this shield, there are also two different models for the evolution of the Precambrian in the Sinai. Shimron (1980, 1983) interprets the tectonic development in terms of a compressional island-arc setting with two deformation phases: a syn-sedimentary D1 phase, responsible for the folding of the bedding ( $S_0$ ), and a D2 thrust-phase, mainly represented by the sub-horizontal foliation found throughout most of the Wadi Kid area. On the other hand, Reymer (1983, 1984) postulates that there was a D1 compressional phase which took place in an island-arc setting similar to Shimron's D1 phase, but he relates the D2 structures to the diapiric emplacement of granites.

The aim of the present study is to investigate in particular the D2 phase of deformation in the Wadi Kid area. Detailed field mapping, followed by a microstructural analysis of carefully selected samples, was undertaken. The combined results indicate that the sub-horizontal foliations, described by Shimron (1980, 1983) and Reymer (1983, 1984), are mylonitic in origin and related to extension. Consequently, we propose a radically different tectonic interpretation for the Wadi Kid area: that of a widespread core complex, resulting from orogenic collapse. The data supporting this conclusion are presented and discussed below, along with their implications for the tectonic evolution of the Wadi Kid area.

## **5.2 Geological background**

### *5.2.1 Introduction*

The Sinai peninsula consists at the surface mainly of sedimentary rocks (80%), ranging from Cambrian to Quaternary age, overlying the Precambrian crystalline basement. This basement forms a part of the Arabo-Nubian Shield, which extends over most of NE Africa and Arabia.

The recent geology of the Sinai is strongly influenced by the rifting of the Red Sea. Two orientations of faults are active since the Miocene: a NNE-SSW trend and a NW-SE trend. The metamorphic assemblages indicate that the total uplift did not exceed 15 km. The main phase of uplift took place during the Cambrian and was responsible for an uplift of at least 12 km. The post-Cretaceous tectonics are responsible for block rotation and another phase of uplift of 3 km (Kohn & Eyal 1981).

### *5.2.2 Lithology*

The metamorphic and magmatic rocks making up the basement in the Wadi Kid area have been described by Shimron (1980, 1983, 1984), Furnes et al. (1985) and Reymer (1983, 1984). Their distribution is shown in Figure 5-1. The metamorphic and magmatic rock suites are referred to as 'Formations' in the literature and we follow this terminology. The Umm Zariq Fm., Malhaq Fm., Heib Fm. and Tarr Fm. contain metasedimentary and metavolcanic rocks. The Quneia Fm. and the Sharira Gabbro/Diorite Fm. contain plutonic and meta-plutonic rocks. All these



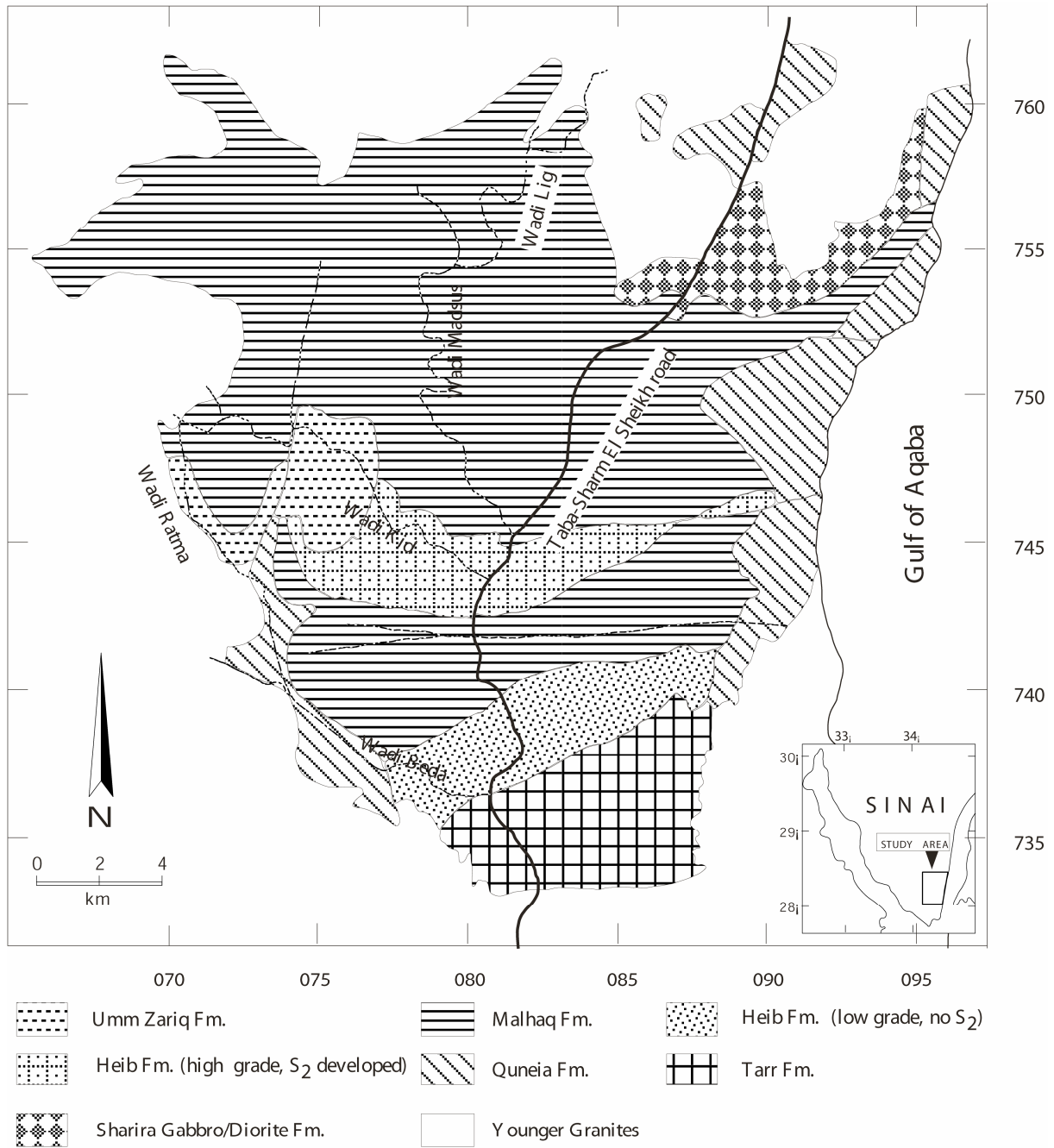


Figure 5-1 Generalized geological sketch-map of the Wadi Kid area, modified after Shimron (1987).

formations have been intruded by granites. The area is cross-cut by swarms of mafic and felsic dykes. The total thickness of the Precambrian metamorphic formations in the Sinai is at least 1.5 km.

The *Umm Zariq Fm.* is a metasedimentary sequence, mainly formed by metapelites; it contains also some metapsammities. The schistose metapelites contain biotite, muscovite,

retrograde chlorite and feldspar along with porphyroblasts of garnet, andalusite and cordierite, indicating amphibolite facies of the low-pressure/high-temperature (LP/HT) type. Relict sedimentary structures, such as bedding, cross-bedding, slump structures and fining upward sequences, are found in the less schistose lenses. The rocks of the Umm Zariq Fm. are interpreted as metagreywackes.

The *Malhaq Fm.* is a metavolcanic sequence (Furnes et al. 1985) containing mainly schists and minor non-schistose massive equivalents. The schistose metavolcanics consist of feldspars, quartz, biotite and hornblende, indicating upper-amphibolite facies. The massive equivalents occur as layers and blocks within the schists and contain biotite, muscovite, chlorite, some quartz and feldspar.

The *Heib Fm.* is a mixed sequence of metasediments and metavolcanics. Rhyolitic and andesitic volcanics can be recognized. The metasedimentary sequence contains conglomerates and turbidites (the Beda Turbidites). The rocks display a lower metamorphic grade than the Umm Zariq and Malhaq Fms and are less deformed. In the more schistose parts, biotite and muscovite are observed, indicating a higher metamorphic grade. The lower-grade parts overlie the higher-grade parts of the Heib Fm. and of the Malhaq Fm. The rocks are thought to be of island-arc volcanic origin, deposited in a marine environment (Furnes et al. 1985).

The *Tarr Fm.*, found in the southern parts of the Wadi Kid, is dominantly a metasedimentary sequence consisting of metaconglomerates, metapelites and metapsammities, in which melanges and felsic flows can be recognized. The formation displays greenschist-grade metamorphism which is lower than that of the Malhaq and Umm Zariq Fms.

The *Quneia Fm.* consists of foliated and lineated diorites and tonalites with occasional biotite-rich xenoliths. Identical intrusives occur in the Nuweiba area, 100 km N of the Wadi Kid Complex, and these were interpreted, from geochemical data, as subduction-related I-type intrusives (Ahmed et al. 1993). Similar intrusives in the Timna area, 150 km N of the Wadi Kid area, were interpreted as I-type granitoids related to crustal thickening in an island-arc environment (Beyth et al. 1994).

Furnes et al. (1985) concluded on basis of major and trace-element studies that the rocks of the metamorphic formations, described above, are subduction-related.

The *Sharira Gabbro/Diorite Fm.* occurs as a single large intrusive body in the northern part of the Wadi Kid Complex. It was described by Furnes et al. (1985) as a layered gabbroic and dioritic intrusion.

The Wadi Kid metamorphic complex is bordered to the north, west and south by *Younger Granites*. Three phases of granitoid intrusions were described (Bentor 1984; Ahmed et al. 1993). The oldest plutonic rocks are the deformed tonalitic to granodioritic rocks of the Quneia Fm. The second phase consists of muscovite granites, which only occur in the most northern part of the Wadi Kid area. The youngest are the biotite-rich granites. Geochemical data indicate that the oldest granitoids are I-type, the muscovite-rich granites S-type, and the youngest biotite granites A-type granites (Ahmed et al. 1993). The S- and A-type intrusives are younger than any of the metamorphic rocks and mostly show intrusive contacts with these rocks. Trace-element studies of late Precambrian A-type granites in southern Israel indicate that these were formed in a thinned crust due to extension, where mantle melts were able to rise near

to the surface (Beyth et al. 1994).

### 5.2.3 Metamorphism

Metamorphic grades of the Wadi Kid area range from lower-greenschist to amphibolite facies with a general trend of increase towards the central and northern parts of the area. Lower-greenschist-facies rocks dominate the southern areas. Sillimanite, garnet and andalusite porphyroblasts appear in the central Wadi Kid Complex where the metamorphic grade reaches upper-amphibolite facies. Here, staurolite is overgrown by andalusite and biotite, which indicates that a medium-pressure phase (> 5 kbar) preceded a LP/HT metamorphic phase. In the northern part of the area, where metavolcanic rocks are found, garnet and hornblende porphyroblasts occur. In the north-eastern part, migmatites are present.

Reymer et al. (1984) calculated a temperature of 700° C and a pressure of 3 to 4 kbar for the Malhaq and Umm Zariq Fms in the central Wadi Kid. Temperatures of 300° C and pressures of 2 kbar have been deduced for the lower-greenschist-facies rocks in the southeastern part of the complex. The metamorphic grade in the Heib Fm. increases from lower greenschist in the Bada Turbidites in the southeast, to higher greenschist in the west and north where biotite-schists appear. Reymer et al. (1984) estimated that the thermal gradient was higher than 50°C/km in the rocks showing amphibolite-grade metamorphism. Shimron (1987) constructed a clockwise P-T-t path for the metamorphic rocks in the Wadi Kid (Figure 5-2).

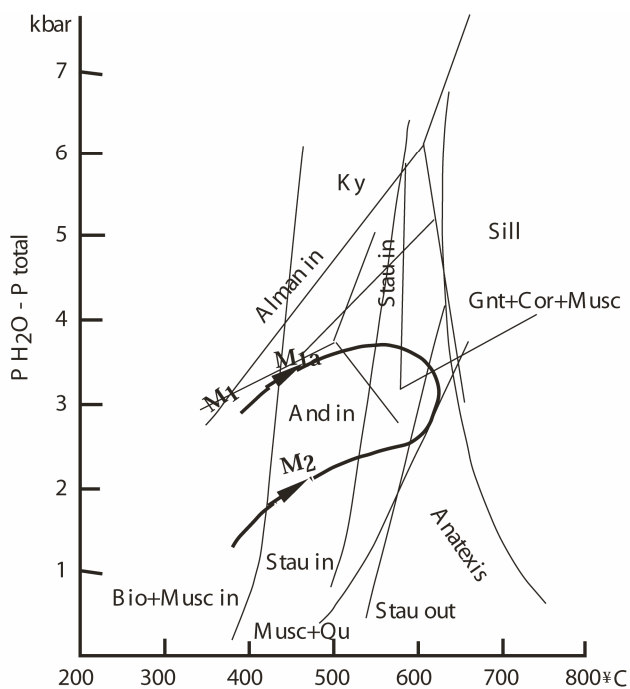


Figure 5-2 P-T-t path for aluminosilicate metamorphic rocks in the Wadi Kid area after Shimron (1987). The plot shows a clockwise path, starting with LP/LT (M1) and moving to medium P and T. After upper greenschist facies was reached (M1a), P remained constant at first and then started to go down but T continued to rise. Eventually, P and T both decreased during retrograde metamorphism related to uplift (M2).

### 5.2.4 Geochronology

The limited number of isotopic ages available for the wider Wadi Kid area are summarized in Table 5-1. From these data it can be concluded that deposition of sediments and volcanics took place after 770 Ma and until 650 Ma ago (Priem et al. 1984), when the metamorphism started. The main amphibolite phase of metamorphism started at about 620 Ma ago. Pulses of metamorphism and the intrusion of granites continued till the early Cambrian and were accompanied by the intrusion of dykes (Ayalon et al. 1987).

Table 5-1 Summary of isotopic ages of Precambrian rocks in the wider Wadi Kid area. Bio, biotite; WR, whole rock; Zr, zircon.

Formation	Metamorphic grade	Age in Ma	Technique	Reference
Heib Fm. (rhyolitic flow)	-	770 ± 150	U-Pb (Zr)	H.N.A. Priem (unpubl. data)
Heib Fm. (granitic pebbles)	-	848 ± 61 735 ± 25	U-Pb (Zr) U-Pb (Zr)	H.N.A. Priem (unpubl. data) ”
Tarr Fm.	upper greenschist	616 ± 30	Rb - Sr (WR)	Halpern & Tristan (1981)
Umm Zariq Fm.	amphibolite	609 ± 12	Rb - Sr (WR)	Bielski (1982)
Malhaq Fm.	amphibolite	609 ± 12	Rb -Sr (WR)	Bielski (1982)
Metavolcanic Ataqa schists (10 km N of Wadi Kid area)	lower amphibolite	600 ± 10 566 -- 529	Rb - Sr (WR) K - Ar	Ayalon et al. (1987) ”
Def. diorite/tonalite	-	608 ± 7	Rb - Sr (WR)	Siender et al. (1974)
Monzodiorite (150 km N of Wadi Kid area)	-	625 ± 5	U-Pb (Zr)	Beyth et al. (1994)
Dykes	-	591 ± 9	Rb - Sr (WR)	Stern & Manton (1987)
Younger Granite	-	580 -- 530	K - Ar (Bio)	Bielski (1982)

## 5.3 The structural geology

### 5.3.1 Introduction

The late Precambrian tectonic history of the Sinai has been divided by most authors (e.g. Shimron 1980, 1983; Reymer 1983, 1984) into two deformation phases, namely D1 and D2. The results of our structural study are presented in Figure 5-3. Our study focuses on the D2 event because of its controversial nature in the tectonic models for the Sinai.

### 5.3.2 D1 structures

The S1 foliation is well developed in the lower-grade parts of the Heib Fm., such as the Bada Turbidites in the southern Wadi Kid area. The S1 slaty cleavage, formed by white micas, is easily recognizable in the shaly layers within these meta-turbidites. It is oblique to the bedding. Inversion of the bedding can be recognized through bedding and cleavage relationships and through sedimentary structures such as cross bedding and coarsening upward sequences. Upright isoclinal F1 folds are thus associated with the formation of the axial planar S1 foliation. Shimron (1983) concluded that D1 has taken place at shallow depth, soon after deposition. We agree with this, since the Heib Fm. was interpreted to have been deposited in an island-arc

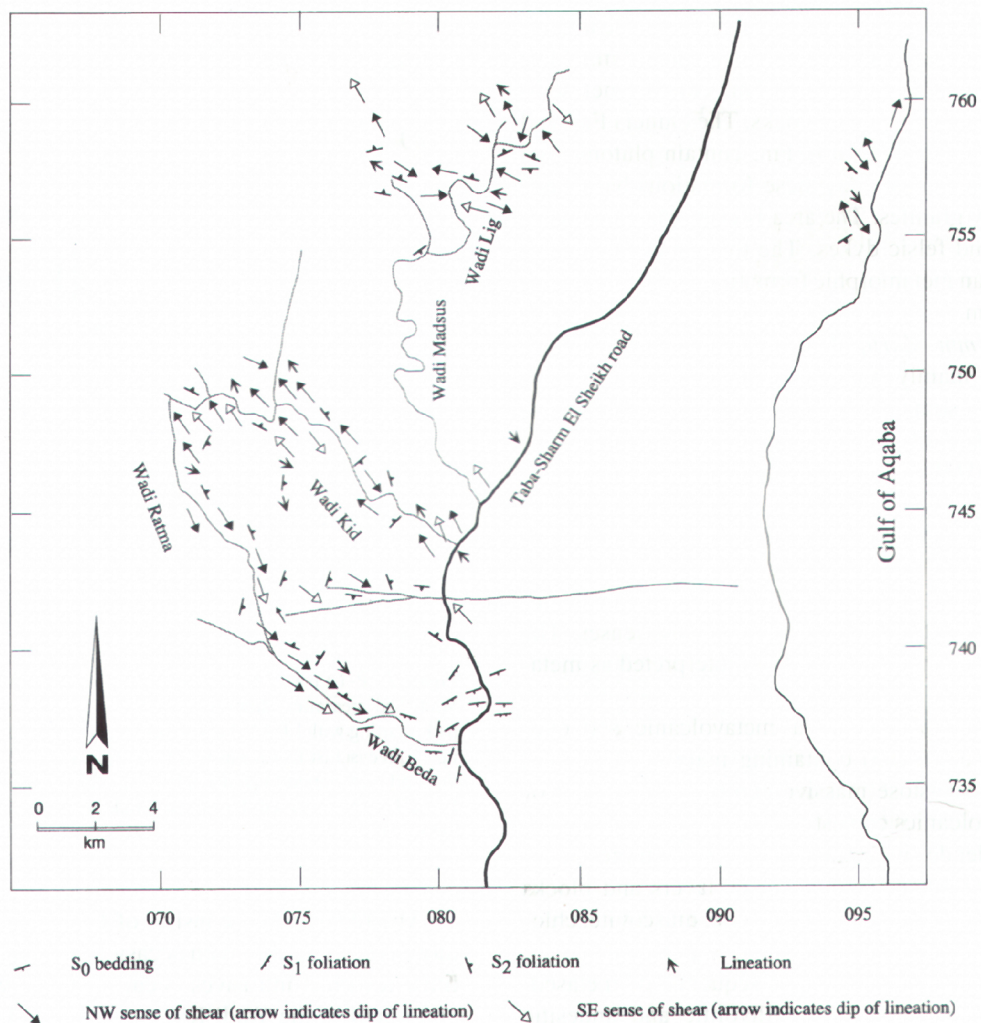


Figure 5-3 Map showing structures related to Precambrian tectonics in the Wadi Kid area.

environment (Furnes et al. 1985), since these rocks display a low metamorphic grade where sedimentary structures are recognizable, and since accretion is the oldest tectonic process recognized in other parts of the Arabo-Nubian Shield (Bentor 1985). The D1 structures were thus formed in a compressional island-arc setting. F1 folds and the associated cleavage are occasionally recognized in the Umm Zariq Fm., with a steep foliation formed by muscovite and biotite. The D1 structures in this formation were overprinted by a later foliation.

### 5.3.3 D2 structures

#### 5.3.3.1 S2 foliation

The S2 foliation is widely developed and dominates the studied area. It is flat-lying to gently dipping ( $< 30^\circ$ , Figure 5-4) and in most areas it totally masks the earlier foliation. It is a disjunctive and sometimes anastomosing foliation, formed by biotite, muscovite and chlorite. The grains in the microlithons show a rather strong preferred orientation.

The general trend in the Wadi Kid Complex is that S2 is better developed to the west

and north. S2 is best developed in the Malhaq, Umm Zariq and Quneia Fms. It is continuous through the higher-grade parts of the Heib Fm. into the Quneia Fm., indicating that the deformed tonalites and diorites of the Quneia Fm. were intruded before the development of S2. Rocks containing D1 structures overlie rocks displaying D2 structures. Slightly foliated granites were observed in the western part of the Wadi Kid Complex. These intrusives were dated at 580-530 Ma as the youngest rocks of the Sinai basement (Bielski 1982) and are thus critical for the timing of the deformation.

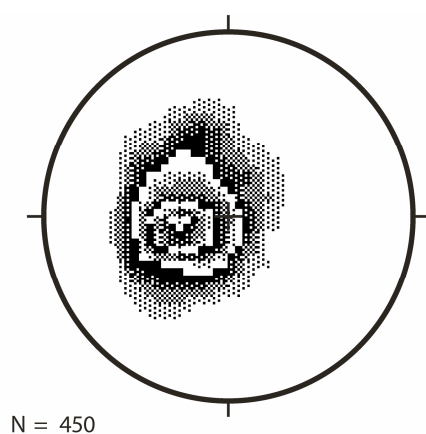


Figure 5-4 Contoured stereographic plot (equal area) of the poles to the S2 foliation in the Wadi Kid area. Contour interval = 2.0%, significance level = 3.0.

### 5.3.3.2 Lineations associated with S2

A lineation is associated with the S2 foliation and arises from an alignment of minerals such as andalusite and hornblende or from elliptical objects such as elongate xenoliths and pebbles. The lineation is sub-horizontal ( $< 30^\circ$ ), plunging either NW or SE (Figure 5-5), that is in opposite directions due to later folding. The two trends reflect one strain regime.

The mineral lineation is best developed on the S2 plane in the schists. It is mainly defined by individual minerals that grew in one uniform direction: amphiboles, sillimanite, andalusite, quartz and feldspar. Some mineral lineations are formed by elongated pods of biotite, muscovite and by quartzo-feldspathic segregations. At some places the mica pods, andalusites, quartz and feldspars are mechanically elongated and define a stretching lineation (5-6a). It is concluded that the lineation was formed partly by stretching, partly by orientated growth. The stretching lineation indicates an extensional strain in NW-SE direction; this will be discussed later. In a number of cases the elongated minerals, mainly andalusites and hornblendes, grew in random directions; this was observed in the Umm Zariq and Malhaq Fms. Their significance will likewise be discussed later.

Elongated pebbles were found in the conglomerates of the high-grade parts of the Heib

Fm., and elongated xenoliths in the deformed intrusives of the Quneia Fm. They are parallel to the general trend of the mineral lineation.

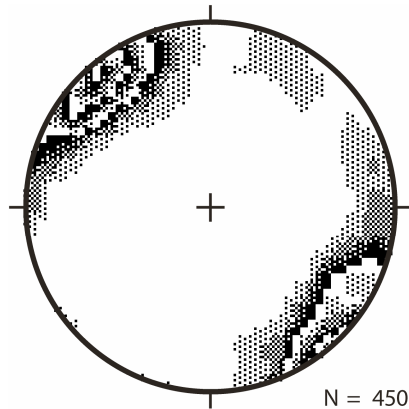


Figure 5-5 Contoured stereographic plot (equal area) of the lineations in the Wadi Kid area, showing maxima at NW and SE. Contour interval = 2.0%, significance level = 3.0.

#### 5.3.3.3 Dykes

The area is cross-cut by vertical felsic and mafic dyke swarms of Precambrian age. They are sub-parallel and strike 35 to 50°, i.e. NE-SW (Figure 5-7). Both types of dykes intruded at 590-580 Ma (Halpern 1980; Stern & Manton 1987). This age is close to the D2 ages. Along with their orientation, the contemporaneity suggests that the intrusion was related to the D2 phase.

Dyke swarms require lateral extension in the crust and the intrusion plane will be perpendicular to  $\sigma_3$ , the direction of greatest extension (Price & Cosgrove 1990). The dykes thus indicate extension in the NW-SE direction at the time of D2, the same direction as can be deduced from the stretching lineation.

#### 5.3.4 Evidence of non-coaxial strains during D2

##### 5.3.4.1 Introduction

Previously, D2-structures have been interpreted as due to an irrotational and a coaxial strain regime (e.g. Reymer 1983, 1984, Shimron 1983, 1984). However, in the course of this study we consistently found that rotational strains were present. Several possible indicators of non-coaxial strain were observed: extensional crenulation cleavage, S-C shearbands, rotated clasts with pressure shadows, asymmetric folds, deformed elliptical objects and quartz c-axis fabrics. The importance and reliability of these indicators will be discussed below.

Figure 5-3 shows the distribution of shear indicators with the sense of shear and the recorded stretching and mineral lineations. The strain was evaluated for elliptical markers.

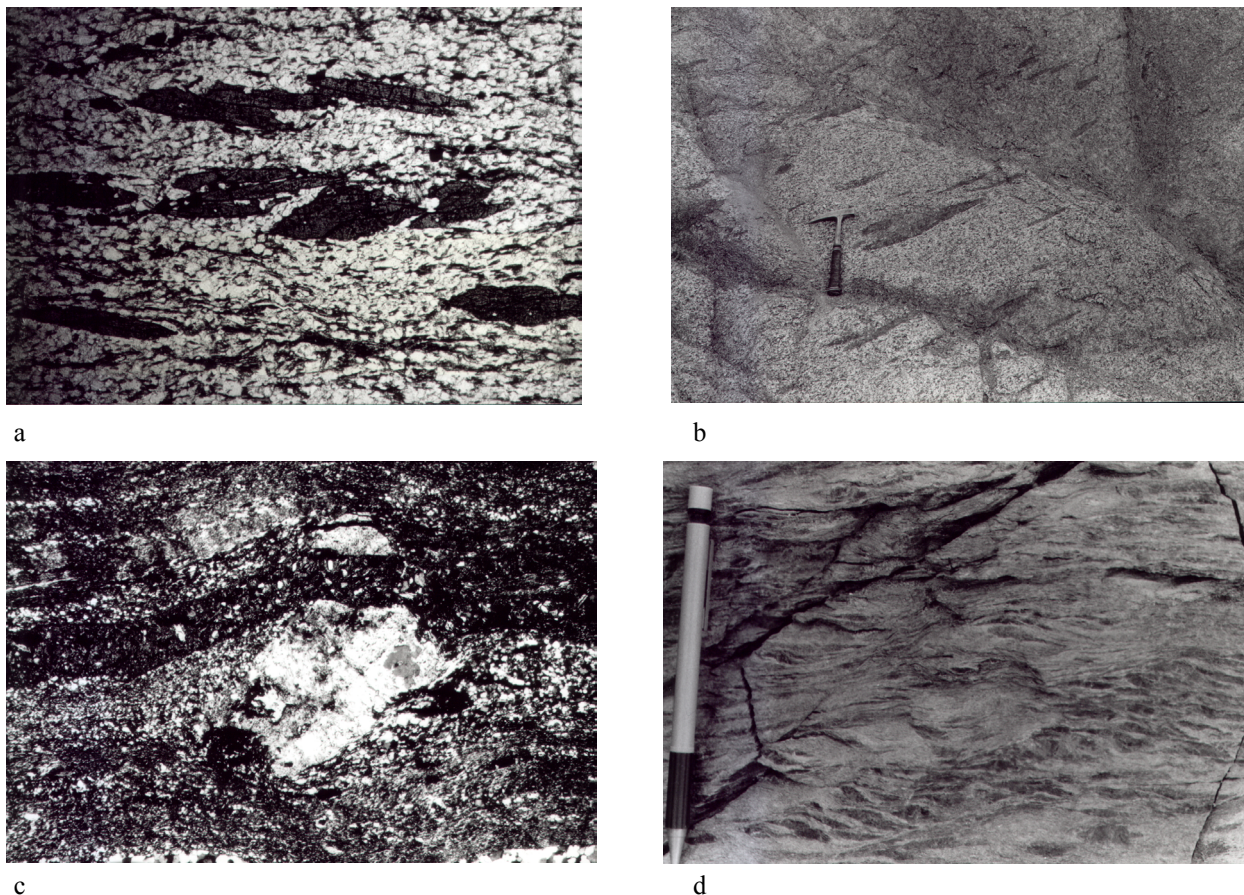


Figure 5-6 Photographs. a) Lineated hornblende, Malhaq Fm., northern Wadi Kid area. Area shown is 4.9mm x 3.4mm. b) Deformed xenoliths, Quneia Fm., NE part of Wadi Kid area. c) Rotated clast with pressure shadows indicating sinistral sense of shear Malhaq Fm., central Wadi Kid area. Area shown is 4.9mm x 3.4mm. d) Macroscopic extensional crenulation cleavage, indicating sinistral sense of shear, Umm Zariq Fm, central Wadi Kid area. Area shown is 4.9mm x 3.4mm.

#### 5.3.4.2 Finite Strain Markers

Throughout the Wadi Kid area, elliptical markers, namely xenoliths, conglomerate pebbles and boudins, were found. They can be used for a qualitative and quantitative strain analysis. These markers are regarded as good indicators of the total finite strain (Lisle 1985), which is very useful in areas with a complicated strain history. Different methods were developed to determine the strain of deformed elliptical objects, taking into account that the initial shape was not spherical and that the markers had a non-random initial orientation.

The tests for non-coaxiality were performed on deformed xenoliths, conglomerate pebbles and boudins. The xenoliths were used to perform a strain analysis with the  $Rf/\Phi$  method (Dunnet 1969; Lisle 1985). The deformed conglomerate pebbles and boudins were used for qualitative analysis and in this framework their relationships with other structural features were studied.

In the northeastern part of the Wadi Kid area, elliptical mafic xenoliths were found in a foliated and lineated syn-kinematic diorite which intruded during D2 (Figure 5-6b). The foliation in the schistose xenoliths continues into the diorite. The stretching lineation of hornblendes in the diorite is sub-parallel with the longest axes of the xenoliths.



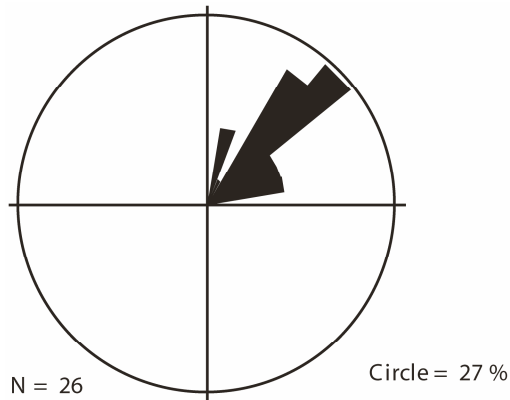


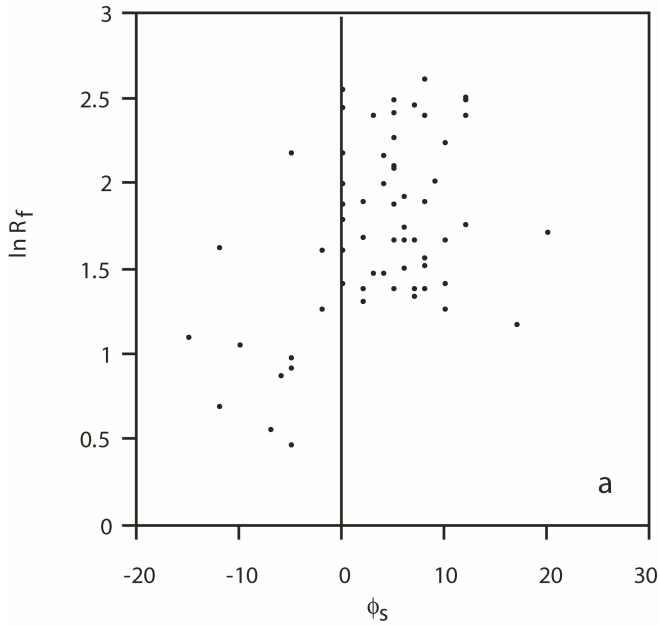
Figure 5-7 Rose diagram of the orientation of the mafic and felsic dykes in the Wadi Kid area.

The basic method, used to compute the strain, is that of Ramsay-Dunnet modified by Lisle (1985) for elliptical markers with an initial ellipticity ( $R_i$ ). This is a graphical method to compute the ellipticity of the strain ellipse ( $R_s$ ) from  $R_f$  (the final ellipticity) and the angle between the long axis of the elliptical marker and the orientation plane, in the deformed state,  $\Phi_s$ . The results of the  $R_f/\Phi$  method were compared to the harmonic mean,  $H$ , which gives a good approximation for  $R_s$  (Lisle 1977).

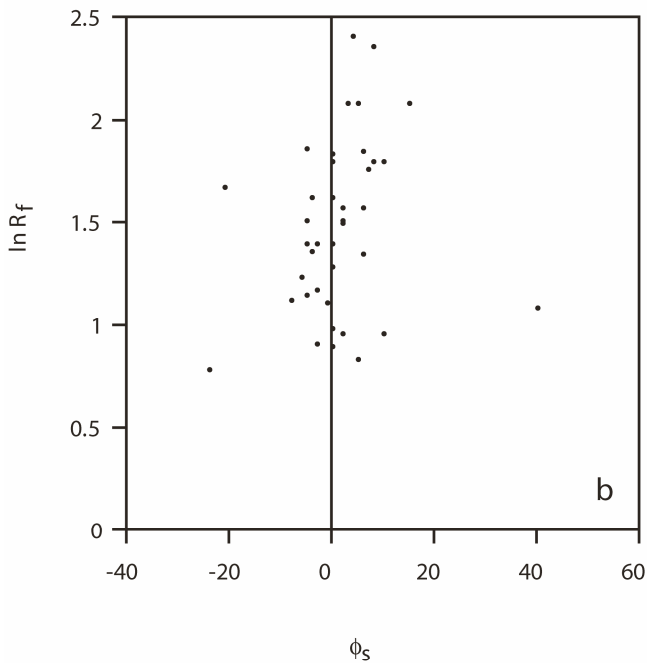
The xenoliths in the Wadi Kid area have an elliptical form and show a uniform direction of their principal axes, with the longest axis (X-axis) sub-parallel with the mineral lineation. The Z-axis is the axis of greatest shortening, so that  $X > Y > Z$ . The foliation was chosen as the reference plane. The X : Z ratio was measured on a plane parallel with the lineation and perpendicular to the foliation.  $\Phi_s$  is the angle between the X-axis and the foliation in the case of the X-Z section, and that between the Y-axis and the foliation in the case of the Y-Z section.  $\Phi_s$  was chosen positive when the orientation of the X-axis was dipping steeper to the southeast than the reference plane. The Y : Z ratio was measured on a plane perpendicular to the lineation and perpendicular to the foliation.

Eighty-five measurements were made on the X-Z plane. The final ellipticity,  $R_f$  for X-Z ranges from 1.58 to 13.5. Figure 5-8a shows the  $R_f/\Phi$  plot for X-Z. The plot shows an asymmetric distribution of points around the mean vector  $\Phi = 3.41^\circ$ . From the  $R_f/\Phi$  diagram, values for  $R_s = 4.6$  and  $R_i = 2-2.5$  are deduced. The harmonic mean,  $H$ , is 4.71. From  $H$  and the  $R_f/\Phi$  plot it can be concluded that  $R_s = 4.6-4.7$ . The mean vector,  $H$ , is  $3.41^\circ$  and so the distribution of points is asymmetric with respect to  $\Phi = 0$ . The longest axis of the plot is not parallel to the vertical base axis, revealing an internal asymmetry.

Forty measurements were made on the Y-Z plane. The  $R_f$  for Y-Z ranges from 2.167 to 11. Figure 5-8b shows the  $R_f/\Phi$  diagram for Y-Z. The distribution of the points is symmetrical around the  $\Phi = 0$  axis. From the diagram, values for  $R_s = 4.2$  and  $R_i = 1.5-2.0$  are deduced. The harmonic mean,  $H$ , gives a value of 3.95. Since  $H$  is expected to give lower values than  $R_s$



a



b

Figure 5-8  $R_f/\Phi$  plots of deformed xenoliths, Quneia Fm., NE part of Wadi Kid area. a) The X-Z section reveals the asymmetry with respect to  $\Phi = 0$  and the internal asymmetry. b) In the Y-Z section no asymmetry is visible.

(Lisle 1977), 3.95 should be a good indication for the maximum of  $R_s$  in the Y-Z plane.

Other deformed elliptical objects, such as elongated conglomerate pebbles and asymmetric elongated boudins, occur throughout the Wadi Kid area. The former were found in the relatively high-grade parts of the Heib Fm. in the central Wadi Kid area and the latter where S2 was developed. These elliptical objects have their longest axis sub-parallel with the mineral lineation and plunge slightly steeper to the southeast than the foliation, thus showing the same

structural relationships with the lineation and the foliation as the xenoliths. The deformed conglomerates and boudins show, like the deformed xenoliths, a movement of the top block to the northwest. The identical morphology and structural relations of all the deformed elliptical markers indicate a similar deformation history for all the total finite strain markers.

*Conclusions on finite strain markers:* The  $Rf/\Phi$  method is a suitable method to analyse the strain of the xenoliths, but additional data from statistic and geometrical methods are required to obtain a precise indication of the amount of strain and the initial form. Lisle (1985) showed that  $H$  gives a good approximation for  $R_s$  and used this method in cases of asymmetric distribution in  $Rf/\Phi$  plots. Best values for the  $X : Y : Z$  relationship were calculated to be 4.6 : 3.95 : 1. From this relationship it is clear that a large component of flattening is present.

The mean vector of the X-Z plane is  $3.41^\circ$  and thus asymmetric with respect to  $\Phi = 0$ . The  $Rf/\Phi$  plot for this plane also shows an internal asymmetric distribution. The mean vector  $\Phi$  for the Y-Z plane is close to  $0^\circ$  and the  $Rf/\Phi$  plot shows a symmetric distribution, and thus no asymmetry with respect to the reference plane exists. Internal asymmetries in  $Rf/\Phi$  plots are ascribed to a preferred initial orientation of the elliptical objects (Lisle 1985), which can be explained by the fact that xenoliths in syn-kinematic intrusions will have a preferred initial orientation. The asymmetry with respect to  $\Phi = 0$  is best explained as due to non-coaxial deformation (Le Theoff 1979, Choukroune et al. 1987). The X-axis is parallel to the stretching lineation but plunges steeper to the southeast than the foliation and lineation, and thus the finite strain markers indicate a NW-vergent movement of the top block during a regional shear event.

The deformed pebbles, xenoliths and boudins show the same relationships with other structural features: lineation and foliation. Since they were deposited or initially formed under different conditions, their final stage of deformation must have been similar. The asymmetry is found in the X-Z plane, parallel with the lineation and the movement direction. No asymmetry was observed in the Y-Z direction. This indicates non-coaxial deformation with the axis of rotation perpendicular to the X-Z section and movement of the top block to the northwest.

#### 5.3.4.3 Kinematic indicators

*Rotated clasts* with asymmetric pressure shadows were observed in a number of thin sections from the Wadi Kid area (5-6c). They are regarded as good indicators of the sense of displacement (Simpson & Schmid 1983) if applied as indicated by Ten Brink (1996). The rotated pressure shadows are of the displacement-controlled type with deformable fibers. These fibers indicate relatively high temperatures, allowing dynamic recrystallization. Table 5-2 and Figure 5-3 show that shear took place in two opposite directions, with the top-to-the-NW direction dominating. Some clasts are accompanied by symmetric pressure shadows. This can indicate a component of coaxial deformation, or a reversal of the shear direction, re-deforming the fibers.

Throughout the area, *extensional crenulation cleavages* (e.c.c.) were observed. They develop in the late stages of shear zone activity (Platt & Vissers 1980) and are regarded as a good indication of local shear movement.

The e.c.c.'s in the Wadi Kid are found both on meso-scale (Figure 5-6d) and on micro-

scale. They contain biotites, white micas, hornblendes and andalusites, depending on the metamorphic assemblage in the country rock. Table 5-2 and Figure 5-3 show that the e.c.c.'s, like the rotated clasts, display a top-to-the-NW as well as a top-to-the-SE shear, with the NW transport dominating. Hornblende occurs mostly in the e.c.c.'s with a sense of shear to the northwest. White mica appears in e.c.c.'s with a NW sense of shear as well as in e.c.c.'s with a SE sense of shear, but is relatively abundant in the latter e.c.c.'s. We relate the formation of the white mica with a phase of retrograde metamorphism and so the SE sense of shear postdated the NW sense of shear.

Although *asymmetric folds* can be used as shear indicators, they are not very reliable (Bell & Hammond 1984). Their reliability improves when they are viewed perpendicular to the stretching lineation, as was done in this study. During progressive deformation, fold axes tend to rotate parallel to the movement direction and are thus of little value in determining the sense of movement. The few asymmetric folds that were found in the Wadi Kid area indicate a NW sense of shear.

#### 5.3.4.4 Quartz c-axes as indicators for non-coaxial deformation

Quartz fabrics record deformation caused by plastic deformation mechanisms and can give information about the type and conditions of deformation (Price 1985). Coaxial deformation produces symmetrical patterns with respect to the principal axes of finite strain and thus with respect to the foliation, whereas non-coaxial deformation produces an asymmetric fabric. The latter points to a mylonitic origin of a schistose rock. The type of slip system in the quartz grains can be deduced from the quartz c-axis fabric, thus providing an indication of the relative temperature at which the deformation took place.

The samples used in the quartz c-axis studies were cut parallel to the lineation and perpendicular to the foliation. Twelve samples were chosen from the Wadi Kid Complex. A minimum of 125 grain measurements were made on each sample. Figure 5-9 shows the location and quartz fabrics of the studied samples. Figure 5-10 shows the position of the different maxima in a quartz c-axis plot (after Fueten et al. 1991); this plot was used for the interpretation of the fabrics. Table 5-2 summarizes the results of the quartz c-axis studies. On the basis of their patterns, the quartz c-axis fabrics were divided into three groups. These groups indicate different slip systems and consequently different conditions of deformation.

Samples WJ 9, WJ 22 and WJ 42 belong to the *first group*. Their fabrics display single girdles and maxima are best developed at I or II. The maxima are at angles of 30° with the lineation. This fabric indicates slip along the basal plane in the <a> direction plus minor activity on the rhomb and prism in an <a> direction and is indicative of relatively low temperatures of deformation (Jessel & Lister 1990).

WJ 42 comes from the transitional area between low-grade and high-grade Heib Fm. and formed at relatively low temperature. The fabric asymmetry indicates top-to-the-NW movement. Rotated clasts in this sample show a reverse shear direction. Quartz c-axis fabrics will, in most cases, record the last stages of deformation (Lister & Hobbs 1980) and it is also likely that the last increments of deformation will be concentrated in the quartz-rich bands. The

rotated clasts are thus indicative of the earlier stages of deformation and the quartz fabric of WJ 42 is reflecting a later overprint. Sample WJ 9 shows the same characteristics of deformation as WJ 42, but the mineralogy of this rock indicates a higher metamorphic grade. The fabric shows movement of the topblock to the northwest indicating deformation after peak metamorphism.

Sample WJ 22 did not show any macroscopic or microscopic shear indicators, but a clear quartz fabric asymmetry was observed, indicating movement of the top block to the northwest. The c-axis fabric indicates basal  $\langle a \rangle$  slip with a significant rhombic component, which takes place at low-to-medium temperatures. From WJ 22 it can be concluded that deformation continued to take place until the later stages of cooling and thus relatively late in the development of the Sinai basement.

The *second group* of quartz c-axis fabrics is distinguished from other groups by the fact that the fabrics contain a maximum at III. This maximum is connected with the maxima at I and/or II via a girdle, depending on the shear-direction. The maximum at III indicates that the prism  $\langle a \rangle$  slip system was active, which indicates that deformation took place at medium temperatures (Tullis et al. 1973; Schmid & Casey 1986). The basal  $\langle a \rangle$  and prism  $\langle a \rangle$  slip systems are thus active in this group.

Samples B 20, B 29, P 37 and WJ 29 belong to this group. In sample B 29, c-axes appear between III and I, indicating that also the rhomb  $\langle a \rangle$  slip system was active and that deformation took place at intermediate-high temperatures. This sample indicates a movement of the top block to the southeast. Sample WJ 29 is a biotite schist from the high-grade part of the Heib Fm. near the contact with granitoid rocks. It displays a NW-vergent sense of shear. Sample B 20 is from the relatively high-grade rocks of the Malhaq Fm. and indicates a top-to-the-SE movement. Sample P 37 comes from the slightly foliated tonalites in the Wadi Quneia/Wadi Ratma area and displays a movement of the top-block to the northwest. It shows less evidence for rhomb slip, as the prism and basal sections are more isolated.

The samples of the *third group* have strong maxima at I and at II, but in all cases one of the two maxima was better developed than the other and no maxima are found in III. The angles between the I and II maxima are  $50^\circ$ . They resemble small-circle girdle fabrics and are a special case of type-I crossed girdles (Schmid & Casey 1986). This fabric shows strong flattening. The active slip systems were basal  $\langle a \rangle$  with rhomb  $\langle c+a \rangle$ , indicative of deformation at medium to higher temperatures.

Samples B 18, B 61, P 16 and P 39 belong to this third group. Samples B 18 and B 61 are from the high-grade biotite schists of the Malhaq Fm. Both show a NW sense of shear with a rather strong flattening. Sample P 16 is from the high-grade metapelites of the Umm Zariq Fm. The fabric indicates movement to the southeast but other shear indicators in this sample show a NW movement. At other outcrops in this area SE-vergent shear indicators were observed. Sample P 39 is from the gneissic tonalites of the Quneia Fm., and displays a NW sense of shear.

All studied samples show a well-developed quartz c-axis fabric. The individual fabrics display an asymmetry, indicating non-coaxial deformation. The three groups were distinguished on the basis of the fabric, which is related to the temperature of deformation. Deformation temperatures vary from relatively low to intermediate-high metamorphic conditions. The

Table 5-2 Results of quartz c-axis studies from the Wadi Kid area. For locations see Figure 5-9.

Sample	Rock type	Metamorphic grade	Fabric group (see text)	Likely slip system	Movement deduced from quartz c-axis fabrics	Movement deduced from other features	Comments
B 18	hbl-bio schist	amphibolite	3	basal <a> and $\pm$ rhomb <c+a>	NW	NW (e.c.c. and rotated clasts)	A component of flattening
B 20	hbl-bio schist	amphibolite	2	prism <a> with basal <a>	SE	NW (e.c.c.)	-
B 29	hbl-bio schist	upper greenschist-- lower amphibolite	2	prism <a> with basal <a> and rhomb <a>	SE	SE (rotated clasts)	A component of flattening
B 61	hbl-bio schist	upper amphibolite	3	basal <a> and $\pm$ rhomb <c+a>	NW	NW (e.c.c.)	A small component of flattening
P 16	and-gnt-bio schist	amphibolite	3	basal <a> and $\pm$ rhomb <c+a>	SE	NW (e.c.c.)	Outcrops in this area show SE shear.
P 17	sill-gnt-bio schist	amphibolite	2	prism <a> with basal <a>	SE	SE (e.c.c.)	A component of flattening
P 37	deformed tonalite	-	2	prism <a> with basal <a>	NW	NW (deformed xenoliths)	A small component of flattening
P 39	deformed tonalite	-	3	basal <a> and $\pm$ rhomb <c+a>	NW	-	A component of flattening
WJ 9	and-gnt-bio gneiss	amphibolite	1	basal <a> and minor prism and rhomb <a>	NW	NW (e.c.c.)	-
WJ 22	deformed granite	-	1	basal <a> with significant rhomb <a>	NW	-	Deformed younger granite
WJ 29	bio schist	greenschist	2	prism <a> with basal <a>	NW	NW (e.c.c.)	A component of flattening
WJ 42	bio schist	greenschist	1	basal <a>	SE	NW (rotated clasts)	-

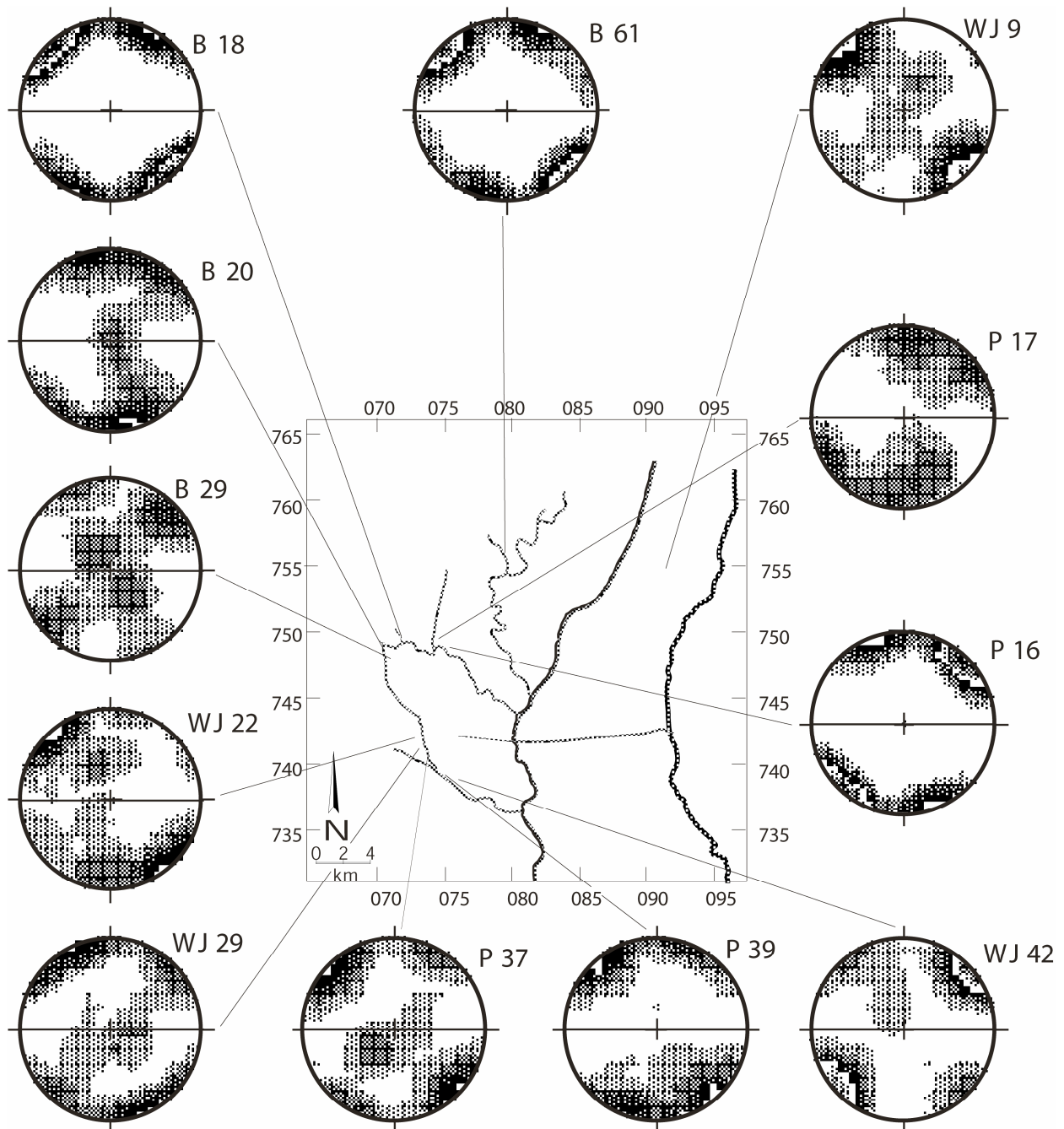


Figure 5-9 Locations and quartz *c*-axis fabrics of the studied samples listed in Table 2. Contour interval = 2.0%, significance level = 3.0.

single-girdle fabrics (group 1) come from the lower-grade rocks, which are found at the upper structural levels. Higher-grade rocks (groups 2 and 3) were deformed at higher temperatures and are from a structurally lower level throughout the complex. These high-grade samples show a more coaxial type of deformation. Movement reversals appear also in the quartz *c*-axis fabrics and will be discussed later.

Sample WJ 22 shows non-coaxial deformation in a relatively late granite (530 Ma,

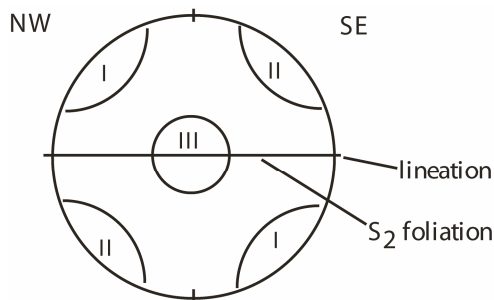


Figure 5-10 Positions of the different maxima in the quartz c-axis plot.

Bielski 1982) implying that the deformation continued after the intrusion of this body.

## 5.4 Discussion

### 5.4.1 Interpretation of regional structural data

Our study indicates that in the Wadi Kid area a clear distinction can be made between D1 and D2 structures on the basis of the types of structures and their metamorphic grades. The D1 structures consist of an axial planar slaty cleavage, namely S1 foliations related to F1 isoclinal folds. The F1 folds in lower-grade rocks were formed in a compressional regime. No indicators of non-coaxial deformation were observed in these relatively low-grade rocks.

The second deformation phase, D2, formed a flat-lying foliation (S2) which is the most important structure in the area. The abundant evidence of asymmetry indicates that the areas of intense foliation-development mark D2 shear zones.

The elongated minerals, formed on S2 surfaces, are mostly orientated in NW-SE direction. Stretching of the elongated minerals indicates that peak-metamorphism started before or during D2. The growth in a preferred parallel orientation of hornblende, andalusite and sillimanite indicates that peak-metamorphism continued during D2. Randomly orientated hornblendes and andalusites were also found and could indicate either that peak-metamorphism outlasted D2 or that the randomly orientated minerals grew in low-strain pockets, implying that the strain regime was not active through the whole shear zone during the entire deformation phase. The latter interpretation seems to fit best the observations in the Wadi Kid area.

The Wadi Kid area is cross-cut by dykes in NE-SW direction, perpendicular to the NW-SE trending lineation. This indicates that extension took place in NW-SE direction.

The indicators of non-coaxial strain were only found in the areas where S2 was developed. Table 5-3 summarizes the different types of shear indicators with the sense of movement. Deformed pebbles, boudins and xenoliths are indicators of total finite strain and all show a non-coaxial deformation with movement of the top block to the northwest. Other non-coaxial shear indicators, such as rotated clasts with pressure shadows, extensional crenulation cleavages and quartz c-axis fabrics, predominantly produce a NW sense of shear but some



Table 5-3 The numbers and senses of movement of the different shear indicators, observed in the Wadi Kid area.

Type of shear sense indicator	Macro.		Micro.	
	NW	SE	NW	SE
Deformed elliptical objects	10	-	-	-
Rotated clasts	5	4	12	5
Extensional crenulation cleavage	20	11	21	8
S-C fabrics	1	-	1	-
Asymmetric folds	6	1	-	-
Quartz c-axis fabrics	-	-	7	5

indicate the reverse direction. From the structural map (5- 3) it is difficult to indicate certain areas with one sense of shear and other areas with the reverse sense, but it was rare that within one outcrop (i.e. on a metre scale) shear indicators with opposite sense were found. The distribution of the sense of shear is thus heterogeneous.

The duality in shear sense may be ascribed to coaxial deformation when flexural slip took place in different limbs of a fold. However, this does not agree with the trend of the S2 foliation and the direction of extension, nor with many of the asymmetric features. Because these latter features are abundant and form synthetically a well-developed stretching lineation, the foliation can be interpreted as a mylonitic foliation resulting from flat-lying shear zones. The main movement of the top block in the Wadi Kid area was interpreted to be to the northwest, since finite strain markers and some 70% of the shear indicators were found to indicate a NW sense of shear.

#### 5.4.2 A core-complex model for the Wadi Kid area

A cross section of the Wadi Kid area according to our interpretation is shown in Figure 5-11. The relationship between the sub-horizontal mylonitic sequences formed in an extensional regime, the upper-crustal low-grade rocks related to an early compressive tectonic phase, the high metamorphic gradients, and the syntectonic granitoids as observed in the area, indicate together a core-complex development. This is investigated below. Much has been published about core complexes in a variety of localities such as the Basin and Range province, U.S.A. (Davis 1980; Davis & Lister 1988), the Canadian Cordillera (Malavieille 1987; Liu & Furlong 1993), the Aegean Sea, Greece (Lister et al 1984), and Variscan core complexes in the Massif Central, France (Malavieille 1993). Below, some of the most important characteristics found in these core complexes are reviewed and compared to those of the Wadi Kid Complex.

The ideal core complex consists of a core of granitoids, gneisses and other lower crustal rocks, overlain by a major mylonite zone. Relatively low-grade rocks, preserving relicts of an earlier deformation phase, overlie this zone. The mylonite zone tends to be sub-horizontal with a near-constant direction of the stretching lineation through the whole area (Davis 1980). The mylonites form at depths of at least 10 km and at temperatures of at least 500° C, with a thermal

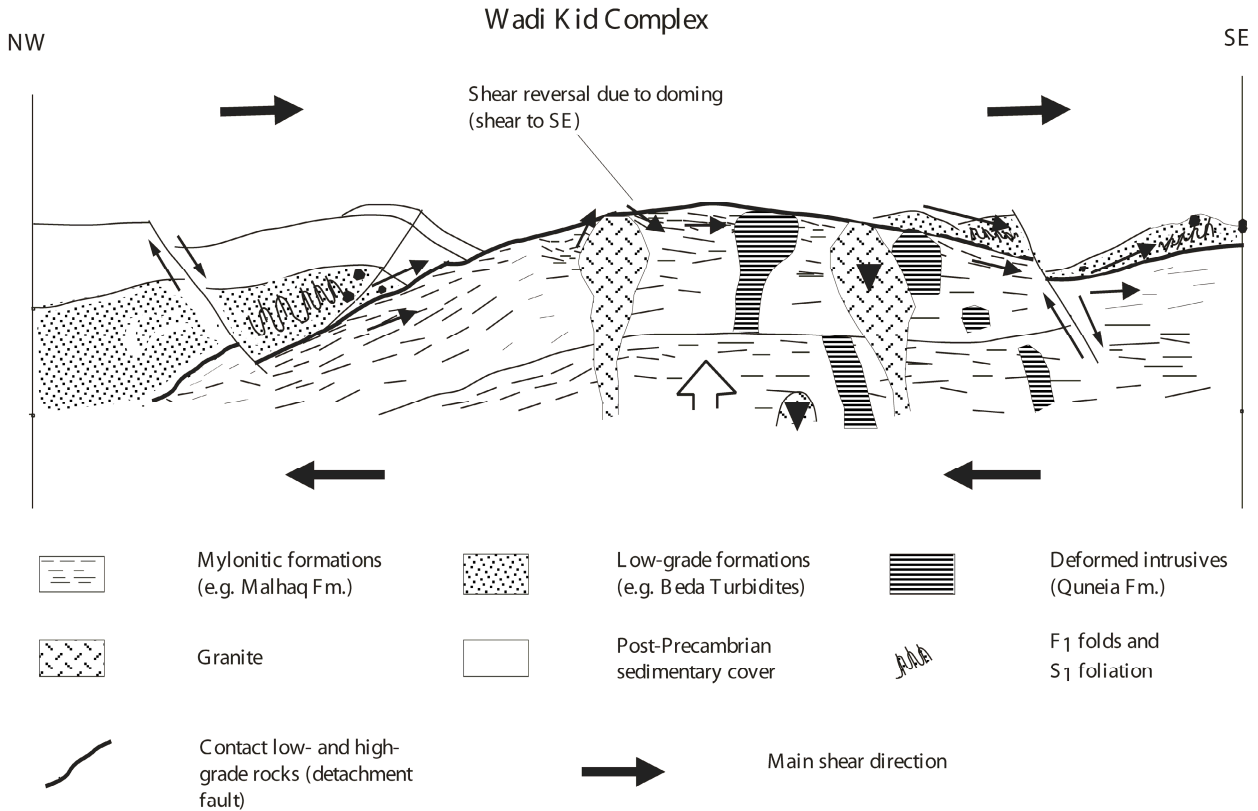


Figure 5-11 Schematic interpreted cross-section through the Wadi Kid Complex. High-angle normal faults were formed during the opening of the Gulf of Aqaba in the Miocene. The sedimentary cover is found to the northwest of the Wadi Kid area mapped in Figure 1. Length of section is approximately 50 km, height is approximately 10 km.

gradient of  $\geq 50^\circ/\text{km}$ , and at pressures of 3.5 to 4.5 kbar (Davis & Lister 1988). The mylonitic zones normally have a thickness of about 1 km but may reach a thickness of 3.5 km (Davis & Lister 1988). The mylonitic rocks are generally interpreted as gently dipping low-angle normal shear zones of the type envisaged by Wernicke (1985), and are related to continental extension. The mylonites contain indicators of non-coaxial deformation which show the general direction of movement. However, in many cases a mixed mode of deformation, i.e. non-coaxial and coaxial deformation, is found and reversal of the sense of shear is observed (Malavieille 1993). The complicated deformation history makes kinematic interpretation difficult but this is characteristic of strain development in an extensional core-complex setting (Malavieille 1993). Undeformed younger intrusives cross-cut all other sequences of the complex.

The core in the Wadi Kid metamorphic complex consists of deformed tonalites and diorites of the Quneia Fm., which have a gneissic appearance. Gneissic rocks were also described in other parts of the Sinai (Shimron 1980; Stern & Manton 1987). The mylonitic Malhaq and Umm Zariq Fms. and the northern and western high-grade parts of the Heib Fm. form the mylonitic drape over the core. This drape is approximately 1.5 km thick. These formations contain a sub-horizontal foliation with a constant NW-SE trending stretching lineation. The low-grade rocks of the Heib Fm., overlying the mylonitic formations, form the upper part of the core complex, with the D1 compressive phase as a relict of an earlier

deformation event. Metamorphism in the mylonitic formations is of a LP/HT type (Shimron 1987). The thermal gradient was  $\geq 50^\circ/\text{km}$  and the foliated formations were formed at a depth of at least 10 km (Reymer et al. 1984).

In the Wadi Kid area a large variety and large number of shear sense indicators were observed. The axis of rotation of the sense of asymmetry from the kinematic indicators is always perpendicular to the stretching lineation. About 70% of the shear sense indicators show movement of the top block to the northwest; the rest shows movement to the southeast (Table 5-3). Part of the non-coaxial strain markers show a coaxial component. All the finite strain markers, indicators of the total strain, point to a sense of shear to the northwest. For this reason the mylonitic formations are interpreted as low-angle shear zones with a movement of the top block to the northwest.

The formation of core complexes is accompanied by extensive magmatism. Basaltic intrusives and syn-kinematic dykes intruded perpendicular to the direction of extension (Anderson & Cullers 1990; Hazlett 1990). Diorites and granodiorites, often syn-kinematic, are the oldest intrusives in core complexes (Barton 1990; Anderson & Cullers 1990). Younger granitoids, intruded during the extensional phase, have a more alkaline granitoid composition (Barton 1990; Anderson & Cullers 1990). In the Wadi Kid area the dykes strike NE-SW, perpendicular to the lineation and thus indicating extension in the NW-SE direction during D2. The older intrusives are I-type granitoids, and younger intrusives are A-type alkaline granites (Ahmed et al. 1993). In other parts of the Arabo-Nubian Shield the older I-type granites are interpreted to have been related to a phase of crustal thickening during orogenic compression, while the A-type granites are interpreted to have been related to extension and crustal thinning when melts were arising from the mantle (Beyth et al. 1994; Greiling et al. 1994).

The features observed in core complexes such as that in the Wadi Kid area, are best explained as developing during orogenic collapse (Dewey 1988). The orogenic history starts with a period of compression and crustal thickening. When convergence slows down, thermal re-equilibration will start. Erosion and convective thinning of the root will cause extension and associated with this, there will be an increase in magmatic activity. The thermal gradient will increase rapidly. The extension may be accommodated by low-angle shear zones (Wernicke 1985). The metamorphism will show a clockwise P-T-t path, characterizing uplift in an extensional setting after a compressional phase, as is the case in the Wadi Kid area.

#### *5.4.3 Reversal in the sense of shear and coaxial overprint in core complexes*

The presence of opposing senses of shear and of components of coaxial deformation posed problems in the kinematic interpretation of the Wadi Kid area, where some 70% of the shear indicators show a top-to-the-NW movement and the rest shows movement to the southeast. Since all finite strain markers show the top-to-the-NW movement, the main deformational event is interpreted to have this sense of shear. Reversal of shear sense and minor components of coaxial deformation are regarded as characteristic features of core complexes (Malavieille 1987, 1993; Davis & Lister 1988; Spencer 1984; Reynolds & Lister 1990; Gautier & Brun 1994). Reynolds & Lister (1990), Malavieille (1993) and Gautier & Brun (1994) suggested that upward bending of the lower plate as an isostatic response to tectonic denudation and doming

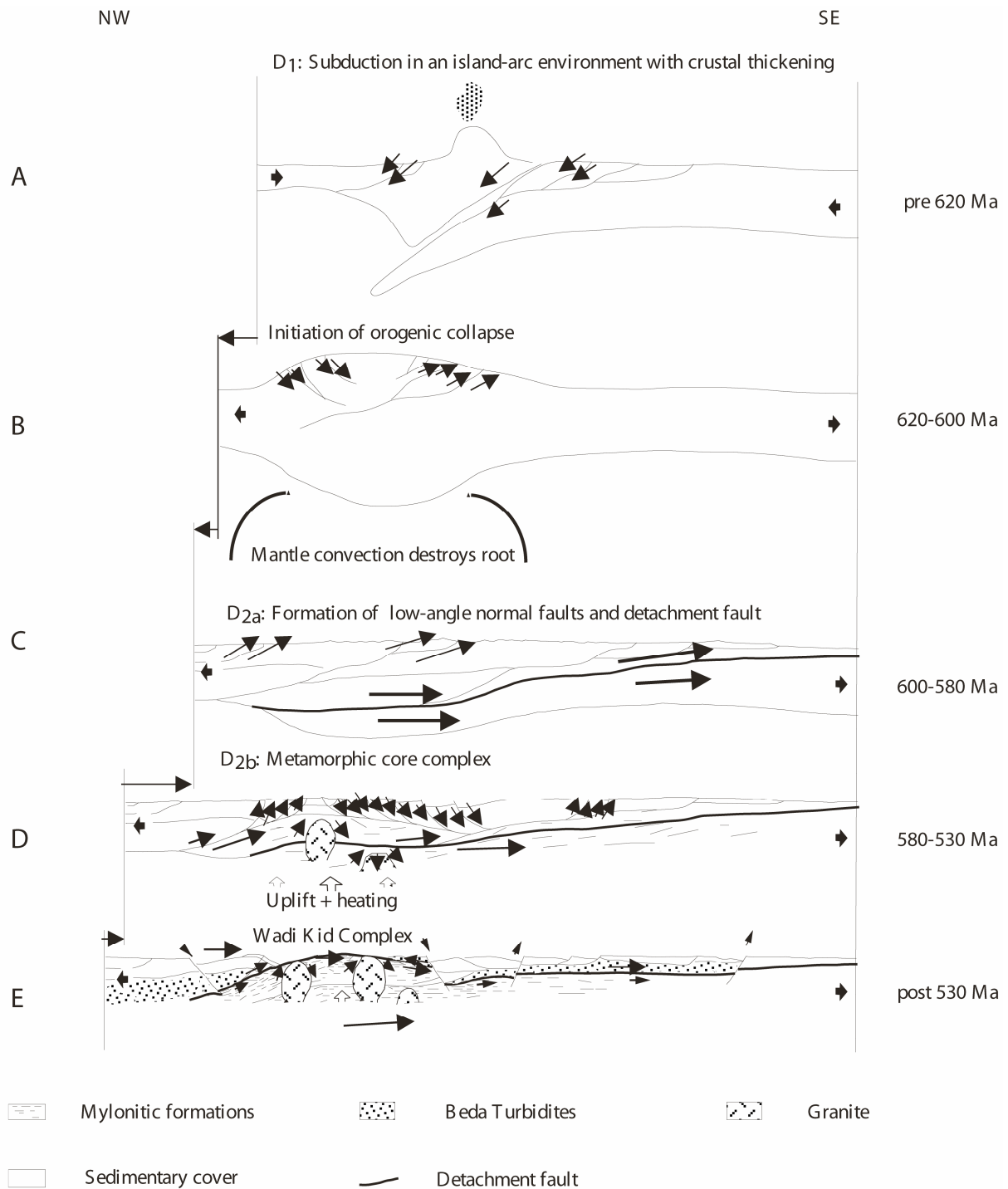


Figure 5-12 Model for the different stages of the formation of the Wadi Kid Core Complex. At stage A, shortening took place with subduction in an island-arc setting, and extensive crustal thickening (D1). At stage B, convection at the root initiated extension. At C the actual collapse started with the formation of low-angle normal faults, including the detachment fault (D2a). At stage D granitoids intruded, causing local reversal of the sense of shear due to upwarping of the detachment fault (D2b). Stage E shows the situation as observed today (Figure 11) with the late Precambrian shear directions. Ages are interpreted from literature data (Table 4).

Table 5-4 Timing of the different phases of metamorphism and deformation in the Wadi Kid area as deduced from the literature (see 'Geological background').

\* In the literature (e.g. Bielski 1982, Halpern & Tristan 1981) some D2 rocks were dated pre-620 Ma, whereas D1 was also dated at pre-620 Ma. To the north, older ages were recorded for D1. No dates are available for the low-grade rocks in the Wadi Kid area (e.g. the Beda Turbidites). These dates, interpreted by Bielski (1982) and Halpern & Tristan (1981) as D1, may very well reflect D2 ages. Mafic xenoliths resembling rocks of the Malhaq and Heib Fms were found in deformed diorites dated at 620 Ma and indicate that volcanism took place well before 620 Ma ago.

Age	Deformation	Deformation features	Metamorphism (facies)
pre-620 Ma*	D1	S1, F1 folds.	M1 (lower greenschist)
620* --560 Ma*	D2 (Main phase)	S2, lineation, deformed elliptical objects, rotated clasts, e.c.c.'s, asymmetric folds, quartz c-axis fabrics.	M2 (upper greenschist to amphibolite)
post-560 Ma	D2 (Shear sense reversal)	”	”

above plutons can cause shear reversal. In such cases the shear zone will undergo uplift and flexure, and parts of the shear zone will eventually dip to the opposite direction. Movement in the initial direction will stop in these parts of the shear zone, and reverse movement will start. The reverse sense of shear is thus a later overprint feature.

Gravimetric and aeromagnetic studies indicate the presence of elongate NE-SW trending intrusive bodies in the Sinai (Folkman & Assael 1980a, b; Ghazala 1995). The reversal of shear sense took place in the later stages of the development of the Wadi Kid area and is thus related to the intrusion of the younger NE-SW trending granitic plutons near this area, when uplift at LP/HT conditions occurred. These intrusions caused the uplift and flexure of the shear zone, and normal movement to the southeast started at their southeasterly sides. The SE movement, as recorded in some 30% of the shear indicators, is thus an overprint. This is in accordance with our metamorphic studies, which show that white micas are predominantly present in the SE-vergent shear-indicators. The SE movement was due to normal movement in a shear zone along the SE side of an intruding granite, northwest of the Wadi Kid area, at the later stages of the formation of the core complex. Ayalon et al. (1987) found evidence in amphibolite schists for a second thermal pulse at 560-530 Ma, after the main phase at 600 Ma. This phase can be related to the intrusion of younger plutons and so the shear reversal event can be dated at 560-530 Ma.

The general trend of the quartz c-axis fabrics shows a transition from a stronger coaxial component at the lower structural levels to a stronger non-coaxial component at higher structural levels. This is in agreement with findings of Malavieille (1993) for quartz c-axis studies of the core complexes in the Basin and Range province, U.S.A. He concluded that low-angle normal shear zones will show a strain distribution through such a shear zone as described above for the quartz c-axis fabrics, contrary to compressional settings, where a homogeneous distribution of strain is to be expected (Malavieille 1993). He attributes this variation in the style of deformation through extensional shear zones to the different amount of rotational strain between the highly deformed upper crustal rocks of the hanging wall and the less deformed basement in the footwall, below the shear zone. This also explains the coaxial component of

strain, as observed in the deformed xenoliths within the gneissic lower-crustal diorites. Malavieille (1993) also demonstrated that deformation, in the shearzone, will be increasingly non-coaxial away from the axis of the dome. This all explains the complex strain patterns in the Wadi Kid area.

#### 5.4.4 A model for the tectonic history of the Wadi Kid area

Our model for the tectonic development of the Wadi Kid area in the late Precambrian is summarized in Figure 5-12 and Table 5-4. In an island-arc setting, volcanics of the Heib and Tarr Fms. were deposited prior to 620 Ma. In this period, compression caused by the subduction was responsible for the D1 deformation phase. At the same time, or slightly afterwards, I-type granitoids intruded. After a phase of crustal thickening related to the subduction of an oceanic plate, orogenic collapse started with extension in NW-SE direction, starting at 620 Ma. The schistose units of the Malhaq, the Umm Zariq, and the northern and western Heib Fms, and the deformed tonalites and diorites testify to the low-angle shear zone. During the extensional phase, dyke swarms intruded with a NE-SW strike. All the units were intruded by granites. The main movement along the shear zone was to the northwest, as deduced from the indicators of finite strain. Doming of younger NE-SW trending granitoid bodies near the Wadi Kid area caused upwarping of the main shear zone and reversal of the sense of shear. The heterogeneous strain distribution through the shear zone was responsible for the coaxial component as observed in the deformed xenoliths and the c-axis fabrics. Deformation continued until after intrusion of the late granites.

The core-complex model explains why the D1 shortening phase is only found at the upper crustal levels, while the horizontal cleavage is observed at lower crustal levels.

## 5.5 Conclusions

The Precambrian rocks in the Wadi Kid area display two main phases of deformation: D<sub>1</sub> and D<sub>2</sub>. The present study offers new data and interpretations and leads to the following conclusions:

- 1) D<sub>1</sub> is a compressional phase related to island-arc subduction as recorded from F<sub>1</sub> folds and the S<sub>1</sub> foliation. It took place before 620 Ma.
- 2) A D<sub>2</sub> deformation phase, dated at 620-580 Ma, was responsible for the main structural features in the area, i.e. the sub-horizontal foliation and the well-developed stretching lineation. The foliation was formed due to mylonitization in a low-angle normal shear zone. The mineralogy indicates that the deformation took place at LP/HT conditions.
- 3) Shear indicators and quartz c-axis fabrics confirm that non-coaxial deformation took place. Finite strain markers such as deformed xenoliths and pebbles indicate a movement of the top block to the northwest in the shear zones. Most of the shear indicators, such as rotated clasts with pressure shadows, extensional crenulation cleavage, and quartz c-axis fabrics also indicate NW-vergent shear, but some indicate movement to the southeast.
- 4) The reversal of movement along mylonites was caused by upwarping due to the intrusion of granitoid bodies near the Wadi Kid area at the latest stages of the Pan-African orogenesis, 560-

530 Ma ago.

5) Dyke swarms, dated at 590-580 Ma, striking NE-SW and perpendicular to the lineation indicate extension in NW-SE direction.

6) The structures and metamorphism observed, support a core complex model for the Wadi Kid area.

7) The transition from the D1 compressional regime to the D2 extensional regime was due to orogenic collapse.





## **A new geodynamic model for the Neoproterozoic of the Arabian-Nubian Shield**

### **6.1 Introduction**

In the framework of this study, research was performed in a number of areas of the ANS that are thought to represent examples of the typical tectonic stages in its Neoproterozoic development: 1) the oceanic stage, which includes mainly remnants of intra-oceanic subduction, 2) the arc-accretion stage and 3) a late extensional stage which is still controversial (see chapter 2). The main goal of this chapter is to integrate the data from the different areas in this thesis, together with relevant data from literature, and to create an updated tectonic model for the Neoproterozoic evolution of the ANS.

### ***6.2 Summary of newly obtained data for the three main tectonic phases in the Arabian-Nubian Shield***

#### *6.2.1 Introduction*

The most important data that were obtained in the framework of this study include kinematic data for the Bi'r Umq Complex and kinematic and geochronological data for the Tabalah and Tarj Complex and the Wadi Kid Complex. Their results are summarized in Figure 6-1. Also included in Figure 6-1, are similar published data for the Nabitah Belt. The location of the studied areas and key structures in the ANS is shown in Figure 6-2.

#### *6.2.2 The Bi'r Umq Complex: Relicts of the oceanic stage and the arc-accretion stage*

Research was performed in the framework of this thesis in the Bi'r Umq Complex in Saudi Arabia (Figure 6-2) because it is thought to contain relicts of two of the three main tectonic phases in the ANS, namely the oceanic stage and arc-accretion stage. The Bi'r Umq Complex is part of the Nakasib-Bi'r Umq suture and is described in detail in chapter 3. The study focused on the detailed structural/kinematic analysis of the key structure in the area, the Bi'r Umq Shear Zone (BUSZ).

The Bi'r Umq Complex consists of a lithological sequence with ultramafics, basalts and cherts. In other parts of the Nakasib-Bi'r Umq suture, complete ophiolitic sequences were found (e.g. Johnson et al., 2002) and therefore the Bi'r Umq Complex (BUC) is assumed to be a dismembered ophiolite. In Chapter 3, it was interpreted as a suprasubduction ophiolite that was formed in a fore-arc or a back-arc because it contains a mixed MORB/OIB geochemistry and is located close to the island-arc relicts of the Jiddah Terrane and Hijaz Terrane. This is in agreement with the interpretations of Johnson et al. (2002) and Dilek and Ahmed (2003) and it was thus formed at an intra-oceanic subduction environment. The ophiolite was thought to have

been formed at ~830 Ma (Pallister et al., 1988).

The detailed structural/kinematic research, described in Chapter 3, focused on the WSW-ENE trending BUSZ. In this shear zone, three phases of deformation were identified. D1-structures include sub-vertical WSW-ENE trending foliations, steeply NW plunging lineations and shear sense indicators that indicate top-to-SE movement. On the basis of these structural observations, it was concluded that the D1-phase resulted in SE-vergent thrusting on the BUSZ. Thrusting was also observed on other WSW-ESE to SW-NE trending shear zones in the BUC and the surrounding areas. Therefore, it was concluded that the D1-structures formed during NW-SE to NNW-SSE compression (Figure 6-1). The emplacement of the Bi'r Umq ophiolite took place during the NW-SE compressional regime of D1 which happened at an intra-oceanic subduction zone. D2-structures, only observed in the central part of the WSW-ENE-trending BUSZ, included sub-horizontal WSW trending lineations that were formed on the S1-foliation, and dextral shear sense indicators. These structures indicated dextral strike-slip with a minor transpressional component. The D2-structures resulted from WNW-ESE compression. The D3-structures, like the D2-structures, were only observed in the BUSZ. They consist of sinistral shear sense indicators. These were developed along the sub-horizontal WSW lineations that were initially formed during D2. Consequently, these structures indicated sinistral strike-slip shear reversal on the BUSZ and were interpreted to result from NNE-SSW compression.

D1, D2 and D3 all took place after 820 Ma and before 760 Ma however no constraining dates are available for each of these phases independently. During this period, arc-accretion along the NE-SW trending ophiolitic sutures was the prevailing tectonic process in the ANS (see Chapter 2). This, combined with the fact that the Bi'r Umq Complex contains features that are typical for ophiolitic sutures that were formed during arc-accretion, implies that the deformation that was observed for D1, D2 and D3 resulted from a process that involved accretion of terranes at a subduction zone. The arc-accretion resulted in the compression that was observed during the deformation phases in the Bi'r Umq Complex. This sequence of events is summarized in Figure 6-1. In Chapter 3, it was proposed that the changes in the directions of compression of the different deformation phases were caused by the change of the direction of plate motion of subducting plates during arc-accretion. The reasons for the changes in the directions of compression will be discussed in more detail below.

### *6.2.3 The Tabalah and Wadi Tarj Complex: Relicts of the oceanic stage and the arc-accretion stage*

The Tabalah and Wadi Tarj Complex in Saudi Arabia (Figure 6-2) was chosen as a research area because it contains relicts of two of the three main tectonic phases of the ANS, namely, the oceanic/island-arc phase and the arc-accretion phase. The Tabalah and Wadi Tarj Complex is in the central part of the Asir Terrane and its geology will thus reflect intra-terrane relicts of the oceanic phase and the arc-accretion phase, opposed to the Bi'r Umq Complex which contains features that were formed at a plate margin. The geology of this area is described in detail in chapter 4.

The Tabalah and Tarj Complex contains amphibolites, gabbros, quartz-diorites, diorites,

tonalites and granodiorites. Geochemical analyses that were presented in chapter 4 show that the gabbros and quartz-diorites were formed in an island-arc environment. Tonalites and granodiorites display geochemical characteristics of rocks that intruded at an active continental margin. The island-arc related rocks were formed at an intra-oceanic subduction environment and were interpreted to be older than ca. 780 Ma. The granodiorite was dated at ca. 761 Ma.

The detailed structural/kinematic analysis in the Tabalah and Tarj Complex focused on the 5-10 km wide NNW-SSE to NW-SE trending Tabalah/Ta'al Shear Zone. Two Neoproterozoic deformation phases were observed on this shear zone. The D1-phase was responsible for the formation of steep NNW-SSE to NW-SE trending foliations, E- to ESE-plunging lineations and top-to-W shear sense indicators. These structures indicate thrusting that was caused by E-W to WNW-ESE compression (Figure 6-1). Geochronological analyses that were performed in the framework of this thesis showed that this phase took place at ca. 779 Ma. The D2-phase displayed dextral strike slip, as indicated by NNW-SSE trending lineations and shear sense indicators. These structures were formed by NNE-SSW compression. The  $^{40}\text{Ar}/^{39}\text{Ar}$ -analyses showed that this event took place at ca. 765 Ma. These two deformation phases took place in a period when arc-accretion and (oblique) subduction along the NE-SW sutures were the prevailing tectonic processes (see also Chapter 2). The structures of the Tabalah and Tarj Complex are thus intra-terrane responses to arc-accretion at the terrane margins. The changes in the directions of compression of the deformation phases were ascribed to the change of plate motion of subducting plates during arc-accretion.

#### *6.2.4 The Wadi Kid Complex: A core complex*

In the framework of the research for this thesis, a mainly structural based research was performed in the Wadi Kid Complex in Egypt (Figure 6-2). These results of this study are described in Chapter 5 and Appendix 1. In the Wadi Kid Complex, a sequence of thick sub-horizontal amphibolite HT/LP grade schists was interpreted as a low-angle normal shear zones and was associated with upper-crustal normal shear zones which displayed top-to-the-NW movement. The high-grade schists are overlain by slightly to non-metamorphosed sediments and volcanics (Chapter 5 and Appendix 1). The high-grade and low-grade sequences are separated by a clear metamorphic break (Appendix 1). Undeformed granites intruded the lower-crustal sequence of the Wadi Kid Complex. Geochemical analyses showed that these granites are similar to the A-type granites found in other parts of the ANS which are interpreted to be related to extension. The intrusion of NE-SW trending dykes, perpendicular and synchronous to the movement on the shear zone, indicated that the shear zones were formed in a NW-SE extensional regime (Figure 6-1).  $^{40}\text{Ar}/^{39}\text{Ar}$ -analyses in this thesis showed that the deformation on the low-angle shear zone took place at ca. 595 Ma. In Chapter 5 and Appendix 1 it is demonstrated that the geological features observed in the Wadi Kid area justify its interpretation as a core complex that was formed during NW-SE extension.

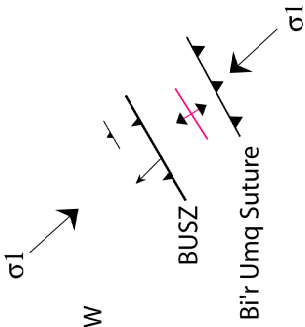
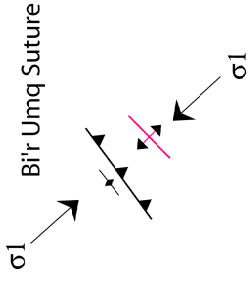
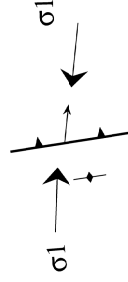
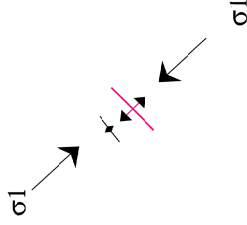

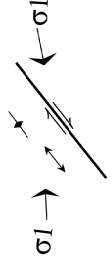
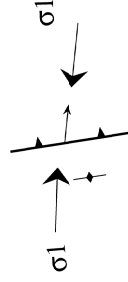
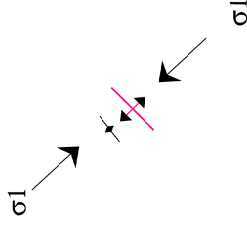
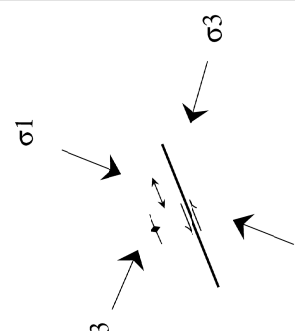
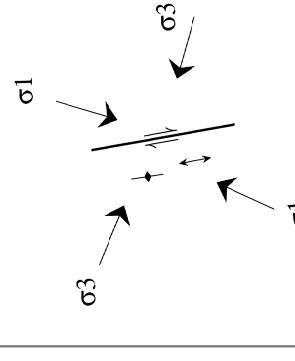



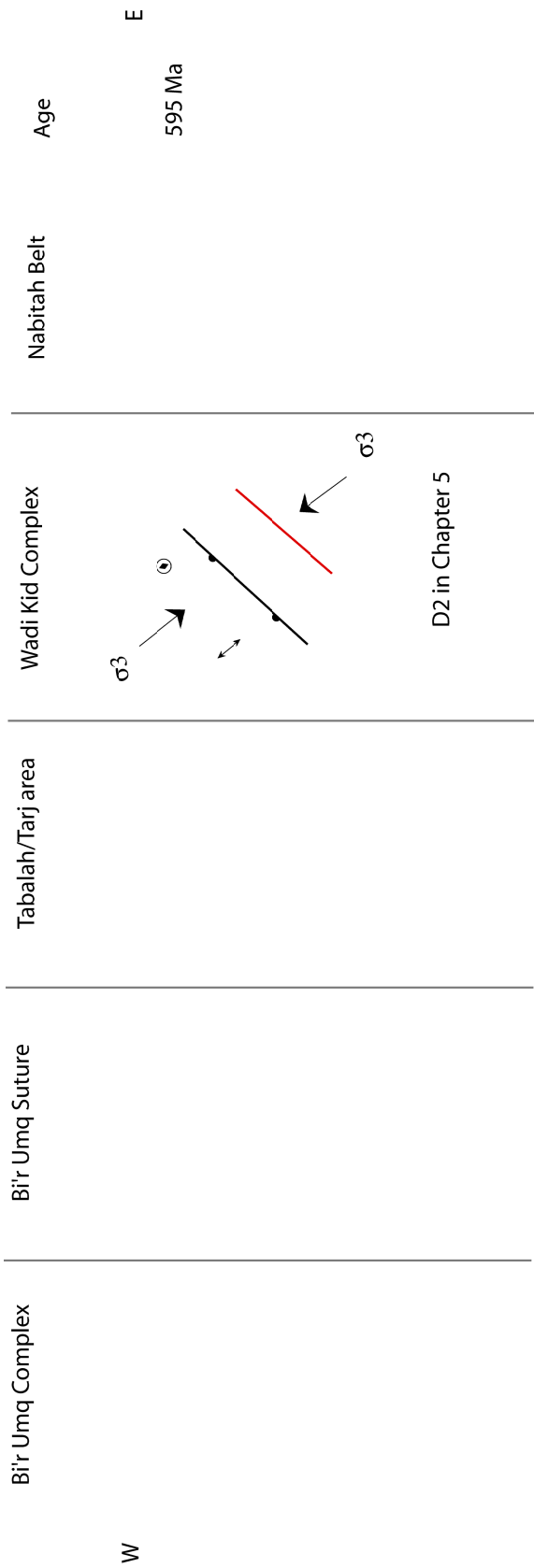
	Bi'r Umq Complex	Nakasib and Bi'r Umq Sutures	Tabalah/Tarj area	Wadi Kid Complex	Nabitah Belt	Age
	 <p>W</p> <p>BUSZ</p> <p>Bi'r Umq Suture</p> <p><math>\sigma_1</math></p> <p>D1 in Chapter 3</p>	 <p>Bi'r Umq Suture</p> <p><math>\sigma_1</math></p> <p>Abdelsalam and Stern, 1996; Wipfler, 1996; Johnson et al., 2002; Johnson, 1998</p>	 <p><math>\sigma_1</math></p> <p>D1 in Chapter 4</p>	 <p>? Ma (however pre-600 Ma)</p> <p><math>\sigma_1</math></p> <p><math>\sigma_1</math></p>		820 Ma ? E
	 <p><math>\sigma_1</math></p> <p>D2 in Chapter 3</p>	 <p><math>\sigma_1</math></p> <p>Abdelsalam and Stern, 1996; Wipfler, 1996; Johnson et al., 2002; Johnson, 1998</p>	 <p><math>\sigma_1</math></p> <p>D1 in Chapter 4</p>	 <p><math>\sigma_1</math></p>		780 Ma

Figure 6-1 Sketch table of the major deformation phases in the Arabian-Nubian Shield. The major deformation phases are drawn for each of the areas that were studied in detail within the framework of this thesis.

Bi'r Umq Complex	Bi'r Umq Suture	Tabalah/Tarj area	Wadi Kid Complex	Nabitah Belt	Age
 <p>W <math>\sigma_3</math> <math>\sigma_1</math> <math>\sigma_3</math> <math>\sigma_1</math></p> <p>D3 in Chapter 3</p>		 <p><math>\sigma_1</math> <math>\sigma_3</math> <math>\sigma_1</math> <math>\sigma_3</math></p> <p>D2 in Chapter 4</p>		 <p><math>\sigma_1</math> <math>\sigma_1</math></p> <p>Quick, 1991</p>	<p>E</p> <p>765 Ma</p>
				 <p><math>\sigma_1</math> <math>\sigma_1</math></p> <p>Quick, 1991</p>	<p>710 Ma</p>
				 <p><math>\sigma_1</math> <math>\sigma_1</math></p> <p>Quick, 1991 Johnson, 2001</p>	<p>680-630 Ma</p>

Continuation Figure 6-1 Sketch table of the major deformation phases in the Arabian-Nubian Shield. The major deformation phases are drawn for each of the areas that were studied in detail within the framework of this thesis.



W

### Legend

- Thrust (plate margin)
- Thrust (local: BUSZ)
- Strike-slip
- Lineation
- (Sub-)horizontal lineation
- Foliation
- (Sub-)horizontal foliation
- (Sub-)horizontal foliation
- (Sub-)horizontal fold axis
- Low-angle normal shear zone
- Dyke

Continuation Figure 6-1 Sketch table of the major deformation phases in the Arabian-Nubian Shield. The major deformation phases are drawn for each of the areas that were studied in detail within the framework of this thesis.

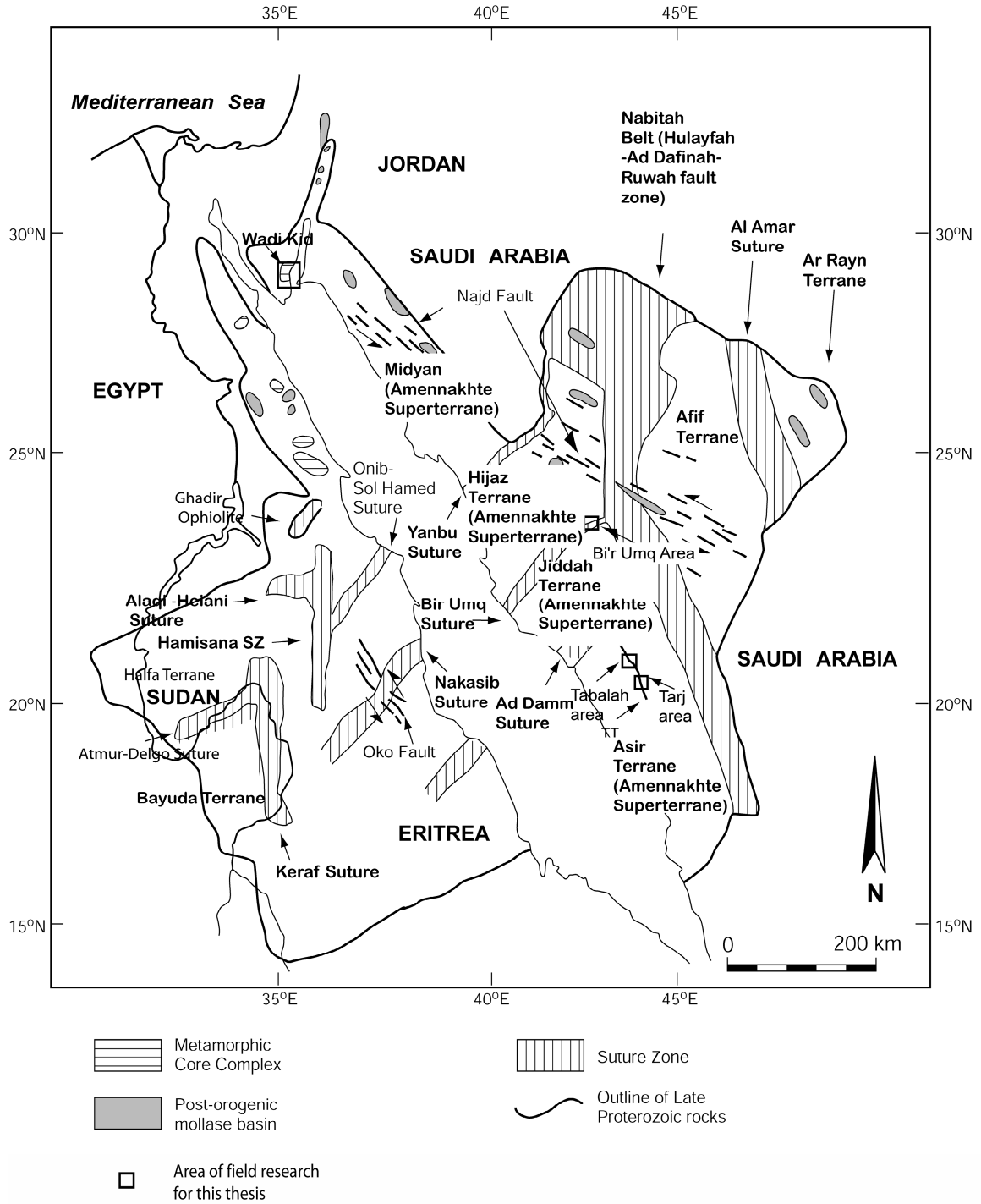


Figure 6-2 A map showing the main Neoproterozoic features in the Arabian Nubian Shield.

### **6.3 A synthesis of the newly obtained data from the Bi'r Umq area, the Tabalah and Wadi Tarj area and the Wadi Kid area**

In the framework of this thesis a number of key areas were chosen in order to compile a geodynamic model for the Neoproterozoic development of the ANS. The areas were chosen in order to represent the three main tectonic phases: 1) the oceanic subduction stage, which is reflected by remnants of intra-oceanic subduction, 2) the arc-accretion stage and 3) a late extensional stage which is still controversial (see chapter 2). The oldest Neoproterozoic relict that was observed in any of the areas in the framework of this study was the Bi'r Umq ophiolite. It was dated at ca. 830 Ma by Pallister et al. (1989) and was formed in an intra-oceanic suprasubduction setting. Another relict of the intra-oceanic subduction phase was represented by the island-arc related gabbro-diorite suite that was observed in the Tabalah and Wadi Tarj Complex. No ages are available for these intrusives however structural relations indicate this suite intruded before ca. 780 Ma. In chapter 3, the three phases of deformation that were observed in the Bi'r Umq Complex, were related to arc-accretion along the SE-NW trending sutures. The two deformation phases that were observed in the Tabalah and Wadi Tarj Complex were also related to arc-accretion (see Chapter 4).

No age constraints are available for the separate deformation phases in the Bi'r Umq Complex however dates from literature (e.g. Johnson et al., 2002; Pallister et al., 1989) indicate the D1-D3 took place at ca. 820-760 Ma. The two deformation phases at the Tabalah and Tarj Complex were dated in the framework of this study: D1 was dated at ca. 779 Ma and D2 was dated at ca. 765 Ma. The earliest deformation phase in the Bi'r Umq Complex resulted from NW-SE compression (Figure 6-1). During D2 in the Bi'r Umq Complex, WNW-ESE compression caused dextral strike-slip along the WSW-ENE trending BUSZ (Figure 6-1). A NNE-SSW compressional phase was responsible for shear reversal during D3 at the Bi'r Umq Suture (Figure 6-1). The D1-phase in the Tabalah and Tarj Complex caused top-to-the-W thrusting on a NNW-SSE trending shear zone (Figure 6-1). This deformation phase resulted from an approximately E-W to WNW-ESE compression and was dated at ca. 779 Ma. The youngest deformation phase in the Tabalah and Tarj area was dated at ca. 765 Ma and resulted from NNE-SSW compression.

Since the deformation phases of both the Bi'r Umq Complex and the Tabalah and Tarj Complex took place at the same timeframes, it is justified to relate them to each other (it should be noted that the deformation at the Bi'r Umq Complex started earlier than the deformation at the Tabalah and Tarj Complex however it ended approximately simultaneously at both complexes). The direction of compression of D2 for the Bi'r Umq Complex is sub-parallel to the direction of compression of the D1 phase of the Tabalah and Tarj Complex (Figure 6-1). From an Andersonian perspective (Anderson, 1951),  $\sigma_3$  is vertical for thrusts and horizontal during strike-slip deformation and therefore the trends of  $\sigma_3$  for D2 in the Bi'r Umq Complex and for D1 in the Tabalah and Tarj Complex should not be the same. However, this Andersonian framework is only valid for newly formed shear zones. Strike-slip faults often take advantage of pre-existing zones of weakness (e.g. Davis, 1984) and so upon a change of a compressional regime, a strike-slip fault may form at a re-activated older structure even though the stress regime may not require it to form. This may explain the apparent difference in



orientation of  $\sigma_2$  and  $\sigma_3$  for D2 in the Bi'r Umq Complex and for D1 in the Tabalah and Tarj Complex. It should be noted that the re-activation of thrusts as strike-slip shear zones in accretionary orogens takes place when the new orientation of compression is at an angle of 30°-45° with the sense of shear of the new strike-slip shear zone (Ellis and Watkinson, 1987).

As noted in Chapter 3, many examples have been recorded for strike-slip shear during arc-accretion and oblique subduction. These examples include the Cretaceous strike-slip shear zones that were formed during arc-accretion along the continental margin of western North America (e.g. Oldow et al., 1989; Cole et al., 1999; Wolf and Saleeby, 1992) and neotectonic strike-slip faults as observed in El Salvador, Central America (Corti et al., 2005).

The co-existence of strike-slip shear zones along plate margins, and thrusts within terranes, is also observed during the Late Cretaceous arc-accretion in western North America. Bergh (2002) described intra-terrane thrusting for the San Juan fault system at the Cascades Orogen, western USA (Figure 6-3). These thrusts were related to oblique subduction along a sinistral strike-slip fault (Bergh, 2002). Cole et al (1999) described the co-existence of strike-slip shear zones and thrusts during arc-accretion during the Late Cretaceous in central Alaska (Figure 6-3). Also in this area, oblique subduction along a strike-slip shear zone led to intra-terrane thrusting (Cole et al., 1999).

On the basis of the above, it can be assumed that the dextral strike-slip deformation of the D2-phase in the Bi'r Umq Complex and the thrusting of the D1 in the Tabalah and Tarj Complex belong to the same regional WNW-ESE to E-W compressional regime which took place at ca 779 Ma. The D1-phase in the Tabalah and Tarj Complex was thus the intra-terrane response to the D2-event at the BUSZ.

The D3-phase in the Bi'r Umq Complex resulted from a NNE-SSE compressional regime (Figure 6-1). This is parallel to the compressional regime that caused the dextral strike-slip along the NNW-SSE Tabalah/Ta'al shear zone during D2 (Figure 6-1). Consequently, the Tabalah/Ta'al Shear Zone was conjugate to the BUSZ in this period (Figure 6-1). Since these shear zones form a conjugate set, it may be assumed that  $\sigma_3$  is horizontal and trends WNW-ESE (Figure 6-1). The D2-deformation in the Tabalah and Tarj Complex was dated at ca.765 Ma and therefore this should also be the approximate age for D3 in the Bi'r Umq Complex. The timing of the NNE-SSE compressional regime in both areas indicates that it was related to the arc-accretion along the NE-SW trending sutures. The structures in the Tabalah and Tarj Complex were thus the intra-terrane response to the deformation at the BUSZ.

It was postulated in Chapter 3 and 4 that the changes in the sense of shear between the different deformation phases resulted from the changes in plate motion of a subducting plate at a plate margin. Approximately 90° of anti-clockwise movement was observed for the shift from the WNW-ESE compression in the D1-phase of Tabalah and Tarj Complex and D2-phase in Bi'r Umq Complex, towards the NNE-SSW compression for the D2-phase of Tabalah and Tarj Complex and D3-phase in Bi'r Umq Complex. This anti-clockwise shift occurred within 15 Ma. It may appear a short time for such large rotations however similar large scale rapid rotations have been described in the geological record. Wolf and Saleeby (1992) assumed a rotation of plate motion of up to 90° for the Proto-Pacific plate during the Jurassic accretion at the Cordillera which took place in a time span of 15-20 Ma. Wallace et al. (1989) assumed a

rotation of plate motion of up to 90° at the margin of Alaska during the Cretaceous in a time span of 15-20 Ma. Also in present-day tectonics, rapid plate rotations have been observed. Wallace et al. (2005) describe such rotations for microplates in the southeastern Pacific where the South Bismarck microplate rotates at ~ 9°/m.y.

The earliest deformation phase in the Wadi Kid Complex was only observed in its upper-crustal rocks and resulted from NW-SE compression. No dates are available to relate this phase to the deformation phases in the Bi'r Umq Complex and the Tabalah and Tarj Complex. Its trend however indicates that it could have been related to the arc-accretion.

D2 is the main phase of deformation in the Wadi Kid Complex (see Chapter 5 and Appendix 1). During this phase, a low-angle normal shear zone was developed in a NW-SE extensional regime (Figure 6-1). Continuing extension and thinning of the crust led to the intrusion of late orogenic granites and the formation of core complex. The main activity on the shear zone of the Wadi Kid Complex was dated at ca. 595 Ma (see Chapter 5 and Appendix 1). In Chapter 5, it was postulated that the extension in the Wadi Kid Complex resulted from gravitational collapse. This form of collapse requires to be preceded by a lithospheric thickening (e.g. Dewey, 1988; Platt and England, 1993). The arc-accretion observed in the Bi'r Umq Complex and in the Tabalah and Tarj Complex could have caused lithospheric thickening that could lead to gravitational collapse. The 'arc-accretion related deformation' in these areas ceased however at ca. 760 Ma and so it is not likely that this phase of arc-accretion led to the gravitational collapse. Later in this chapter, it will be investigated if other arc-accretion phases in the ANS have been described in literature that could lead to lithospheric thickening and gravitational collapse.

#### **6.4 A model for the tectonic evolution of the Arabian-Nubian Shield based on the Bi'r Umq Complex, the Tabalah and Tarj Complex and the Wadi Kid area**

##### *6.4.1 The oceanic/island-arc phase in the ANS*

The ANS contains numerous relicts of the oceanic phase in the form of ophiolites and remnants of island-arcs (see chapter 2). In Chapter 3, the Bi'r Umq ophiolite was interpreted as a suprasubduction ophiolite. It is generally accepted that other ophiolitic sequences in the ANS also were formed in oceanic environment (e.g. Stern, 1994, Pallister et al., 1989). Some of the ophiolites in the ANS, like the Bi'r Umq Complex, are thought to have originated in an intra-oceanic suprasubduction environment (Al-Salah and Boyle, 2001; El-Sayed and El-Nisr, 1999; Zimmer et al., 1995).

Island-arc remnants are very common in the ANS (see also chapter 2) and they form the core of the main Neoproterozoic terranes as the Asir, the Hijaz, the Jiddah and the Midyan terranes in Saudi Arabia (see Figure 6-2 for locations) (Jackson 1986; Brown et al., 1989). The mixed gabbro-diorite suite in the Tabalah and Wadi Tarj area shows geochemical characteristics of island-arcs. Island-arcs form important parts of many of the Neoproterozoic complexes in Egypt and Sudan (e.g. Bentor 1985; El Gaby et al., 1984; El Din et al., 1991;

Rashwan, 1991).

The geochemical studies that were performed in the framework of this thesis in the Bi'r Umq Complex and the Tabalah and Wadi Tarj areas confirm the presence of rocks with oceanic/intra-oceanic subduction origin in the ANS.

Many of the ophiolites and island-arcs in the ANS are generally believed to have originated in intra-oceanic subduction environments in the Mozambique Ocean, that was formed upon rifting of Rodinia at ~900Ma (e.g. Abdelsalam and Stern, 1996; Pallister et al., 1988; Rogers et al, 1995; Shackleton, 1996; Unrug, 1996).

#### *6.4.2 Arc-accretion phase in the ANS*

Most of the ophiolitic belts in the ANS are strongly deformed and trend SW-NE and N-S (see Figure 6-2). The ophiolites mark the borders between the different terranes (e.g. Abdelsalam and Stern, 1996; Johnson et al., 1987; Stoeser and Camp, 1985). They are thought to represent the zones of closure of the oceanic basins between the juvenile terranes and the continental terranes (e.g. Abdelsalam and Stern, 1996; Stoeser and Camp, 1985). The closure took place along subduction zones and so these ophiolitic sutures are thought to represent relicts of ancient subduction zones (Abdelsalam and Stern, 1996; Shackleton, 1996; Stoeser and Camp, 1985).

The Bi'r Umq Complex, at the NW-margin of the Bi'r Umq-Nakasib Suture is an example of area that displays evidence for arc-accretion at the border of two terranes, namely the Hijaz Terrane and the Jiddah Terrane. The detailed structural research in Chapter 3 showed three phases of deformation on the main structure in the area, the Bi'r Umq Shear Zone.

It is generally thought that the initial movement on the Bi'r Umq Suture and the Nakasib Suture (the continuation of the Bi'r Umq Suture in Sudan, see Figure 6-2 for location) was related to NW- or SE-vergent thrusting that resulted from NW-SE compression (e.g. Abdelsalam and Stern, 1993; Abdelsalam and Stern, 1996; Wipfler, 1996; Johnson et al., 2002) like D1 in the Bi'r Umq Suture. Most studies of the Nakasib and Bi'r Umq Sutures also indicate that the earlier thrusting was followed by a major phase of dextral transpression (e.g. Abdelsalam and Stern, 1996; Wipfler, 1996; Johnson et al., 2002) as observed for the D2-phase in the Bi'r Umq area.

The three deformation phases in the Bi'r Umq Complex, described in Chapter 3, recorded the deformation that was responsible for the juxtaposition of the Jiddah Terrane and the Hijaz Terrane. Consequently, the deformation in Bi'r Umq Complex was related to the arc-accretion. The deformation in the Bi'r Umq Complex took place at ca. 820-760 Ma, an era when arc-accretion along NE-SW trending sutures was the main "tectonic driver" in the ANS.

The main structure in the Tabalah and Tarj areas is the Tabalah/Ta'al Shear Zone. It displays two phases of deformation. This shear zone lies in the central part of the Asir terrane and is thus an intra-terrane structure. The timing of the Tabalah/Ta'al Shear Zone, ca. 780-760 Ma (see Chapter 4), indicates that it was active in the same period as the Bi'r Umq Shear Zone. As shown above, it can be assumed that D1 and D2 in the Tabalah and Tarj Complex were formed during the same trend of compression as D2 and D3 in the Bi'r Umq Complex. The deformation in Tabalah and Tarj Complex was thus interpreted to represent intra-terrane response to arc-accretion along the NE-SW trending sutures.

From chapter 2, it can be concluded that subduction at the N-S trending active continental margins, as the Nabatah Belt, started not earlier than 700 Ma, after the arc-accretion along the NE-SW trending sutures had ceased. Therefore, the juxtaposition of the island-arcs of the Jiddah Terrane and Hijaz Terrane, as reflected by the deformation along the Bi'r Umq Shear zone, was arc-arc collision. Typically, arc-arc collision can only take place when both island-arcs would have had a mature (> 20 m.y.) and thicker crust with a relatively low density (Cloos, 1993). The subduction zone at the Jiddah island-arc, which was also responsible for the emplacement of the Bi'r Umq ophiolite, would have been the place where the actual arc-accretion of the Hijaz Terrane upon the Jiddah Terrane took place (see Figure 6-2 for locations of Terranes). The Hijaz island-arc would have collided on the Jiddah Terrane after its back-arc basin or fore-arc had been subducted at the Jiddah island-arc, which happened during the D1-phase and which was recorded as such at the Bi'r Umq Complex. It is thus very possible that the Bi'r Umq ophiolite itself was a part of the back-arc or the fore-arc of the Hijaz island-arc. The Hijaz Terrane and the Jiddah Terrane formed thus a superterrane at 820-760 Ma.

The Asir Terrane (see Figure 6-2 for its location) was formed at 900-800 Ma and probably represents the oldest island-arc in the Arabian part of the ANS (Brown et al., 1989; Jackson, 1986; Stoesser and Camp, 1985). Structural data from the Asir terrane were recorded in the Tabalah SZ and the Wadi Ta'al SZ of the Tabalah/Tarj Complex. As demonstrated above, it may be assumed that D2 in the Bi'r Umq Complex and D1 in the Tabalah and Tarj Complex formed simultaneously. Furthermore, it was concluded that D3 in the Bi'r Umq Suture formed parallel to the direction of compression during D2 in the Tabalah and Tarj Complex. These facts may indicate that the Jiddah Terrane and the Asir Terrane underwent the same deformation history from D1 and D2 at the Tabalah and Wadi Tarj Complex and from D2 and D3 at the Bi'r Umq Complex and that the two terranes formed one "superterrane" before the start of D1 in the Tabalah/Wadi Tarj Complex. Johnson (1999) postulated that the amalgamation of the Asir Terrane and the Jiddah Terrane took place around 790 Ma and this is in accordance with the data from this thesis.

The amalgamation of the Hijaz Terrane and its northerly neighbor, took place along the Yanbu Suture (see Figure 6-2 for its location). The formation of the ophiolitic rocks of the Yanbu Suture itself was dated at ~740 Ma (Claeson et al., 1984; Pallister et al., 1988). No solid age data are available for this suturing event, however it was estimated at 740-696 Ma (Johnson, 1999; Stoesser and Camp, 1985). The Onib-Sol Hamed Suture is the extension of the Yanbu Suture into the Nubian part of the ANS. The subduction at this suture was estimated at 740-690 Ma (Abdelsalam and Stern, 1996; Shackleton, 1994). Consequently, no arc-accretion took yet place north of the BUSZ within the ANS while the deformation took place at the Bi'r Umq SZ. The Bi'r Umq SZ represented thus the most northerly subduction zone of the ANS until after its D3-deformation phase. The D1-, D2- and D3- deformation phases at the BUSZ display thus different phases of arc-accretion at the subduction of which the Bi'r Umq Suture is a remnant. Since no other deformation was observed to have impacted the Asir Terrane at 820-760 Ma, the D1- and D2-deformation phase at the Tabalah/Wadi Tarj Complex represent intra-terrane deformation during the D3-deformation phases at the Bi'r Umq SZ.

Geochemical studies indicate that the undeformed granodiorite of the Tabalah and Tarj

Complex was intruded at a continental margin at ca. 761 Ma. This is before the start of subduction at the “real” active continental margins of East and West Gondwanaland. However, the granodiorite formed within the superterrane consisting of the Asir Terrane and Jiddah Terrane, which, by 761 Ma, could be treated as a microcontinent, which will be referred to as the Amennakhte Superterrane (named after the Theban scribe who is thought to have prepared the pharaonic map of the Wadi Mammamat area) (Figure 6-2). It had an amphibolite crust that was relatively stable from an “island-arc magmatic” point of view (pure island-arc magmatism at the Asir Terrane ceased before 800 Ma). Continental sedimentary processes were active and the crust contained large volumes of island-arc plutons. The latest stages of subduction at the Bi’r Umq suture could have led to the partial melting of a lithosphere that had been thickened by the accretion of the Midyan and Hijaz Terranes up on the Asir/Jiddah Superterrane. The partial melting of a thickened amphibolite crust with continental affinity would have led to the formation of granodiorites such as those in the Wadi Tarj area.

In chapters 3 and 4, it is shown that both the BUSZ and the Tabalah/Ta’al SZ initiate as thrusts. Both shear zones display later phases of deformation, strike-slip shearing, that result from changes in plate motion. Little detailed structural studies are available for ophiolitic sutures in the ANS however a study by Johnson et al. (2002) indicated that along the entire the Bi’r Umq-Nakasib Suture thrusting was followed by strike-slip movement.

As argued already in chapter 3 and 4, the emplacement of ophiolites and accretion of terranes shows similarity with the arc-accretion in western North America. Like in the ANS, thrusting and strike-slip faults were related to the different phases of arc-accretion in the Cordilleran of western North America (e.g. Oldow, 1989; Stewart and Crowell, 1992). The strike-slip faults in western North America were related to oblique subduction (Stewart and Crowell, 1992) or to intra-terrane response to deformation at plate boundaries (Chardon et al., 1999). These strike-slip faults often showed shear-reversal (Cole et al., 1999; Stewart and Crowell, 1992). The transition from convergence to oblique subduction at the plate boundaries in western North America was related to a change in the direction of plate motion of the subducting plate (e.g. Cole et al., 1999; Oldow et al., 1989; Stewart and Crowell, 1992). Shear reversal on strike-slip faults was also related to changes in the directions of plate motions (e.g. Cole et al., 1999; Oldow et al., 1989; Stewart and Crowell, 1992). The transition from convergence to strike-slip faulting and the strike-slip shear reversal as observed in the study of the Bi’r Umq SZ and the Tabalah/Ta’al SZ is interpreted to be a result of changes in the directions in plate motion of the subduction plate.

The accretion of island-arcs and composite island-arc terranes upon continental margins was not recorded in any of the areas that were studied during this research. From Chapter 2 and references within, it can be concluded that arc-continent collision, subduction at the active continental margin at the western boundary of the ANS started at ca. 730 Ma along the Keraf Suture and the Kabus Suture (Abdelsalam and Stern, 1996; Bailo et al., 2003). Here, the oceanic basin between continental Bayuda Terrane and the island-arc terranes of the ANS was closed during the arc-continent collision. HP-metamorphism at supra-subduction N-S trending shear zones in Eritrea, were formed before 650 Ma (De Souza Filho and Drury, 1998). No other reliable constraints exist on the end of the subduction at the western margin of the ANS, and no

features that are typically associated with the arc-accretion at the western margin of the ANS, post-date 650 Ma.

The arc-continent collision at the eastern margin of the ANS took place along the N-S trending Nabitah Belt (Agar, 1985; Abdelsalam and Stern, 1996). This structure is bordered at its western margin by the Hijaz, Jiddah and Asir Terranes, which are part of the Amennakhte Superterrane. Subduction at this active continental margin started ca. 700 (Abdelsalam and Stern, 1996; Johnson and Kattan, 1999; Quick, 1991). By ca. 650 Ma activity along the Nabitah Belt ended (Abdelsalam and Stern, 1996), and so the accretion of the Amennakhte Superterrane upon the continental Afif Terrane was completed. The Nabitah Belt contains ophiolites and their obduction was related to the closure of a fore-arc at a subduction zone (Quick, 1991). The Nabitah Belt is interpreted to be the feature where the final closure of the Mozambique Ocean and the island-arcs that were formed within this ocean, took place (Shackleton, 1996) and so the end of activity on the Nabitah Belt marks the end of arc-accretion at the ANS. Miller and Dixon (1992) proposed that the latest stage of compressional deformation along N-S trending Hamisana SZ in Sudan may have taken place when arc-accretion was completed and that this compression resulted from continent-continent collision between East- and West-Gondwanaland. The arc-accretion as described above, for the different island-arcs in the ANS is similar to arc-accretion of terranes that was described in western North America by Coney (1989) and Oldow et al. (1989).

#### *6.4.3 Extensional features in the ANS*

The presence of extensional features in the ANS has been subject of discussion over the past decade. In the past it was thought that the main structural features of Neoproterozoic of the ANS were formed in compressional regimes (e.g. Bentor, 1985; Vail, 1985; Ries et al., 1983). Over the last decade, a number of authors have proposed that the Neoproterozoic development of the ANS ended with extension. This was often based on geochemical research of igneous rocks which were thought to have originated from mantle derived magmas that were intruded and extruded in a thinned and extending crust (e.g. Beyth et al., 1994; Hassanen, 1997; Jarrar et al., 2003). Sedimentary basins that were formed at the very late stages of the Neoproterozoic in the ANS were also associated with extension (Jarrar et al., 1991; Jarrar et al., 1992; Greiling et al., 1994).

The Wadi Kid Complex resembles the “gneissic domes” that are found in other parts of the ANS as described in chapter 2. The Meatiq dome and the Hafafit dome are examples of other “gneissic domes” in the ANS. Like the Wadi Kid Complex, these “gneissic domes” contain a lower-crustal unit with a thick mylonitic sequence of amphibolite-grade, overlain by an upper-crustal sequence (see chapter 2 and references within). The mylonitic sequences consist of sub-horizontal foliations, well developed lineations and abundant shear sense indicators (see chapter 2 and references within). A number of authors interpreted the low-angle shear zones of the “gneissic domes” as thrusts (Fowler and Osman, 2001; Habib et al., 1985). This would however require the presence of thrust-duplexes with a vertical repeat of the metamorphic sequence. This is not observed in the domes of the ANS where in fact strong metamorphic breaks were found (see appendix 2). Others interpreted the “gneissic domes” in

the ANS as core complexes that are expressions of local extension in the NW-SE strike-slip systems of the Najd SZ (e.g. Bregar et al., 2002; Fritz et al., 2002; Loizenbauer et al., 2001). In such a scenario, the sinistral strike-slip Najd shear zone was thought to have been formed at the later stages of the collision between East and West Gondwanaland (e.g. Bregar et al., 2002; Fritz et al., 2002; Loizenbauer et al., 2001). Core complexes associated with strike slip shear zones generally form with their linear trends parallel to the direction of  $\sigma_3$  of the strike slip regime or with their linear trends parallel to the strike slip shear zone (Yin, 2004). If the linear trends of the core complexes of the ANS would have formed parallel to  $\sigma_3$  of a major strike-slip zone as the sinistral NW-SE Najd SZ, the linear features of the core complex would have to trend WNW-ESE. However, they all trend NW-SE, which is in fact parallel to the Najd SZ (e.g. Bregar et al., 2002; Fritz et al., 2002; Loizenbauer et al., 2001). Core complexes that are formed parallel to the strike-slip shear zones should form in a pull-apart regime within the strike slip shear zone. The core complexes of the ANS are however formed outside of the main strike slip shear zones as the Najd SZ. Therefore the formation of the core complexes in the ANS is not related to pull-apart in a strike-slip shear zone.

As demonstrated for the Wadi Kid Complex, the combination of LP-HT sub-horizontal shear zones with NW-SE lineations that are formed at the same time as the NE-SW trending dykes with A-type granites can best explained to have been formed in an extensional regime. Because of their similarity to the core complex of the Wadi Kid Complex, all core complexes in the ANS can be interpreted to have formed in an extensional regime. Consequently, the schistose sequences, overlying the gneissic cores, are interpreted as low angle extensional detachment faults of the type envisaged by Wernicke (1985) and which caused considerable crustal thinning. Isostatic rebound together with the intrusion of granites lead to doming of the lower crust. The doming was responsible for the formation of typical extensional core complexes similar to those formed in the Mesozoic and Early Cenozoic of western North America (e.g. Coney and Harms 1984; Davis and Lister 1989).

Minor strike-slip zones are associated with some of the core complexes in the ANS however this feature is common for core complexes in extensional regimes. The strike-slip zones accommodate part of the extension in the crust (Lister et al., 1986; Faulds and Stewart, 1998).

#### *6.4.4 The transition from compression to extension in the ANS*

This study shows that the ANS contains abundant evidence for both a regional compressional regime as well as a regional extensional regime. However in the areas studied during this research, there appears to be no close relation, from a timing perspective, between the compressional regime and the extensional regime. The compressional regimes in the Bi'r Umq Complex and the Tabalah and Tarj Complex ended 160 Ma before the extension that was observed in the Wadi Kid Complex. However, from chapter 2, it can be concluded that compression in the ANS must have continued until 650 Ma on the N-S trending structures throughout the shield. This age is close to the earliest relicts of extension which were dated at 620 Ma (see chapter 2).

In this research, it was shown that the observed geological features in the ANS, as the

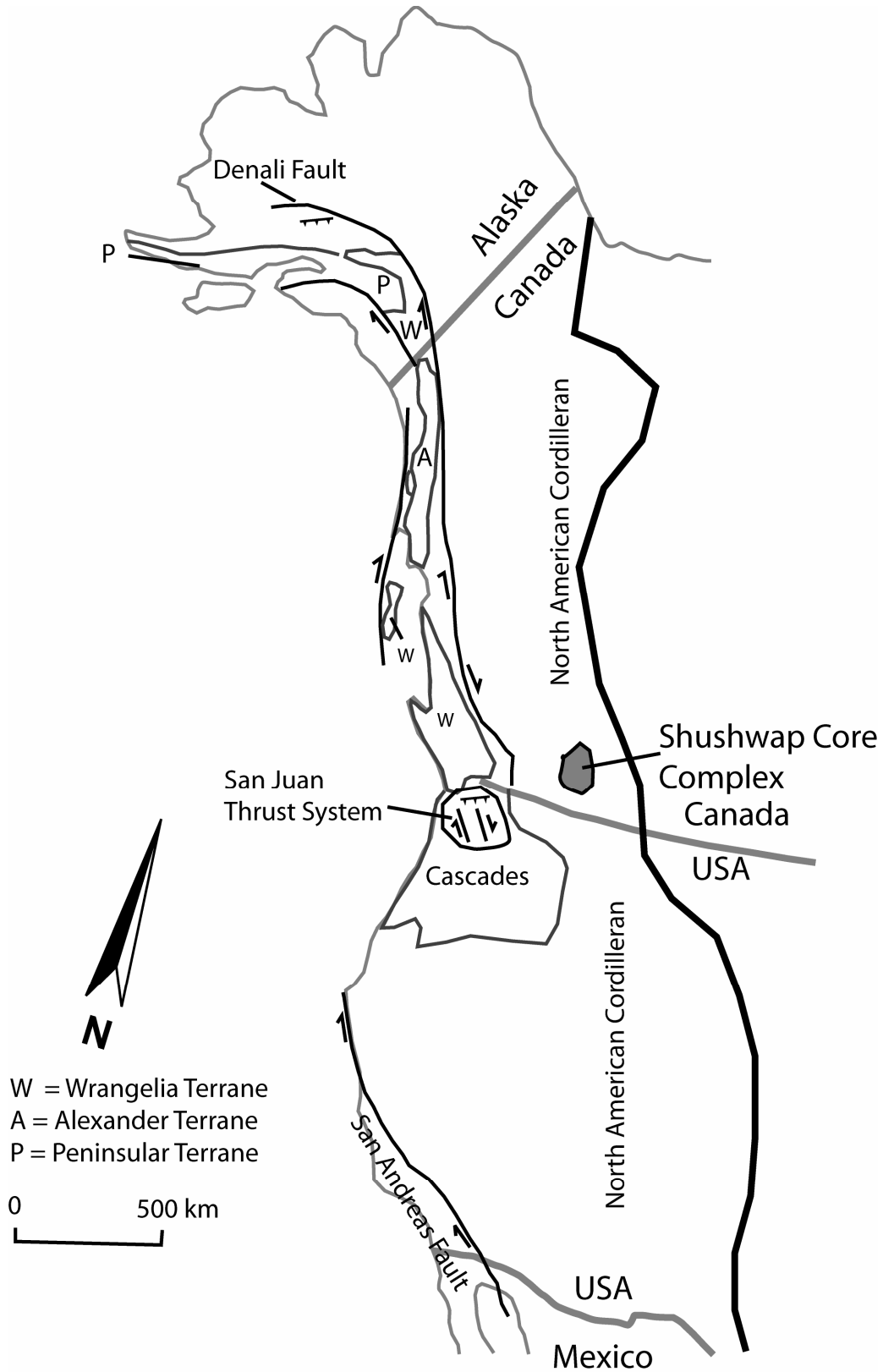


Figure 6-3 Overview of main Cordilleran structures in western North America that are mentioned in this Chapter.



island-arcs, the ophiolitic sutures and the extensional core complexes, justify a comparison with the geological development of western North America during the Mesozoic and Early Cenozoic. The different terranes in the ANS, as the Asir, Jiddah and Hijaz Terranes, consisting of juvenile crust, and bordered by ophiolitic sutures, as the Bi'r Umq Suture, can be compared to the Cordillera of western North America. There, terranes of mainly juvenile composition accreted upon each other to form superterranes before accretion upon the continental margin to form new continental crust (Coney 1989). An example of such a superterrane that underwent "offshore amalgamation", as the Amennakhte Superterrane, is the Wrangellia Superterrane (Coney, 1989; Burchfiel et al., 1992). This superterrane consists of the Wrangellia Terrane, the Alexander Terrane and the Peninsular Terrane (see Figure 6-3 for locations) (Coney, 1989). These terranes consist of island-arc remnants with marine sediments (Coney, 1989). The independent terranes within the Wrangellia Superterrane are bordered by ophiolites (Coney, 1989; Burchfiel et al., 1992). The "offshore amalgamation" of the Wrangellia Superterrane started in the Late Paleozoic but the actual accretion upon the North American continental margin took only place during the Cretaceous (Coney, 1989). The main shear zones that recorded the deformation of the arc-accretion in western North America display extensive strike slip faulting (e.g. Coney, 1989; Burchfiel et al., 1992).

The continuing accretion of superterranes and other allochthonous terranes upon the active continental plate margin of western North America during the Mesozoic, caused fast growth of the continental crust and substantial lithospheric thickening at 155-60 Ma (Liu, 2001; Livacari, 1991; Platt and England, 1993). A reduction in the rate of convergence during accretion allowed for thermal re-equilibration of the lithosphere and consequent weakening and slow thinning of the thickened lithosphere (Platt and England, 1993; Liu, 2001). At this stage conductive heating of the lithospheric root decreased the strength of the crust (Platt and England, 1993; Liu, 2001). The thickened crust of the Cordilleran became isostatically unstable and consequent delamination of its lithospheric root led to gravitational collapse (Meissner and Mooney, 1998; Liu, 2001; Vanderhaeghe and Teyssier, 2001). This, in turn, led to extension and lithospheric thinning which started at ~55 Ma in the Canadian Cordillera and continued until ~16 Ma in the central Basin and Range (e.g. Dewey, 1988; Platt and England, 1993; Liu, 2001; Livacari, 1991). Lithospheric thinning, through large low-angle normal shear zones, allowed the intrusion of magmas at higher crustal levels and caused the initiation of core complexes as the Shushwap core complex in the Canadian Cordillera (see Figure 6-3 for location) (Vanderhaeghe and Teyssier, 2001) where the process of transition from compression to extension took place within 20 Ma (Ranalli et al, 1989). The isostatic rebound and the intrusion of these magmas contributed to the doming of the lower crust and the development of metamorphic core complexes (Wernicke and Axen, 1988). Extensive magmatism was associated with the extension throughout the Cordillera (Liu, 2001). Continental sedimentary basins, bordered by normal faults, were formed at upper crustal levels as a response to the extension and allowed the deposition of late orogenic molasse sequences (Beard, 1996; Lucchita and Suneson; 1996).

Many of the geological features observed in the North American Cordillera are also observed in the ANS. Island-arcs, as observed in the Tabalah and Tarj areas and ophiolitic

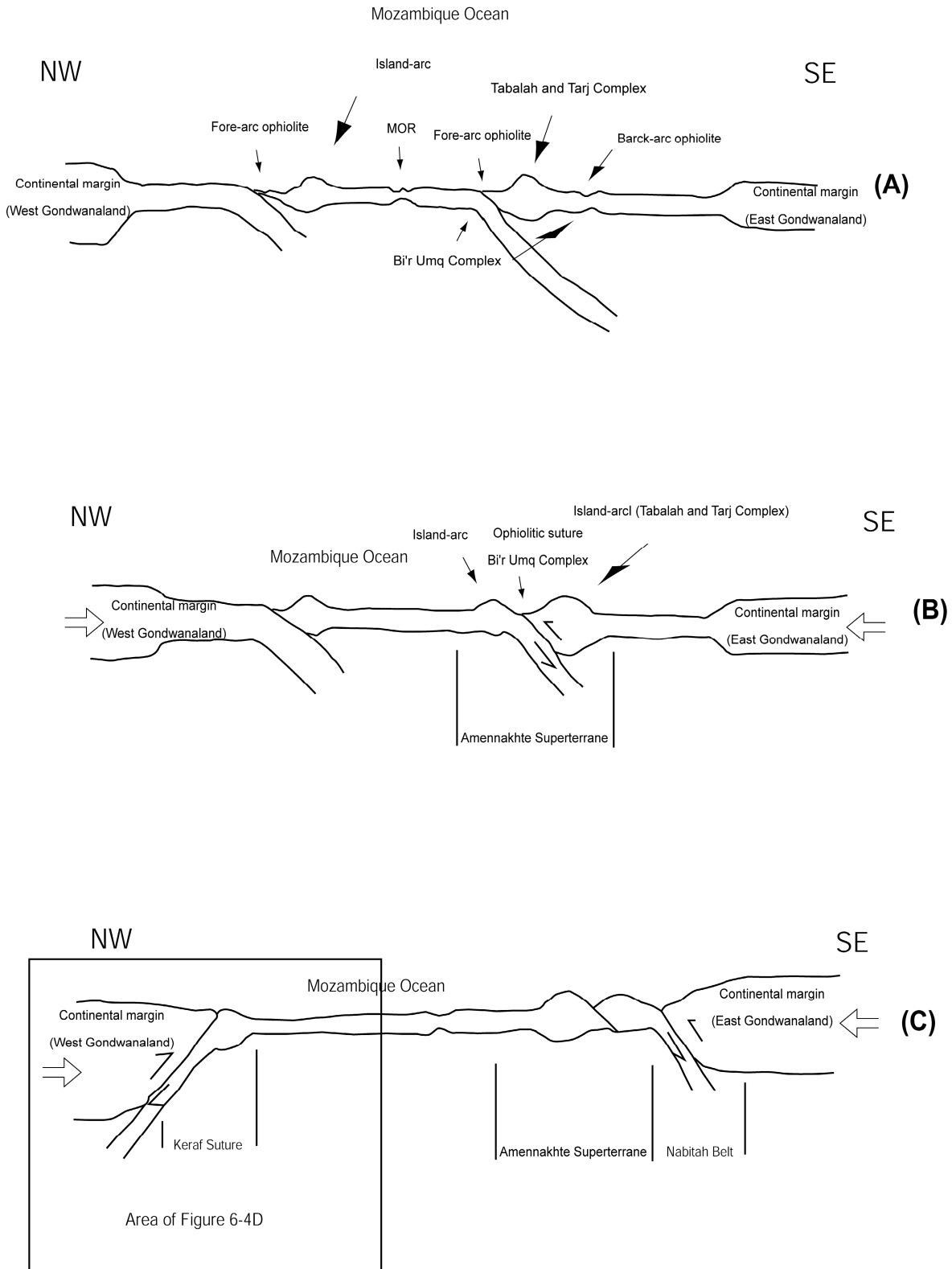
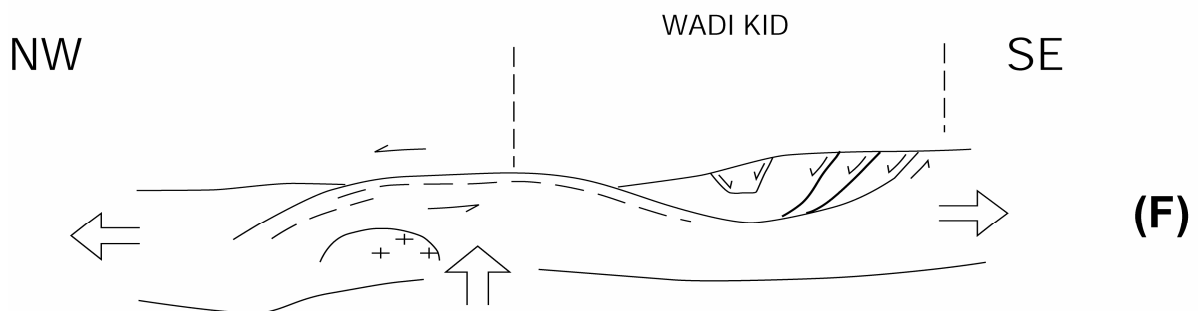
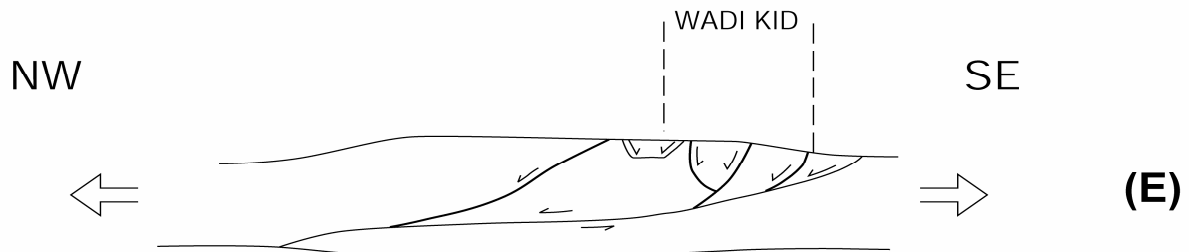
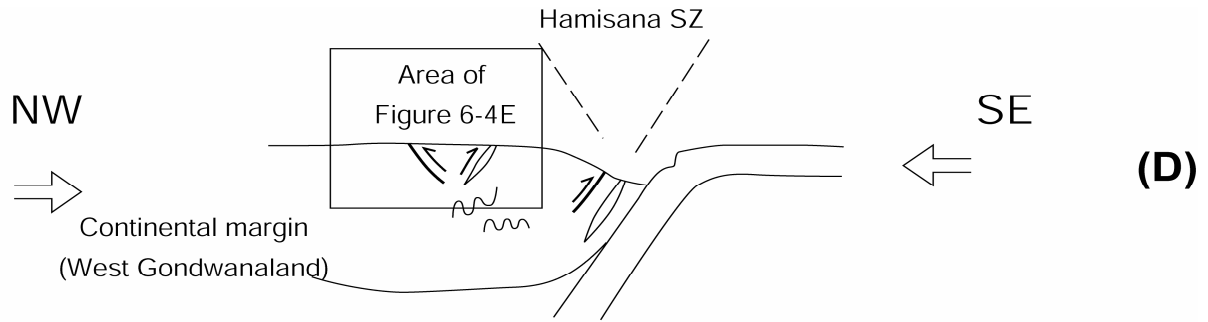


Figure 6-4 A cartoon displaying the different stages of the evolution of the Arabian Nubian Shield. The oceanic phase is shown in (A), with island-arcs developing in the Mozambique Ocean. Remnants of the island-arcs were found in the Tabalah and Tarj areas. Oceanic crust was formed at the MOR, in fore-arcs and back-arcs. Remnants of the fore-arcs or back-arcs were found in the ophiolite of the Bi'r Umq Complex. At stage (B), "off-shore amalgamation" or arc-accretion took place. The Bi'r Umq SZ is the location where the Hijaz Terrane accreted upon the Jiddah Terrane to form a superterrane. At (C), subduction at the continental margins took place and accretion of the island-arcs and superterranes started.



Continuation Figure 6-4 At (D), continuing arc-accretion led to lithospheric thickening. multiple arc-accretion led to lithospheric thickening. When convergence slowed down, thermal re-equilibration caused slow thinning of the thickened lithosphere and the conductive heating of the lithospheric root decreased the strength of the crust. Stages (E) and (F) refer to the tectonic development of the core complexes as the Wadi Kid area in more detail and a smaller scale with the start of extension in stage (E) and the development of a metamorphic core complex in (F). At stage (E) the lithosphere became gravitationally unstable and collapsed which led to extension and thinning of the crust through crustal-scale shear zones. At (F), tectonic denudation by the main detachment, together with isostatic rebound and the intrusion of A-type granites were resulted in the development of metamorphic core complexes.

Table 6-1 Table that displays the main tectonic phase in the ANS and their relicts as observed in this study and as described by others.

Main tectonic phase	In this study	Others (see Chapter 2 and references within)	Age	Stage in Figure 6-
Oceanic phase	Ophiolites in BUC		~830 Ma	A
	Island-arc related rocks in Tabalah/Ta'al Complex		>780 Ma	A
		Ophiolites throughout ANS	900-740 Ma	A
		Island-arcs throughout ANS	900-780 Ma	A
Arc-accretion phase	Three phases of deformation along suture at BUC		820-760Ma	B
	Two phases of intra-terrane deformation along Tabalah/ Ta'al SZ		780-765 Ma	B
		Arc-accretion along NE-SW trending sutures throughout ANS	820-700 Ma	B
		Arc-accretion along continental margin at N-S trending Nabitah Belt	700-630 Ma	C/D
Gravitational collapse			~620 Ma	D/E
Extensional phase	D2 extensional phase in the Wadi Kid Complex		595 Ma	F
		Core complexes in the Nubian part of the ANS	620-580 Ma	F

sutures, as the Bi'r Umq Suture, are the remnants of arc-accretion in the ANS. The Wadi Kid Complex and other core complexes in the ANS, the A-type granites, acid and basic volcanic sequences and the late orogenic sedimentary sequences as the Hamammat Gp. and Saramuj Gp. represent late orogenic extensional features in the ANS. On the basis of the similarity between the North America Cordillera and the ANS, the transition from compression to extension in the ANS can be best explained by gravitational collapse. A phase of lithospheric thickening needs to pre-date the gravitational collapse. The gap of 160 Ma between the compressional phases of the Bi'r Umq Complex and Tabalah and Tarj Complex, and the extension of the Wadi Kid Complex, is too large. However, compression continued on other structures in the ANS. The shortening along the N-S trending sutures, which included the accretion of the Amennakhte Superterrane at the Nabitah Belt, continued until ~650 Ma. This phase of deformation along N-S trending sutures as the Hamisana SZ and the Nabitah Belt should have caused the lithospheric thickening that led to the gravitational collapse and extension in the ANS.

### 6.5 Summary of a new tectonic scenario for the Arabian-Nubian Shield

A synthesis of the geological features of the main geological phases in the ANS, justifies the comparison with the Mesozoic and Early Cenozoic development of western North America. The ANS consists, like the Cordillera of western North America, of accreted mostly juvenile terranes which are separated by ophiolitic sutures. These sutures display a complex structural history which includes significant stages of strike slip movement. The younger geological features in the ANS, as core complexes, sedimentary basins and A-type granites, all indicate

extension and lithospheric thinning. Consequently, a new tectonic scenario for the ANS is proposed here (see also Figure 6-4 and Table 6-1). It is similar to the tectonic scenario that is described above for the Mesozoic and Early Cenozoic Cordilleran development of western North America:

The Neoproterozoic era of the ANS started with the formation of the Mozambique Ocean upon the rifting of Rodinia at ca. 900 Ma (e.g. Abdelsalam and Stern, 1996; Rogers et al, 1995; Shackleton, 1996; Unrug, 1996). Island arcs, of which remnants can be found in the Asir Terrane (the Tabalah and Tarj Complex) and other terranes of the ANS, were formed in the Mozambique Ocean (Figure 6-4A). The island-arcs were formed soon after the opening of the Mozambique Ocean and the youngest of these island-arcs were formed as late as 730 Ma. Meanwhile ophiolites, as the Bi'r Umq Suture, were formed at the fore-arcs and back-arcs of the island-arcs (Figure 6-4A).

“Offshore amalgamation” of island-arcs led to the accretion of island-arcs and the formation of a superterrane that consisted of the Asir Terrane, the Jiddah Terrane and the Hijaz Terrane (Figure 6-4B). The accretion took place along the ophiolitic sutures as the Bi'r Umq Suture. This suture recorded the earliest stage of accretion after ~820 Ma. Later stages of deformation that were recorded on the Bi'r Umq Suture and at the intra-terrane shear zones of the Tabalah and Tarj shear zones, indicate strike-slip movement along terrane-boundaries. The changes in sense of shear on the shear zones during arc-accretion are attributed to the change in plate motion during arc-accretion. The activity at the Bi'r Umq Suture and the intra-terrane shear zones of the Asir Terrane ended at ca. 760 Ma. This date indicates the end of the “offshore amalgamation” of the Asir, Jiddah and Hijaz Terranes that formed the Amennakhte Superterrane.

The subduction at the N-S trending continental margins of East Gondwanaland (the Nabitah Belt) and West Gondwanaland (the Keraf Suture and Kabus Suture) started at ca. 730-700 Ma (Figure 6-4C). The arc-accretion at these sutures led to lithospheric thickening (Figure 6-4D). The subduction at the continental margins caused the closure of the Mozambique Ocean at ca. 650 Ma which is the youngest date for deformation on the shear zones which are thought to represent the continental margins. No actual collision of the continental masses of East and West Gondwanaland took place, however the continuing accretion of large amounts of juvenile crusts should have caused significant lithospheric thickening. The findings in this thesis confirm the conclusions of Burke and Sengör (1986) and Stern (1994) who state that the Najd SZ formed during the compressional regime. It would then represent a large intra-terrane strike slip shear zone as also observed during arc-accretion in western North America.

A reduction in the rate of convergence at the continental margins of the ANS, initiated thermal re-equilibration of the lithosphere. This caused slow thinning of the thickened lithosphere and initiated the actual gravitational collapse at 650-620 Ma. At this stage conductive heating of the lithospheric root decreased the strength of the crust (Figure 6-4D). The thickened crust became gravitationally unstable. Delamination of the lithospheric root of the ANS caused the actual collapse (Figure 6-4E). This gravitational collapse led to extension in NW-SE direction (Figure 6-4F). Lithospheric thinning, through large low-angle normal shear zones, caused heating and the intrusion of A-type granites, as those that were observed in the

Wadi Kid Complex. The isostatic rebound and the intrusion of these granites contributed to the doming of the lower crust and the development of metamorphic core complexes such as the Wadi Kid complex, and the El Sibai and Meatiq domes in a NW-SE extensional regime at 600 Ma (Figure 6-4F). Sedimentary basins, bordered by normal faults, were formed at upper crustal levels as a response to the extension and allowed the deposition of post orogenic molasse sequences as the Hammamat Gp. and the Saramuj Conglomerate Gp (Figure 6-4F). The extension was accompanied by large igneous activity in the form of the intrusion of A-type granites, the intrusion of NE-SW dykes and volcanics as the undeformed rhyolites in the Wadi Kid Complex.

## 6.6 Conclusions

The tectonic development of Arabian-Nubian Shield displays many similarities with the Cordilleran Mesozoic and Early Cenozoic development of western North America. The different tectonic stages in the ANS can be summarized as follows:

1. Ophiolitic sequences and island-arcs formed at ca. 900-750 Ma in the Mozambique Ocean. The lithologies of the Tabalah and Tarj Complex and the Bi'r Umq Complex are remnants of this phase.
2. "Offshore amalgamation" led to accretion of island-arcs in the Mozambique Ocean and the formation of the Amennakhte Superterrane. Different compressional and transcurrent deformation phases that were observed in the Bi'r Umq Complex and Tabalah and Tarj areas are remnants of this phase. The intra-oceanic arc-accretion took place at ca. 820 – 760 Ma.
3. Literature indicates that subduction at N-S active continental margins started at ca. 700 Ma. Arc-accretion at these continental margins led to lithospheric thickening.
4. The start of gravitational collapse of the thickened lithosphere took place at ca. 650 – 620 Ma.
5. Gravitational collapse led to extension. This extension was accommodated by low-angle shear zones of the type that was observed at the Wadi Kid Complex.
6. Isostatic rebound and the rise of mantle derived magmas in the extending crust led to doming of the low-angle shear zones and the actual formation of the core complexes as the Wadi Kid Complex at ca. 600 Ma.

## 6.7 Recommendations for future research

This research, based on the detailed studies of three key areas, has produced an improved model for the tectonic evolution of the Arabian-Nubian Shield. It provides a pointer for the direction of future research. Similar detailed studies in other areas are needed to further improve our understanding of the tectonic evolution of the Arabian-Nubian Shield. There are other subjects of research that deserve attention in the Arabian-Nubian Shield. These include:

1. The real nature (suprasubduction or MOR) of the ophiolites remains still subject of discussion. Geochemical investigations may help in getting a better view on their origin. .
2. Generally, little attention has been given to the arc-accretion in the ANS, although it was

this process, which gave the ANS much of its current face. Detailed structural, geochemical and metamorphic research is needed to improve the understanding of this phase so that it can help us to understand the lithospheric thickening, which led to gravitational collapse, in more detail. The relatively low abundance of HP-metamorphism also requires attention.

3. The extend of extension in the ANS is not really clear. NW-SE extension is clearly observed through the core complexes in the Nubian part of the ANS, however it is not clear if, and in which way extension took place in the Arabian part of the ANS.





## References

- Abdelsalam, M.G. 1994. The Oko Shear Zone, Sudan: post-accretionary deformation in the Arabian-Nubian Shield. *Journal of the Geological Society, London*, 151: 767-776.
- Abdelsalam, M.G. and Stern, R.J. 1996. Sutures and shear zones in the Arabian Nubian Shield. *Journal of African Earth Sciences*, 23: 289-310.
- Abdelsalam, M.G. and Stern, R.J., 1993, Structure of the late Proterozoic Nakasib suture, Sudan. *Journal of the Geological Society*, 150: 1065-1074.
- Abdelsalam, M.G., Abdeen, M.M., Dowaidar, H.M., Stern, R.J. and Abdelghaffar, A.A., 2003a. Structural evolution of the Neoproterozoic Western Allaqi–Heiani suture, southeastern Egypt, *Precambrian Research*, 124: 87-104.
- Abdelsalam, M.G., Abdel-Rahman, E.M, El-Faki, E.M., Al-Hur, B., El-Bashier, F.M., Stern, R.J. and Thurmond, A.K., 2003b. Neoproterozoic deformation in the northeastern part of the Saharan Metacraton, northern Sudan. *Precambrian Research*, 123: 203-221.
- Abu El-Ela, FF., 1999. Neoproterozoic tholeiitic arc plutonism: petrology of gabbroic intrusions in the El-Aradiya area, Eastern Desert, Egypt. *Journal of African Earth Sciences*, 28: 721-741.
- Agar, R.A., 1985. Stratigraphy and palaeogeography of the Siham group: direct evidence for a Neoproterozoic continental microplate and active continental margin in the Saudi Arabian Shield. *Journal of the Geological Society*, 142: 1205-1220.
- Agar, R.A., 1986. The Bani Ghavy Group; sedimentation and volcanism in pull-apart grabens of the Najd strike-slip orogen, Saudi Arabian shield. *Precambrian Research*, 31: 259-274.
- Ahmed, A.M., El Sheshtawi Y.L., and El Tokhi, M.M., 1993. Origin and geochemistry of Egyptian granitoid rocks in Nuweiba area, eastern Sinai. *Journal of African Earth Sciences* 17: 399-413.
- Al-Husseini, M.I., 2000. Origin of the Arabian Plate structures: Amar Collision and Najd Rift. *Georabia*, 5: 527-542.
- Al-Rehaili, M.H., 1980, Geology of the mafic-ultramafic complex of the Bir Umq area: Jiddah, King Abdulaziz University, Faculty of Earth Sciences, M.Sc. thesis, 160 p.
- Al-Saleh, A.M. and Boyle, A.P., 2001. Neoproterozoic ensialic back-arc spreading in the eastern Arabian Shield: geochemical evidence from the Halaban Ophiolite. *Journal of African Earth Sciences*, 33: 1-15.
- Al-Saleh, A.M. and Boyle, A.P., 2001. Neoproterozoic ensialic back-arc spreading in the eastern Arabian Shield: geochemical evidence from the Halaban Ophiolite. *Journal of African Earth Sciences*, 33: 1-15.
- Al-Saleh, A.M., Boyle, A.P. and Musset, A.E., 1998. Metamorphism and  $^{40}\text{Ar}/^{39}\text{Ar}$  dating of the Halaban Ophiolite and associated units: evidence for two-stage orogenesis in the Arabian Shield. *Journal of the Geological Society, London*, 155: 165-175.
- Anderson, E.M., 1952. The dynamics of faulting and dyke formation with applications to Britain. Oliver & Boyd, 206 pp.
- Anderson, J.L. and Cullers, R.L., 1990. Middle to upper crustal plutonic construction of a magmatic arc; An example from the Whipple Mountains metamorphic core complex. In: J.L. Anderson (ed.) *The nature and origin of Cordilleran magmatism. Geological Society of America Memoir* 174: 47-69.
- Ayalon, A., Steinitz G., and Starinsky, A., 1987. K-Ar and Rb - Sr whole rock ages reset during Pan-African event in the Sinai Peninsula (Ataq Area). *Precambrian Research* 37: 191-197.
- Bailo, T., Schandelmeier, H, Franz, G., Sun, C.H. and Stern, R.J., 2003. Plutonic and metamorphic rocks from the Keraf Suture (NE Sudan): a glimpse of Neoproterozoic tectonic evolution on the NE margin of W. Gondwana. *Precambrian Research*, 123: 67-80.
- Bakor, A. R., Gass, I. G. and Neary, C. R., 1976. Jabal al Wask, northwest Saudi Arabia: An Eocambrian back-arc ophiolite. *Earth and planetary science letters*, 30: 1-9.
- Barton, M.D., 1990. Cretaceous magmatism, metamorphism and metallogeny in the east-central Great Basin. In: J.L. Anderson (ed.) *The nature and origin of Cordilleran Magmatism. Geological Society of America Memoir* 174: 283-302.
- Beard, L.S. 1996. Paleogeography of the Horse Spring Formation in relation to the Lake Mead fault system, Virgin Mountains, Nevada and Arizona. In Beratan, K.K. (ed.) *Reconstructing the history of the Basin and Range extension using sedimentology and stratigraphy. Geological Society of America Special Paper*, 303: 27-59.
- Bell, T.H. and Hammond, R.L., 1984. On the internal geometry of mylonite zones. *Journal of Geology* 92: 667-686.
- Bentor, Y.K., 1985 The crustal evolution of the Arabo-Nubian Massif with special reference to the Sinai Peninsula. *Precambrian Research* 28: 1-74.
- Berman, R.G., 1990. Mixing properties of Ca-Mg-Fe-Mn garnets. *American Mineralogy* 75: 328-344.
- Beyth, M, Avigad, D., Wetzell, H.-U., Matthews A. and S. M. Berhe, 2003. Crustal exhumation and indications for Snowball Earth in the East African Orogen: north Ethiopia and east Eritrea. *Precambrian Research*, 123: 187-201
- Beyth, M., Stern, R.J., Altherr, R. and Kröner, A., 1994. The late Precambrian Timna igneous Complex, Southern Israel: Evidence for comagmatic-type sanukitoid monzodiorite and alkali granite magma. *Lithos* 31: 103-124.
- Bielski, M., 1982. Stages in the Arabian-Nubian Massif in Sinai (unpublished Ph.D. Thesis) - Hebrew University, Jerusalem. 155 pp
- Blasband B., White, S., Brooijmans, P., De Boorder, H., and Visser, W., 2000, Neoproterozoic extensional collapse in the Arabian-Nubian Shield: *Journal of the Geological Society*, 157, 615-628.
- Blasband, B., Brooijmans, P., Dirks, P., Visser, W. & White, S., 1997. A Pan-African core complex in the Sinai, Egypt. *Geologie en Mijnbouw*, 73: 247-266.
- Bogoch, R., Avigad, D and Weissbrod, T., 2002. Geochemistry of the quartz-diorite – granite association, Roded area, southern Israel. *Journal of African Earth Sciences*, 35: 51-60.

- Bowden, R.A., Smith, G.H., and Hopwood, T., 1981, Reconnaissance geological map of the Jabal Sayid District: : Saudi Arabian Deputy Ministry for Mineral Resources Open File Report RF-OF-01-8.
- Bregar, M., Bauernhofer, A., Pelz, K., Kloetzli, U., Fritz, H. and Neumayr, P., 2002. A late Neoproterozoic magmatic core complex in the Eastern Desert: emplacement of granitoids in a wrench-tectonic setting. *Precambrian Research*, 118: 59-82.
- Brooijmans, P., Blasband, B., White, S. H., Visser, W. J. and Dirks, P., 2003. Geothermobarometric evidence for a metamorphic core complex in Sinai, Egypt. *Precambrian Research*, 123: 249-268.
- Brown, G.F., Schmidt, D.L. and Huffman, A.C. Jr., 1989. Geology of the Arabian Peninsula; shield area of Western Saudi Arabia. USGS Professional Paper, 560-A.
- Buick, I.S. and Holland, T.J.B., 1989. The P-T-t path associated with crustal extension, Naxos, Cyclades, Greece. In: Daly, J.S., Cliff, R.A., Yardley, B.W.D. (Eds.), *Evolution of Metamorphic Belts*. Geological Society London Special Publication 43: 365-369.
- Burchfiel, B.C., Cowan, D.S., and Davis, G.A., 1992. Tectonic overview of the Cordilleran orogen in the western United States. In Burchfiel, B.C., Lipman, P.W. and Zoback, M.I., (eds), *The Cordilleran orogen: conterminous U.S. (The Geology of North America – G.3)*: 407-479.
- Burke, K. and Sengor, C., 1986. Tectonic escape in the evolution of the continental crust. *American Geophysical Union Geodynamics Series*, 14: 41-53.
- Calvez, J.Y. and Kemp, J., 1982, Geochronological investigations in the Mahd adh Dhahab quadrangle, central Arabian Shield: Saudi Arabian Deputy Ministry for Mineral Resources Technical Record BRGM-TR-02-5, 41 p.
- Chardon, D., Andronicos, C.L., and Hollister, L.S., 1999. Large-scale transpressive shear zone patterns and displacements within magmatic arcs: The Coast Plutonic Complex, British Columbia. *Tectonics*, 18: 278-292.
- Choukroune, P., Gapais, D. and Merle, O. 1987. Shear criteria and structural symmetry. *Journal of Structural Geology* 9: 525-530.
- Claeson, S., Pallister, J.S. and Tatsumoto, M., 1984. Samarium-Neodymium data on two Neoproterozoic ophiolites of Saudi Arabia and implications for crustal and mantle evolution. *Contributions to Mineralogy and Petrology*, 85: 244-252.
- Clark, M.D., 1985. Late Proterozoic crustal evolution of the Midyan region, northwestern Saudi Arabia. *Geology*, 13: 611-615.
- Cloos, M., 1993. Lithospheric buoyancy and collisional orogenesis: Subduction of oceanic plateaus, continental margins, island arcs, spreading ridges, and seamounts. *Geological Society of America Bulletin*, 105: 715-737.
- Cobbold, P.R. and Gapais, D., 1987. Shear criteria in rocks: an introductory review. *Journal of Structural Geology* 9: 521-523.
- Cole, R.B., Ridgway, K.D., Layer, P.W. and Drake, J., 1999, Kinematics of basin development during the transition from terrane accretion to strike-slip tectonics, Late Cretaceous-early Tertiary Cantwell Formation, south central Alaska: *Tectonics*, 18 1224-1244.
- Coney, P.J. and Harms, T.A., 1984. Cordilleran metamorphic core complexes: Cenozoic relicts of Mesozoic compression. *Geology*, 12: 550-554.
- Coney, P.J., 1989. Structural aspects of suspect and accretionary tectonics in western North America. *Journal of Structural Geology*, 11: 107-125.
- Corti, G., Carminati, G., Mazzarini, F. and Garcia, M.O., 2005, Active strike-slip faulting in El Salvador, Central America. *Geology*, 33: 989–992.
- Davis, G.A. and Lister G.S., 1988. Detachment faulting in continental extension; Perspectives from the Southwestern U.S. Cordillera. *Geological Society of America, Special Paper* 218: 133-159.
- Davis, G.A., 1980. Structural characteristics of metamorphic core complexes, southern Arizona. *Geological Society of America Memoir* 153: 35-77.
- Davis, G.A., 1987. A shear-zone model for the structural evolution of metamorphic core complexes in southeastern Arizona. In: Coward, M.P., Dewey, J.F., Hancock, P.L. (Eds.), *Continental Extensional Tectonics*. Geological Society London Special Publication 28: 247-266.
- Davis, G.H., 1980. Structural characteristics of metamorphic core complexes, southern Arizona. In: Crittenden, M.D., Coney, P.J. and Davis, G.H. (eds) *Cordilleran Core Complexes*. Geological Society of America Memoir 153: 35-77.
- Davis, G.H., 1984, *Structural geology of rocks and regions*. John Wiley and sons, 492 pp.
- De Souza Filho, C.R., Drury S.A., 1998. A Neoproterozoic supra-subduction terrane in northern Eritrea, NE Africa. *Journal of the Geological Society*, 155: 551-566.
- De Yoreo, J.J., Lux, D.R. and Guidotti, C.V., 1991. Thermal modeling in low-pressure/high-temperature metamorphic belts. *Tectonophysics* 188: 209-238.
- Dewey, J.F., 1988. Extensional collapse of orogens. *Tectonics* 7: 1123-1139.
- Dick, H.J.B. and Bullen, T., 1984, Chromian spinel as a petrogenic indicator in abyssal and alpine peridotites and spatially associated lavas: *Contributions to mineralogy and Petrology*, v.86, p. 54-76.
- Dilek, Y. and Ahmed, Z., 2003. Proterozoic ophiolites of the Arabian Shield and their significance in Precambrian tectonics. In Dilek, Y. and Robinson, P.T., 2003 (eds) *Ophiolites in earth history*. Geological Society Special Publications, 218: 685-700.
- Dilek, Y., 2003. Ophiolite concept and its evolution. In Dilek, Y. and Newcomb, S., (eds) *Ophiolite concept and the evolution of geological thought*. Geological Society of America Special Paper, 373: 1-16.
- Dixon, T.H., Stern, R.J. and Hussein, I.M., 1987. Control of Red Sea rift geometry by Precambrian structures. *Tectonics*, 6: 551-571.
- Dodge, F.C.W., 1979. The Uyaijah ring structure, Kingdom of Saudi Arabia. U.S. Geological Survey Professional Paper, 774-E.
- Dunlop, H.M., Kemp, J., and Calvez, J.Y., 1986, Geochronology and isotope geochemistry of the Bir Umq mafic-ultramafic complex and Arj-group volcanic rocks, Mahd adh Dhahab quadrangle, central Arabian Shield: Saudi Arabian Deputy Ministry for Mineral Resources Open-File Record BRGM-OF-07-7, 38 p.

- Dunnet, D., 1969. A technique of finite strain analysis using elliptical particles. *Tectonophysics* 7: 117-136.
- El Akhal, H., 1993. Transect of a tectonic melange to an island-arc in the Pan-African of SE Egypt (Wadi Ghadir area). Scientific series of the International Bureau/Forschungszentrum Jülich GmbH, 20.
- El Akhal, H., 1993. Transect of a tectonic melange to an island-arc in the Pan-African of SE Egypt (Wadi Ghadir area). Scientific series of the International Bureau/Forschungszentrum Jülich GmbH, 20.
- El Din, G.M.K., 1993. Geochemistry and tectonic significance of the Pan-African El Sibai Window, Central Eastern Desert, Egypt. Scientific series of the International Bureau/Forschungszentrum Jülich GmbH, 19.
- El Din, K.G.M., Khudeir, A.A. and Greiling, R.O., 1991. Tectonic evolution of a Pan-African gneiss culmination, Gabal El Sibai area, Central Eastern Desert, Egypt. *Zentralblatt fuer Geologie und Palaeontologie, Teil I*, 11: 2637-2640.
- El Gaby, S., El Nady, O. and Khudeir, A., 1984. Tectonic evolution of the basement complex in the Central Eastern Desert of Egypt. *Geologische Rundschau*, 73: 1019-1036.
- El Shazly, S.M. and El Sayad, M.M., 2000. Petrogenesis of the Pan-African El-Bula suite, central Eastern Desert, Egypt. *Journal of African Earth Sciences*, 31: 317-336.
- Ellis, M. and Watkinson, A.J., 1987. Orogen-parallel extension and oblique tectonics: the relation between stretching lineations and relative plate motions. *Geology*, 15: 1022-1026.
- El-Nisr, S. A., El-Sayed, M. M. and Saleh, G. M., 2001. Geochemistry and petrogenesis of Pan-African late- to post-orogenic younger granitoids at Shalatin-Halaib, south Eastern Desert, Egypt. *Journal of African Earth Sciences*, 33: 261-282
- El-Sayed, M.M. and El-Nisr, S.A., 1999. Petrogenesis and evolution of the Dineibit El-Quleib hyperaluminous leucogranite, Southeastern Egypt: petrological and geochemical constraints. *Journal of African Earth Sciences*, 28: 703-720.
- Ernest Anderson, R., 1977. *Geology of the Wadi Tarj Quadrangle, Sheet 19/42 A, Kingdom of Saudi Arabia: Saudi Arabian Directorate General of Mineral Resources Geologic Map GM-24, 24p. Scale 1:100.000.*
- Ernst, W.G., 2003. High-pressure and ultrahigh-pressure metamorphic belts – Subduction, recrystallization, exhumation, and significance for ophiolite study. In Dilek, Y and Newcomb, S., (eds) *Ophiolite concept and the evolution of geological thought. Geological Society of America Special Paper*, 373: 365-384.
- Eyal, E., Eyal, M. and Kroner, A., 1991. The geochronology of the Elat terrain, metamorphic basement, and its implication for crustal evolution of the NE part of the Arabian-Nubian Shield. *Israel Journal Earth Sciences* 40: 5-16.
- Faulds, J.E. and Stewart, J.H. 1998. Accommodation zones and transfer zones: The regional segmentation of the Basin and Range Province. *Geological Society of America Special Paper*, 323.
- Fisher, D. M., Gardner, T.M., Marshall, J.S. and Montero, W. P., 1994. Kinematics associated with late Cenozoic deformation in central Costa Rica: Western boundary of the Panama microplate. *Geology* 22: 263–266.
- Fleck, R.J., Greenwood, W.R., Hadley, D.G., Anderson, R.E and Schmidt, D.L., 1980. Rubidium-strontium geochronology and plate-tectonic evolution of the southern part of the Arabian Shield. *U.S. Geological Survey Professional Paper*, 1131.
- Flower, M.F.J, 2003. Ophiolites, historical contingency, and the Wilson cycle. In Dilek, Y and Newcomb, S., (eds) *Ophiolite concept and the evolution of geological thought. Geological Society of America Special Paper*, 373, 111-135.
- Folkman, Y. and Assael, R., 1980b. Aeromagnetic map of Sinai; 1:500 000. Survey of Israel, Jerusalem.
- Folkman, Y. and Assael, R., 1980a. Gravity map of Sinai (relative Bouguer anomalies); 1:500 000. Survey of Israel, Jerusalem.
- Fowler, T. J. and Osman, A. F., 2001. Gneiss-cored interference dome associated with two phases of late Pan-African thrusting in the Central Eastern Desert, Egypt. *Precambrian Research*, 108: 17-43
- Fritz, H., Dallmeyer, D.R., Wallbrecher, E., Loizenbauer, J., Hoinkes, G., Neumayer, P. and Khudeir, A.A., 2002. Neoproterozoic tectonothermal evolution of the Central Eastern Desert, Egypt: a slow velocity tectonic process of core complex exhumation. *Journal of African Earth Sciences*, 34: 137-155.
- Fritz, H., Wallbrecher, E., Khudeir, A.A., Abu El Ela, F. and Dallmeyer, D.R., 1996. Formation of Neoproterozoic metamorphic core complexes during oblique convergence (Eastern Desert, Egypt). *Journal of African Earth Sciences*, 23: 311-329.
- Fueten, F, Robin, P-Y.F. and Stephens R., 1991. A model for the development of a dominal quartz c-axis fabric in a coarse-grained gneiss. *Journal of Structural Geology* 13: 1111-1124.
- Furnes, H., Shimron, A.E. & Roberts, 1985. Geochemistry of Pan-African volcanic arc sequences in southeastern Sinai Peninsula and plate tectonic implications. *Precambrian Research*. 29: 359-382.
- Gans, P.B., Mahood, G.A. and Schermer, E., 1989. Synextensional magmatism in the Basin and Range Province; a case study from the eastern Great Basin. *Geological Society of America Special Paper* 233.
- Garson, M. S. and Shalaby, I. M., 1976. Precambrian-Lower Paleozoic plate tectonics and metallogenesis in the Red Sea region. *Geol. Assoc. Canada, Special Paper*, 14: 573-96.
- Gass, I. G., 1977. The evolution of the Pan African crystalline basement in NE Africa and Arabia. *Journal of the Geological Society*, 134:129-138.
- Gautier, P. and Brun, J.P., 1994. Ductile crust and exhumation and extensional detachments in the central Aegean (Cyclades and Evvia Islands). *Geodinamica Acta* 7: 57-85.
- Ghazala, H.H., 1995. Structural interpretation of the Bouguer and aeromagnetic anomalies in the central Sinai. *Journal of African Earth Sciences* 19: 35-42.
- Ghebreab, W., 1999. Tectono-metamorphic history of Neoproterozoic rocks in eastern Eritrea. *Precambrian Research*, 98: 83-105.
- Ghent, E.D. and Stout, M.Z., 1981. Geobarometry and geothermometry of Plagioclase-Biotite-Garnet-Muscovite assemblages. *Contributions to Mineralogy and Petrology* 76: 92-97.
- Gibson, R.L., 1992. Sequential, syndeformational porphyroblast growth during Hercynian low-pressure/high-temperature metamorphism in the Canigou massif, Pyrenees. *Journal of metamorphic Geology* 10: 637-650.

- Green, T.H., 1982. Anatexis of mafic crust and high pressure crystallization of andesite: *in* Thorpe, R.S, (ed.) Andesites; Orogenic andesites and related rocks, John Wiley and Sons: 465-488.
- Greene, R.C., 1982. Reconnaissance geology of the Thaniyah Quadrangle, Sheet 20/42 C, Kingdom of Saudi Arabia, Saudi Arabian Deputy Ministry for Mineral Resources Open-File Report USGS-OF-02-84, 22p., scale 1: 100.000.
- Greenwood, W. R, Jackson, R.O. and Johnson, P.R., 1986. Geologic Map of the Jabal Hasir Quadrangle, sheet 19 F, Kingdom of Saudi Arabia: Saudi Arabian Deputy Ministry for Mineral Resources Map GM 94-C, 31p., scale 1: 250.000.
- Greiling, R.O., Abdeen, M.M., Dardir, A.A, El Akhal, H., El Ramly, M.F., Kmal El Din, G.M., Osman, A.F., Rahwan A.A., Rice, A.A. and Sadek, M.F., 1994. A structural synthesis of the Proterozoic Arabian-Nubian Shield in Egypt. *Geologisches Rundschau*, 83: 484-501.
- Greiling, R.O., El Ramly, M.F., El Akhal, H. and Stern, R.J., 1988. Tectonic evolution of the northwestern Red Sea margin as related to basement structure. *Tectonophysics*, 153: 179-191.
- Greiling, R.O., Kröner, A. and El Ramly, M.F.. 1984. Structural interference patterns and their origin in the Pan-African basement of the southeastern Desert of Egypt. In Greiling, R. and Kröner, A. (eds) *Precambrian Tectonics Illustrated*: 401-413.
- Grothaus, B., Eppler, D. and Ehrlich, R., 1979. Depositional environment and structural implications of the Hammamat Formation. *Annals of the Geological Survey of Egypt*, 9: 564-590.
- Habib, M.E., Ahmed, A.A. and El Nady, O.M., 1985. Tectonic evolution of the Meatiq infrastructure, Central Eastern Desert. *Tectonics*, 7: 613-627.
- Hadley, D.G. and Schmidt, L.S., 1980. Sedimentary rocks of the Arabian Shield and their evolution. *I.A.G. Bulletin*, 3: 26-50.
- Halpern, M. and Tristan N., 1981. Geochronology of the Arabian-Nubian Shield in southern Israel and eastern Sinai. *Journal of Geology* 89: 639-648.
- Halpern, M., 1980. "Pan-African" isochron ages of Sinai igneous rocks. *Geology* 8: 639-648.
- Hammer, S., 1986. Asymmetrical pull-aparts and foliation fish as kinematic indicators. *Journal of Structural Geology* 8: 111-112.
- Harms, U, Darbyshire, D.B.F., Denkler, T., Hengst, M and Schandelmeier, H., 1994. Evolution of the Neoproterozoic Delgo suture zone and crustal growth in Northern Sudan.: geochemical and radiogenic isotope constraints. *Geologisches Rundschau*, 83: 591-603.
- Harrel, J.A. and Brown, V.M, 1992. The world's oldest geological map: the 1150 B.C. Turin Papyrus from Egypt. *Journal of Geology*, 100: 3-18.
- Harris, N.B.W, Hawkesworth, C.J and Tindle, A.G, 1993. The growth of continental crust during the Neoproterozoic: geochemical evidence from the Arabian Shield: *in* Prichard, H.M., Harris, N.B.W. and Neary, C.R. (eds.), *Magmatic processes and plate tectonics*, Geological Society Special Publication, 76: 363-371.
- Hassanen, M. A. , El-Nisr, S.A. and Mohammed, F.H., 1996. Geochemistry and petrogenesis of Pan-African I-type granitoids at Gabal Iгла Ahmar, Eastern Desert, Egypt. *Journal of African Earth Sciences*, 22: 29-42.
- Hassanen, M.A., 1997. Post-collisional A-type granites of Homrit Waggat Complex, Egypt: Petrological and geochemical constraints on its origin. *Precambrian Research*, 82: 211-236.
- Hawkins, J.W., 2003. Geology of supra-subduction zones – Implications for the origin ophiolites. In Dilek, Y and Newcomb, S., (eds) *Ophiolite concept and the evolution of geological thought*. Geological Society of America Special Paper, 373: 227-268.
- Hazlett, R.W., 1990. Extension related Miocene volcanism in the Mopah Range volcanic field, southeastern California. In Anderson, J.L.(ed.) *The nature and origin of Cordilleran magmatism Geological of Society of America Memoir* 174: 133--145
- Hildreth, W. and Moorbath, S., 1988. Crustal contribution to arc magmatism in the Andes and central Chile. *Contributions to Mineralogy and Petrology*, 98: 455-489.
- Holland, T.J.B. and Blundy, J., 1994. Non-ideal interactions in calcic amphiboles and their bearing on amphibole-plagioclase thermometry. *Contributions to Mineralogy and Petrology* 116: 433-447.
- Holland, T.J.B. and Powell, R., 1992. Plagioclase feldspars: activity-composition relations based upon Darken's Quadratic Formalism and Landau theory. *American Mineralogy* 77: 53-61.
- Hopwood, T., An exploration study of metal deposits in the Jabal Sayid region: Saudi Arabian Directorate General of Mineral Resources RFO-1979-9, 169 p.
- House, M.A., Hodges, K.V. and Bowring, S.A., 1997. Petrological and geochronological constraints on regional metamorphism along the northern border of the Bitterroot batholith. *Journal of metamorphic Geology* 15: 753-764.
- Husseini, M.I. and Husseini, S.I., 1990. Origin of the Infracambrian salt basins of the Middle East. In: Brooks, J., (ed) *Classic Petroleum Provinces*. Geological Society London Special Publications, 50: 279-292.
- Husseini, M.I., 1988. The Arabian Infracambrian extensional system. *Tectonophysics* 148: 93-143.
- Husseini, M.I., 1989. Tectonic and deposition model of Late Precambrian-Cambrian Arabian and adjoining plates. *The American Association of Petroleum Geologists Bulletin*, 73: 1117-1131.
- Jackson, J.N. and Ramsay, C.R., 1984. Time-space relationships of Upper Precambrian volcanic and sedimentary units in the Central Arabian Shield. *Journal of the Geological Society*, 140: 617-628.
- Jackson, N.J., 1986. Petrogenesis and evolution of Arabian felsic plutonic rocks. *Journal of African Earth Sciences*, 4, 47-59.
- Jarrar, G, Stern, R.J., Saffarini, G. and Al-Zubi, H., 2003. Late- and post orogenic Neoproterozoic intrusions of Jordan: implications for crustal growth in the northernmost segment of the East African Orogen. *Precambrian Research*, 123: 295-319.
- Jarrar, G., Wachendorf, H. and Saffarini, G., 1992. A Neoproterozoic bimodal volcanic/subvolcanic suite from the Wadi Araba, southwest Jordan. *Precambrian Research*, 56: 51-72.
- Jarrar, G., Wachendorf, H. and Zellmer, H., 1991. The Saramuj Conglomerate: Evolution of a Pan-African molasse sequence from southwest Jordan. *Neues Jahrbuch Geologie Paläontologie Mh.*, 6: 335-356.
- Jessel, M.W. and Lister, G.S, 1990. A simulation of temperature dependence of quartz fabrics. In: Knipe, R.J. & E.H. Rutter

- (eds) Deformation mechanisms, rheology and tectonics. Geological Society Special Publication 54: 335-352.
- Johnson, P.R. 1999. Tectonic development of the Arabian Shield. Contribution to IUGS/UNESCO Deposit Modelling Workshop, p.1
- Johnson, P.R. and Kattan, F. 1999a, The timing and kinematics of a suturing event in the northeastern part of the Arabian Shield, Kingdom of Saudi Arabia: Saudi Arabian Deputy Ministry for Mineral Resources Open File Report USGS-OF-99-3, 29p.
- Johnson, P.R. and Kattan, F. 1999b, The Ruwah, Ar Rika, and Halaban-Zarghat fault zones: northwest-trending Neoproterozoic brittle-ductile shear zones in west-central Saudi Arabia: In De Wall, H. & Greiling, R.O. (eds) Aspects of Pan-African Tectonics Proceedings of a discussion meeting at Heidelberg, October 1998. Series International Cooperation, Bilateral Seminars, Forschungszentrum Jülich, 32, 75-79.
- Johnson, P.R. and Kattan, F., 2001. Oblique sinistral transpression in the Arabian shield: the timing and kinematics of a Neoproterozoic suture zone. *Precambrian Research*, 107: 117-138.
- Johnson, P.R. and Stewart, I.C.F., 1995. Magnetically inferred basement structure in central Saudi Arabia. *Tectonophysics*, 245: 37-52.
- Johnson, P.R., 1996. Geochronologic and isotopic data for rocks in the east-central part of the Arabian Shield: stratigraphic and tectonic implications. Saudi Arabian Deputy for Mineral Resources, Open-File Report USGS-OF-3.
- Johnson, P.R., 1998. The structural geology of the Samran-Shayban area, Kingdom of Saudi Arabia: Saudi Arabian Deputy Ministry for Mineral Resources Open File Report USGS-OF-98-2, 45p.
- Johnson, P.R., 2003. Post-amalgamation basins of the NE Arabian shield and implications for Neoproterozoic III tectonism in the northern East African orogen. *Precambrian Research*, 123: 321-337.
- Johnson, P.R., Abdelsalam, M, and Stern, R.J., 2002, The Bir Umq-Nakasib fault zone: Geology and structure of a Neoproterozoic suture, Kingdom of Saudi Arabia and Sudan: Saudi Geological Survey Open-File Report SG-OF-2002-1.
- Johnson, P.R., Kattan, F.H. and Wooden, J.L., 2001. Implications of SHRIMP and Microstructural Data on the Age and Kinematics of Shearing in the Asir Terrane, Southern Arabian Shield, Saudi Arabia. *Gondwana Research*, 4: 172-173
- Johnson, P.R., Scheibner, E and Alan Smith, E. 1987, Basement fragments, accreted tectonostratigraphic terranes, and overlap sequences: elements in the tectonic evolution of the Arabian Shield. In: Kroner, A.(ed.) Proterozoic lithospheric evolution. American Geophysical Union Geodynamics Series, 17, 235-257.
- Johnson, P.R., Kattan, F. and A-Salah, A., 2004. Neoproterozoic ophiolites in the Arabian-Shield: field relations and structures. In *ed: Kusky, T. 2004. Precambrian ophiolites*, 13
- Kay, S.M., Mpodozis, C, Ramos, V.A. and Munizaga, F., 1991. Magma source variations for mid-late Tertiary magmatic rocks associated with a shallowing subduction zone and a thickening crust in the central Andes (28 to 33°). In: Harmon, R.S. and Rapela, C.W., eds. Andean magmatism and its tectonic setting, Geological Society of America Special Paper 265, 113-137.
- Kemp, J., 1996. The Kuara Formation (northern Arabian Shield); definition and interpretation: a probable fault-trough sedimentary succession. *Journal of African Earth Sciences*, 22: 507-523.
- Kemp, J., Pellaton, C. and Calvez, J.Y., 1980. Geochronological investigations and geological history in the Precambrian of northwestern Saudi Arabia. Saudi Arabian Deputy Ministry for Mineral Resources Open-File Report, BRGGM-OF-01-1.
- Kessel, R., Stein, M. and Navon, O., 1998. Petrogenesis of Late Neoproterozoic dikes in the Northern Arabian-Nubian Shield. Implications for the origin of A-type granites. *Precambrian Research*, 92: 195-213.
- Kleemann, U. and Reinhardt, J., 1994. Garnet-biotite thermometry revisited: The effect of AlVI and Ti in biotite. *European Journal of Mineralogy* 6: 925-941.
- Kohn, B.P. and Eyal, M., 1981. History of the uplift of the crystalline basement of Sinai and its relation to the opening of the Red Sea as revealed by fission track dating of apatites. *Earth and Planetary Science Letters* 52: 129-141.
- Kröner, A., 1985. Ophiolites, and the evolution of tectonic boundaries in the Neoproterozoic Arabian-Nubian Shield of Northeast Africa and Arabia. *Precambrian Research*, 27: 235-257.
- Kröner, A., Greiling, R., Reischman, T., Hussein, I.M., Stern, R.J., Durr, S., Kruger, J. and Zimmer, M., 1987. Pan-African crustal evolution in the Nubian segment of northeast Africa. In: Kröner, A.(ed.) Proterozoic lithospheric evolution. American Geophysical Union Geodynamics Series, 17: 235-257.
- Kröner, A., Todt, W., Hussein, I.M., Mansour, M. and Rashwan, A.A., 1992. Dating of Neoproterozoic ophiolites in Egypt and the Sudan using the single grain zircon evaporation technique. *Precambrian Research*, 59: 15-32.
- Kuster, D. and Harms, U., 1998. Post-collisional potassic granitoids from the southern and northwestern parts of the Late Neoproterozoic East African Orogen: a review. *Lithos*, 45: 177-195
- Küster, D. and Liégeois, J.P., 2001. Sr, Nd isotopes and geochemistry of the Bayuda Desert high-grade metamorphic basement (Sudan): an early Pan-African oceanic convergent margin, not the edge of the East Saharan ghost craton? *Precambrian Research*, 109: 1-23.
- Laird, J. and Albee, A.L., 1981. Pressure, temperature and time indicators in mafic schists: their application to reconstructing the polymetamorphic history of Vermont. *American Journal of Science* 281: 127-175.
- Law, R.D. 1990 Crystallographic fabrics: a selective review of their applications to research in structural geology. In: Knipe, R.J. & E.H. Rutter (eds) Deformation mechanisms, rheology and tectonics. Geological Society Special Publication 54: 335-352.
- Le Bel, L and Laval, M., 1986. Felsic plutonism in the Al Amar-Idsas area, Kingdom of Saudi Arabia. *Journal of African Earth Sciences*, 4: 87-98.
- Le Metour, J., Johan, V., and Tegvey, M., 1982, Relationships between ultramafic-mafic complexes and volcanosedimentary rocks in the Precambrian Arabian Shield: Saudi Arabian Deputy Ministry for Mineral Resources Open File Report BRGM-OF-02-15, 108 p.
- Le Theoff, B., 1979. Non-coaxial deformation of elliptical particles. *Tectonophysics* 53: T7-T13.
- Leake, B.E., 1978. Nomenclature of amphiboles. *American Mineralogy* 63: 1023-1052.

- Lisle, R.J., 1977. Estimation of the tectonic strain ratio from the mean shape of deformed elliptical markers. *Tectonophysics* 56: 140-144.
- Lisle, R.J., 1985. *Geological Strain Analysis: A Manual for the Rf/Φ Technique*. Pergamon, Oxford, 99 pp.
- Lister, G.S. and Baldwin, S.L., 1993. Plutonism and the origin of metamorphic core complexes. *Geology* 21: 607-610.
- Lister, G.S. and Hobbs, B.E., 1980. The simulation of fabric development during plastic deformation and its application to quartzite: the influence of the deformation history. *Journal of Structural Geology* 2: 355-370.
- Lister, G.S., Banga, G. and Feenstra, A., 1984. Metamorphic core complexes of the Cordilleran type in the Cyclades, Aegean Sea, Greece. *Geology* 12: 221-225.
- Lister, G.S., Etheridge M.A. and Symonds P.A., 1986. Detachment faulting and the evolution of passive continental margins. *Geology*, 14: 246-250.
- Liu, M. and Furlong, K.P., 1993. Crustal Shortening and Eocene extension in the southeastern Canadian Cordillera: Some thermal and rheological considerations. *Tectonics* 12: 776-786.
- Loizenbauer, J., Wallbrecher, E., Fritz, H., Neumayer, P., Khudeir, A.A. and Kloetzli, U., 2001. Structural geology, single zircon ages and fluid inclusion studies of the Meatiq metamorphic core complex: Implications for Neoproterozoic tectonics in the Eastern Desert of Egypt. *Precambrian Research*, 110: 357-383.
- Lucchitta, I. and Suneson, N.H. 1996. Timing and character of deformation along the margin of a metamorphic core complex, west-central Arizona. In Beratan, K.K. (ed.) *Reconstructing the history of the Basin and Range extension using sedimentology and stratigraphy*, Geological Society of America Special Paper, 303: 27-59.
- Mahar, E.M., Baker, J.M., Powell, R., Holland, T.J.B. and Howell, N., 1997. The effect of Mn on mineral stability in metapelites. *Journal of metamorphic Geology* 15: 223-238.
- Malavieille, J. 1993 Late orogenic extension in mountain belts: Insights from the Basin and Range and the Late Paleozoic Variscan Belt. *Tectonics* 12: 1115—1130.
- Malavieille, J., 1987. Kinematics of compressional and extensional ductile shearing deformation in a metamorphic core of the northern Basin and Range. *Journal of Structural Geology* 9: 541-554.
- Marzouki, F. and Divi, R., 1989. Geology, petrology and geochemistry of Jabal Afaf, western Arabian Shield, Kingdom of Saudi Arabia. *N. Jb. Geol. Paläont. Mh.*, 1989, 11: 656-670.
- McDougall, I. and Harrison, T.M., 1999. *Geochronology and thermochronology by the <sup>40</sup>Ar/<sup>39</sup>Ar Method*. Oxford University Press, 269pp.
- Means, W.D., 1994. Rotational quantities in homogeneous flow and the development of small scale structures. *Journal of Structural Geology* 16: 437-445.
- Meissner, R. and Mooney, M., 1998. Weakness of the lower continental crust: a condition for delamination, uplift, and escape. *Tectonophysics*, 296: 47-60.
- Liu, M., 2001. Cenozoic extension and magmatism in the North America Cordillera: the role of gravitational collapse. *Tectonophysics*, 342: 407-433.
- Merrill, C and Turner, G., 1966. Potassium-argon dating by activation with fast neutrons. *Journal of Geophysical Research*, 71: 2852-2857.
- Miller M.M. and Dixon T.H., 1992. Neoproterozoic evolution of the northern part of the Hamisana zone, northeast Sudan: constraints on Pan-African accretionary tectonics. *Journal of the Geological Society*, 5: 743-750.
- Miller, M.M. and Dixon, T.H., 1992. Proterozoic evolution of the northern part of the Hamisana zone, northeast Sudan: Constraints on Pan-African accretionary tectonics. *Journal of the Geological Society*, 149: 743-750.
- Miyashiro, A., 1994. *Metamorphic Petrology*: UCL Press, 404p.
- Moghazi, A.M., Mohamed, F.H. and Kanisawa, F., 1999. Geochemical and petrological evidence of calc-alkaline magmatism in the Homrit Wagat and El-Yatima areas of eastern Egypt. *Journal of African Earth Sciences*, 29: 535-549.
- Moghazi, A.M., 2003. Geochemistry and petrogenesis of a high-K calc-alkaline Dokhan Volcanic suite, South Safaga area, Egypt: the role of late Neoproterozoic crustal extension. *Precambrian Research*, 125: 161-178.
- Moghazi, A.M., Andersen, T., Oweiss, G.A. and El Bouseily, A.M., 1998. Geochemical and Sr-Nd-Pb isotopic data bearing on the origin of Pan-African granitoids in the Kid area, southeast Sinai, Egypt. *Journal of the Geological Society*, 155: 697-710.
- Mohammed, F.H. and Hassanen, M.A., 1996. Geochemical evolution of arc-related mafic plutonism in the Umm Naggat district, Eastern Desert of Egypt. *Journal of African Earth Sciences*, 3: 269-283.
- Monger, J.W.H., Price, R.A. and Tempelman-Kluit, D.J., 1982. Tectonic accretion and origin of two major metamorphic and plutonic belts in the Canadian Cordillera. *Geology*, 10: 71-75.
- Moore, J.M., 1979. Tectonics of the Najd Transcurrent Fault System, Saudi Arabia. *Journal of the Geological Society, London*, 136: 441-454.
- Moore, J.M., 1979. Tectonics of the Najd Transcurrent Fault System, Saudi Arabia. *Journal of the Geological Society, London*, 136: 441-454.
- Nelson Eby, G., 1990. The A-type granitoids: a review of their occurrence and chemical characteristics and speculations on their petrogenesis. *Lithos*, 26: 115-134.
- Oldow, J.S., Bally, A., W., Avé Lallemant, H.G., and Leeman, W.P., 1989. Phanerozoic evolution of the North American Cordillera; United States and Canada, In Bally A.W. and A.R. Palmer, eds., *The Geology of North America-An overview*. The Geological Society of America., p. 139-232,
- Pallister, J.S., Stacey, J.S., Fischer, L.B. and Premo, W.R., 1988. Precambrian ophiolites of Arabia: geologic settings, U-Pb geochronology, Pb-isotope characteristics, and implications for continental accretion. *Precambrian Research*, 38: 1-54.
- Pallister, J.S., Stacey, J.S., Fischer, L.B. and Premo, W.R., 1988. Precambrian ophiolites of Arabia: geologic settings, U-Pb geochronology, Pb-isotope characteristics, and implications for continental accretion. *Precambrian Research*, 38: 1-54.
- Passchier, C.W. and Trouw, R.A.J., 1996. *Microtectonics*: Springer, 289p.

- Pearce, J.A. and Parkinson, I.J., 1993. Trace element models for mantle melting: application to volcanic arc petrogenesis. In Prichard, H.M., Harris, N.B.W. and Neary, C.R. (eds.), *Magmatic processes and plate tectonics*, Geological Society Special Publication, 76: 373-403.
- Pearce, J.A., 2003. Supra-subduction zone ophiolites: The search for modern analogues. In Dilek, Y and Newcomb, S., (eds) *Ophiolite concept and the evolution of geological thought*. Geological Society of America Special Paper, 373: 269-293.
- Pearce, J.A., 2003. Supra-subduction zone ophiolites: The search for modern analogues. In Dilek, Y and Newcomb, S., (eds) *Ophiolite concept and the evolution of geological thought*. Geological Society of America Special Paper, 373: 269-293.
- Pearce, J.A., Harris, N.B and Tindle, A.G., 1984. Trace element discrimination diagrams for the tectonic interpretation of granitic rocks. *Journal of Petrology*. 25: 956-983.
- Platt, J.P. & Vissers, R.L.M., 1980. Extensional structures in anisotropic rocks. *Journal of Structural Geology* 2: 397-410.
- Powell, R. and Holland, T.J.B., 1988. An internally consistent dataset with uncertainties and correlations: 3. Applications to geobarometry, worked examples and a computer program. *Journal of metamorphic Geology* 6: 173-204.
- Price, G.P., 1985. Preferred orientation in quartzites. In: Wenk, H.R. (ed.) *Preferred orientation in deformed metals and rocks*. Academic Press. Orlando: 385-406.
- Price, N.J. and Cosgrove, J.W., 1990. *Analysis of geological structures*. Cambridge University Press, 502 pp
- Priem, H.N.A., Eyal, M., Hebeda, E.H. and Verdurmen, E.A.Th., 1984. U-Pb zircon dating in the Precambrian basement of the Arabo-Nubian Shield of the Sinai Peninsula. A progress report, ECOG VIII. *Terra Cognita* 4: 30-31.
- Pudlo, D. and Franz, G., 1994. Dike rock and magma interactions in the Bir Safsaf igneous complex, south-west Egypt: Implications for the Pan-African evolution in north-east Africa. *Geologisches Rundschau*, 83: 523-536.
- Quick, J.E., 1991. Neoproterozoic transpression on the Nabitah fault system - implications for the assembly of the Arabian Shield. *Precambrian Research*, 53: 119-147.
- Ragab, A.I., 1993. A geodynamic model for the distribution of the oceanic plate slivers within a Pan-African orogenic belt, Eastern Desert, Egypt. *Journal of Geodynamics* 17: 21-26.
- Ramsey, J.G. and Huber, M.I., 1983. *The techniques of modern structural geology*. 700 pages.
- Ranalli, G., Brown, R.L. and Bosdachin, R., 1989. A geodynamic model for extension in the Shuswap core complex, southeastern Canadian Cordillera. *Canadian Journal of Earth Sciences*, 26: 1647-1653.
- Rashwan, A.A., 1991. Petrography, geochemistry and petrogenesis of the Migif-Hafifit at Hafifit Mine area, Egypt. Scientific series of the International Bureau/Forschungszentrum Jülich GmbH, 5.
- Reymer, A.P.S., 1983. Metamorphism and tectonics of a Pan-African terrain in southeastern Sinai. *Precambrian Research* 19: 225-238.
- Reymer, A.P.S., 1984a. Metamorphism and tectonics of a Pan-African terrain in Southeastern Sinai - a reply. *Precambrian Research* 24: 189-197.
- Reymer, A.P.S., Matthews, A. and Navon, O., 1984. Pressure-temperature conditions in the Wadi Kid metamorphic Complex: implications for the Pan-African event in SE Sinai. *Contributions Mineralogy Petrology* 85: 336-345.
- Reynolds, S.J. and Lister, G.S., 1990. Folding of mylonitic zones in Cordilleran core complexes: Evidence from near the mylonitic front. *Geology* 18: 216-219.
- Rice, A.H.N., Greiling, R.O., Dardir, A.A., Rashwan, A.A. and Sadek, M.F., 1991. Pan-African extensional structures in the area south of the Hafafit Antiform, Eastern Desert of Egypt. *Zentralblatt für Geologie und Paläontologie*, Teil 1, 11: 2461-2651.
- Ries, A.C., Shackleton, R.M., Graham, R.H. and Fitches, W.R., 1983. Pan-African structures, ophiolites and melanges in the Eastern Desert of Egypt: a traverse at 26°N. *Journal of the Geological Society*, London, 140: 75-95.
- Rogers, J.J.W., Unrug, R. and Sultan, M., 1995. Tectonic assembly of Gondwana. *Journal of Geodynamics*, 19: 1-34
- Saleeby, J.B., 1982. Polygenetic Ophiolite Belt of the California Sierra Nevada: geochronological and tectonostratigraphic development. *Journal of Geophysical Research*, 87, B3, 1803-1824.
- Samson, S.D. and Patchett, P.J., 1991. The Canadian Cordillera as a modern analogue of Proterozoic crustal growth. *Australian Journal of Earth Sciences*, 38: 595-611.
- Schandelmeier, H., Abdel Rahman, E.M., Wipfler, E., Küster, D., Utke, A. and Mathejs, G., 1994. Neoproterozoic magmatism in the Nakasib suture, Red Sea Hills, Sudan. *Journal of the Geological Society*, 151: 485-497.
- Schmid, S.M. and Casey, M., 1986. Complete fabric analysis of some commonly observed quartz c-axis patterns. *American Geophysical Union, Geophysical monograph* 36: 263-286.
- Schmidt, D.L., Hadley, D.G. and Stoesser, D.B. 1980. Neoproterozoic crustal history of the Arabian Shield, Southern Najd Province, Kingdom of Saudi Arabia. *I.A.G. Bulletin*, 3: 41-58.
- Schürmann, H.M.E., 1966. *The Pre-Cambrian along the Gulf of Suez and the Northern part of the Red Sea*. Brill, Leiden.
- Sengupta, P., Dasgupta, S., Bhattacharya, P.K. and Mukherjee, M., 1990. An orthopyroxene-biotite geothermometer and its application in crustal granulites and mantle derived rocks. *Journal of metamorphic Geology* 8: 191-197.
- Shackleton, R. M., 1996. The final collision zone between East and West Gondwana: where is it? *Journal of African Earth Sciences*, 23: 271-287
- Shackleton, R.M., Ries, A.C., Graham, R.H., and Fitches, W.R., 1980. Late Precambrian ophiolitic melange in the eastern desert of Egypt. *Nature* 285: 472-474.
- Shalaby, A., Stüwe, K., Makroum, F., Fritz, H., Kebede, T. and Klötzli, U., 2005. The Wadi Mubarak belt, Eastern Desert of Egypt: a Neoproterozoic conjugate shear system in the Arabian–Nubian Shield. *Precambrian Research*, 136: 27-50
- Shervais, J.W., Murchey, B. L., Kimbrough, D. L., Renne, P. R. and Hanan, B, 2005. Radioisotopic and biostratigraphic age relations in the Coast Range Ophiolite, northern California: Implications for the tectonic evolution of the Western Cordillera. *Geological Society of America Bulletin*, 117: 633–653.
- Shantie, M. And Roobol, M.J., 1979. A late Neoproterozoic ophiolite complex at Jebel Ess in northern Saudi Arabia. *Nature*, 279: 488-491.

- Shimron, A.E., 1980. Proterozoic island arc volcanism and sedimentation in Sinai. *Precambrian Research* 12: 437-458.
- Shimron, A.E., 1983. The Tarr Complex revisited. The Tarr Complex: folding, thrusts and melanges in the southern Wadi Kid region, Sinai Peninsula. *Israel Journal of Earth Sciences* 32: 123-148.
- Shimron, A.E., 1984. Metamorphism and tectonics of a Pan-African terrain in southeastern Sinai. A discussion. *Precambrian Research* 24:173-188.
- Shimron, A.E., 1987. Pan-African metamorphism and deformation in the Wadi Kid Region, Sinai Peninsula: Evidence from porphyroblasts in the Umm Zariq Formation. *Israel Journal of Earth Science* 36: 173-193.
- Siender, G., Pringle, J.R. and Shimron, A.E., 1974. Age of relationships in basement rocks of the Sinai Peninsula. *Proceedings, International Meetings Geochronology, Cosmochronology and Isotope Geology, Paris.*
- Simpson, C. and Schmid, S.M., 1983. An evaluation of criteria to deduce the sense of movement in sheared rocks. *Geological Society of America Bulletin* 94: 1281-1288.
- Spear, F.S. and Cheney, J.T., 1989. A petrogenetic grid for pelitic schists in the system  $\text{SiO}_2\text{-Al}_2\text{O}_3\text{-FeO-MgO-K}_2\text{O-H}_2\text{O}$ . *Contributions to Mineralogy and Petrology* 101: 149-164.
- Spear, F.S., 1991. On the interpretation of peak metamorphic temperatures in the light of garnet diffusion during cooling. *Journal of metamorphic Geology* 9: 379-388.
- Spencer, J.E., 1984. Role of tectonic denudation in warping and uplift of low-angle normal faults. *Geology* 12: 95-98.
- Stern, R.J. and Bloomer, S.H., 1992. Subduction zone infancy; examples from the Eocene Izu-Bonin-Mariana and Jurassic California arcs. *Geological Society of America Bulletin*, 104: 1621-1636.
- Stern, R.J. and Hedge, C.E., 1985. Geochronologic and isotopic constraints on Late Precambrian crustal evolution in the Eastern Desert of Egypt. *American Journal of Science*, 285: 97-127.
- Stern, R.J. and Manton, W.I., 1987. Age of Feiran basement rocks, Sinai: implications for late Precambrian crustal evolution in the northern Arabian-Nubian Shield. *Journal of the Geological Society* 144: 569-575.
- Stern, R.J., 1985. The Najd fault system, Saudi Arabia and Egypt: A late Precambrian rift related transform system? *Tectonics* 4: 497-511.
- Stern, R.J., 1985. The Najd fault system, Saudi Arabia, and Egypt: A late Precambrian rift-related transform system? *Tectonics*, 4: 497-511.
- Stern, R.J., 1994. Arc assembly and continental collision in the Neoproterozoic East African Orogen: Implications for the consolidation of Gondwanaland. *Annual Reviews of Earth and Planetary Sciences*, 22: 319-351.
- Stern, R.J., 2005. Evidence from ophiolites, blueschists, and ultrahigh-pressure metamorphic terranes that the modern episode of subduction tectonics began in Neoproterozoic time. *Geology*, 33: 557-560.
- Stern, R.J., Gottfried, D. and Hedge, C.E., 1984. Late Precambrian rifting and crustal evolution in the Northeastern Desert of Egypt. *Geology*, 12: 168-172.
- Stern, R.J., Nielsen, K.C., Best, E., Sultan, M., Arvidson, R.E. and Kröner, A., 1990. Orientation of late Precambrian sutures in the Arabian-Shield shield. *Geology*, 18: 1103-1106.
- Stern, R.J., Johnson, P.R., Kröner, A. and Yibas, B., 2004. Neoproterozoic ophiolites of the Arabian-Nubian Shield. In *ed: Kusky, T.* 2004. *Precambrian ophiolites*, 13
- Stewart, J. H., and J. C. Crowell, 1992. Strike-slip tectonics in the Cordilleran region, western United States. In Burchfiel, B.C., Lipman, P.W. and Zoback, M.I., (eds.), *The Cordilleran orogen: conterminous U.S. (The Geology of North America – G.3):* 609-628.
- Stoeser, D.B. and Stacey, J.S., 1988, Evolution, U-Pb geochronology, and isotope geology of the Pan-African Nabitah orogenic belt of the Saudi Arabian Shield, in S. El-Gaby and R.O. Greiling, eds., *The Pan-African belt of Northeast Africa and adjacent areas: Braunschweig/Wiesbaden, Vieweg and Shn*, 227-288.
- Stoeser, D.B. and Camp, V.E. 1985, Pan-African microplate accretion of the Arabian Shield: *Geological Society of America Bulletin*, 96, 817-826.
- Stoeser, D.B., 1986. Distribution and tectonic setting of plutonic rocks of the Arabian Shield. *Journal of African Earth Sciences*, 4: 21-46.
- Sturchio, N.C., Sultan, M. and Batiza, R., 1983. Geology and origin of Meatiq Dome, Egypt: A Precambrian metamorphic core complex? *Geology*, 11: 72-76.
- Sultan, M., Arvidson, R.E., Duncan, I.J., Stern, R.J. and El Kaliouby, B., 1988. Extension of the Najd Shear System from Saudi Arabia to the Central Eastern Desert of Egypt based on integrated field and Landsat observations. *Tectonics*, 7: 1291-1306.
- Sylvester, P.J., 1989. Post-collisional alkaline granites. *Journal of Geology*, 97: 261-280.
- Symmes, G.H. and Ferry, J.M., 1992. The effect of whole-rock MnO content on the stability of garnet in pelitic schists during metamorphism. *Journal of metamorphic Geology* 10: 221-237.
- Teklay, M, Kröner, A, and Mezger, K., 2002. Enrichment from plume interaction in the generation of Neoproterozoic arc rocks in northern Eritrea: implications for crustal accretion in the southern Arabian-Nubian Shield. *Chemical Geology*, 184: 167-184.
- Ten Brink, C. E., 1996. Development of porphyroblast geometries during non-coaxial flow: An experimental and analytical investigation. *Geologica Ultraiectina* 142, 163 pp.
- Thompson, P.H., 1989. Moderate overthickening of thinned sialic crust and the origin of granitic magmatism and regional metamorphism in low-P-high-T terranes. *Geology* 17: 520-523.
- Tormey, D.R., Hickey-Vargas, R., Frey, F.A. and Lopez-Escobar, L., 1991. Recent lavas from the Andean volcanic front (33 to 42°); Interpretations of along-arc compositional variations. In Harmon, R.S. and Rapela, C.W., eds. *Andean magmatism and its tectonic setting*, Geological Society of America Special Paper, 265: 57-77.
- Tullis, J., Christie, J.M. and Griggs, D.T., 1973. Microstructures and preferred orientations of experimentally deformed quartzites. *Geological Society of America Bulletin* 84: 297-314.
- Twiss, R.J. and Moores, E.M. 1992. *Structural Geology*. Freeman, 532 pp.



- Unrug, R., 1996. The assembly of Gondwanaland, *Episodes*, 19: 11-20.
- Vail, J.R., 1985. Pan-African (Late Precambrian) tectonic terrains and the reconstruction of the Arabian-Nubian Shield. *Geology*, 13: 839-842.
- Van der Heyden, P., 1992. A middle Jurassic to early Tertiary Andean-Sierran arc model for the coast belt of British Columbia. *Tectonics*, 11: 82-97.
- Vanderhaeghe, O. and Teyssier, C., 2001. Crustal-scale rheological transitions during late-orogenic collapse. *Tectonophysics*, 335: 211-228.
- Wakabayashi, J., and Dilek, Y., 2003. What constitutes "emplacement" of an ophiolite?: mechanisms and relationship to subduction initiation and formation of metamorphic soles: In Dilek, Y., and Robinson, P.T., (eds), *Ophiolites in earth history*, Geological Society of London Special Publication 218: 427-447.
- Wallace, L.M., McCaffrey, R., Beavan, J. and Ellis, S., 2005. Rapid microplate rotations and backarc rifting at the transition between collision and subduction. *Geology*, 33: 857-860.
- Wallace, W.K., Hanks, L.C. and Rogers, J.F., 1989. The southern Kahiltna terrane: Implications for the tectonic evolution of southwestern Alaska. *Geological Society of America Bulletin*, 101: 1389-1407.
- Wernicke, B. and Axen, G.J., 1988. On the role of isostasy in the evolution of normal fault systems. *Geology*, 16: 848-851.
- Wernicke, B., 1985. Uniform-sense normal simple shear of the continental lithosphere. *Canadian Journal of Earth Sciences* 22: 108-125.
- Wijbrans, J.R., Pringle, M.S., Koppers, A.A.P., and Scheveers, R., 1995. Argon geochronology of small samples using the Vulkaan argon laserprobe. *Proceedings of the Koninklijke Nederlandse Akademie van Wetenschappen*, 98: 185-218.
- Willis, K.M., Stern, R.J. and Clauer, R.F., 1988. Age and geochemistry of late Precambrian sediments of the Hammamat series from Northeastern Desert of Egypt. *Precambrian Research*, 42: 173-187.
- Wilson, M., 1989. *Igneous Petrogenesis*. 450 pages
- Wipfler, E.P., 1996. Transpressive structures in the Neoproterozoic Ariab-Nakasib Belt, northeast Sudan: evidence for suturing by oblique collision. *Journal of African Earth Sciences*: 23, 347-362.
- Wolf, M.B. and Saleeby, J.B., 1992. Jurassic Cordilleran dike swarm-shear zones: Implications for the Nevadan orogeny and North American plate motion. *Geology*, 20: 745-748.
- Worthing, M.A., 1984. Rotated boudins associated with Caledonian thrusting from Seiland, North Norway. *Norsk Geologisk Tidsskrift* 64: 275-285.
- Yardley, B.H.W., 1989. *An Introduction to Metamorphic Petrology* - Longman Essex 248pp
- Yin, A., 2004. Gneiss domes and gneiss dome systems. In Whitney, D.L., Teyssier, C., Siddoway, C.S., eds., *Gneiss domes in orogeny*, Geological Society of America Special Paper, 380: 1-14.
- Zimmer, M., Kröner, A., Jochum, K. P., Reischmann, T. and Todt, W., 1995. The Gabal Gerf complex: A precambrian N-MORB ophiolite in the Nubian Shield, NE Africa. *Chemical Geology*, 123: 29-51



## Samenvatting (Summary in Dutch)

Het Midden Oosten heeft in recente tijden veel aandacht getrokken van geologen. Dit heeft met name te maken met het feit dat er veel olie en gas wordt gevonden in de Phanerozoïsche gesteenten (jonger dan 600 miljoen jaar). De Neoproterozoïsche gesteenten van het Midden Oosten (1000 tot 600 miljoen jaar oud) trekken echter ook aandacht van geologen. Deze oudere gesteenten worden met name gevonden in het westelijke deel van het Midden Oosten, in streken zoals het oosten van Egypte en het westen van Saudi Arabië, en vormen het Arabisch-Nubische Schild.

In enkele gevallen werd er tijdens het onderzoek naar olie en gas in het Midden Oosten, ook aandacht besteed aan de oudere Neoproterozoïsche gesteenten. Zo onderzocht dr. H.M.E. Schürmann van de Koninklijke Olie/Shell in het begin van de jaren twintig de Neoproterozoïsche sedimenten in het oosten van Egypte. Dit onderzoek had tot doel om het verschil tussen de “droge” Neoproterozoïsche sedimenten en de olie-houdende Phanerozoïsche sedimenten te begrijpen.

Het Egyptische deel van het Arabisch-Nubische Schild is de locatie van het oudste geologisch onderzoek ter wereld. De oude Egyptenaren zochten in hun land naar goud en zij vonden het in de Neoproterozoïsche gesteenten. Een kaart die de geologie van het Wadi Hammamat gebied in het oosten van Egypte beschrijft, is gemaakt rond 1150 v. Chr. door Amennakhte van Thebe (Harrel en Brown, 1992). Deze kaart laat verschillende kleuren zien, die ieder met een specifieke gesteente-soort is te correleren (zie Figuur 1-2).

Het doel van het onderzoek, zoals beschreven in dit proefschrift, was om een beter begrip te verkrijgen van de geodynamische ontwikkeling van het Neoproterozoïsche Arabisch-Nubische Schild. Traditioneel wordt de geodynamische ontwikkeling van het Arabisch-Nubische Schild in drie fases verdeeld:

1. Een oceanische fase met overblijfselen van intra-oceanische subductie
2. Een arc-accretie fase
3. Een laat-orogene fase; over de achtergronden van deze fase zijn de geologen het onderling niet eens.

Om een beter inzicht te krijgen in de geodynamische fases van het Arabisch-Nubische Schild, is onderzoek gedaan in drie gebieden in Egypte en Saoedie Arabië:

1. Het Bi'r Umq Complex (Saoedie Arabië) – dit complex wordt gevormd door een ophioliet (een stuk oceanische lithosfeer) die arc-accretie heeft ondergaan. In het gebied ligt een grote NO tot ONO lopende duktiele breukzone.
2. Het Tabalah en Tarj Complex (Saoedie Arabië) – dit complex wordt gevormd door overblijfselen van een eiland-boog, ontstaan tijdens intra-oceanische subductie. In het gebied ligt een NNW lopende duktiele breukzone.
3. Het Wadi Kid Complex (Egypte) – een complex dat gevormd wordt door één van de “gneissische koepels” van het Arabische Nubische Schild.

Het Bi'r Umq Complex is onderdeel van de NO-ZW lopende “Bi'r Umq –Nakasib

Suture” en ligt in het centrum van het Arabische deel van het Arabisch-Nubische Schild. Het vormt de grens tussen het Jiddah Terrein en het Hijaz Terrein. De ophioliet van het Bi’r Umq Complex is ongeveer 830 miljoen jaar oud. De gesteenten in het Bi’r Umq Complex zijn heel erg gedeformeerd. Tijdens de eerste deformatie fase, D1, werden foliaties, lineaties en indicatoren van non-coaxiale deformatie gevormd in de Bi’r Umq breuk en in de kleinere breuken van het Bi’r Umq Complex. Deze structuren geven aan dat de breuken werden gevormd als overschuivingen tijdens NW-ZO compressie. Tijdens de tweede deformatie fase in het Bi’r Umq Complex, D2, vond er dextrale strike-slip beweging plaats op de WZW-ONO lopende Bi’r Umq breuk. Deze fase was een gevolg van WNW-OZO compressie. Tijdens D3, de jongste Neoproterozoïsche deformatie fase in het Bi’r Umq Complex, vond er een omdraaiing van beweging plaats op de Bi’r Umq breuk zodat daar sinistrale strike-slip beweging plaats vond. Deze sinistrale beweging was het resultaat van NNO-ZZW compressie. De deformatie in het Bi’r Umq Complex vond plaats gedurende de obductie van de Bi’r Umq ophioliet. Deze obductie eindigde 760 miljoen jaar geleden. De veranderingen van de bewegings-richtingen op de breuken van het Bi’r Umq Complex waren het resultaat van de veranderingen in de richting van beweging van de subducerende plaat. De structuren en structurele geschiedenis in dit gebied worden geassocieerd met de sluiting van een oceanisch bekken gebied door middel van subduction en zij vormen overblijfselen van de “off-shore amalgamation” van een aantal eiland-bogen in het Arabische schild. De “off-shore amalgamation” leidde tot de formatie van de Amennakhte Superterrein.

Het Tabalah en Wadi Tarj Complex, in het centrale deel van het Neoproterozoïsche Asir Terrein in Saoedi Arabië, vertoont typische intra-terrein kenmerken. Het Tabalah en Wadi Tarj Complex bevat gabbros en kwarts-diorieten, die in een eiland boog zijn geïntroduceerd, en tonalieten en granodiorieten, die kenmerken vertonen van intrusies die zijn gevormd tijdens subductie bij een actieve continentale marge. De gesteenten in het Tabalah en Wadi Tarj Complex werden tijdens twee deformatie-fasen gedeformeerd: D1 en D2. De D1-fase werd gekarakteriseerd door overschuivingen. D1 vond plaats rond 779 Ma en was het gevolg van E-W tot WNW-OZO compressie. De D2-fase werd door dextrale strike-slip beweging gekarakteriseerd die het gevolg was van NNO-ZZW compressie. D2 vond plaats rond 765 miljoen jaar geleden. De deformatie fasen en late intrusiva in het Tabalah en Wadi Tarj Complex zijn ook gerelateerd aan de “off-shore amalgamation” die het Amennakhte Superterrein vormden.

In het Wadi Kid Complex in de Sinai, Egypte, werden dikke lagen van sub-horizontale schisten, die gevormd werden bij een hoge temperatuur en een lage druk, geïnterpreteerd als een sub-horizontale afschuivings breuk. Deze breuk toonde een beweging van het top-blok naar het NW. Ongedeformeerde granieten in het Wadi Kid Complex lijken op A-type granieten die worden gevonden in andere delen van het Arabisch-Nubische Schild. Deze granieten zouden zijn gerelateerd aan extensie. De intrusie van NE-SW lopende dijken, loodrecht op, en synchroon aan de beweging langs de afschuiving, geeft aan dat deze afschuiving is gevormd tijdens NW-ZO extensie. De afschuiving is rond 595 miljoen jaar geleden gevormd. De geologische kenmerken geven aan dat het Wadi Kid Complex een typisch kern-complex is, dat tijdens NW-ZO extensie is gevormd. Andere “gneissische koepels” in het Arabisch-Nubische

Schild lijken heel erg op het Wadi Kid Complex en worden dus ook als extensie-gerelateerde kern-complexen geïnterpreteerd.

Gepubliceerde data geven aan dat de extensie zoals die is beschreven voor het Wadi Kid Complex, werd voorafgegaan door een fase van arc-accretie langs de N-Z lopende actieve continentale marges van Oost- en West-Gondwanaland rond 700-650 miljoen jaar geleden. Tijdens deze fase botsten onafhankelijke eiland-bogen en de superterreinen die in de oceaan waren gevormd, op deze continentale marges. De arc-accretie bij de continentale marges resulteerde in verdikking van de lithosfeer. Toen convergentie vertraagde, leidde dit tot een thermale re-equilibratie en een afname van sterkte van de lithosfeer. Dit leidde weer tot inzakken van de lithosfeer onder de invloed van de zwaartekracht. Het inzakken van de lithosfeer leidde tot de extensie waarbij de kern-complexen werden gevormd. De Neoproterozoïsche ontwikkeling van het Arabisch-Nubische Schild lijkt daardoor op de mesozoïsche geodynamische ontwikkeling van de Cordillera in westelijk Noord-Amerika.



## Acknowledgements

First and foremost, I would like to thank the Dr. Schürmann Fund for their financial support of my laboratory and field research in Egypt and Saudi Arabia with grant numbers 1994/06, 1997/07, 1999/04 and 2000/04a.

The period of my Ph.D. studies was slightly longer than normal (it took me the better part of 10 years of part-time dedication). And with such long studies one really needs the support of teachers, family and friends. It was a great time: I was able to do the research I wanted and meanwhile I travelled wonderful countries and met great people.

I want to thank my promoter Stan White. You gave me the opportunity to do the research that I wanted to do and gave me the freedom to go the direction that I wanted. You were patient and always available to read, correct and help me improve my work (even if there had been a year-long silence from my side).

I want to thank Harry Priem who has been motivating me from the early stages to do this research and helped out in all possible ways.

Paul Dirks was the supervisor of the 1<sup>st</sup> Sinai; it was great fun working together. Hugo de Boorder joined the 2<sup>nd</sup> Sinai fieldwork. Afterwards, you were always available to review new chapters and have discussions on the geology of the ANS (while sharing your own ANS-experiences from the old Marsa Alam-days, including your recollections of the mating of the local camels). I want to thank Dr. Ibrahim Shalaby, formerly at EGSMA, for his support during the Sinai fieldworks. I thank Jan Wijbrans for his help with Ar-Ar dating at the Vrije Universiteit lab. I thank Hanan Kisch for the great discussions during the Egyptian trips and his constructive comments on the different parts of my thesis.

Peter Johnson of the Saudi Geological Survey (formerly the USGS Saudi Arabia mission) was the key to all the research I did in Saudi Arabia; you made all arrangements so that I could do my research in the Kingdom. This included all the visa-work, the logistics, ideas for research areas and the many great discussions on the geology of the ANS. I want to thank Dr. M.A. Tawfiq, the president of the Saudi Geological Survey for his support. I want to thank all people at the Saudi Geological Survey who helped me during my fieldtrips to Saudi Arabia and made it into an unforgettable experience. I also would like to thank Ron Worl, Jeff Doebrich and James Elliot of the former USGS Saudi Arabia mission for their support.

I really enjoyed the enthusiastic support from Reinhard Greiling from Heidelberg. You invited me for the meetings you organised on the geology of the ANS and you let me and Kike join the excursions you organised in Egypt. During these excursions I learned a lot about the geology of the ANS and we had lots of fun (e.g. leaving behind weird graffiti on tonalites at the Wadi Ghadir in Egypt).

I did the two Sinai-fieldworks together with Patrick and Wouter. We worked hard but also had loads of fun (being in Egypt, staying at Yasser's place, dancing on oildrums, trying to cross minefields (calling back Wouter when he was half-way) and smoking shisha. You continued to be among my best friends and I am grateful for your support during my Ph.D. studies.

I want to thank all of my friends who supported me during my studies. I know that I was not always able to spend enough time with them, as good friends should. However they remained my friends during these years.

I want to thank my current employer, LogicaCMG for their flexibility during my studies. I thank my colleagues who listened patiently whenever I was telling boring stories about the rocks and my research (I am pretty sure you didn't (want to) understand a word of it).

My parents, Tet and Ignace, helped out wherever they could and were patient whenever I was busy with my studies. THANKS. To Jacques, my brother, and Sonja, I promise that we will visit you more often in Milan now that I have finished my Ph.D. Also the remainder of my family, my uncles and aunts and all my cousins, have been very supportive throughout my studies.

My family-in-law, the Beintemas, have always been supportive and patient (for example when I was working on my thesis during our Christmas visits).

Finally my greatest help during my Ph.D. studies was Kike. Much of the work was done during our "holidays" (who wants to go on a geological excursion to Egypt as a holiday? Well, Kike doesn't mind!) and weekends. You were patient and helped out wherever you could. While helping me with ANS, you also taught me about Archean geology and the Pilbara in Australia. THANKS!



## **Curriculum Vitae**

I was born on May 22<sup>nd</sup>, 1966 in the Hague. I spend most of my high-school days at the Haganum and graduated from Noctua in 1986. I obtained my “doctoraal” in geology from Utrecht University in 1995. From early 1996 until the end of 1999 I worked as a geologist at Halliburton. Since early 2000 I work at LogicaCMG as a project manager. Between 1996 and 2005 I spent the better part of my free time on geological research in the Middle East and writing a PhD thesis.



## **Appendices**



# Appendix 1

## A1 Additional geological data for the Wadi Kid area, Sinai, Egypt

### Abstract

New data from the Wadi Kid Complex show that the low-angle shear zone, described in detail in chapter, was formed at ~ 595 Ma. Geochemical data from undeformed plutonic and volcanic rocks are comparable to those observed in A-type granites and other late orogenic rocks in other parts of the ANS. These igneous rocks were interpreted to have been derived from mantle magmas in a thinned and extending crust. Shear zones in the upper-crustal rocks display normal movement with top-to-NW movement. These newly obtained data confirm the core complex model for the Wadi Kid Complex that was presented in Chapter 5.

### A1.1 Introduction

After the publication of Chapter 5 as a peer-reviewed paper in *Geologie en Mijnbouw* (Blasband et al., 1997), additional research was performed in the Wadi Kid Complex. It was decided to maintain the integrity of this paper for the purpose of future reference. The results of additional research in the form of new relevant field-data, geochronological and geochemical data, will be presented in this appendix.

### A1.2 Geological background

In order to present the newly obtained data in this Appendix, the rock-section of the Wadi Kid area was divided in a lower-crustal sequence consisting of metavolcanic and metasedimentary schists of amphibolite grade, foliated and gneissic diorites, tonalites and granodiorites, and an upper-crustal sequence consisting of weakly metamorphosed (lower-greenschist grade) to non-metamorphosed sedimentary and volcanic units (Figure A.1-1). The lower-crustal unit includes the Umm Zariq Fm., Malhaq Fm., Qenaia Fm. and the high grade part of the Heib Fm., which were all described in chapter 5 of this thesis. The upper-crustal rocks, only found in the SE part of the Wadi Kid area, include sandstones, claystones, conglomerates, andesites, basalts and agglomerates. The upper-crustal unit includes the low grade part of the Heib Fm. and the Tarr Fm. which were described in detail in chapter 5. During detailed research that was performed after the publication of Blasband et al. (1997), locally, 50 to 100 m thick bands of chlorite- and biotite-schists, striking NE-SW, were observed within the low-grade metamorphic rocks in the southeastern Wadi Kid Complex. These schists are foliated equivalents of their neighboring rocks, the low-grade metavolcanics and metasediments (Figure A.1-1 and Figure A.1-3b). It was observed that the contact between the lower- and upper-crustal rocks is marked by a brittle cataclastic layer (ca. 0.5 m thick), overlying a chlorite-schist, at the southeastern contact of these units, and a post-Oligocene brittle fault at the northeastern contact of these two units. During the recent research, it was also observed that undeformed and non-metamorphosed rhyolites and ignimbrites overlie all other low-grade rocks in SE part of the Wadi Kid

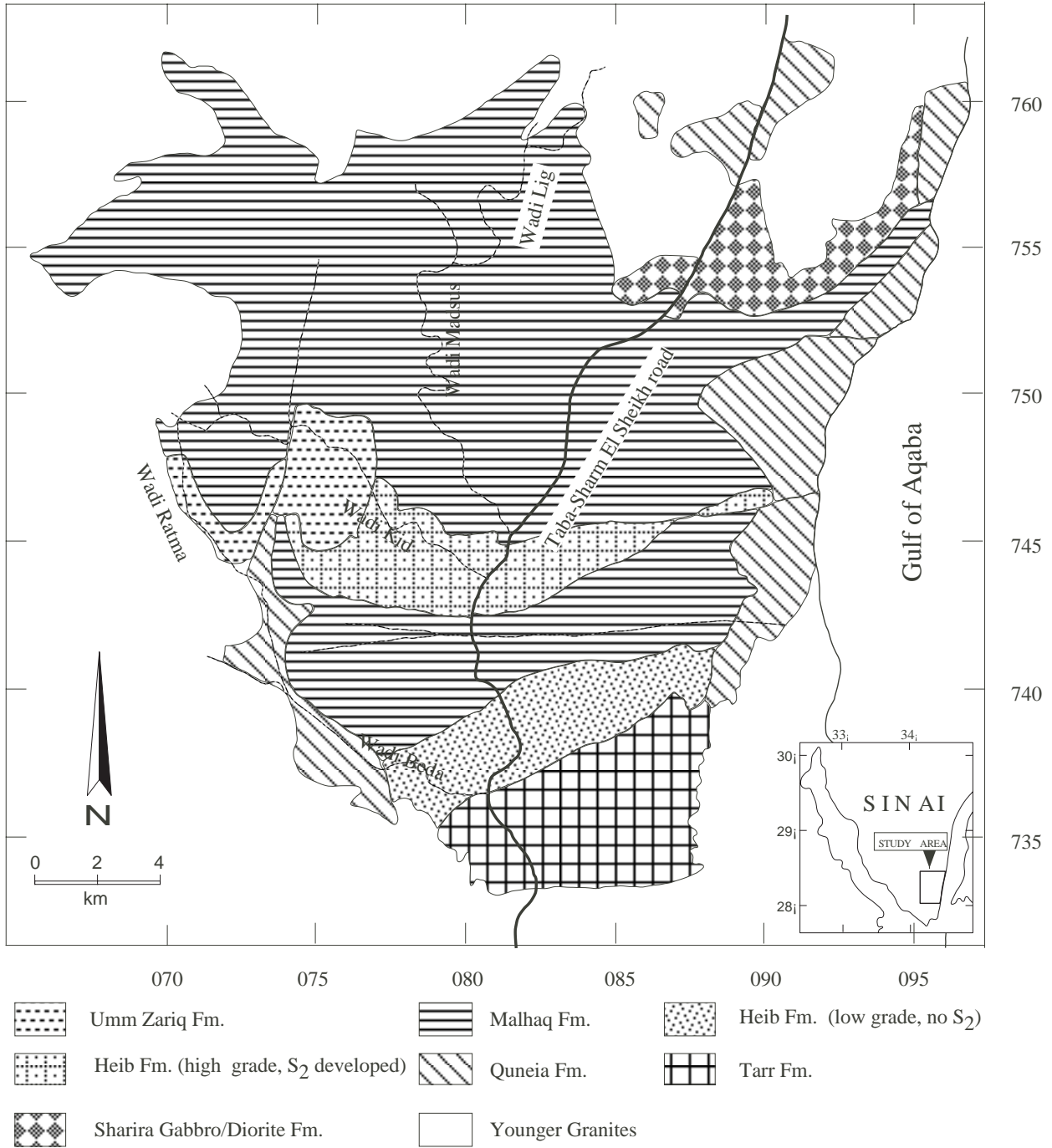


Figure A.1-1 Map of the Wadi Kid Complex presents newly obtained geological data.

Complex..

Brooijmans et al. (2003) postulated two main metamorphic phases: the M1-phase that was responsible for the greenschist grade that was observed in the upper-crustal rocks in the SE part of the Wadi Kid Complex; the M2-phase was responsible for the low-pressure/high-temperature amphibolite grade metamorphism that was observed in the lower-crustal schists.

Structural research that was performed after the publication of Blasband et al. (1997) showed that the oldest deformation phase (D1) in the Wadi Kid area is represented by an S1-foliation that was formed in the greenschist-grade metasedimentary rocks of the southern Wadi Kid area, during M1. This foliation is axial planar to isoclinal F1-folds with NNE-SSW to NE-SW trending fold axes (Figure A.1-1 and Figure A.1-3a). The D1-deformational phase, responsible for the formation of S1 and F1, indicates regional WNW-ESE to NW-SE shortening. In view of the tectonic development of other parts of the ANS and the parallelism of the shortening in the Wadi Kid area to the compressional regime in the Neoproterozoic rocks of NW Saudi Arabia (Stoeser and Camp 1985; Quick 1991), this phase is attributed to arc-

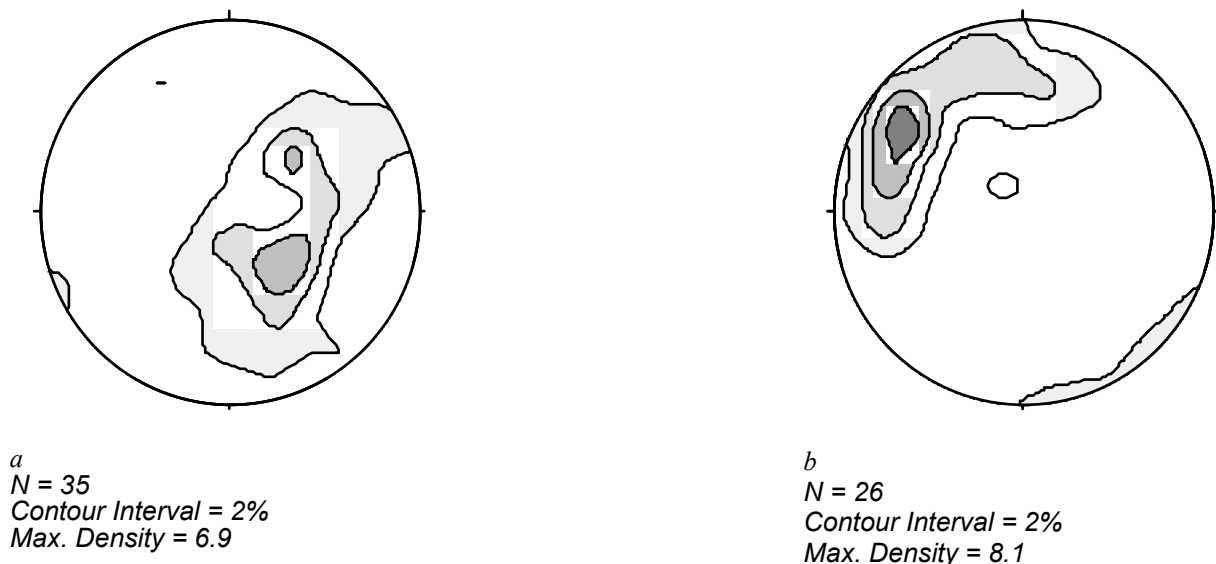


Figure A.1-2 (a) Contoured stereographic plot (equal area) of the poles to the S2 foliation in the upper-crustal rocks. (b) Contoured stereographic plot (equal area) of the poles to the L2 lineation in upper-crustal rocks, showing maximum at NW.

accretion with a WNW-ESE to NW-SE compressional stress field.

The D2-phase is mainly represented by the deformation features in the lower-crustal rocks. These have been described in detail in chapter 5. The S2-foliation is subhorizontal and best developed in the amphibolite-grade schists (see Chapter 5). A NW-SE trending mineral and stretching lineation is developed on the S2-foliation (Figure 5-5 in Chapter 5). A large variety of indicators of non-coaxial strain have been described in Chapter 5 and they indicate a main phase of top-to- NW movement that was followed by shear reversal and a top-to-SE movement (see Chapter 5). Recent research shows that the thin chlorite- and biotite-schists that cross-cut the upper-crustal greenschist-grade rocks represent D2 features in the upper-crustal



a



b

Figure A.1-3 (a) F1-folds, folding a S0-bedding, and S1-foliation in the low-grade metasediments of the SE Wadi Kid area. (b) NE-SW striking chlorite-schist in the SE Wadi Kid, representing splays off the deeper shear in the upper-crustal rocks. Extensional crenulation cleavages indicate dextral movement (in this case top-to-the-NW).

section (Figure A.1-1). Asymmetric features as extensional crenulation cleavages (Figure A.1-3b), indicate that these moderately NW dipping mylonitic zones (Figure A.1-2a), with a NW plunging lineation (Figure A.1-2b), all display a top-to-the-NW-movement.

The Wadi Kid area is cross-cut by NE-SW trending mafic, felsic and composite dykes. The mineral and stretching lineations are orthogonal to the strike of the dykes and the fact that these two features are synchronous, indicate NW-SE extension (See Chapter 5).



### A1.3 Geochemistry of undeformed igneous rocks in the Wadi Kid Complex

#### A1.3.1 Introduction

Geochemical studies may prove useful in discriminating between magmatic processes and tectonic regimes and have been widely used for tectonic interpretations in the Arabian-Nubian Shield (e.g. Brown et al., 1989; Hassanen, 1996; Jarrar et al., 2003). In this appendix, the results of the major element and trace element analyses for undeformed key-samples from the Wadi Kid Complex were compared with those of other trace element studies in the Arabian-Nubian Shield and other areas. The methods for the geochemical analyses were identical to those that were used for the analyses of the samples from the Tabalah/Tarj area. These methods were described in Chapter 4 of this thesis.

#### A1.3.2 Samples

Five samples, that are representative for the undeformed igneous rocks from Wadi Kid Complex, were analyzed for geochemical studies through ICP-MS. These samples are:

- A *basalt* from a mafic dyke in the central Wadi Kid Complex area that trends 40°. This type of dyke is often found cross-cutting the undeformed granites and was related to the later stage of extension in Wadi Kid Complex.
- A *rhyolitic rock* from a felsic dyke from the central Wadi Kid Complex area that trends 45°. This type of dyke is often found cross-cutting the undeformed granites and was related to the later stage of extension in Wadi Kid Complex. Similar dykes, near the Wadi Kid area, were dated at 620-560 Ma (Stern & Manton 1987).
- An *undeformed granite* from the northern Wadi Kid Complex. These granite rocks were dated at 590–530 Ma (Bielski, 1982) and intrude the lower crustal schists and thus also represent a relict of the later stages in the Wadi Kid Complex.
- A *massive rhyolite* that overlies the greenschist grade schist in the southern Wadi Kid Complex. Similar rhyolites in southwest Jordan were dated at 553 Ma (Jarrar *et al.* 1992).
- An *undeformed basaltic flow* that overlies the greenschist grade schist in the southern Wadi Kid Complex.

#### A1.3.3 Results

The results of the major-element analysis are shown in Table A.1-1 and the results for the trace element analyses are shown in Table A.1-2. The N-MORB normalized diagrams in Figure A.1-4 and the REE chondrite-normalized diagrams in Figure A.1-5 justify the division into 2 groups of the samples from the Wadi Kid Complex:

I) The mafic rocks: The basaltic dyke and the basalt flow

II) The felsic rocks: the alkali- granite, the rhyolitic dyke and the massive rhyolite

Generally, the relative young and undeformed granites in the Arabian Nubian Shield were interpreted to be late- or post-orogenic A-type granites (Kuster and Harms, 1998). The

Appendix 1

Table A.1-1 Major element analyses for the analyzed samples from the Wadi Kid Complex

Sample	Basalt	Massive rhyolite	Rhyolitic dyke	Undeformed granite	Basaltic dyke
Na <sub>2</sub> O	4,22	4,48	4,54	4,29	3,23
MgO	2,19	0,456	0,456	0,718	6,61
Al <sub>2</sub> O <sub>3</sub>	15,8	13,6	13,8	13,7	14,9
SiO <sub>2</sub>	61,9	70,1	71,3	69,5	44,6
P <sub>2</sub> O <sub>5</sub>	0,292	0,127	0,122	0,188	0,373
K <sub>2</sub> O	2,41	4,62	4,64	4,59	0,599
CaO	4,87	1,27	1,27	1,66	8,49
TiO <sub>2</sub>	0,842	0,582	0,591	0,588	1,89
MnO	0,088	0,072	0,074	0,081	0,143
Fe <sub>2</sub> O <sub>3</sub>	5,74	3,6	3,85	3,84	13,3

major elements for the undeformed granite, the rhyolitic dyke and the massive rhyolite in the Wadi Kid Complex display the geochemical characteristics of A-type alkaline granites, with concentrations of SiO<sub>2</sub> ≈ 70%, Na<sub>2</sub>O + K<sub>2</sub>O > 7 and CaO < 1.8 (see also table Table A.1-1). These concentrations are typical for rocks with an A-type granite geochemistry (Nelson Eby, 1990). The felsic rocks in the Wadi Kid Complex also display trace-element patterns which characterize A-type granites in other parts of the Arabian Nubian Shield as in eastern Egypt (Hassanen, 1996), southwestern Jordan (Jarrar et al, 2003), southern Israel (Kessel et al., 1998) and Sudan (Kuster and Harms, 1998). In these areas, N-MORB normalized diagrams display an enrichment of the LFS-elements relative to the HFS-elements with a pronounced Sr trough; REE-diagrams display enrichment relative to HREE with pronounced negative Eu-anomaly. These patterns are also observed in the Wadi Kid Complex (Figure A.1-4 and Figure A.1-5). Through additional Sr-, Nd-, Pb- and O-isotope studies, Beyth et. al. (1994) and Kuster and Harms (1998) showed that the A-type granites in other parts of the Arabian Nubian Shield were derived from a lithospheric mantle and included evidence for partial melting of a continental crust. Likewise, Jarar et al. (2003) and Kessel et al. (1998) postulate that the A-type granites and their related volcanics were derived from mantle magmas which underwent extensive fractional crystallization. This form of magmatism is best explained to take place in thinned lithosphere in the very late stages of or completely after a compressional event and these igneous rocks was thus interpreted to be late- to pos-tectonic (Kuster and Harms, 1998; Sylvester, 1989)

The mafic rocks of the Wadi Kid Complex must be late because the basaltic dykes are observed intruding the undeformed granites. The N-MORB patterns of the mafic rocks are characterized by enrichment of the LFS-elements relative to the HFS-elements but lack anomalies. The REE-patterns for the mafic rocks show an enrichment of LREE relative to HREE but lack the Eu-anomaly observed in the felsic rocks. These geochemical patterns are similar to geochemical patterns observed for late mafic volcanics in southern Israel (Kessel et

Table A.1-2 Trace element analyses for the analyzed samples from the Wadi Kid Complex

Sample	Basaltic dyke	Undeformed granite	Rhyolitic dyke	Massive rhyolite	Basalt
Rb	8,31	109,3	126,9	81,10	71,44
Sr	330,4	139,9	173,8	94,79	1018,20
Y	11,85	31,22	32,76	10,54	22,55
Zr	86,96	107,8	363,5	101,2	220,72
Nb	7,91	28,05	27,26	7,47	11,13
La	10,06	51,90	42,93	22,27	26,83
Ce	23,84	114,7	98,85	49,09	63,42
Pr	3,24	13,43	12,01	5,54	7,83
Nd	13,85	50,85	45,85	19,54	32,10
Sm	3,25	9,39	9,08	3,52	6,70
Eu	1,08	1,46	1,96	0,50	1,93
Gd	3,29	8,18	8,06	2,82	5,89
Tb	0,51	1,21	1,23	0,42	0,85
Dy	2,79	6,63	6,85	2,34	4,72
Ho	0,54	1,24	1,31	0,44	0,90
Er	1,44	3,52	3,70	1,28	2,41
Tm	0,21	0,53	0,58	0,20	0,36
Yb	1,31	3,54	3,69	1,37	2,35
Lu	0,21	0,57	0,59	0,22	0,37
Hf	2,34	3,46	10,00	3,65	5,89
Ta	1,38	3,57	3,30	1,20	1,51
Th	0,81	11,81	8,92	14,55	5,65

al, 1998), Sudan (Kuster and Harms, 1998) and the Dokhan Volcanics in Eastern Egypt (Moghazi, 2003). These authors interpret the mafic rocks to be part of bi-modal mafic/felsic volcanic suites and consequently relate the mafic rocks to the felsic rocks that were discussed in the previous paragraph. Kuster and Harms (1998) suggested that these mafic rocks originated from the lithospheric mantle. This would have happened in a extending and thinning crust (Moghazi, 2003).

It can be concluded that the undeformed igneous rocks in the Wadi Kid Complex resemble late- to post-orogenic igneous rock-suites in other parts of the Arabian-Nubian Shield. These rocks were suggested to have been derived from mantle magmas in a extending and thinning crust.

#### **A1.4 Geochronology: Ar-Ar dating for the main lower-crustal amphibolite**

Two key-samples were dated in order to constrain the age of the main tectonic phase in the

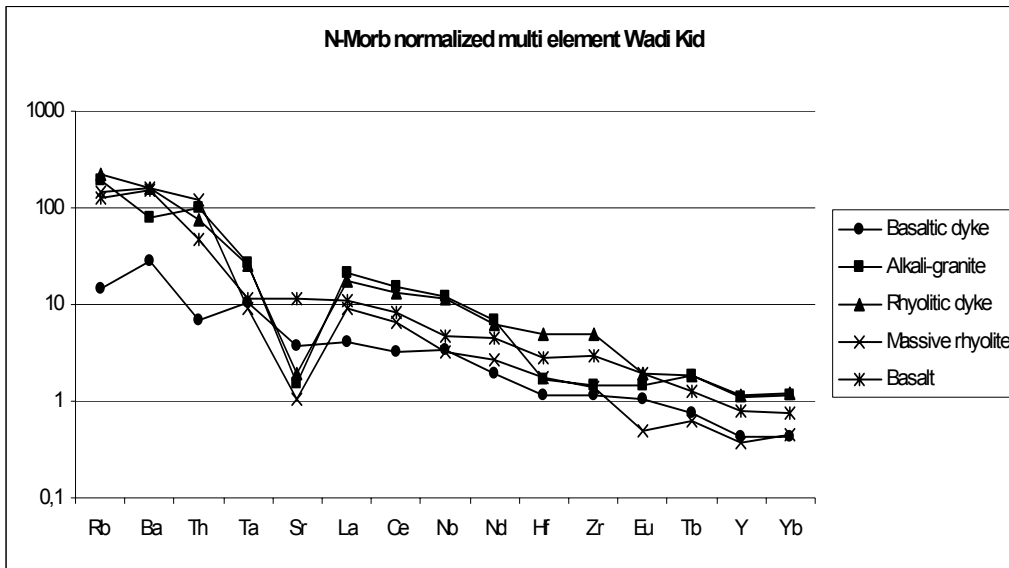


Figure A.1-4 N-MORB normalized multi element diagram for the selected samples from the Wadi Kid Complex.

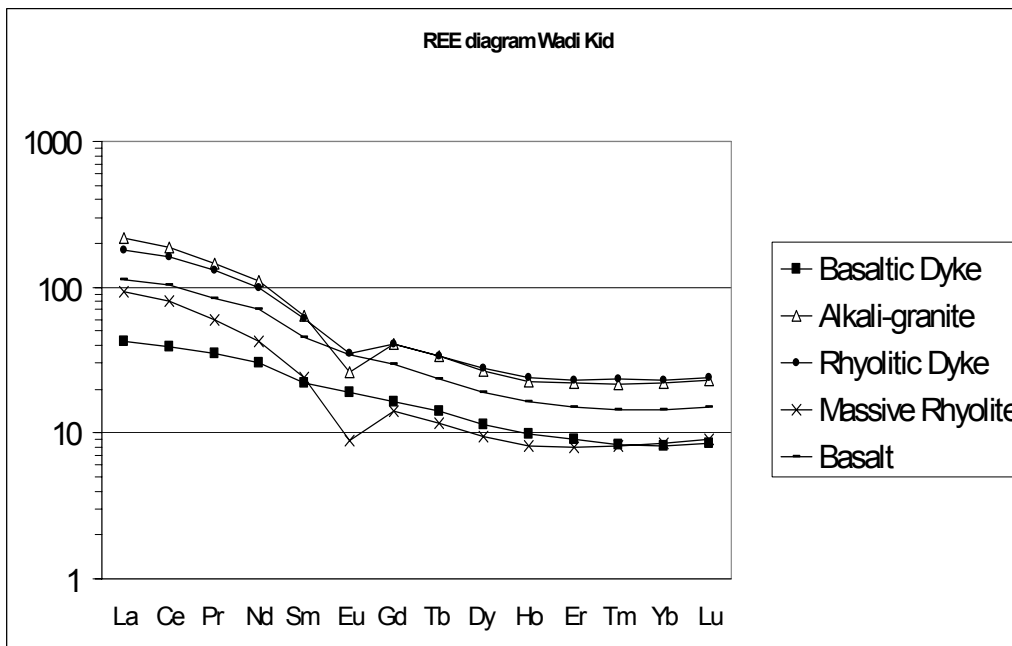


Figure A.1-5 Chondrite normalized REE for the selected samples from the Wadi Kid Complex

Wadi Kid Complex, the D2 phase, as identified in Chapter 5. The  $^{40}\text{Ar}/^{39}\text{Ar}$ -method was chosen for the dating because this allows dating of amphibolite-grade rocks through dating of hornblendes. Furthermore, hornblende has good argon retentivity properties with a closure temperature of 525° C for well crystallized hornblende (McDougall & Harrison, 1999). The hornblendes in the samples define the highest metamorphic grades found in these rock-types so their dates would define the age for the peak tectono-metamorphic event. The method for the geochronological analyses was identical to the one that was used for the analyses of the samples from the Tabalah/Tarj area. This method was described in Chapter 4 of this thesis.

The chosen samples, SIN 1 and SIN 2, are both hornblende schists from the central Wadi Kid Complex (for their location see Figure A.1-1) and display relicts of the D2/M2 phases. The

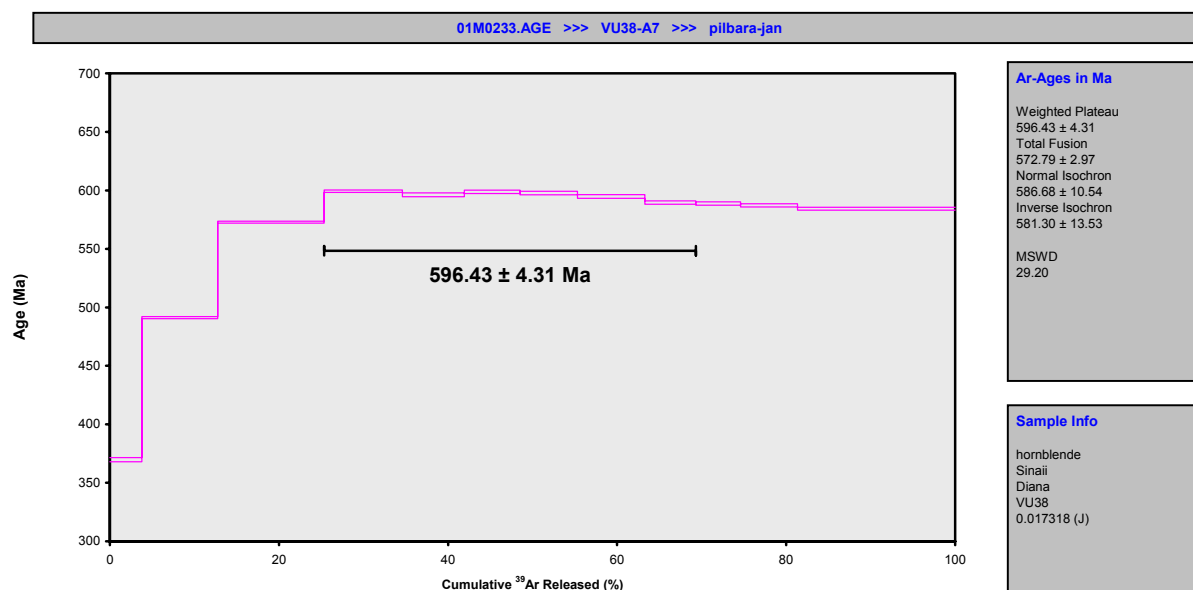
Table A.1-3a Table with detailed tables of the individual step-heating for the  $^{40}\text{Ar}/^{39}\text{Ar}$  dating of samples SIN 1

<b>Incremental Heating</b>										
	$^{36}\text{Ar(a)}$	$^{37}\text{Ar(ca)}$	$^{38}\text{Ar(c)}$	$^{39}\text{Ar(k)}$	$^{40}\text{Ar(r)}$	Age $\pm 2\sigma$ (Ma)	$^{40}\text{Ar(r)}$ (%)	$^{39}\text{Ar(k)}$ (%)	K/Ca	$\pm 2\sigma$
01M0234A	0,25 W	0,00419	0,26863	0,01414	0,63938	500.69 $\pm$ 4.11	90,51	15,14	1,023	$\pm$ 0,772
01M0234B	0,40 W	0,00197	2,16198	0,02393	0,88767	610.21 $\pm$ 3.12	97,25	21,03	0,177	$\pm$ 0,024
01M0234C	0,45 W	0,00039	1,10876	0,01084	0,34647	599.72 $\pm$ 6.92	98,54	8,21	0,134	$\pm$ 0,027
01M0234D	0,50 W	0,00029	1,11905	0,00956	0,25307	593.38 $\pm$ 10.00	98,53	5,99	0,097	$\pm$ 0,020
01M0234F	0,55 W	0,00068	5,42609	0,04203	0,85154	598.04 $\pm$ 2.61	98,96	20,17	0,067	$\pm$ 0,007
01M0234G	0,58 W	0,00013	0,64596	0,00386	0,10393	597.84 $\pm$ 13.42	98,34	2,46	0,069	$\pm$ 0,009
01M0234H	0,60 W	0,00017	1,06746	0,00670	0,16175	593.54 $\pm$ 9.55	98,64	3,83	0,065	$\pm$ 0,007
01M0234I	0,63 W	0,00008	0,47080	0,00303	0,08232	583.44 $\pm$ 16.08	98,78	1,95	0,075	$\pm$ 0,011
01M0234K	0,70 W	0,00009	1,42096	0,00908	0,18882	590.28 $\pm$ 9.91	99,35	4,47	0,057	$\pm$ 0,006
01M0234L	0,80 W	0,00014	1,45674	0,00887	0,18800	587.95 $\pm$ 10.45	99,02	4,45	0,055	$\pm$ 0,006
01M0234M	fsn	0,00040	3,45736	0,02149	0,51888	590.01 $\pm$ 3.97	98,99	12,29	0,065	$\pm$ 0,007
$\Sigma$		0,00852	18,60378	0,15353	4,22184					
<b>Results</b>										
Sample	VU38-A8					Age $\pm 2\sigma$ (Ma)	MSW D	$^{39}\text{Ar(k)}$ (%)	K/Ca	$\pm 2\sigma$
Material	hornblende					595.18 $\pm$ 4.19	2,34	63,83	0,064	$\pm$ 0,007
Location	Sinai					$\pm$ 0,70%		9		
Analyst	Diana					External Error $\pm$ 12.62				
						Analytical Error $\pm$ 2.89				
Project	pilbara-jan							11	0,098	$\pm$ 0,004
Irradiation	VU38					583.82 $\pm$ 3.42				
J-value	0,017318					$\pm$ 0,59%				
Standard	98,3					External Error $\pm$ 12.17				
						Analytical Error $\pm$ 1.66				
<b>Information on Analysis</b>										
Sample	VU38-A8					40(r)/39(k) $\pm 2\sigma$				
Material	hornblende					22,5685 $\pm$ 0,1286				
Location	Sinai					$\pm$ 0,57%				
Analyst	Diana									
Project	pilbara-jan									
Irradiation	VU38									
J-value	0,017318									
Standard	98,3									

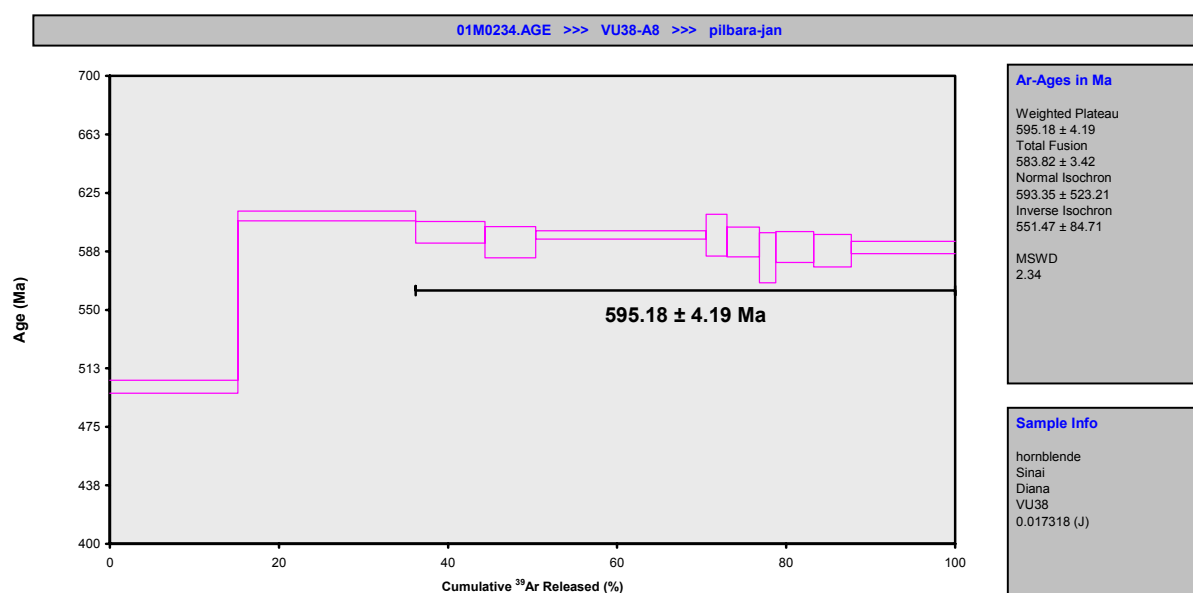
Table A.1-3b Table with detailed tables of the individual step-heating for the  $^{40}\text{Ar}/^{39}\text{Ar}$  dating of samples SIN 2

<b>Incremental Heating</b>		$^{36}\text{Ar}(\text{a})$	$^{37}\text{Ar}(\text{ca})$	$^{38}\text{Ar}(\text{cl})$	$^{39}\text{Ar}(\text{k})$	$^{40}\text{Ar}(\text{r})$	Age $\pm 2\sigma$ (Ma)	$^{40}\text{Ar}(\text{r})$ (%)	$^{39}\text{Ar}(\text{k})$ (%)	K/Ca	$\pm 2\sigma$
01M0233B	0,25 W	0,01551	0,40049	0,02183	0,97980	12,87070	369.78 $\pm$ 1.82	73,73	3,77	1,052	$\pm$ 0,206
01M0233C	0,40 W	0,02031	0,70265	0,03917	2,33704	42,23185	491.20 $\pm$ 0.87	87,55	8,99	1,430	$\pm$ 0,163
01M0233D	0,45 W	0,00955	1,93078	0,05404	3,27098	70,58409	572.81 $\pm$ 0.76	96,15	12,58	0,728	$\pm$ 0,073
01M0233E	0,50 W	0,00430	2,71273	0,04177	2,40940	54,81894	599.30 $\pm$ 1.04	97,73	9,27	0,382	$\pm$ 0,038
01M0233G	0,55 W	0,00223	3,37396	0,03904	1,90634	43,10865	596.19 $\pm$ 1.59	98,49	7,33	0,243	$\pm$ 0,024
01M0233H	0,60 W	0,00226	2,68100	0,03159	1,71535	38,98984	598.80 $\pm$ 1.47	98,31	6,60	0,275	$\pm$ 0,027
01M0233I	0,65 W	0,00172	4,18352	0,04281	1,76553	40,04563	597.73 $\pm$ 1.48	98,74	6,79	0,181	$\pm$ 0,018
01M0233J	0,70 W	0,00242	6,05644	0,05936	2,07375	46,76618	594.80 $\pm$ 1.61	98,48	7,97	0,147	$\pm$ 0,015
01M0233L	0,75 W	0,00171	3,04940	0,03242	1,56320	34,89203	589.61 $\pm$ 1.38	98,57	6,01	0,220	$\pm$ 0,022
01M0233M	0,80 W	0,00133	2,54626	0,02862	1,37926	30,73382	588.75 $\pm$ 1.49	98,73	5,30	0,233	$\pm$ 0,024
01M0233N	0,90 W	0,00191	5,26072	0,04861	1,75462	38,97612	587.19 $\pm$ 1.36	98,57	6,75	0,143	$\pm$ 0,014
01M0233O	fusion	0,00771	16,97158	0,11384	4,84798	107,07849	584.34 $\pm$ 1.19	97,91	18,64	0,123	$\pm$ 0,012
$\Sigma$		0,07095	49,86952	0,55310	26,00327	561,09637					

<b>Information on Analysis</b>		<b>Results</b>			Age $\pm 2\sigma$ (Ma)	MSW D	$^{39}\text{Ar}(\text{k})$ (% <sub>n</sub> )	K/Ca	$\pm 2\sigma$
Sample	VU38-A7	40(r)/39(k) $\pm 2\sigma$			596.43	29,20	43,97	0,203	$\pm 0,053$
Material	hornblende	$\pm 0,1356$	$\pm 0,60\%$						
Location	Sinai	Error Plateau			External Error $\pm 12.68$				
Analyst	Diana				Analytical Error $\pm 3.05$				
Project	pilbara-jan	Total Fusion Age			572.79		12	0,224	$\pm 0,009$
Irradiation	VU38	$\pm 0,0169$	$\pm 0,08\%$						
J-value	0,017318	External Error $\pm 11.83$							
Standard	98,3	Analytical Error $\pm 0.39$							



a



b

Figure A.1-6 Age spectra for (a) SIN 1 and (b) SIN 2

rocks contain hornblende, biotite, plagioclase and quartz. The samples were well linedated and foliated. The hornblendes define the lineations. The samples represent the main low-angle shear zone that was described in detail in chapter 5. The age spectra for the analyzed samples from the Wadi Kid Complex areas are shown in Figure A.1-6. The detailed tables of the individual step-heating can be found in table A.1-3. All analyzed samples display clear plateaus with no evidence of a secondary event outside of event that formed the main plateau. The results of  $^{40}\text{Ar}/^{39}\text{Ar}$  dating for sample SIN 1 displays an age of  $596 \pm 4$  Ma and for SIN 2 an age of  $595 \pm 4$  Ma (Figure A.1-6). These dates represent the ages of the M2 and D2 phases which formed the low-angle shear zone.

### A1.5 Conclusions

This appendix presents new geological data for the Wadi Kid Complex that is additional to the data that was presented in Chapter 5. These new data include the following geological information:

- Undeformed and non-metamorphosed rhyolites and ignimbrites overlie the low-grade deformed rocks. Geochemical data show that these were formed during extension.
- F1-folds with NNE-SSW to NE-SW trending fold axes and a related S1-foliation were formed during the D1-deformational phase. These structures formed during WNW-ESE to NW-SE compression. This trend of compression is also observed in the Later Proterozoic of northwestern Saudi Arabia, where this phase is attributed to arc-accretion (Stoeser & Camp 1985; Quick 1991).
- Moderately NW-dipping shear zones, with a thickness of 50 to 100 m, cross-cut the upper-crustal unit. These shear zones display a top-to-NW sense of shear. This sense of shear is also the initial sense of movement that was observed on the sub-horizontal lower-crustal shear zone that was formed during D2 (see also chapter 5). Therefore I interpret the moderately NW-dipping shear zones in the upper-crustal unit also to have been formed during D2.
- Locally, the contact between the lower- and upper-crustal rocks is marked by a brittle cataclastic layer.
- Geochemical data for the non-deformed igneous rocks, A-type granites, rhyolites and basalts indicate that these were derived mantle magmas that were intruded into a thinned and extending crust.
- The low-angle shear zone in the lower-crustal rocks, formed during D2, was dated at  $\approx 595$  Ma

An updated section across the Wadi Kid area is shown in Figure A.1-7a and an interpretation is presented in Figure A.1-7b. In this interpretation it is shown that upper-crustal rocks, metavolcanics and metasediments, display the compressional features that are indicative of the D1 -deformation phase. These rocks structurally overlie lower-crustal rocks, mainly mylonites, in the form of amphibolites and metaplutonic rocks, which were formed in an NW-SE extensional regime during the D2 -deformation phase (see also chapter 5). These shear zones were dated at  $\approx 595$  Ma.

The NE-SW striking shear zones in the upper-crustal metamorphics are interpreted as original splays off the deeper shear and were also formed during the extensional D2-phase. The lower- and upper-crustal rocks are separated by a brittle shear. Undeformed A-type granites intruded the lower-crustal mylonitic sequence. Geochemical studies show that these are alkaline granites that were derived through fractional crystallization from mantle magmas. This happened in a thinned and extended crust. The basaltic and felsic dykes, and the undeformed rhyolites and undeformed basalts that overlie the upper-crustal deformed rocks, were also derived from the same mantle magmas. In chapter 5, it is suggested that the SE-sense of movement in the lower-crustal mylonitic sequence postdated the NW-sense of movement and that this reversal was a result of doming. A cataclasite separates the lower- and upper-crustal units.



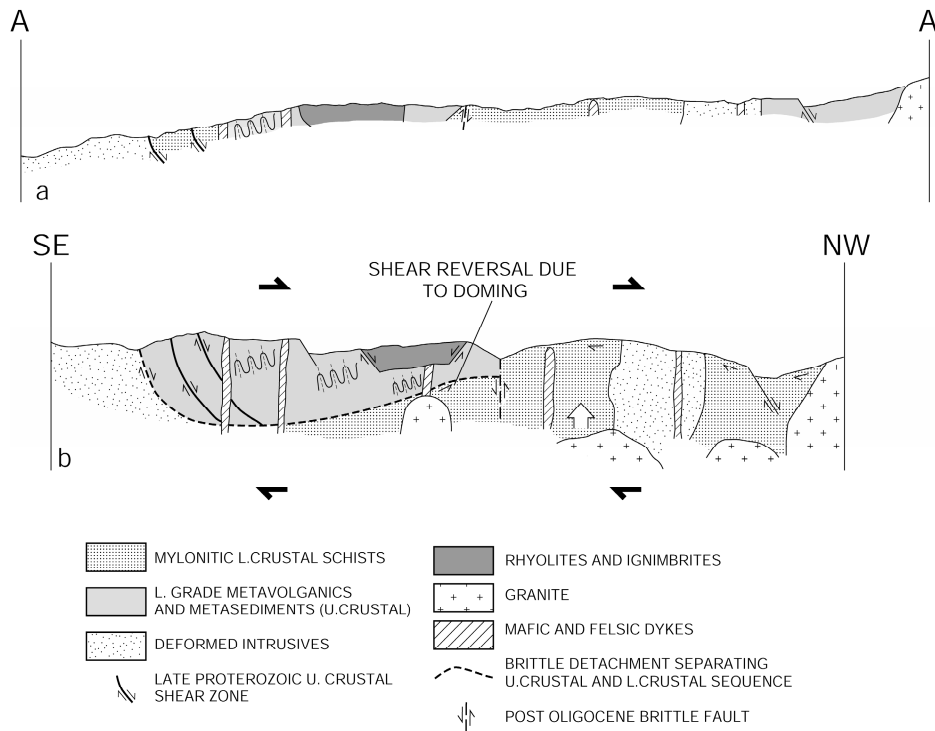


Figure A.1-7 Schematic cross-section through the Wadi Kid (section A-A' in Figure A.1-1)

The newly presented data in this appendix confirm the core-complex model for the Wadi Kid Complex that was presented in chapter 5. The sequence consisting of deformed plutons, of thick subhorizontal amphibolite-grade schists with uniformly trending lineations (described in detail in chapter 5), and which were formed at HT/LP conditions in an extensional regime, overlain by rocks displaying relicts of older compressional phases, with a cataclasite separating the two sequences.



## A.2 Geothermobarometric evidence for a metamorphic core-complex in Sinai, Egypt

*Published in Precambrian Research: 123 (2003): 249-268. Brooijmans, P., Blasband, B., White, S.H., Visser W.J. and P. Dirks*

### Abstract

Blasband et al. (1997, 2000) postulated a metamorphic core complex model for the Wadi Kid area, south Sinai, Egypt. This core complex was formed in an extensional setting after gravitational collapse of the East African Orogen in the Late Proterozoic. Arc-accretion was responsible for the closure of the Mozambique Ocean. Blasband et al (1997, 2000) based their theory mainly on structural data. In order to justify this model geothermobarometric evidence is crucial. Therefore the metamorphic rocks of the Wadi Kid area were the subject of a detailed metamorphic study.

The M<sub>1</sub> metamorphic phase is characterized by greenschist facies conditions and is related to arc-accretion. The M<sub>2</sub> metamorphic phase is the main subject of this paper. The petrologic characteristics of pelitic and mafic rocks that were metamorphosed during M<sub>2</sub> show that the lower crustal rocks in the Wadi Kid area were subjected to upper-greenschist to upper-amphibolite conditions of the low-pressure/high-temperature type at the end of the Late Proterozoic. Garnet-biotite and amphibole-plagioclase geothermometry reveal temperatures of 488-684 °C. Plagioclase-biotite-muscovite-garnet geothermometry and amphibole-plagioclase geobarometry indicate pressures of 3.42-4.28 kbar.

The M<sub>2</sub> metamorphic phase is associated with a D<sub>2</sub> deformation phase. This phase is a relict of gravitational collapse during the final stages of the collision of East and West Gondwanaland.

### A.2.1 Introduction

Blasband et al. (1997) were the first to acknowledge the presence of core complexes in the Arabian Nubian Shield, more specifically the Wadi Kid area (S.E. Sinai, Egypt). Structural studies in this area indicated the presence of a core complex as a result of extensional collapse during the Late Proterozoic (Blasband et al. 1997, 2000). Because core complexes display a typical metamorphic evolution, we believe that a detailed metamorphic study is necessary to demonstrate that the core complex model is valid for the Wadi Kid area.

Previous studies in the Wadi Kid area indicate that two metamorphic phases can be recognized (Shimron 1980, 1984, 1987; Reymer 1983, 1984a, 1984b). Phase M<sub>1</sub> is characterized by greenschist facies conditions (Shimron, 1987). Pressure and temperature conditions were estimated at 3-4 kbar and 300-400 °C. The M<sub>1</sub> phase was believed to have been

related to compression at upper crustal levels (Reymer, 1983, 1984a; Shimron, 1980, 1984, 1987) The M<sub>2</sub> phase is associated with deformation phase D<sub>2</sub> (Blasband et al., 1997, 2000). Studies by Reymer et al. (1984) and Shimron (1987) indicate upper-amphibolite facies conditions for this phase.

The aim of this research was to study and re-evaluate the metamorphic evolution of the Wadi Kid area and the metamorphic conditions in the lower crustal rocks in particular on the basis of new geothermobarometric data from the metapelitic and metavolcanic rocks of the Wadi Kid area.

This study indicates that the M<sub>1</sub> stage of greenschist-facies metamorphism was associated with a phase of arc-accretion. The M<sub>2</sub> stage of high-temperature/low-pressure type was associated with extension and the subsequent intrusion of large volumes of granitoids. The temperatures were between 488-684 °C and pressures between 3.42 kbar and 4.23 kbar respectively. The M<sub>2</sub> metamorphism is Furthermore we show that the metamorphic petrology and the geothermobarometric data support the core complex model for the Wadi Kid area as described by Blasband et al. (1997, 2000).

### **A.2.2 Lithology**

The Wadi Kid area consists of low- to high-grade metamorphic rocks and plutonic rocks of Late Proterozoic age which have been described and discussed by Shimron (1980, 1983, 1984), Furnes et al. (1985), and Reymer (1983, 1984a). The distribution of these rocks in the Wadi Kid Area is shown in Figure A.2-1. The Malhaq Fm., Umm Zariq Fm., the Heib Fm., and the Tarr Fm. represent the metamorphic sequence. The total thickness of this sequence is estimated to be 1.5 km. The Quneia Fm., the Sharira Diorite, and alkaline granites represent the (meta-) plutonics. Dikes crosscut all formations.

The *Umm Zariq Fm.* is a sequence of meta-pelites and meta-psammities. Within the Umm Zariq Fm., relict sedimentary structures, such as bedding, cross-bedding, slump structures and fining upward sequences are found in the less schistose lenses.

The strongly foliated metapelites contain fine-grained biotite, muscovite, (retrograde) chlorite, plagioclase and K-feldspar along with porphyroblasts of garnet, andalusite, staurolite, biotite and cordierite. The foliation is defined by biotite and muscovite flakes and flattened quartz grains. Garnets are present as anhedral and subhedral crystals between 0.3 and 2.4 mm in diameter. They contain only few inclusions of quartz, plagioclase, K-feldspar and ilmenite. Inclusion trails are absent. Staurolites occur as anhedral porphyroblasts up to 3.5 mm. Biotite, muscovite and quartz (Figure A.2-2) partly replace them. Andalusite porphyroblasts are anhedral, up to 4 mm and are locally replaced by biotite or muscovite (Figure A.2-3). Andalusites with inclusion trails were found in the Wadi Umm Zariq. Chiastolite is common and shows re-entrant zones with feather structures and growth inclusions. Inclusions in the chiastolite consist of biotite, quartz and ilmenite. Cordierite porphyroblasts are spherical, up to 5 mm in size and show sector twinning. Inclusions are numerous and consist of groundmass components.

The *Malhaq Fm.* is a metavolcanic sequence (Furnes et al., 1985) of biotite-schists and minor amounts of fine-grained, less-deformed, massive, metamorphosed volcanics. The biotite-

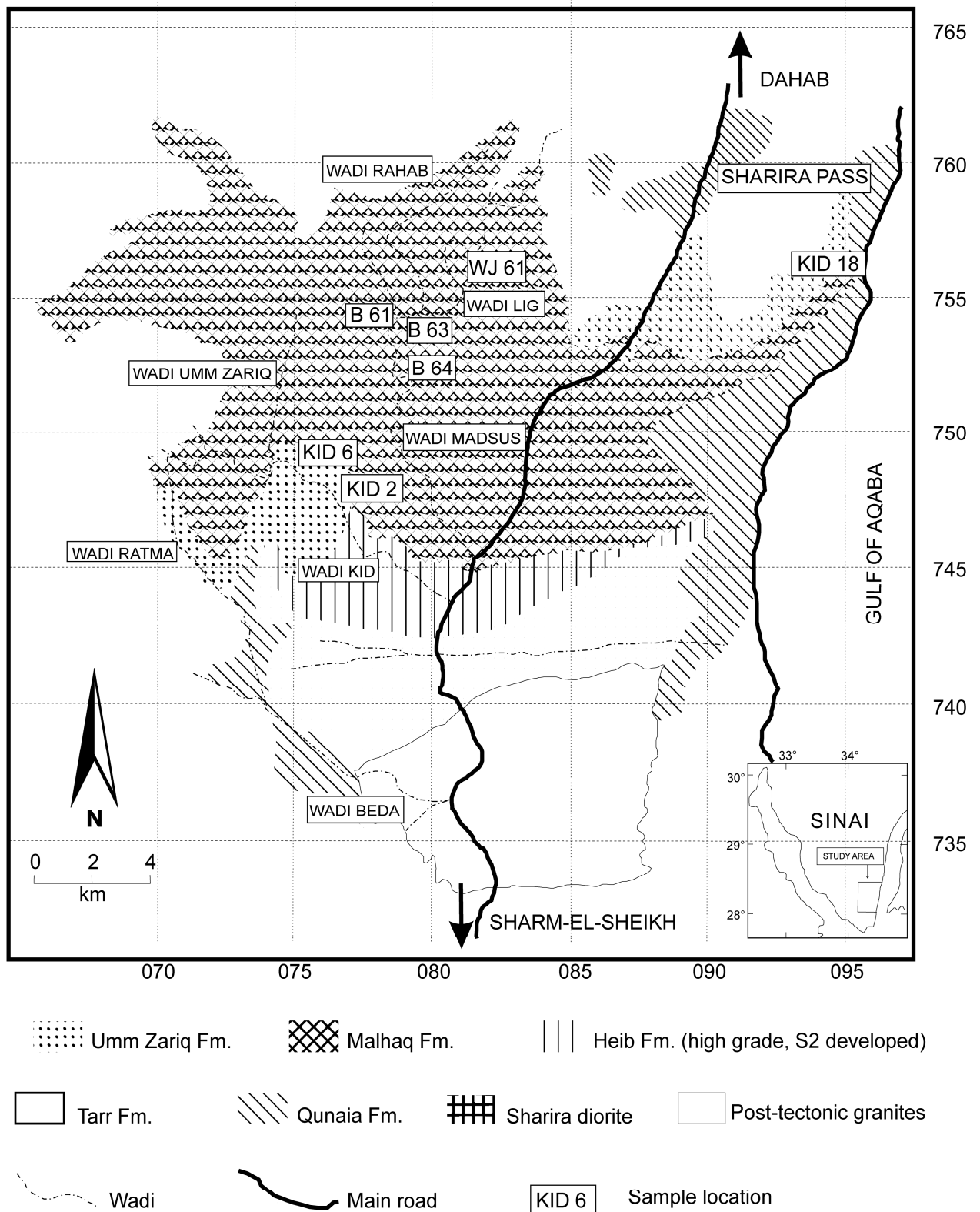


Figure A.2-1 Map of the Wadi Kid belt with an outline of the geological units and sample locations (modified after Shimron, 1987 and Blasband et al., 1997).

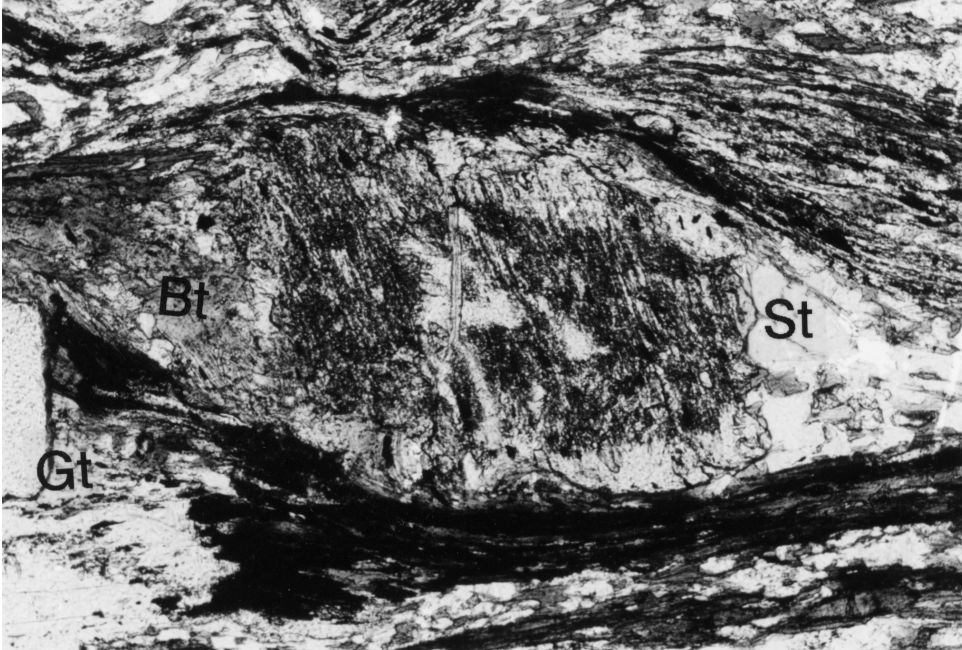


Figure A.2-2 Staurolite porphyroblasts in sample Kid 6, a pelitic schist from the Umm Zariq Fm., with in the left

schists contain feldspar, quartz, biotite and hornblende. Hornblende, biotite, flattened quartz and minor chlorite define the schistosity in the rocks of the Malhaq Fm. The massive equivalents of these schists occur as layers and blocks within the schists and contain biotite, muscovite, chlorite, some quartz and K-feldspar. Garnet, andalusite and staurolite are also present, as porphyroblasts in the Malhaq Fm. Quartz is present as flattened grains, which display undulatory extinction. Chlorite is brown to colorless. Staurolite porphyroblasts show mutual contacts with muscovite, andalusite and feldspar, and are partially replaced by muscovite. Anhedral andalusite porphyroblasts are up to 5 mm in size and contain inclusions of

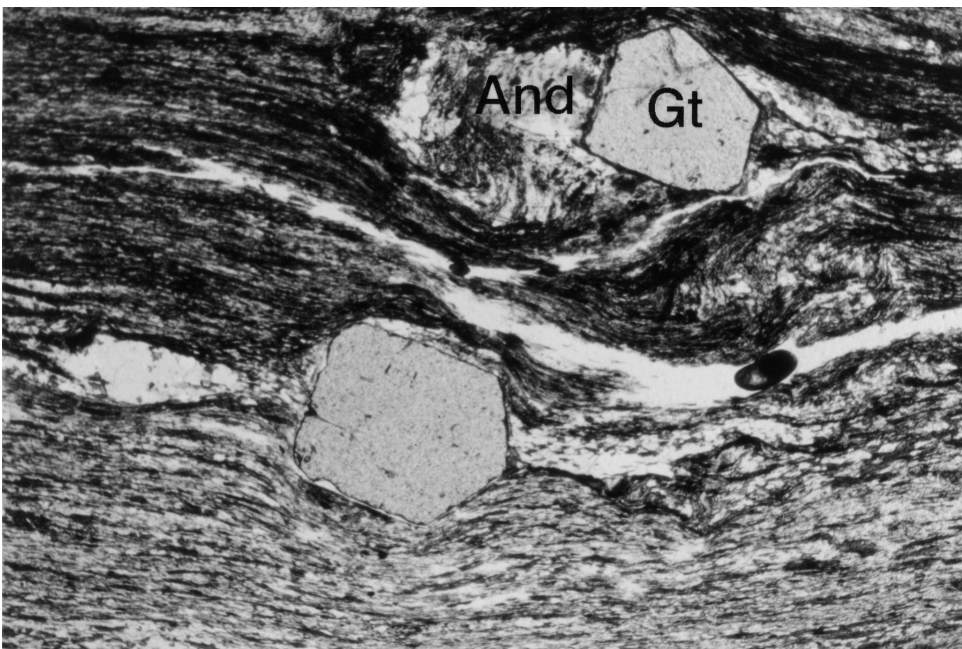


Figure A.2-3 Garnet in mutual contact with andalusite in sample Kid 6, Umm Zariq Fm.. Garnet and biotite are replacing andalusite. Magnification 30x.

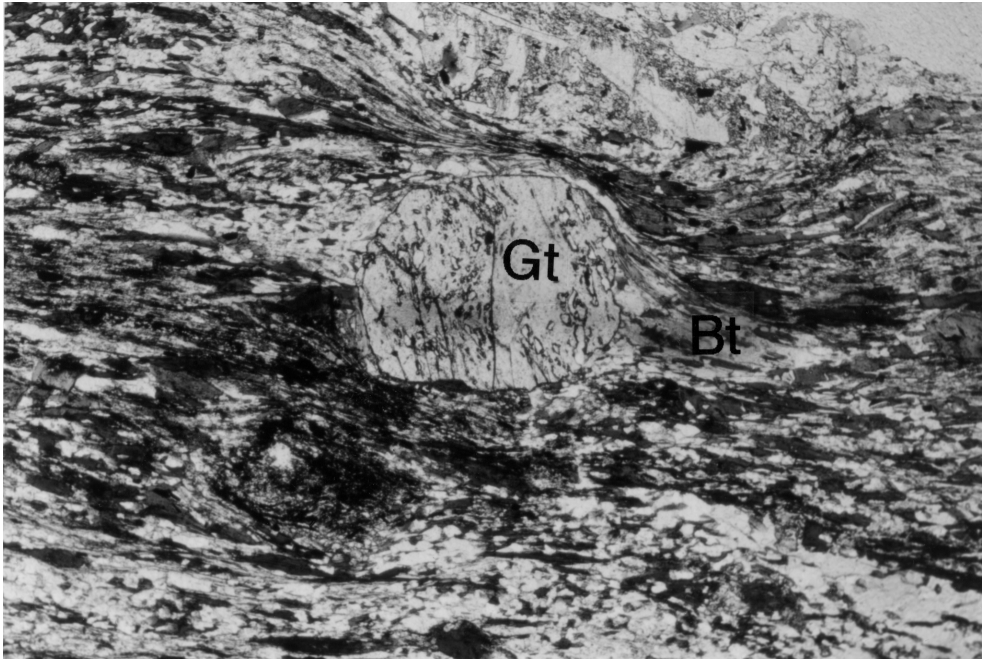


Figure A.2-4 Garnet in sample Kid 18, Malhaq FM., enclosed by muscovite, plagioclase and quartz. Pressure shadows on the edges are clearly visible. Magnification 30x.

quartz, plagioclase, garnet and ilmenite. No clear inclusion trails are observed in the andalusites. The andalusites are partially replaced by biotite and muscovite. Anhedral and subhedral garnet porphyroblasts with irregularly shaped rims are up to 1.4 mm in size (Figure A.2-4). The inclusions in the garnets consist of plagioclase, quartz and ilmenite. Garnets enclosed by andalusite crystals were observed, however garnet was not consumed during andalusite growth (Figure A2.-5). Biotite porphyroblasts are 1.0-2.0 mm in size and sometimes

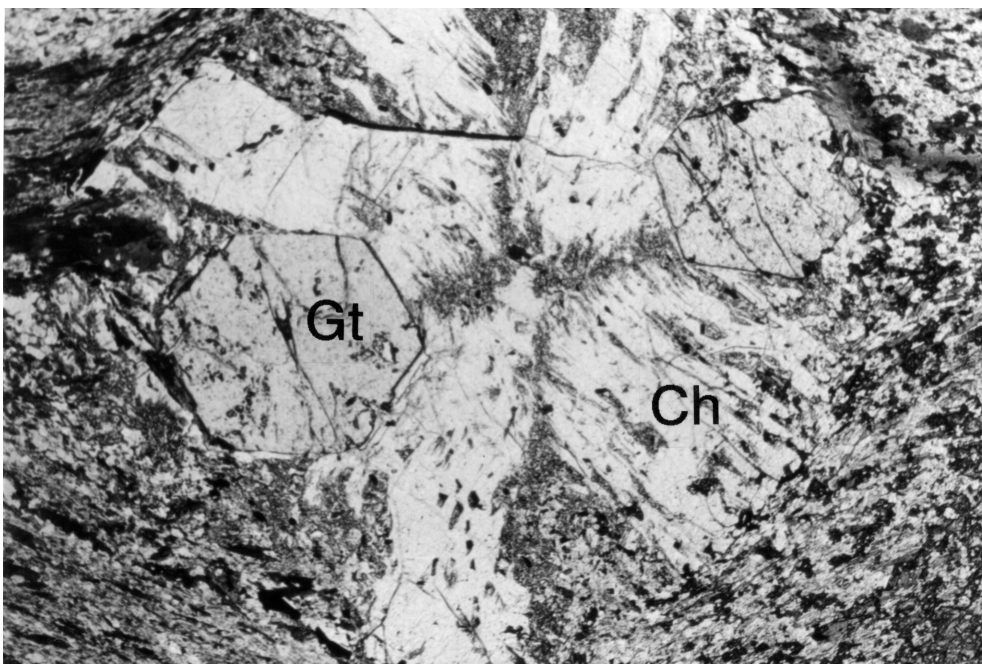


Figure A.2-5: Garnet enclosed by chiastolite in sample Kid 18 from the Malhaq Fm.. The garnet rims are well preserved, indicating no reaction of garnet during chiastolite growth. Magnification 30x.

overgrow the foliation. Hornblende is also present as porphyroblasts and up to 1 mm in size. They are found in the form of flakes and aggregates. Chlorite is only present in minor quantities. Ilmenite and magnetite are accessory minerals.

The *Heib Fm.* consists of upper-greenschist to lower-amphibolite-grade biotite-muscovite schists. These contain fine-grained feldspar, quartz, biotite, muscovite and chlorite. Porphyroblasts consist of cordierite, biotite and garnet. Biotite, muscovite and chlorite define the foliation.

The *Tarr Fm.* consists of low-grade schists, mudstones, sandstones, conglomerates and andesitic flows. The Tarr Fm. comprises the Beda Turbidites that formerly had been included in the Heib Fm (Blasband et al., 1997). The turbidites show sedimentary structures, such as fining-up sequences and low angle structures. The conglomerates contain granitic, andesitic and pelitic pebbles. Biotite schists form shear zones, 50-100m thick, that cross cut the Tarr Fm. These shear zones are formed in the highly schistose parts of the Tarr Fm. and are considered to be splays off the deeper shear (Blasband et al., 2000). The Tarr Fm. overlies the Heib Fm. On the basis of major and trace element studies Furnes et al. (1985) concluded that the protoliths of the Malhaq Fm., Heib Fm., Umm Zariq Fm. and Tarr Fm. exhibit trace element abundance's and ratios that characterize subduction-related rocks.

The *Quneia Fm.* is plutonic in origin and consists of foliated and lineated diorites and tonalites. Similar intrusives in the Nuweiba area (100 km north of the Wadi Kid Complex) were interpreted as subduction-related I-type intrusives (Ahmed et al., 1993).

The *Sharira Diorite* is an undeformed hornblende-diorite in the northern part of the Wadi Kid area and was dated at  $570 \pm 4$  Ma (Moghazi et al, 1998).

All formations, except the Tarr Fm., are intruded by undeformed to slightly deformed biotite bearing alkaline granites, which were interpreted as A-type granites by Ahmed et al. (1993). Trace-element studies on similar granites in the Timna Area show that these granites are related to crustal thinning in an extensional regime (Beyth et al., 1994). Mafic and felsic composite dykes crosscut the upper and lower crustal rocks in NE-SW direction. Undeformed ignimbrites and rhyolites overlie the Tarr Fm.

### A.2.3 Structures

An extensive structural study of the Wadi Kid area was conducted by Blasband et al. (1997, 2000). They recognized two deformation phases in the Late Proterozoic history of the Wadi Kid area. The older phase, hereby referred to as  $D_1$  produced a steep regional foliation, axial planar to  $F_1$  folds with WSW-ENE fold-axes. This phase is only observed in upper-crustal rocks of the Tarr Fm. Deformation took place at greenschist facies conditions. This  $D_1$  phase is thought to have been related to arc-accretion and was interpreted to have taken place at 720-650 Ma (Blasband et al., 2000).

The younger deformation phase,  $D_2$ , produced structures in the lower- and upper-crustal rocks (Blasband et al., 1997, 2000). The structures include an  $S_2$ -foliation, a NW-SE trending  $L_2$  lineation formed by hornblende, andalusite, mica pods and stretched feldspars (Blasband et al., 1997). Dikes intruded in a NE-SW direction, perpendicular to the stretching lineation, and indicate NW-SE extension during  $D_2$ . Shear sense indicators, specifically deformed xenoliths



and conglomerates, extensional crenulation cleavages, rotated porphyroclasts with pressure shadows and S-C fabrics, indicate that the schists were formed as normal shear zones in an extensional environment (Blasband et al., 1997, 2000). The main sense of movement was to the NW but local reversals to the SE were recorded (Blasband et al., 1997). The reversal was related to the doming of the lower crust, which is caused by isostatic rebound of the crust and intrusion of A-type granites (Blasband et al., 1997, 2000).

#### **A.2.4 Petrology**

Seven samples from the Malhaq Fm. and Umm Zariq Fm. were selected for geothermobarometry. The petrology of these samples will be described below. The objective of this paragraph is to unravel the P-T conditions of the mineral assemblages in the samples and to compare it with a P-T diagram showing the univariant curves for the reactions that control the appearance and breakdown of the phases present. The order of mineral growth and mineral reactions seen in the thin sections define a PTt path, where as geothermobarometry studies will define a single point in PTt-space.

Sample Kid 18 is a garnet-andalusite-biotite schist from the Malhaq Fm. In sample Kid 18 garnet is enclosed by andalusite (Figures A.2-4 and A.2-5), suggesting garnet grew before andalusite through the reaction

- chlorite + muscovite = garnet + biotite + quartz + H<sub>2</sub>O.

Andalusite grew through the reaction, thereby not consuming garnet as garnet remained stable during andalusite growth,

- pyrophyllite = andalusite + quartz + H<sub>2</sub>O.

In sample Kid 18 we also observed breakdown of andalusite overgrown by muscovite through the reaction

- andalusite + K-feldspar + H<sub>2</sub>O = muscovite.

Sample B 63 is a garnet-biotite schist from the Malhaq Fm. hereby we assume that as a resultant of metamorphism during D<sub>1</sub> sample B 63 is a chlorite-muscovite schist comparable with the Beda turbidites and during D<sub>2</sub> garnet and biotite were formed through the reaction

- chlorite + muscovite = garnet + biotite + quartz + H<sub>2</sub>O.

The order of mineral growth in sample Kid 6, Umm Zariq Fm., is probably staurolite, followed by garnet and andalusite. Staurolite (Figure A.2-2) can exist in low and medium pressure rocks and can be formed by the following reactions (Yardley, 1989)

- chloritoid + quartz = staurolite + garnet + H<sub>2</sub>O or
- garnet + muscovite + chlorite = staurolite + biotite + quartz + H<sub>2</sub>O or
- chlorite + muscovite = staurolite + biotite + quartz + H<sub>2</sub>O.

In the samples no relicts of chloritoid is found and garnet is formed after staurolite, thereby leaving the third reaction as most likely.

Garnet was formed not at the expense of staurolite through the reaction

- chlorite + muscovite = garnet + biotite + quartz + H<sub>2</sub>O,

thereby forming the stable assemblage staurolite-garnet-biotite.

Transformation of staurolite into andalusite was observed in sample Kid 6 through the reaction

- staurolite + muscovite + quartz = andalusite + biotite + H<sub>2</sub>O.

Andalusite breakdown observed in sample Kid 6 to form muscovite through the reaction (Figure A.2-3)

- andalusite + K-feldspar + H<sub>2</sub>O = muscovite.

During the last phase of metamorphism H<sub>2</sub>O is needed for retrograde reactions. During this phase the post-tectonic granites were probably the main source of H<sub>2</sub>O.

Sample Kid 2 is a garnet-biotite schist where garnet and biotite formed through the reaction like sample B 63

- chlorite + muscovite = garnet + biotite + quartz + H<sub>2</sub>O.

## A.2.5 Mineral composition

### A.2.5.1 Methods

The purpose of obtaining exact mineral compositions is to use the data for geothermobarometry and to derive exact pressure and temperature conditions for the samples. Geothermobarometry is the name given to the application whereby the pressure and temperature dependence of the equilibrium constant is used to infer metamorphic pressures and temperatures. The most common geothermometer in pelitic schists is based on the cation exchange reaction of Fe and Mg between garnet and biotite.

Mineral compositions were determined by analyzing carbon-coated, polished thin sections on the JEOL JXA-8600 microprobe at Utrecht University. Operating conditions were 15 kV accelerating potential and 10 nA beam current. A focused beam diameter of <1 μm was used for all minerals. Standard ten-element analyses were performed on all minerals. SiO<sub>2</sub>, Al<sub>2</sub>O<sub>3</sub>, FeO, CaO, MgO and K<sub>2</sub>O were analyzed on the energy dispersive X-ray spectrometer and TiO<sub>2</sub>, Na<sub>2</sub>O, Cr<sub>2</sub>O<sub>3</sub> and MnO were analyzed on the wavelength dispersive X-ray spectrometer. Analyses on garnets were core-rim in small steps. Core and rim analyses were made on biotite porphyroblasts, andalusites, amphibole porphyroblasts, K-feldspars, plagioclase and staurolite. Measurements on muscovite, chlorite, biotite and ilmenite were spot analyses.

Biotite grains near garnet, but not in physical contact with garnet, were used for geothermometry, because these biotites are considered to reflect the composition at the peak temperature. It was assumed that the composition of biotite is not influenced by post-metamorphic diffusion.

Conditions of metamorphism reflected by the pelitic schists were estimated by using biotite-garnet thermometry using the calibration of Kleemann and Reinhardt (1994). In the Kleemann and Reinhardt (1994) model, Mg-Fe mixing is assumed to be ideal, whereas the activity model is non-ideal for Mg, Fe-Al and Mg, Fe-Ti mixing. The titanium mixing parameters used in this study were taken from Sengupta et al. (1990). According to Kleemann and Reinhardt (1994) the influence of Ti on garnet-biotite thermometry is small compared to the effect of <sup>VI</sup>Al and is considered to be negligible. The garnet activity model was taken from Berman (1990). Pressures were estimated using the plagioclase-biotite-muscovite-garnet geobarometer of Powell and Holland (1988), originally calibrated by Ghent and Stout (1981). This barometer is especially suitable for rocks in which aluminosilicate polymorphs are absent.

The best estimate for peak temperatures during M<sub>2</sub> comes from thermobarometry

combining matrix phases with the low  $\text{Fe}/(\text{Fe}+\text{Mg})$  region of the garnet (the “well”) just inside the rim. (Spear, 1991). This low  $X_{\text{Fe}}$  region represents the minimum estimate of peak temperature (Spear, 1991).

Geothermobarometry on mafic schists is based on the chemical interaction between plagioclase and hornblende. Several geothermometers are available and geobarometers are rare. In this study the hornblende-plagioclase geothermometer of Holland and Blundy (1994) was used. The Holland and Blundy (1994) thermometer is based on an ideal mixing-on-sites model for amphibole and plagioclase non-ideality is modeled on the basis of Darken’s quadratic formalism (Holland and Powell, 1992). A problem associated with the use of amphiboles and plagioclase in geothermobarometry is that both solid solutions show miscibility gaps. Furthermore, the disadvantage of this thermometer is that it uses fixed pressures. Results obtained by the Holland and Blundy (1994) calibration were calculated using HBL-PLAG, a computer program that requires raw microprobe data and the activity of albite. It computes temperatures for different pressures.

#### *A.2.5.2 Chemical compositions*

##### *A.2.5.2.1 Pelitic schists of the Malhaq Formation*

The samples Kid 18 and B 63 represent the metapelites of the Malhaq Fm. Kid 18 is a garnet-andalusite-biotite schist and sample B 63 is a garnet-biotite schist. Tables A.2-1 and A.2-2 summarize the chemical compositions of the minerals from this pelitic schist. Sample locations are shown in Figure A.2-1. In the garnets the mole fractions of almandine ranges between 0.67 and 0.80 (see Figures A.2-6 and A.2-7). Pyrope, spessartine and grossular contents vary between 0.03 and 0.17. Most garnets show an increase in almandine and pyrope from core to rim, whereas spessartine and grossular decrease (see Figures A.2-6 and A.2-7). Biotite composition differs between sample Kid 18 and sample B 63.  $X_{\text{Fe}}$  varies between 0.65 and 0.71 in sample Kid 18 and between 0.52 and 0.56 in sample B 63. The potassium content of muscovite varies between 0.81-0.92 (Kid 18) and 0.95-0.98 (sample B 63). Plagioclase feldspars in sample Kid 18 are rich in albite ( $X_{\text{Ab}}= 0.63\text{-}0.88$ ) with only minor amounts of orthoclase ( $X_{\text{Or}}= 0.0\text{-}0.08$ ).

##### *A.2.5.2.2 Pelitic schists of the Umm Zariq Formation*

Tables A.2-3 and A.2-4 summarize representative microprobe analyses for sample Kid 6, a garnet-andalusite-staurolite-biotite schist, and sample Kid 2, a garnet-biotite schist. The sample locations are shown in Figure A.2-1. The mole fraction of almandine in garnets from the Umm Zariq Fm. ranges between 0.61-0.80 (Figures A.2-8 and A.2-9). The mole fractions of pyrope, spessartine and grossular are lower and vary between 0.04-0.16 (Figures A.2-8 and A.2-9). Almandine increases from core to rim in all samples, pyrope shows a flat profile or a slight decrease, spessartine decreases from core to rim in both samples (Figures A.2-8 and A.2-9).  $X_{\text{Fe}}$  in biotite varies between 0.58-0.66 in sample Kid 6 and between 0.48-0.52 in sample Kid 2.  $X_{\text{Mg}}$  in biotite varies between 0.21 and 0.39. Muscovite in sample Kid 6 has potassium content

Appendix 2

Table A.2-1 Representative results of electron microprobe analyses of garnet, biotite, muscovite and plagioclase in sample Kid 18. For location see Figure A.2-6. Oxygen basis of the analysis: Pl 8; Grt 24; Bt, Ms 22.  $X_{Fe} = Fe/(Fe+Mg)$ ;  $X_{Alm} = Fe/(Fe+Mg+Mn+Ca)$ ;  $X_{Sps} = Mn/(Fe+Mg+Mn+Ca)$ ;  $X_{Prp} = Mg/(Fe+Mg+Mn+Ca)$ ;  $X_{Grs} = Ca/(Fe+Mg+Mn+Ca)$ ;  $X_{Ab} = Na/(Na+K+Ca)$ .

Kid 18

	Gt 1 core	Gt 1 rim	Gt 4 core	Gt 4 rim	90 Bt matrix	126 Bt matrix	9 Ms matrix	78 Ms matrix	13 Pl matrix	1 Pl matrix
SiO <sub>2</sub>	36.26	37.82	36.43	37.05	33.07	32.13	47.99	48.01	61.04	61.41
TiO <sub>2</sub>	0.03	0.07	0.98	-	2.37	2.07	0.28	0.47	-	-
Al <sub>2</sub> O <sub>3</sub>	20.71	20.82	20.58	20.63	18.89	18.69	38.05	37.68	25.09	24.53
Cr <sub>2</sub> O <sub>3</sub>	-	-	-	-	-	-	0.01	0.04	-	-
FeO	33.28	36.27	32.06	35.76	24.71	26.80	1.07	1.22	-	0.32
MnO	6.77	3.65	6.83	3.85	0.15	0.17	0.04	-	-	-
CaO	2.28	2.38	2.20	2.27	-	0.17	-	-	6.56	5.88
MgO	1.23	1.66	0.91	1.81	5.94	6.96	0.13	0.23	-	-
K <sub>2</sub> O	-	-	-	-	8.82	6.77	8.84	8.49	0.14	-
Na <sub>2</sub> O	0.12	-	0.09	-	0.08	0.11	0.65	0.54	8.10	8.69
Total	100.68	102.67	100.08	101.37	94.03	93.87	97.06	96.68	100.93	100.83
Si	5.914	6.012	5.944	5.972	5.254	5.124	6.170	6.188	2.691	2.712
Ti	0.003	0.007	0.121	-	0.283	0.239	0.027	0.045	-	-
Al	3.982	3.901	3.956	3.921	3.674	3.511	5.769	5.725	1.304	1.277
Cr	-	-	-	-	0.001	-	0.001	0.003	-	-
Fe	4.541	4.820	4.373	4.821	3.283	3.575	0.116	0.132	-	0.012
Mn	0.934	0.492	0.944	0.525	0.020	0.023	0.003	-	-	-
Ca	0.399	0.406	0.383	0.393	-	0.029	-	-	0.310	0.278
Mg	0.300	0.391	0.221	0.436	1.404	1.655	0.025	0.046	-	-
K	-	-	-	-	1.787	1.377	1.451	1.397	0.008	-
Na	0.040	-	0.031	-	0.026	0.034	0.162	0.133	0.693	0.744
Total	16.113	16.029	15.973	16.068	15.732	15.568	13.724	13.669	5.006	5.023
$X_{Fe}$	0.960	0.925	0.952	0.917	0.701	0.684	-	-	-	-
$X_{Alm}$	0.747	0.789	0.739	0.781	-	-	-	-	-	-
$X_{Sps}$	0.153	0.081	0.159	0.085	-	-	-	-	-	-
$X_{Prp}$	0.031	0.064	0.037	0.071	-	-	-	-	-	-
$X_{Grs}$	0.070	0.066	0.065	0.064	-	-	-	-	-	-
$X_{Ab}$	-	-	-	-	-	-	-	-	0.685	0.728

Table A.2-2: Representative results of electron microprobe analyses of hornblende, plagioclase and chlorite in sample B 64. For location see Figure A.2-6. Oxygen basis of the analysis: Hbl 23; Pl 8; Chl 28.  $X_{Fe} = Fe/$ 

B 64										
	Hbl 2.1	Hbl 2.3	Hbl 2	Hbl 4	Hbl 5	Hbl 12	Pl 1	Pl 5	Pl 8	Chl 1
	blast	blast	matrix	matrix	matrix	matrix	matrix	matrix	matrix	matrix
SiO <sub>2</sub>	44.04	44.37	48.07	45.04	44.91	44.12	46.36	47.51	67.49	25.64
TiO <sub>2</sub>	0.72	0.65	0.53	0.58	0.59	0.66	-	0.06	0.01	0.08
Al <sub>2</sub> O <sub>3</sub>	12.5	12.75	8.58	11.78	12.40	13.34	35.23	34.40	20.74	21.46
Cr <sub>2</sub> O <sub>3</sub>	0.03	-	0.04	-	-	0.29	-	-	0.01	0.03
FeO	20.19	19.55	18.95	19.75	19.98	19.59	0.23	0.27	0.36	28.16
MnO	0.45	0.43	0.51	0.50	0.49	0.45	0.02	-	-	0.34
CaO	12.17	11.73	11.59	11.65	11.89	11.76	18.75	17.62	1.49	-
MgO	8.06	8.53	10.26	8.72	8.06	8.03	-	-	-	15.04
K <sub>2</sub> O	0.61	0.48	0.33	0.40	0.44	0.61	-	-	1.70	-
Na <sub>2</sub> O	0.91	1.08	0.78	0.94	1.05	1.09	1.25	1.81	8.64	0.03
Total	99.69	99.57	99.64	99.34	99.81	99.95	101.83	101.67	100.43	90.79
Si	6.539	6.558	7.037	6.668	6.629	6.507	2.101	2.150	2.950	5.293
Ti	0.081	0.072	0.059	0.064	0.066	0.073	-	0.002	0.001	0.012
Al	2.187	2.221	1.480	2.055	2.157	2.319	1.882	1.835	1.068	5.220
Cr	0.003	-	0.005	-	-	0.033	-	-	-	0.006
Fe	2.507	2.417	2.320	2.445	2.466	2.416	0.009	0.010	0.013	4.862
Mn	0.057	0.054	0.063	0.062	0.062	0.056	0.001	-	-	0.058
Ca	1.937	1.858	1.818	1.848	1.880	1.858	0.910	0.855	0.070	-
Mg	1.784	1.880	2.238	1.924	1.774	1.766	-	-	-	4.627
K	0.116	0.090	0.062	0.076	0.083	0.114	-	-	0.095	-
Na	0.262	0.308	0.221	0.269	0.301	0.313	0.110	0.159	0.732	0.012
Total	15.473	15.458	15.303	15.411	15.418	15.455	5.013	5.011	4.929	20.090
X <sub>Fe</sub>	0.584	0.562	0.509	0.560	0.582	0.578				0.512
X <sub>Ab</sub>							0.108	0.157	0.816	

## Appendix 2

Table A.2-3: Representative results of electron microprobe analyses of garnet, biotite, muscovite, staurolite and plagioclase in sample Kid 6. For location see Figure A.2-6. Oxygen basis of the analysis: Pl 8; Grt 24; Bt, Ms 22; St 32.  $X_{Fe} = Fe/(Fe+Mg)$ ;  $X_{Alm} = Fe/(Fe+Mg+Mn+Ca)$ ;  $X_{Sps} = Mn/(Fe+Mg+Mn+Ca)$ ;  $X_{Prp} = Mg/(Fe+Mg+Mn+Ca)$ ;  $X_{Grs} = Ca/(Fe+Mg+Mn+Ca)$ ;  $X_{Ab} = Na/(Na+K+Ca)$ .

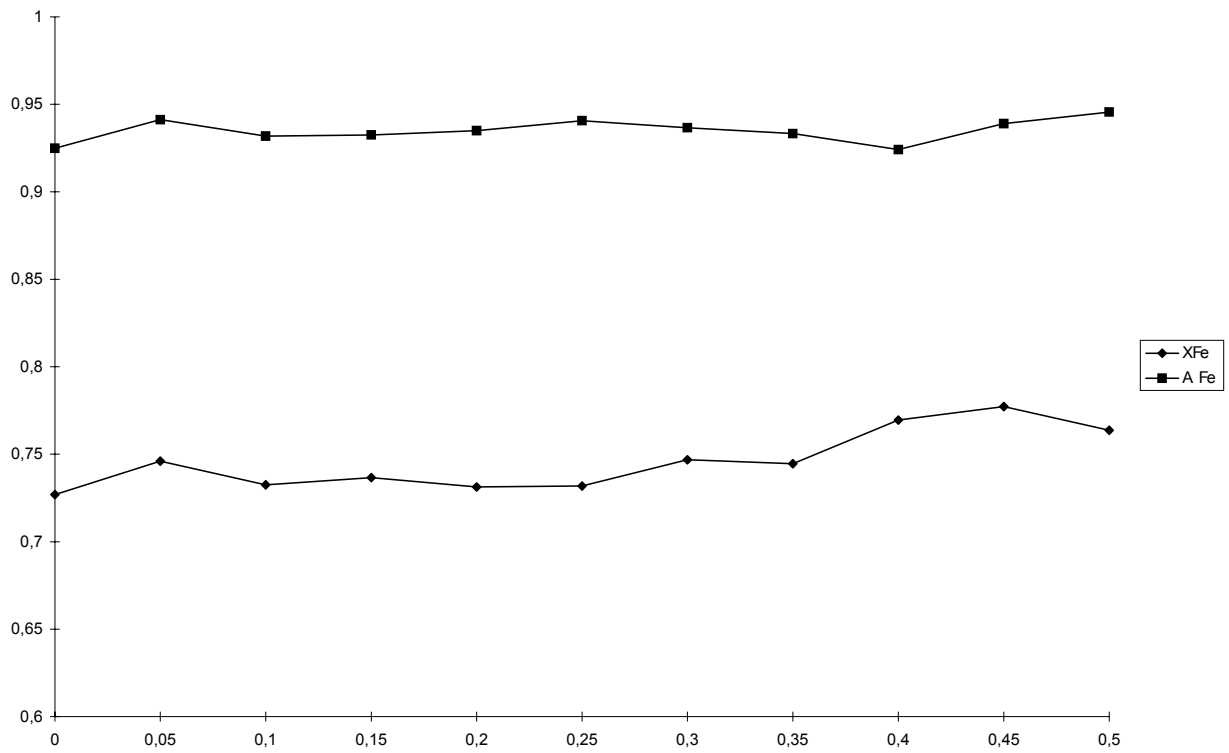
## Kid 6

	Gt 3 core	Gt 3 rim	Gt 6 core	Gt 6 rim	Bt 1 matrix	Bt 8 matrix	Ms 1 matrix	St 1	Pl 4 matrix	Pl 7 matrix
SiO <sub>2</sub>	37.58	37.31	36.52	37.55	35.36	34.68	46.59	27.53	60.87	59.90
TiO <sub>2</sub>	-	0.01	-	-	0.98	2.13	0.44	0.52	-	0.05
Al <sub>2</sub> O <sub>3</sub>	20.93	21.38	20.88	20.84	21.08	20.67	37.51	54.06	25.38	25.31
Cr <sub>2</sub> O <sub>3</sub>	0.04	0.01	0.01	-	-	-	0.04	0.04	0.05	-
FeO	33.27	35.22	33.13	34.99	20.74	21.91	1.03	13.77	-	0.31
MnO	6.27	4.27	6.25	3.89	0.14	0.1	-	0.22	-	-
CaO	1.56	1.88	1.94	1.90	0.13	-	-	-	6.77	6.44
MgO	1.32	1.77	1.66	1.66	8.19	7.22	-	1.09	-	-
K <sub>2</sub> O	0.14	0.11	-	0.10	9.42	9.93	8.87	-	0.18	0.48
Na <sub>2</sub> O	0.03	0.03	0.07	0.11	0.22	0.14	0.64	-	7.75	7.68
Total	101.15	102.00	100.46	101.04	96.26	96.79	95.12	97.23	100.99	100.16
Si	6.049	5.959	5.938	6.039	5.347	5.271	6.125	5.347	2.682	2.669
Ti	-	0.001	-	-	0.112	0.244	0.043	0.075	-	0.002
Al	3.970	4.025	4.003	3.953	3.757	3.702	5.812	12.372	1.318	1.329
Cr	0.005	0.001	0.002	-	-	-	0.004	0.007	0.002	-
Fe	4.479	4.704	4.505	4.708	2.623	2.786	0.114	2.235	-	0.012
Mn	0.855	0.577	0.861	0.530	0.017	0.014	-	0.036	-	-
Ca	0.269	0.322	0.338	0.328	0.021	-	-	-	0.220	0.307
Mg	0.317	0.421	0.404	0.399	1.847	1.636	-	0.317	-	-
K	0.029	0.023	-	0.020	1.818	1.926	1.488	-	0.010	0.027
Na	0.010	0.009	0.021	0.039	0.066	0.041	0.164	-	0.663	0.660
Total	15.983	16.042	16.072	16.016	15.608	15.620	13.750	20.389	4.865	5.006
$X_{Fe}$	0.934	0.918	0.918	0.922	0.587	0.630				
$X_{Alm}$	0.757	0.781	0.738	0.789						
$X_{Sps}$	0.144	0.096	0.066	0.067						
$X_{Prp}$	0.054	0.070	0.055	0.055						
$X_{Grs}$	0.045	0.053	0.141	0.089						
$X_{Ab}$								0.876	0.742	0.665

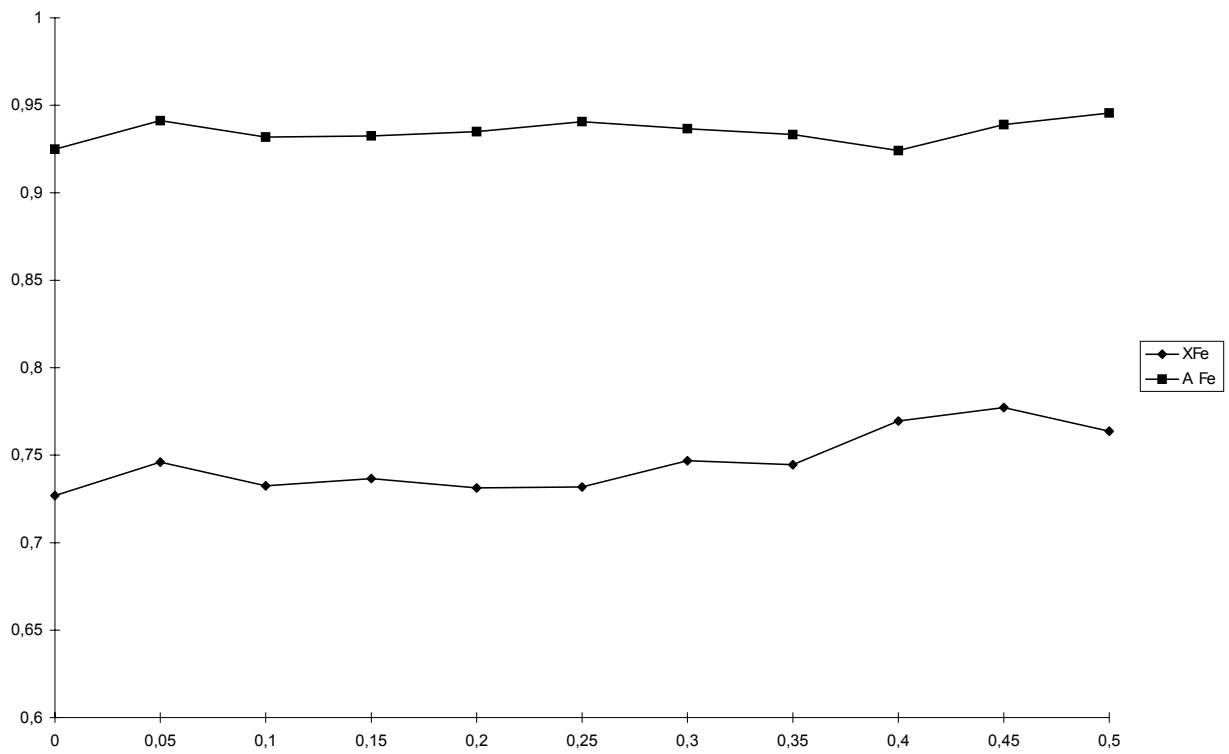
Table A.2-4: Representative results of electron microprobe analyses of garnet, biotite, chlorite and plagioclase in sample Kid 2. For location see Figure A.2-6. Oxygen basis of the analysis: Pl 8; Grt 24; Bt, Ms 22; Chl 28.  $X_{Fe} = Fe/(Fe+Mg)$ ;  $X_{Alm} = Fe/(Fe+Mg+Mn+Ca)$ ;  $X_{Sps} = Mn/(Fe+Mg+Mn+Ca)$ ;  $X_{Prp} = Mg/(Fe+Mg+Mn+Ca)$ ;  $X_{Grs} = Ca/(Fe+Mg+Mn+Ca)$ ;  $X_{Ab} = Na/(Na+K+Ca)$ .

Kid 2								
	Grt 1	Grt 1	Grt 2	Grt 2	Bt 52	Chl 44	Pl 50	Pl 51
	core	rim	core	rim	matrix	matrix	matrix	matrix
SiO <sub>2</sub>	37.01	36.41	37.85	37.82	36.32	26.31	57.55	56.95
TiO <sub>2</sub>	0.07	0.05	0.10	0.10	1.99	0.15	0.02	-
Al <sub>2</sub> O <sub>3</sub>	20.97	21.05	21.29	21.20	18.09	21.79	26.60	27.78
Cr <sub>2</sub> O <sub>3</sub>	0.06	0.07	-	-	-	-	-	-
FeO	29.38	37.42	29.63	32.02	20.42	25.55	0.06	-
MnO	5.69	3.81	5.32	3.83	0.08	0.19	-	-
CaO	4.34	2.88	4.53	2.70	0.03	0.06	8.69	9.60
MgO	1.67	2.24	1.72	2.47	10.48	14.87	0.02	-
K <sub>2</sub> O	-	-	-	-	8.98	0.22	0.06	0.05
Na <sub>2</sub> O	-	0.01	0.01	-	0.04	0.01	6.25	6.30
Total	99.19	97.94	100.45	100.57	96.42	89.15	99.25	100.68
Si	6.009	5.981	6.046	6.031	5.466	5.445	2.592	2.539
Ti	0.010	0.006	0.012	0.011	0.226	0.025	0.001	-
Al	3.977	4.745	4.011	4.034	3.208	5.315	1.412	1.459
Cr	0.008	0.009	-	-	-	-	-	-
Fe	3.846	4.315	3.958	4.409	2.569	4.423	0.002	-
Mn	0.745	0.530	0.720	0.431	0.011	0.034	-	-
Ca	0.849	0.507	0.776	0.385	0.005	0.014	0.420	0.458
Mg	0.399	0.549	0.410	0.640	2.351	4.589	0.001	-
K	-	-	-	-	1.732	0.057	0.004	0.003
Na	-	0.003	0.006	-	0.013	0.004	0.546	0.544
Total	15.974	16.645	15.939	15.941	15.572	19.906	4.798	5.003
$X_{Fe}$	0.908	0.887	0.906	0.873	0.522	0.491		
$X_{Alm}$	0.673	0.731	0.675	0.752				
$X_{Sps}$	0.132	0.090	0.123	0.074				
$X_{Prp}$	0.068	0.093	0.070	0.109				
$X_{Grs}$	0.127	0.086	0.132	0.066				
$X_{Ab}$							0.563	0.541

Appendix 2



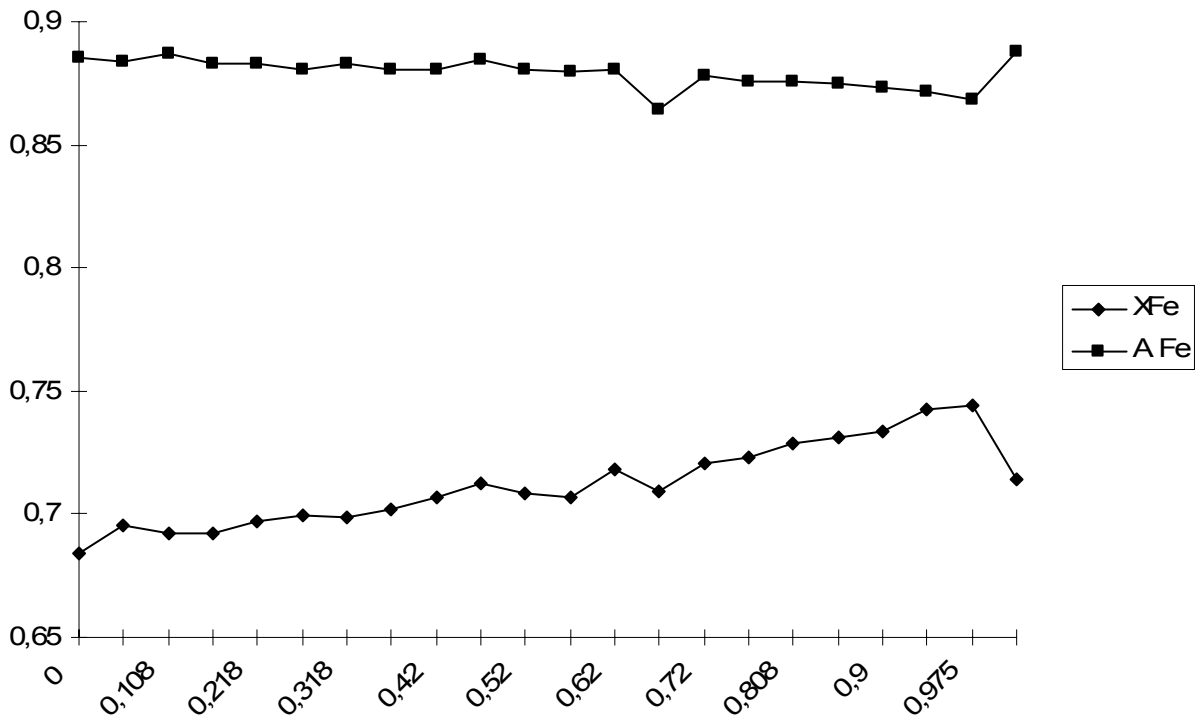
a



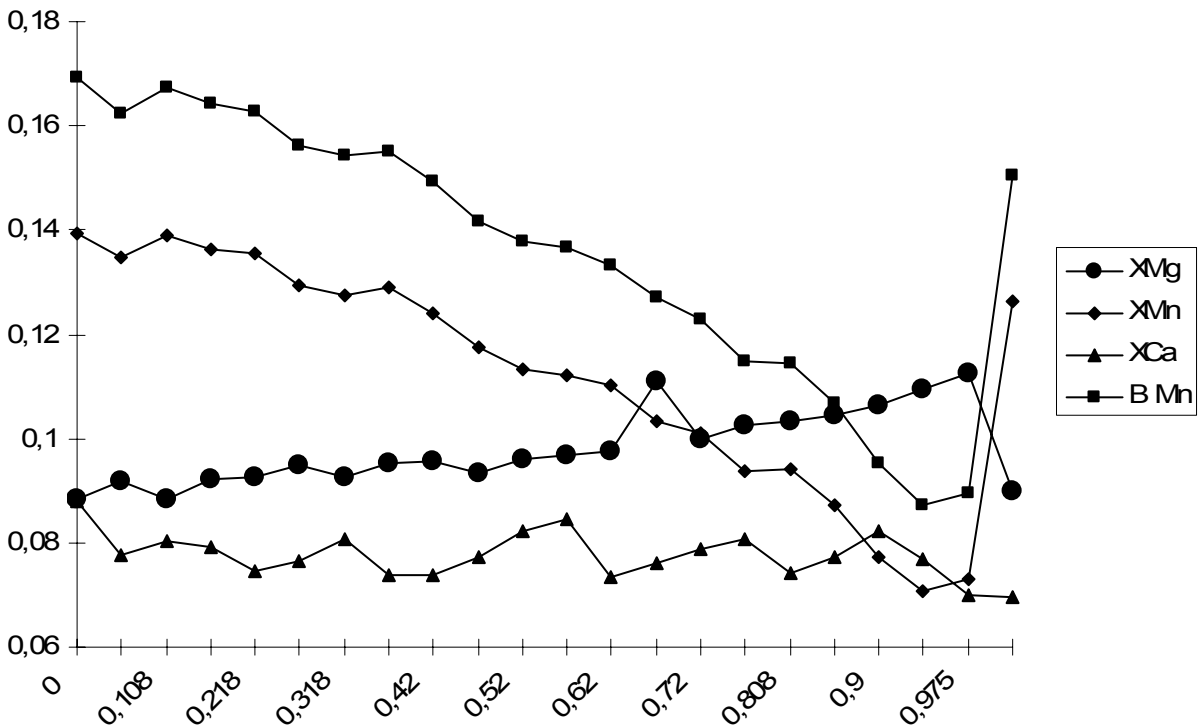
b

Figure A.2-6 a) shows trends for  $A_{Fe}$  (top) and  $X_{Fe}$ , garnet 6, Kid 18; b) Shows trends for  $B_{Mn}$ ,  $X_{Mn}$  (top two lines),  $X_{Mg}$  (at 0,06) and  $X_{Ca}$  for garnet 6, Kid 18.





a



b

Figure A.2-7 a) shows trends of AFe (top) and XFe, garnet 1, sample B63; b) shows trends for BMn and XMn (top two), XMg (third line) and XCa (bottom line), garnet 1, sample B 63.

of 0.90. Plagioclase in sample Kid 6 has an anorthite content between 0.20-0.38. K-feldspar is also observed. Plagioclase is commonly found in Kid 2. The mole fraction of magnesium in staurolite in Kid 6 varies between 0.12 and 0.15. Ilmenite is present in both samples with mole fractions of manganese varying between 0.02 and 0.18.

#### *A.2.5.2.3 Metavolcanics of the Malhaq Formation*

Tables A.2-5 to A.2-7 summarize the composition of minerals from samples of metavolcanic rocks of the Malhaq Fm. Sample locations are shown in Figure A.2-1. Sample B 61 is a biotite-amphibole schist and samples B 64 and WJ 64 are amphibole schists. All amphiboles are calcic in composition according to the classification scheme of Leake (1978). The  $X_{Mg}$  is between 0.43 and 0.82. No zoning is observed. Feldspar composition has grain to grain variations from albite to orthoclase in the different samples. The mole fraction of iron in biotite varies around 0.43 and the mole fraction of magnesium is around 0.46. Chlorite is only present in minor amounts and has an  $X_{Fe}$  between 0.39 and 0.51.

#### *A.2.5.3 PT conditions*

Tables A.2-8 to A.2-10 summarize the calculated temperatures and pressures for the different samples. The pelitic schists of the Central Wadi Kid area recorded garnet rim temperatures of 533 to 567°C (Table A.2-8). Garnet core temperatures are between 488 and 536°C (Table A.2-8). Pressures in the Wadi Kid area are consistent and are in the range 3-4.5 kbar (Table A.2-8).

Metamorphic conditions recorded by the metapelites in the Wadi Lig (sample B 63), in the northern part of the Wadi Kid area (Figure A.2-1), recorded garnet rim temperatures of 604-620°C and a pressure of 4.19 kbar (Table A.2-9), indicating upper-amphibolite facies conditions. Garnet core temperatures are slightly lower between 587 and 590°C. Metamorphic conditions estimated from hornblende-plagioclase thermometry were calculated for all measured amphiboles in the mafic schists (samples B61, B63 and WJ 61). Average temperatures for the amphiboles in the mafic schists range from 565 to 678°C with a pressure of 4 kbar (Table A.2-10).

In order to derive a PTt-path it is useful to compare the petrology and mineral assemblages in the pelitic schists with a petrogenetic grid. In this paper the KFMASH grid of Spear and Cheney (1989, Figure A.2-10) is used. Garnet-andalusite-biotite assemblages are stable between 550-600 °C and below the 3 kbar. Staurolite breakdown occurs between 500-600 °C and 1-3 kbar. Garnet-biotite assemblages are stable above 475 °C and less than 3 kbar up into the sillimanite stability field. The staurolite-andalusite stability field starts at approximately 475 °C. Mineral assemblages in the pelitic rocks indicate greenschist to amphibolite metamorphism. The metamorphic facies classification for mafic rocks is due to less sensitivity of the minerals to changes in pressure and temperature not so clear as for pelitic rocks.

Table A.2-5: Representative results of electron microprobe analyses of hornblende, plagioclase, chlorite and biotite in sample B 61. For location see Figure A.2-6. Oxygen basis of the analysis: Hbl, Bt 23; Pl 8; Chl 28.  $X_{Fe} = Fe/(Fe+Mg)$ ;  $X_{Ab} = Na/(Na+K+Ca)$ .

B 61									
	Hbl 2	Hbl 21	Hbl 24	Hbl 32	Pl 11	Pl 25	Pl 36	Chl 22	Bt 12
	matrix	matrix	matrix	matrix	matrix	matrix	matrix	matrix	matrix
SiO <sub>2</sub>	46.06	46.02	46.34	46.30	60.01	68.91	59.00	27.26	36.41
TiO <sub>2</sub>	0.35	0.37	0.35	0.33	-	0.03	-	0.02	2.20
Al <sub>2</sub> O <sub>3</sub>	9.94	10.15	10.56	10.28	25.55	21.09	26.68	20.05	15.97
Cr <sub>2</sub> O <sub>3</sub>	-	-	-	-	-	0.01	-	-	-
FeO	15.90	15.22	14.29	15.22	0.06	0.06	0.12	23.05	17.42
MnO	0.41	0.43	0.40	0.35	-	-	-	0.27	0.17
CaO	11.98	11.80	11.74	11.74	6.98	2.01	7.67	0.13	0.08
MgO	12.35	12.77	13.13	12.30	-	-	0.02	18.09	13.15
K <sub>2</sub> O	0.33	0.33	0.39	0.27	0.14	0.06	0.13	0.02	8.90
Na <sub>2</sub> O	1.08	1.13	1.15	1.09	7.41	7.70	7.29	0.01	0.09
Total	98.40	98.22	98.35	97.88	100.15	99.87	100.91	88.90	94.39
Si	6.774	6.758	6.759	6.808	2.667	2.982	2.613	5.586	5.794
Ti	0.039	0.041	0.039	0.037	-	0.001	-	0.001	0.265
Al	1.723	1.756	1.815	1.780	1.338	1.075	1.392	4.843	2.995
Cr	-	-	-	-	-	0.0004	-	-	-
Fe	1.955	1.870	1.744	1.871	0.002	0.003	0.004	3.952	2.317
Mn	0.052	0.054	0.049	0.044	-	-	-	0.047	0.023
Ca	1.888	1.855	1.835	1.849	0.333	0.093	0.364	0.029	0.015
Mg	2.708	2.974	2.855	2.695	-	-	0.001	5.527	3.118
K	0.062	0.061	0.071	0.049	0.008	0.004	0.072	0.005	1.806
Na	0.308	0.322	0.326	0.309	0.639	0.646	0.627	0.007	0.029
Total	15.509	15.511	15.493	15.442	4.987	4.804	5.0732	19.637	16.362
$X_{Fe}$	0.419	0.386	0.379	0.410				0.417	
$X_{Ab}$					0.652	0.869	0.590		

Appendix 2

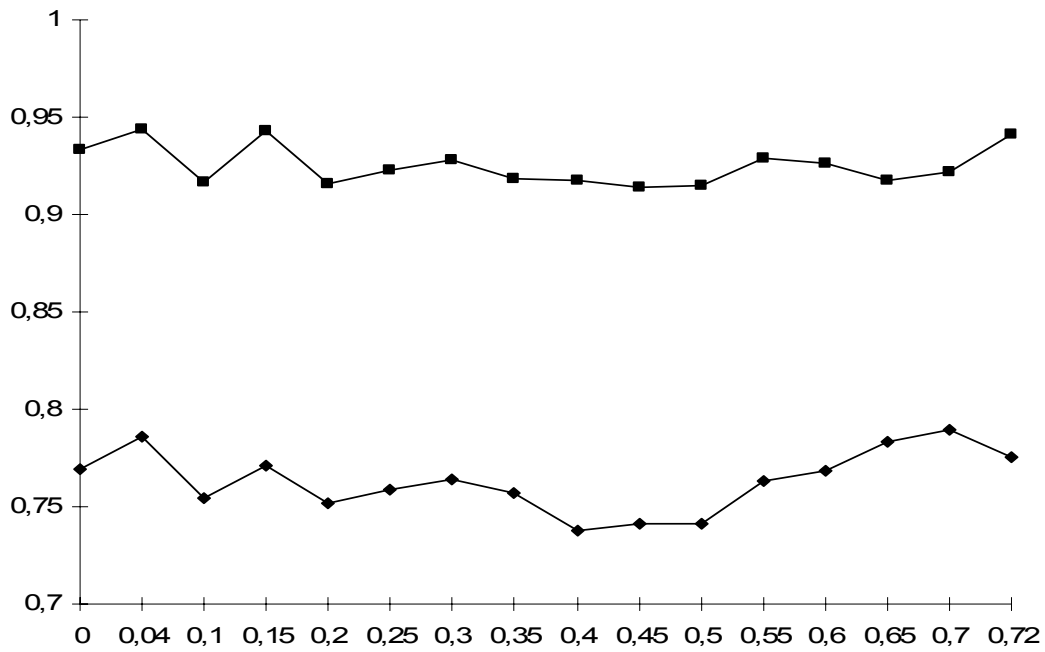
Table A.2-6: Representative results of electron microprobe analyses in sample B 63. For location see Figure A.2-6. Oxygen basis of the analysis: Pl 8; Grt 24; Bt, Ms 22.  $X_{Fe} = Fe/(Fe+Mg)$ ;  $X_{Alm} = Fe/(Fe+Mg+Mn+Ca)$ ;  $X_{Sps} = Mn/(Fe+Mg+Mn+Ca)$ ;  $X_{Prp} = Mg/(Fe+Mg+Mn+Ca)$ ;  $X_{Grs} = Ca/(Fe+Mg+Mn+Ca)$ ;  $X_{Ab} = Na/(Na+K+Ca)$ .

B 63									
	Gt 1	Gt 1	Gt 2	Gt 2	Bt 150	Bt 158	Ms 154	Pl 152	Pl 135
	core	rim	core	rim	matrix	matrix	matrix	matrix	matrix
SiO <sub>2</sub>	37.52	35.21	37.40	34.40	34.55	34.42	47.66	56.44	56.22
TiO <sub>2</sub>	0.07	0.02	0.03	0.02	1.13	1.25	1.07	-	-
Al <sub>2</sub> O <sub>3</sub>	21.07	20.54	21.14	21.96	20.27	20.22	37.51	28.38	28.17
Cr <sub>2</sub> O <sub>3</sub>	-	-	-	0.03	-	0.06	-	-	-
FeO	29.53	31.63	29.02	28.61	21.29	21.10	1.57	-	0.05
MnO	5.94	3.07	6.79	4.47	0.19	0.15	-	0.03	0.03
CaO	2.95	2.32	2.42	2.64	0.04	0.17	0.01	9.57	9.57
MgO	2.14	2.69	2.12	2.11	8.16	9.80	0.81	-	-
K <sub>2</sub> O	-	-	-	0.10	9.93	7.30	6.73	0.10	0.10
Na <sub>2</sub> O	0.01	0.01	0.03	0.08	0.09	0.08	0.19	6.13	5.76
Total	99.23	95.49	98.95	94.42	95.65	94.55	95.55	100.65	99.90
Si	6.064	5.938	6.062	5.834	5.307	5.265	6.159	2.517	2.524
Ti	0.008	0.002	0.004	0.003	0.131	0.145	0.104	-	-
Al	4.013	4.081	4.041	4.388	3.671	3.644	5.713	1.493	1.491
Cr	0.001	-	-	0.003	-	0.007	-	-	-
Fe	3.992	4.463	3.934	4.059	2.734	2.699	0.170	-	0.002
Mn	0.814	0.439	0.933	0.642	0.025	0.019	-	0.001	0.001
Ca	0.512	0.420	0.421	0.481	0.006	0.027	0.002	0.457	0.460
Mg	0.515	0.674	0.514	0.534	1.866	2.235	0.155	-	-
K	-	0.001	-	0.020	1.943	1.425	1.110	0.005	0.006
Na	0.006	0.006	0.089	0.026	0.027	0.022	0.048	0.531	0.501
Total	15.925	16.478	15.998	15.990	15.710	15.488	13.461	5.004	4.985
X <sub>Fe</sub>	0.886	0.869	0.884	0.884	0.594	0.547			
X <sub>Alm</sub>	0.684	0.744	0.678	0.710					
X <sub>Sps</sub>	0.140	0.073	0.161	0.112					
X <sub>Prp</sub>	0.088	0.112	0.089	0.093					
X <sub>Grs</sub>	0.088	0.070	0.073	0.084					
X <sub>Ab</sub>								0.534	0.518

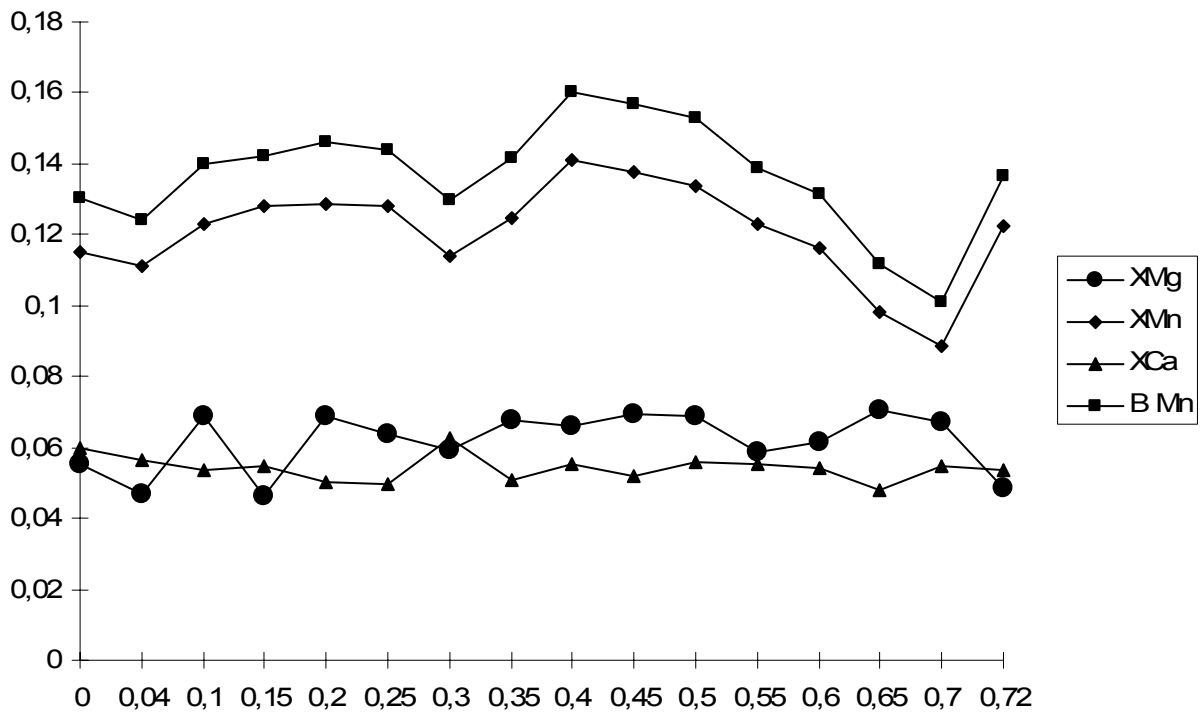
Table A.2-7: Representative results of electron microprobe analyses in sample WJ 61. For location see Figure A.2-6. Oxygen basis of the analysis: Hbl 23; Pl 8; Chl 28.  $X_{Fe} = Fe/(Fe+Mg)$ ;  $X_{Ab} = Na/(Na+K+Ca)$ .

	WJ 61										
	Hbl 72	Hbl 77	Hbl 90	Hbl 94	Hbl 102	Hbl 103	Pl 71	Pl 86	Pl 96	Pl 100	Chl 97
	matrix	matrix	matrix	matrix	matrix	matrix	matrix	matrix	matrix	matrix	matrix
SiO <sub>2</sub>	45.10	45.55	45.16	43.96	46.15	48.50	63.37	64.52	63.13	64.52	26.68
TiO <sub>2</sub>	0.53	0.52	0.53	0.60	0.40	0.42	-	-	-	-	0.15
Al <sub>2</sub> O <sub>3</sub>	10.58	10.17	10.49	11.05	9.60	7.12	23.49	23.71	23.81	21.33	19.61
Cr <sub>2</sub> O <sub>3</sub>	0.01	0.07	0.34	0.04	-	0.03	0.01	-	0.03	-	0.06
FeO	19.63	19.22	19.17	19.85	18.78	18.26	0.17	0.06	0.10	0.08	28.02
MnO	0.37	0.36	0.36	0.30	0.32	0.34	-	0.01	-	0.01	0.19
CaO	10.89	10.82	10.80	11.00	11.12	10.94	4.63	4.58	4.32	0.32	0.15
MgO	9.85	10.10	9.95	9.35	10.74	11.66	-	-	-	0.03	12.62
K <sub>2</sub> O	0.34	0.33	0.33	0.35	0.28	0.22	0.06	0.11	0.06	11.43	0.04
Na <sub>2</sub> O	1.52	1.50	1.52	1.60	1.29	0.97	6.79	9.23	9.44	2.20	-
Total	98.82	98.64	98.65	98.10	98.68	98.46	98.52	102.22	100.89	99.92	87.52
Si	6.713	6.777	6.724	6.619	6.839	7.152	2.816	2.791	2.770	2.922	5.706
Ti	0.061	0.058	0.059	0.067	0.046	0.047	-	-	-	-	0.025
Al	1.858	1.781	1.839	1.961	1.676	1.240	1.130	1.208	1.232	1.139	4.944
Cr	0.001	0.009	0.040	0.004	-	0.003	0.001	-	0.001	-	0.009
Fe	2.444	2.391	2.387	2.500	2.328	2.251	0.006	0.002	0.004	0.003	5.011
Mn	0.047	0.046	0.046	0.039	0.040	0.042	-	0.001	-	0.001	0.035
Ca	1.737	1.724	1.723	1.773	1.765	1.728	0.211	0.212	0.303	0.016	0.036
Mg	2.185	2.239	2.207	2.099	2.374	2.563	-	-	-	0.002	4.023
K	0.063	0.061	0.063	0.068	0.053	0.041	0.003	0.006	0.004	0.660	0.008
Na	0.438	0.432	0.439	0.468	0.370	0.277	0.586	0.774	0.803	0.193	-
Total	15.547	15.518	15.527	15.598	15.491	15.344	4.763	4.994	5.117	4.936	19.797
X <sub>Fe</sub>	0.528	0.516	0.520	0.544	0.495	0.468					0.555
X <sub>Ab</sub>							0.733	0.780	0.723	0.222	

Appendix 2

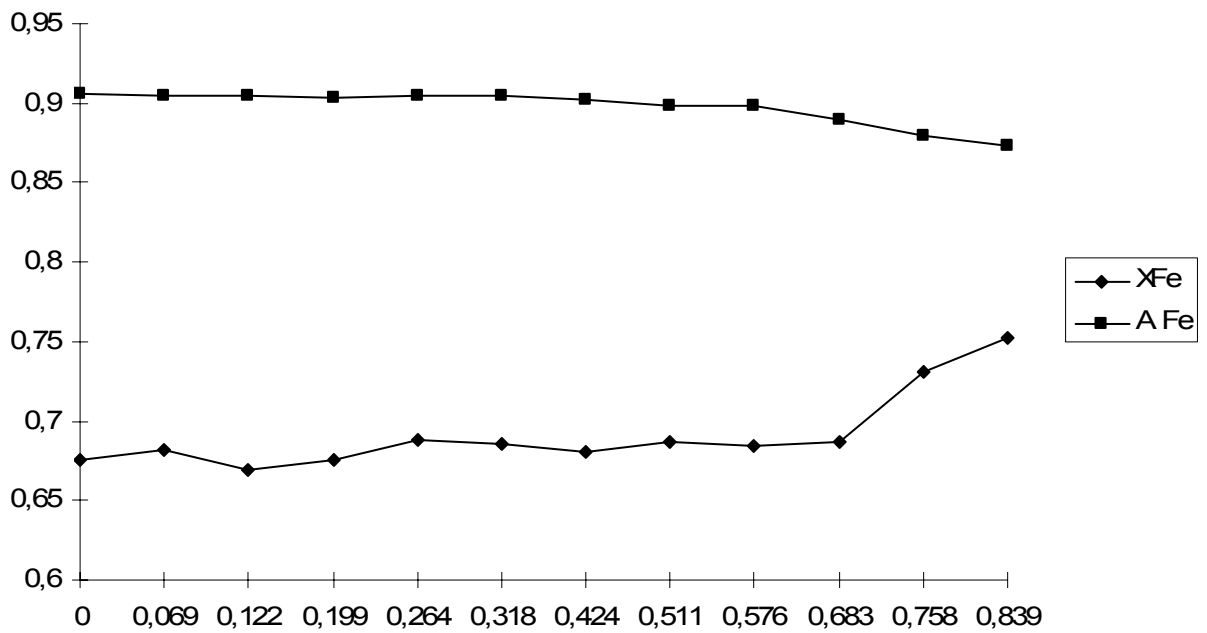


a

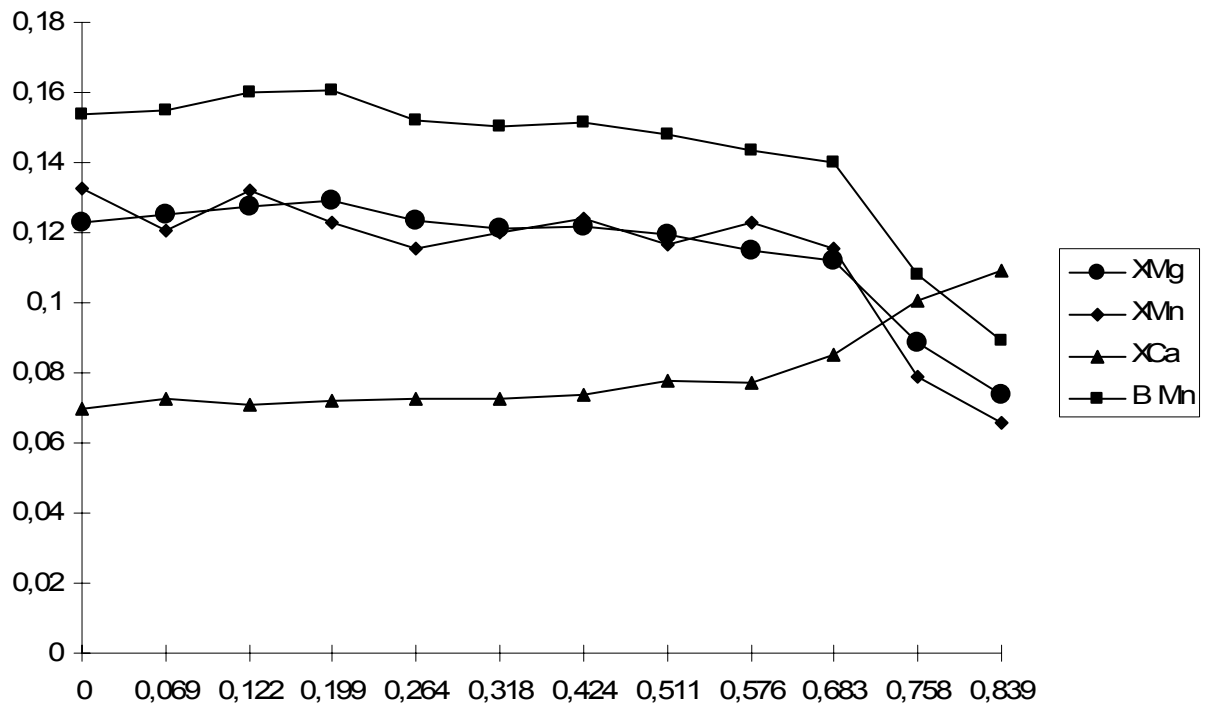


b

Figure A.2-8 a) AFe (top) and XFe for garnet 6, Kid 6; b) Graph showing the trends of BMn, XMn, XCa and XMg (from top to bottom) for garnet 6, sample Kid 6.



a



b

Figure A.2-9 a) Graph of AFe (upper line) and XFe, garnet 2, sample Kid 2; b) Graph showing trends of BMn (upper line), XMn, XMg and XCa (lowest line), garnet 2, Kid 2.

#### A.2.5.4 Discussion of PT results

Geothermobarometry indicates a low-pressure/high-temperature amphibolite facies metamorphism during the M<sub>2</sub> phase in the lower crustal rocks of the Wadi Kid area. Furthermore, the geothermobarometric results show an increase in pressure and temperature from south to north. These results are supported by the petrology of the rocks in the Wadi Kid area.

Garnet rims represent peak temperatures in the Wadi Kid and Wadi Lig, where the cores give the lower temperatures (Table A.2-8). Garnet zoning is the result of prograde metamorphism, i.e. the rims are enriched in almandine and pyrope and cores are enriched in spessartine and grossular (Figures A.2-6 to A.2-9). The zoning is suggested to be the effect of continuous garnet growth during prograde metamorphism. Garnets experienced minor effects of retrograde re-equilibration, as displayed by the decreasing almandine ratio close to the rim and so actual peak temperatures have been slightly higher than shown by our analytical results. Garnet core pressures have not been calculated in this study, due to the fact that the garnet cores are not in equilibrium with three other phases (muscovite, feldspar and biotite) in the rock.

The chemical composition of the amphiboles will give reliable information on the temperatures and pressures (Laird and Albee, 1981). Consequently thermobarometry of the mafic schists of the Malhaq Fm. (Table A.2-10) were used to give additional information on the P-T conditions in the Wadi Kid area because. The pressure used for the calculations was 4 kbar. Geothermometric results of the mafic schists in the Wadi Lig are consistent with the results of geothermometry with the Kleemann and Reinhardt geothermometer (1994) on the pelitic schists (sample B63).

Error estimation on the results of geothermobarometry is essential to reveal the consistency and quality of the results. Standard deviations from the results on the samples of the Wadi Kid and the Wadi Lig (Figure A.2-1) are all less than 50 °C, which is a common standard deviation for geothermometers. Most geobarometers have a standard deviation of 1 kbar. In this study, all standard deviations on the results are less than 1 kbar. The fact that the standard deviations in this study fall within the limits set by the authors of the calibrations used, is a measure for the consistency of our results.

Barrovian as well as Buchan zone metamorphic assemblages are found in the pelitic schists of the Wadi Kid area. The Buchan type Andalusite zone does not contain garnet or staurolite and the Barrovian type Staurolite zone does not contain andalusite. The overall presence of low pressure metamorphic assemblages, such as cordierite, andalusite and sillimanite, and the absence of blueschist facies rocks and kyanite gives rise to the conclusion that staurolite is not the relict of an earlier higher pressure metamorphic phase, but the product of prograde metamorphism.

Differences in temperatures and pressures are noticed when comparing the geothermobarometric results with the petrogenetic grid. Temperatures for the garnet-andalusite-biotite schist of the Malhaq Fm. are lower than the temperature range as predicted by the petrogenetic grid. The calculated pressures are generally more than 1 kbar higher than the pressures read from the petrogenetic grid. Calculated temperatures for garnet-andalusite-biotite-staurolite schist (Umm Zariq Fm.) equal the temperatures from the petrogenetic grid, the



Table A.2-8: P-T results for the pelitic schists of the central Wadi Kid. Bio-gt geothermometry (Kleemann & Reinhardt, 1994) and plag-bio-gt-musc geobarometry (Powell & Holland, 1988). Errors are mean deviations of the reported results.

Sample #	Core T (°C)	Rim T (°C)	P (kbar)
Kid 18			
G1	536	566	4.28
G2	533	559	3.98
G3	530	573	3.97
G4	504	578	4.23
G5	535	571	4.02
G6	527	565	3.98
G7	516	576	4.18
G8	528	550	3.81
Average	526±11	567±9	4.06±0.16
Kid 2			
G1	527	553	-
G2	526	562	-
Average	527±1	558±6	
Kid 6			
G1	505	545	3.45
G3	505	535	3.42
G4	506	546	3.48
G5	519	533	3.50
G6	488	539	3.48
Average	505±11	540±6	3.54±0.17

## Appendix 2

Table A.2-9: P-T results for the pelitic schists of the northern Wadi Kid. Bio-gt geothermometry (Kleemann & Reinhardt, 1994) and plag-bio-gt-musc geobarometry (Powell & Holland, 1988). Errors are mean deviations of

Sample #	Core T (°C)	Rim T (°C)	P (kbar)
B 63			
G1	590	620	4.16
G2	587	604	4.01
G3	-	626	4.20
Average	589±2	617±11	4.12±0.10

Table A.2-10: Temperature results for the Wadi Lig mafic schists (Holland & Blundy (1994)) thermometer, P = 4 kbar. Errors are mean deviations of the reported results.

Sample #	T (ed-tr)	T (ed-ri)	Average
WJ 61(n=15)	684±18	672±13	678±17
B 61 (n=36)	623±22	565±21	594±36
B64 (n=22)	668±18	594±13	631±41

difference between the pressures is 0.5 kbar. The calculated temperatures for the garnet-biotite assemblages (Malhaq and Umm Zariq Fm.) are within the stability field of the petrogenetic grid. Calculated pressures are higher than the pressures predicted by the petrogenetic grid.

Differences between the calculated pressures and temperatures and the PT-space for the stable assemblages on the petrogenetic grid can be explained by the errors involved in estimating pressures and temperatures. Secondly the behavior of natural assemblages differs from an ideal chemical system as is the Spear and Cheny (1989) grid. Thirdly the presence of small quantities of stabilizing elements, like MnO, extends the stability field of the phases present in the rock (Mahar et al, 1997 and Symmes and Ferry, 1992).

### A.2.6 Evidence from PT-data for a core complex in the Wadi Kid Area

Blasband et al. (1997, 2000) have postulated, mainly on the basis of their structural data, that the Wadi Kid area represents a typical core complex. However to accept such an idea, evidence from geothermobarometry is crucial.

Metamorphic core complexes in extensional setting are characterized by LP/HT metamorphism in their lower crustal sequence due to the intrusion of granitoids into thinned crust (Gans et al, 1989; Lister and Baldwin, 1993). Pressures of metamorphism are less than or

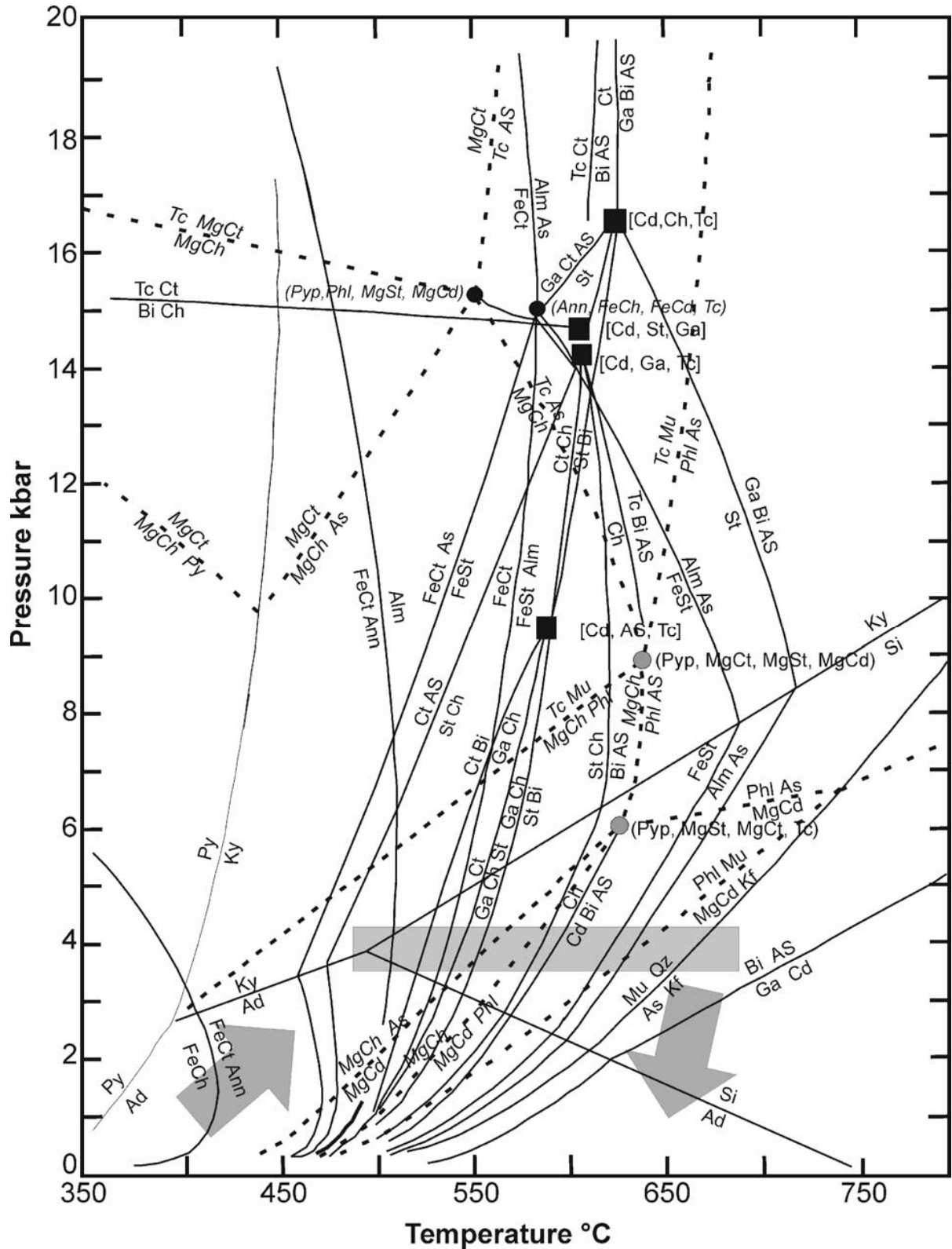


Figure A.2-10 Petrogenetic grid for the KFMASH system after Spear and Cheney (1989). The grey square defines the PT-space for the samples of the Wadi Kid area resulting from geothermobarometry. The arrows indicate the PT-path during the M<sub>1</sub> and uplift phase.

equal to that of the aluminosilicate triple point and the temperatures range from 500-750°C (De Yoreo et al., 1991). Inferred pressure-temperature-time-paths (PTt-paths) are nearly isobaric in the early stages and turn clockwise during the later stages of uplift (De Yoreo et al., 1991). Metamorphic thermal gradients are generally higher than 40°C/km (Thompson, 1989; Barton, 1990). Evidence for isobaric PT-paths are found in garnets and peak temperatures are best represented by garnet rim compositions (Spear, 1991; Buick and Holland, 1989; House et al., 1997). Geothermochronological studies have shown that uplift of core complexes can be very rapid (Davis and Lister, 1988).

Davis (1980, 1987) has shown that there is a difference in structural styles between the upper and lower crustal rocks. Deformation in the upper-crustal rocks is brittle, while lower crustal rocks display ductile deformation. This implies a metamorphic break between the lower and the upper crustal rocks.

Metamorphism in the lower crustal rocks of the Wadi Kid area during  $M_2$  is of the LP/HT-type. Temperatures range from 488 °C in the south to 684 °C in the north and pressures are in the range 3.4 to 4.28 kbar from south to north. Garnet rims define peak temperatures. Metamorphic thermal gradients are in the range 42-50 °C/km (assuming 1 kbar = 3.5 km). Metamorphism is prograde (see Figure A.2-10) as shown by the chemical trends in garnet.

The succession of andalusite after garnet can be observed in the Wadi Kid area. This is interpreted as a result of isothermal decompression (Gibson, 1992). Garnets show small retrograde rims (Figures A.2-6 to A.2-9). Retrograde rims on other metamorphic minerals are absent. These observations lead us to the conclusion that the uplift and cooling rates were relatively rapid.

The data on the metamorphic conditions presented above support the extensional core complex model of Blasband et al. (1997). Metamorphism during  $M_2$  is characterized by low-pressure/high-temperature conditions. The granitoids responsible for heating are the undeformed A-type granites and a non-deformed hornblende diorite in the northern Wadi Kid area. A mantle source is inferred for the hornblende diorite (Moghazi et al., 1998) and thus possibly indicates intrusion into a thinned crust. It is near the hornblende diorite that we found the highest temperatures (sample WJ 61, 687 °C) and thus it may be assumed that the hornblende diorite is the deepest-seated intrusion in the Wadi Kid area.

The upper crustal greenschist facies rocks of the  $M_1$  phase are probably relicts of the arc-accretion phase (Blasband et al., 2000). These authors believe this phase to be responsible for the crustal thickening, which preceded the extensional collapse. The closure of the Mozambique Ocean resulted in arc-accretion and consequently the lithospheric thickening. (Blasband et al., 2000). This collisional phase is generally referred to as the East African Orogen. The  $M_1$  metamorphic phase reflects metamorphism during this orogen. During the collapse stage, extensional core complexes were able to develop where LP/HT metamorphism took place as is observed during the  $M_2$  phase in the Wadi Kid area. Blasband et al. (2000) postulated that the Late Proterozoic extensional phase in the Sinai, in which the core complex was formed, was due to the collapse of a compressed and thickened lithosphere. The HT/LP metamorphism as observed in the Wadi Kid area is a result of the very latest stage of the Late Proterozoic in the Middle East when collapse of this orogen led to extension and core complex formation

(Blasband et al. 2000).

### **A.2.7 Conclusions**

1. Thermobarometry of metamorphic rocks from the Wadi Kid area reveal upper-greenschist to lower-amphibolite facies conditions of the LP/HT-type for the M<sub>2</sub> phase. Peak temperatures and pressures in the Wadi Lig also indicate LP/HT amphibolite facies conditions (687 °C and 4.28 kbar).
2. In the Wadi Kid area, a temperature increase is observed from south to north with highest temperatures recorded adjacent to the Sharira diorite.
3. Garnets show a progressive growth history and peak temperatures are given by garnet rim compositions.
4. M<sub>2</sub> metamorphism is associated with regional extension and the subsequent intrusion of granitoids.
5. The geothermobarometric results of this study support the core complex model, which is a result of collapse of the East African Orogen (Blasband et al., 1997; 2000).

### **Acknowledgements**

The Dr. Schürmann Foundation for Precambrian Research, grants nos. 1994/06 and 1997/04, supported this research. We thank H.N.A. Priem for his support during all stages of this project. We thank H. Kisch for useful discussions in the field. We thank H. de Boorder and H. Kisch for reviewing earlier drafts of the manuscript. R. Dymek, R. Buchwaldt and M. El-Shafei are thanked for constructive reviews, which greatly improved the paper.

